THE PHYSICAL STRUCTURE AND ADSORPTIVE PROPERTIES OF HEAT TREATED POROUS CARBONS

by

D.R.G. WILLIAMS, B.APP.SC.(Hons.)

of the

Department of Mining, Metallurgical
and Chemical Engineering

A Thesis submitted for the
Degree of Doctor of Philosophy
in the Faculty of Engineering,
University of Adelaide.

January, 1964.

ACKNOWLEDGEMENTS

The author is indebted to Dr. R.V. Culver for his guidance and encouragement during the investigation.

The author wishes to acknowledge an equipment grant from The Colonial Sugar Refining Company Limited, Sydney, and financial assistance in the form of a Commonwealth Postgraduate Scholarship from the Commonwealth Government of Australia.

TABLE OF CONTENTS

TABLE OF CONTENTS

TABLE OF CONTENTS

TABLE OF CONTENTS

TABLE OF CONTENTS

TABLE OF CONTENTS

LIST OF TABLES

LIST OF FIGURES

LIST OF FIGURES

LIST OF FIGURES

LIST OF FIGURES

LIST OF FIGURES

SUMMARY

This thesis deals with the changes in the physical structure and the adsorptive properties of porous carbons heat treated at temperatures from 800° to 3,000°C under an inert atmosphere.

A comprehensive review was undertaken of the literature related to the structure and formation of heat treated porous carbons. The final properties of a carbon were found to depend to a large extent on the history of the carbonization and heat treatment steps. It was established that heat treatment decreased the adsorptive capacity and surface area but little attempt had been made to follow the change in the physical structure with heat treatment and so elucidate the mechanism of sintering. A recent article on the properties of sintered cellulose carbon and its possible commercial applications, emphasized the need for further study of the sintering process.

Carbons were prepared from the polymers cellulose acetate, cellulose, phenol-formaldehyde, polyvinylidene chloride and polyvinyl chloride; a commercial activated carbon, Cal Carbon (prepared from coal) was included for purposes of comparison. Heat treatment of these carbons produced a marked drop in the surface area - the largest drop in surface area generally occurring at temperatures between 1,000° and 1,200°C. While steam activation of the carbon prepared from polyvinylidene chloride considerably increased the surface area, heat treatment of the activated carbon reduced the surface area by an amount comparable with that of the unactivated carbon.

Results obtained from mercury density, helium density, pore volume, average pore size and pore size distribution determinations indicated that heat treatment produced constrictions in the pores, the smallest pores becoming blocked, i.e. the maximum in the pore size distribution tended to move towards higher values of the pore diameter. Generally, the helium density and pore volume decreased with increased temperature of heat treatment. On the macro-scale there was little

change, with the mercury density (or bulk density) remaining practically constant.

An extensive study of the kinetics of adsorption of argon on heat treated cellulose acetate and polyvinylidene chloride carbons supported the contention that heat treatment reduced the proportion of pore volume residing in the smaller pores. For the cellulose acetate carbons, the effective diffusion coefficient calculated from an appropriate solution of Fick's Second Law increased with increased temperature of heat treatment. A similar result was obtained for the polyvinylidene chloride carbons except that at 1,400°C, the value of the effective diffusion coefficient decreased instead of increased. The marked reduction in the rate of adsorption for the polyvinylidene chloride carbon heat treated to 1,400°C was attributed to a combination of a very uniform pore size distribution and a growth of constrictions sufficient to retard the passage of molecules into the pore volume.

Values of the heats and entropies of adsorption of argon and benzene suggested that the surface of the carbon becomes more heterogeneous with increased temperature of heat treatment. It was postulated that surface imperfections arose from growth steps and dislocations accompanying crystallite growth.

Several possible sintering processes were examined such as sealing of cracks or the irreversible thermal expansion of crystallites into the pores. However, the only process which could account for the bridging of pores approximately 15 Å in diameter, involved the growth of crystallites into the pore space to form constrictions. Thus crystallite growth is presumed to be accommodated in the pore space as for reversible thermal expansion.

I hereby certify that this Thesis contains no material which has been accepted for the award of any other Degree or Diploma in any University and that, to the best of my knowledge and belief, this Thesis contains no material previously published or written by another person except when due reference is made in the text of the Thesis.

D.R.G. WILLIAMS.

1. INTRODUCTION

In contrast with the many investigations dealing with the activation of carbons, the sintering of porous carbons - usually involving a reduction in surface area and pore volume - has received limited attention, and only recently has some attempt been made to elucidate the sintering mechanism.

The industrial significance of the sintering of porous carbons serves to emphasize the need for a more detailed investigation of the sintering process. Porous carbons used as adsorbents are revivified periodically to remove adsorbed impurities by heating at temperatures above 600°C. If the sintering temperature is exceeded, the adsorptive capacity will be reduced. A similar restriction applies to the manufacture of carbons for subsequent gasification. Loss of surface area on sintering will decrease the accessibility of gases to inner surfaces of the carbon and consequently the rate of gasification. Heat treatment of a porous cellulose carbon reduces its permeability to an immeasurably low value and produces a novel material of construction. The sintered carbon possesses other important qualities such as high strength and impact resistance, which make it suitable for 'canning' fuel elements in high temperature gas-cooled nuclear reactors.

In examining the sintering of porous carbons, it appears that particular reference should be made to changes in adsorptive capacity, pore size and crystallite dimensions resulting from heat treatment. Moreover the porous carbons should possess strictly reproducible physical and chemical properties.

In the investigation therefore, it is proposed to use carbons prepared from polymers of known chemical composition; their properties, as opposed to carbons made from other raw materials, should be reproducible. The experimental work would include:

1. The preparation of porous carbons heat treated at various temperatures.

2. The determination of equilibrium adsorptive capacities using adsorbates of varying physical characteristics.
3. The determination of rates of adsorption and correlation with pore sizes.
4. The measurements of pore volumes by the displacement of helium and mercury.
5. The measurement of crystallite dimensions by X-ray analysis.

This thesis is concerned with the physical structure and adsorptive properties of heat treated porous carbons and is divided into five sections. Firstly, the literature is reviewed and recommendations made for investigating the sintering process. Section 2 outlines the scope of the experimental programme and the experimental procedures to be adopted; the results are given in section 3 and discussed in section 4. In the final section conclusions are drawn and recommendations made for future work.

2. LITERATURE REVIEW

The review commences with an account of the theory underlying the formation and structure of carbons and graphites. This is followed by a survey of the sintering of porous carbons and graphites. The next sections deal successively with the measurement of some of the characteristic properties of carbons such as crystallite size, surface area, pore size, gaseous diffusion coefficients and heats and entropies of adsorption. In the final section progress in the field is summarized and recommendations made for future experimental work.

2.1 Structure and Formation of Carbons and Graphites

An analysis of the factors involved in the formation of a carbon from its parent polymer is essential to an understanding of the effect of heat treatment on the properties and the characteristics of carbons. Firstly, the crystal structure of the carbons is discussed with particular reference to the structural defects. The section deals with the evolution of the carbon crystal structure during the pyrolysis of typical carbons. The last section is concerned with the development and growth of the crystal structure and the removal of structural defects during heat treatment.

2.1.1 Crystal Structure of Carbon and Graphite

2.1.1.1 Ideal Graphite Lattice

There have been two main ideal lattices proposed for graphite. The first is the hexagonal layered lattice proposed by Bernal[1] and is shown in Fig. 1(a). It is composed of aromatic parallel layers with a C-C distance within each layer of 1.42 Å. The parallel layers are weakly held together by van der Waals forces and exhibit a comparatively large interlayer spacing of 3.15 Å. The stacking sequence is of the type ABAB.... where (1) half the carbon atoms in one plane are directly above atoms in the layer beneath, and (2) all the carbon atoms in alternate layers are directly above one another.

The second ideal lattice (Fig. 1(b)) was first suggested by Debye and Scherrer[2], where the packing sequence is now represented by ABCABC...., i.e. carbon atoms in any one layer are directly above those in the fourth layer. This rhombohedral form was suggested to account for certain faint lines found in X-ray powder photographs. Because the hexagonal form is more stable, only a few per cent of the rhombohedral form is usually found in graphite[3].

2.1.1.2 Defect Structures in Carbons and Graphites

The structure of carbons and graphites is usually far removed from the ideal graphite lattice due to the presence of defects. It is these defects which promote such diversity of properties amongst carbons and graphites and therefore it is of fundamental importance that these defects be carefully studied in conjunction with observed physical and chemical properties. Ubbelohde and Lewis[4] in their extensive review of graphite have systematically classified the defects under three convenient headings, viz. layer stacking defects, carbon network bond defects and gross defects. Under these headings, only those defects of particular interest in this project will be dealt with in detail.

(a) Layer Stacking Defects

Turbostratic Packing Because the interlayer attraction forces are comparatively weak, it is usual for a large percentage of the layers to be randomly orientated about an axis perpendicular to the plane. Biscoe and Warren[5] have termed this type of lattice geometry 'turbostratic'.

There is some confusion of terms in this field and it is appropriate at this stage to define more clearly some of the ambiguous ones. Graphitization[6] should mean the process whereby the turbostratic structure reverts to the stable three-dimensionally ordered ideal graphite lattice. However, the term graphitization generally refers to heat treatment at temperatures above

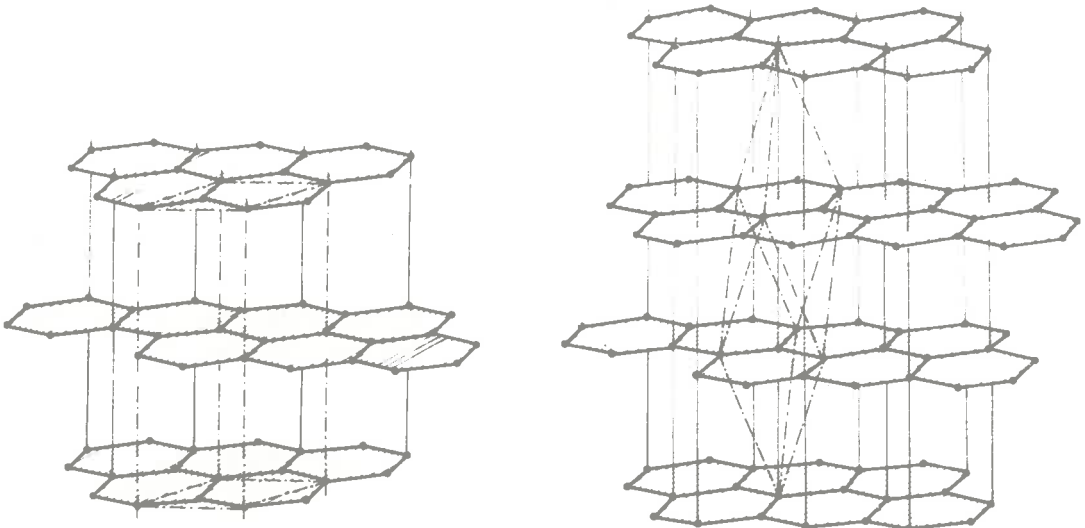

(a)
hexagonal

(b)
rhombohedral

Fig. 1 - Ideal Lattice Structure of Graphite

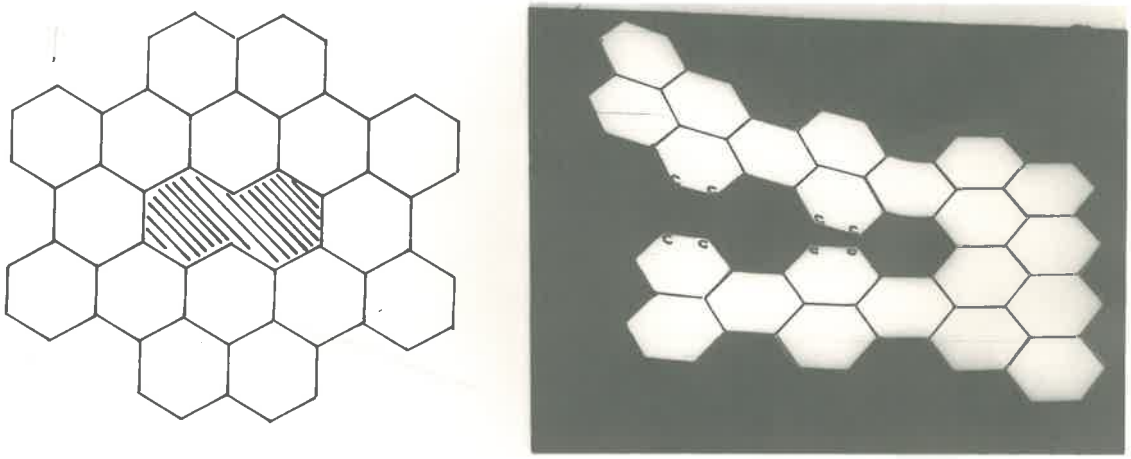

(a)
'hole'

(b)
'claw'

Fig. 2 - 'Hole' and 'Claw' Defects in Carbon Hexagon Networks[4]

approximately 2,000°C, so, to be consistent with current usage in the literature, this is the meaning that will be implied whenever the word graphitization is used in this project. To avoid ambiguity, all carbonaceous solids will be considered as carbons, unless the carbon possesses a near-ideal graphite lattice.

Interlayer Spacing Associated with the graphitization of turbostratic structures is the gradual decrease in the interlayer spacing d, from a value of approximately 3.44 Å to the ideal spacing of 3.35 Å. Various empirical equations have been developed to relate the change in interlayer spacing d with the proportion of disorientated layers[7].

Crystallite Size An assembly of layers of finite size is termed a crystallite and a useful appraisal of the degree of ordering of a carbon can be made in terms of (1) L_a and L_c, the average dimensions of the packets of layers parallel and perpendicular to the layer planes, (2) d, the interlayer spacing, (3) p, the proportion of disorientated layers, and (4) the proportion of disorganized material. A further set of parameters introduced by Steward and Cook[8,9] are M_a and M_c which refer to the size of layer planes over which there is reasonable continuity and regularity of atomic arrangement, i.e. M_a and M_c denote a macro-unit of crystallites which are roughly aligned. For low temperature carbons, where the degree of ordering is far removed from that of highly graphitized carbons, both the crystallites and the disorganized phase must be considered as gross defects.

(b) Carbon Network Bond Defects

It is interesting to consider graphite as the limiting term of the homologous aromatic series, the number of fused benzene rings in a typical graphite layer being of the order of 1,000. Another concept is to regard carbons as thermoset high polymers containing fused aromatic rings, whose mutual orientations conform approximately to that of the ideal graphite lattice. It is to be

expected that in such large systems there will exist bond defects. Principal types include edge defects, internal structure defects and chemical defects.

Edge Defects For carbons composed of small crystallites the proportion of edge atoms will be high and their properties will thus exert a correspondingly large influence on the carbon structure as a whole. In the layered lattice type structure, carbon forms strong trigonal type σ bonds, i.e. in the excited state the σ hybrid bond utilizes only two of the three 2p orbitals.

$$(2s^2\ 2p^2 \longrightarrow 2s\ 2p_x\ 2p_y\ 2p_z)$$

ground state excited state

The remaining $2p_z$ orbitals protruding from above and below the plane, laterally overlap and form a π-bond. The carbon atoms on the edge of the layer will therefore possess a free bond and be able to combine with foreign atoms or groups such as -H, -OH, -C≡H, etc. Coulson[171] has shown that the situation is not necessarily as simple as it appears; for instance, he suggests that certain edge atoms may acquire a partly triple-bond character and certain other edge atoms revert to a divalent state. Pullman[11] has made some interesting calculations of bond order and free valence for aromatic ring systems of increasing size. Pullman's calculations indicate that certain edge atoms will possess relatively large values of free valence compared to others. However, as the free valence for carbon atoms in the edge position is greater than 0.5 compared with a free valence value of less than 0.2 for carbon atoms in the centre of the layer, it is clear that the edge atoms are in the most favourable position for chemisorption of foreign atoms.

When a carbon is initially prepared from a polymer by pyrolysis, non-carbon atoms present in the original polymer or in

the surrounding atmosphere may become bonded to unsaturated carbon atoms around the peripheries of the layers. A carbon prepared from polyvinylidene chloride by pyrolysis under an atmosphere of nitrogen to 800°C will contain some 17% oxygen, 4% chlorine and 2% hydrogen (by weight). Although oxygen is strictly excluded during the carbonization process, it is apparently rapidly chemisorbed when the cooled carbon is exposed to the atmosphere. It is well known that the presence of these foreign atoms exerts a considerable influence on the adsorption of polar molecules[12, 13, 14, 15] and on the electronic properties[16] of the carbons. Further detailed evidence of the nature and reactions of surface complexes may be found in the comprehensive reviews of Culver and Watts[17], Smith[14] and Weiss[18].

Two interesting types of edge defect that have been proposed by Ubbelohde[19] are 'hole' and 'claw' defects. The 'hole' defect is caused by the presence of unsaturated carbon atoms at internal points of layers and an example of a naphthalene gap is shown in Fig. 2(a). The second structure, Fig. 2(b), is the result of a re-entrant 'hole' where the carbon atoms designated by 'c' are bonded to foreign atoms. The repulsion between these foreign atoms causes the layer to buckle into the shape of a claw. A claw defect could also present an ideal site for the beginning of a spiral growth mechanism.

Internal Structural Defects Electron micrographs of graphite have revealed a variety of topographical features such as pyramidal growth, conical growth by a screw mechanism and laminar cleavage along basal planes[20, 21, 22]. While it is well known that such defects and dislocations have a profound influence on the chemical and physical properties of metals and inorganic crystals[23, 24], there is at present little evidence as to how these defects influence the properties of graphite.

Chemical Defects There are four different types of chemical

impurities in carbons and graphites[25]; substitutional impurities, ordered impurities, disordered impurities and impurities chemically bonded to free valencies around layer edges. The last impurity has already been considered in the section on layer stacking defects.

A substitutional impurity occurs where a carbon atom in a layer is directly replaced by a foreign atom. Relatively little is known about the effects of substitutional impurities, mainly because of the difficulty of introducing foreign atoms into the layer. To date, the only substance that can be reliably placed in substitutional position is boron[26, 27]. Because the electron structure and the size of the boron atom (the atomic volume is 0.7 that of carbon) is different from that of carbon, a boron atom in a carbon layer will profoundly influence the surrounding network structure. Bond tautomerism at these sites may explain why carbons containing boron can be more easily graphitized than carbons without boron.

Ordered impurities result when various compounds form monomolecular layers between graphite layers. These compounds[4] are called crystal compounds, lamellar compounds or intercalation compounds. These compounds can generally be recovered without any alteration to the essential structure of the aromatic layers.

Disordered impurities are formed from thermal or chemical decomposition of lamellar compounds. A small fraction is sometimes tenaciously held by carbon and cannot be removed intact without destruction of the carbon structure. Hennig[28] suggested that these disordered impurities were retained at structural defects, such as twin lines and crystallite boundaries.

(c) <u>Gross Defects</u>

Pyrolysis of carbon containing polymers results in the formation of a grossly defective carbon structure containing very small crystallites, a disorganized phase, lattice strains and

pores. These defects play a major role in determining the properties of porous carbons and will therefore be considered in detail.

Crystallites Crystallites have been previously defined in Section 2.1.1.2. They can be regarded as gross defects because, in the initial stages of carbonization and heat treatment, their size is extremely small. For instance, Franklin[29] found that for a polyvinylidene chloride carbon prepared at 1,000°C, the crystallites have a layer diameter of 16 Å and the number of stacked layers is equal to two. The average number of hexagons in a layer of this diameter is approximately 24; the average number of potentially unsaturated border carbon atoms is approximately 26, compared with the total number of carbon atoms of approximately 72. Thus about 36% of the carbon atoms are potentially unsaturated and it can be expected that these carbon atoms around the peripheries of the layers will profoundly influence inter-crystalline linkages.

The assemblage of the crystallites in the bulk phase has an important influence on the reaction of carbon to heat treatment. By the assemblage of crystallites one means the alignment of crystallites, their orientation, and strength and degree of cross-linking. For instance, soft carbons (easily graphitized carbons) are generally formed from raw materials which remain fluid during the initial decomposition process. This allows the aromatic layers to take up positions favourable for crystallite growth at higher temperatures. On the other hand, carbons which are formed from raw materials which solidify early often possess a very rigid structure. It is assumed, in this case, that the aromatic layers have not had the opportunity to align in favourable positions.

There are several models of the assemblage of crystallites which are worth considering. The first model is one that has been widely accepted since its proposal by Biscoe and Warren[5] in 1942. It consists of neat packets of layers in random positions which are connected by a disorganized phase (see Fig. 3(a)). The

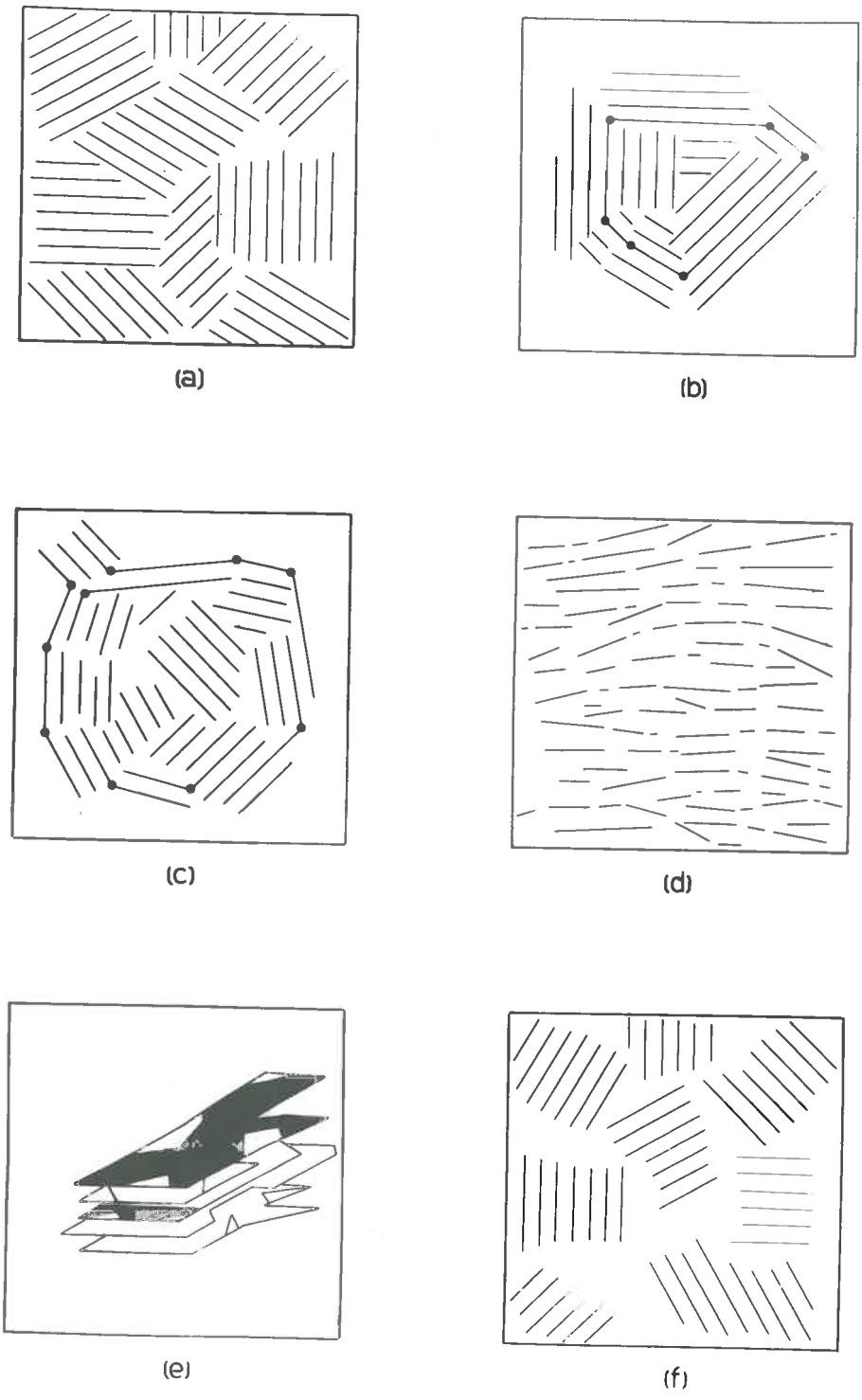

Fig. 3 - Crystallite Assemblage Models

difference in the ease of graphitization of soft carbons and hard carbons was explained in terms of the degree of alignment of the crystallites. To explain the low thermal expansion of carbons, Mrozowski[30] slightly modified the arrangement of the layers to give a ring type configuration (see Fig. 3(b)). Fig. 3(b) illustrates a closed ring configuration while Fig. 3(c) illustrates the more likely random ring configuration.

Mizushima[31] suggested that the model of neat crystallites was too idealized, firstly because layers will generally be of unequal length, and secondly, because the interlayer attraction forces are too weak to form isolated packets of layers. The model proposed by Mizushima is shown in Fig. 3(d). It consists of irregular piles of sheets randomly connected with each other at their edges. For this model the values of L_a and L_c, obtained from X-ray measurements, will refer to a pile of layers of sufficient order to produce coherent interference effects in the diffracted beam. A plan view of this model (see Fig. 3(e)) shows the presence of microscopic voids created by misfits between layers. Mizushima admits that even this model is idealized, since there will remain a certain amount of disorganized phase amongst the sheets. A somewhat similar model has been suggested by Castle[32].

Davidson and Losty[33] found that the mechanical behaviour of carbons could be satisfactorily explained in terms of shear of the crystallite layers. The carbons accommodate an applied stress by movement of one layer over the next, rather like cards in a pack. They supported this suggestion by showing that the modulus of rigidity increased with the degree of neutron irradiation and decreased with increasing temperature of heat treatment. Neutron irradiation is known to produce interstitial atoms and these provide a resistance to layer movement. Heat treatment on the other hand, is said to remove irregularities in the layers and thus lower the force needed to produce shear movement of the layers. These theories were applied to the model of Biscoe and Warren[5], in which

case it was necessary to assume that inter-crystallite bonds were stronger than interlayer bonds. Davidson and Losty suggested an alternative model where the X-ray crystallite dimensions L_a, L_c, referred to regions of parallel layers bounded by structural imperfections. Thus, crystallite growth is merely the removal of imperfections. With this model the question of the relative strength of bonding between crystallites and layers does not arise.

Green[34] has adopted an interesting approach to the study of the mechanical behaviour of carbons and graphites; he suggested that the structure of carbons was similar to that of semi-crystalline polymers. Fig. 3(f) shows the morphology of a semi-crystalline polymer, where crystalline areas are separated by amorphous areas consisting of individual polymer chains. Green was able to successfully apply to carbons the mechanical theory developed by Flory[35] for semi-crystalline polymers.

Disorganized Phase In between the crystallites there exists a disordered phase giving a gas-like contribution to the total X-ray scattering. There have been few quantitative measurements of the amounts of disorganized phase in carbons. Franklin's[29] investigation of carbon (1,000°C) prepared from polyvinylidene chloride showed that 35% of the carbon was in an amorphous form. Austin[36] found that, for a series of carbon blacks, the percentage of carbon in the disordered phase varied from 5% to 25%, depending upon pyrolysis conditions and the type of raw material.

Lattice Strains Graphite single crystals are markedly anisotropic with regard to thermal expansion. X-ray measurements[37] have shown that the coefficient of thermal expansion perpendicular to the layers has a value of approximately 28 x 10^{-6} per °C. In the plane of the layers, the coefficient of thermal expansion is much lower, the value varying between zero and 1.5 x 10^{-6} per °C, depending upon temperature. However, for carbons and graphites, bulk thermal expansion is much lower than that predicted from data

for a single crystal. It is suggested that the discrepancy results from the rigidity of the structure and expansion of some of the crystallites into pore spaces. Mrozowski[30] has suggested that the combination of anisotropic thermal expansion, coupled with the great rigidity of some carbon structures, produces large lattice strains. It is thought that these lattice strains promote layer rearrangement and lead to crystallite growth. This driving force for crystallite growth will be discussed more fully under Section 2.1.3.3.

Mrozowski[30] has further postulated that carbons will possess frozen-in stresses. When a carbon is heated, thermal expansion of the crystallites will occur, and, depending upon the rigidity of the structure, the crystallites will exhibit a certain degree of deformation. On cooling down to room temperature, contraction of the crystallites will be restrained, creating frozen-in stresses. These stresses will be accentuated if the carbon is heated above the viscous creep temperature of approximately 2,300° - 2,500°C. The gradual release of frozen-in stresses as the temperature increases accounts for the increase of the mechanical strength of carbons with temperature until the viscous creep temperature is reached.

Blackman and Ubbelohde[38] recently discovered that pyrolytic graphites are deposited from the gas phase with considerable strain energy and that on annealing recrystallization takes place which, under suitable conditions, can yield graphite of high crystal perfection. In fact, on occasions, the recrystallization was so rapid that the propagation took the form of a 'weak' detonation.

Pores One of the main features of carbons and graphites is their large pore volume. The formation, structure and determination of the pore volume of carbons will be described in Section 2.4.2.

2.1.2 Carbonization of Polymers

It is well known that the ease of graphitization of carbons depends mainly on the composition of the original organic polymer. For instance, two closely related organic polymers are polyvinyl chloride and polyvinylidene chloride, and pyrolysis of these polymers to high temperatures results in the formation of carbons with widely different physical properties. The carbon prepared from polyvinyl chloride has a well ordered crystal structure approaching that of the ideal graphite lattice, while the carbon from polyvinylidene chloride still possesses relatively small crystallites in which the majority of layers are randomly orientated about the axis perpendicular to the plane of the layer. While the carbon from polyvinyl chloride is soft, dense and of low porosity and surface area, that from polyvinylidene chloride is hard and of high porosity and surface area. It is considered that, because of interlocking of layers by strong cross-links, polymerization of various organic molecules can lead to quite different carbons, according to the conditions prevailing during the early stages of increase of molecular size[39]. Therefore, the initial process of carbonization is important, as it plays a dominant role in determining the high temperature characteristics of the carbons.

As the process of carbonization is not well understood, it is desirable to deal with the carbonization of individual polymers and then finally summarize in more general terms. The polymers and the corresponding carbons are typical of those reported in the literature.

There are, however, several terms in use which need definition. Carbonization usually refers to the formation of carbons from organic or inorganic origin where the final temperature is in the range 700° to 800°C. A coke is a carbon formed from materials which fuse before decomposing while a char is a carbon formed from materials which decompose without fusing[40].

Cellulose Tang and Bacon[41] have recently made a comprehensive study of the pyrolysis of cellulose. Using modern techniques such as infra-red analysis, differential thermal analysis and thermogravimetric analysis, they were able to characterize the process by the following steps:

(1) desorption of physically adsorbed water,

(2) the removal of chemically held water from the cellulose molecule,

(3) chain scissions, or depolymerization and breaking of C-O and C-C bonds within ring units, accompanied by evolution of more water, carbon monoxide and carbon dioxide, and

(4) aromatization or formation of graphite-like layers.

From the third stage it is suggested that a four-member carbon radical is formed and that this becomes the building block for aromatization. Tang and Bacon were also able to show from X-ray orientation studies, that the fibrous nature of the original polymer is preserved despite carbonization.

Chemical analysis of the solid residues by Smith and Howard[42] demonstrated that aromatization occurs at quite low temperatures. They charred cotton cellulose at temperatures from 190° to 400°C, and subjected the products to exhaustive oxidation with alkaline permanganate; the magnitude of the yields indicated progressive aromatization as the charring temperature increased. X-ray evidence[43, 44] indicated that at temperatures between 400° and 500°C the residue was beginning to assume the crystal structure of layers of hexagonal networks. Heating[45] to 800°C produced a fairly rapid increase in the L_a dimension of the crystallite from 9 to 18 Å, while the L_c dimension remained practically constant at about 10 Å. At 800°C the crystallites comprise 4 to 5 layer planes each containing an average of 33 hexagons.

Cellulose Acetate Kipling and Wilson[40] appear to have been the only workers who have investigated the pyrolysis of cellulose acetate, which unlike cellulose, forms a coke. The authors suggested that cross-links between adjacent chains were prevented from forming by a blocking action of the acetate groups. The structure during the initial decomposition was therefore less rigid and went through a fluid stage to form a coke.

Phenol-formaldehyde Ouchi and Honda[46] have extensively investigated the thermal cracking of phenolformaldehyde resins. The gaseous products given off at various temperatures are shown in Fig. 4(a). The authors proposed a three stage mechanism of decomposition. Firstly, water is formed by the condensation of -OH radicals. Secondly, methane, carbon monoxide and hydrogen are formed from the reaction of $-CH_2-$ bridges with water. Thirdly, at higher temperatures the hydrogen atoms directly bonded to the benzene nuclei begin to split off in the form of hydrogen and, at the same time, the size of the aromatic nuclei increases suddenly by a partial rearrangement accompanying strong three-dimensional bonding.

Polyvinylidene Chloride This polymer is unique in that it decomposes quantitatively into carbon and hydrogen chloride. This is one of the simplest of carbonization processes and has been carefully studied by several workers[47, 48, 49].

The loss of hydrogen chloride occurs in two stages, corresponding to the loss of two units of hydrogen chloride per unit of polymer. The initial step in the conversion is the loss of one molecule of hydrogen chloride, by a process which follows first order kinetics[49, 50]. It is generally agreed that the mechanism involves the loss of one hydrogen chloride molecule per pair of carbon atoms, which leads to the formation of a linear polyene chain. The removal of the remaining hydrogen chloride almost certainly occurs by the cross-linking of polyene chains by

a Deils-Alder type mechanism. The mechanism proposed by Winslow et al.[51] is as follows:

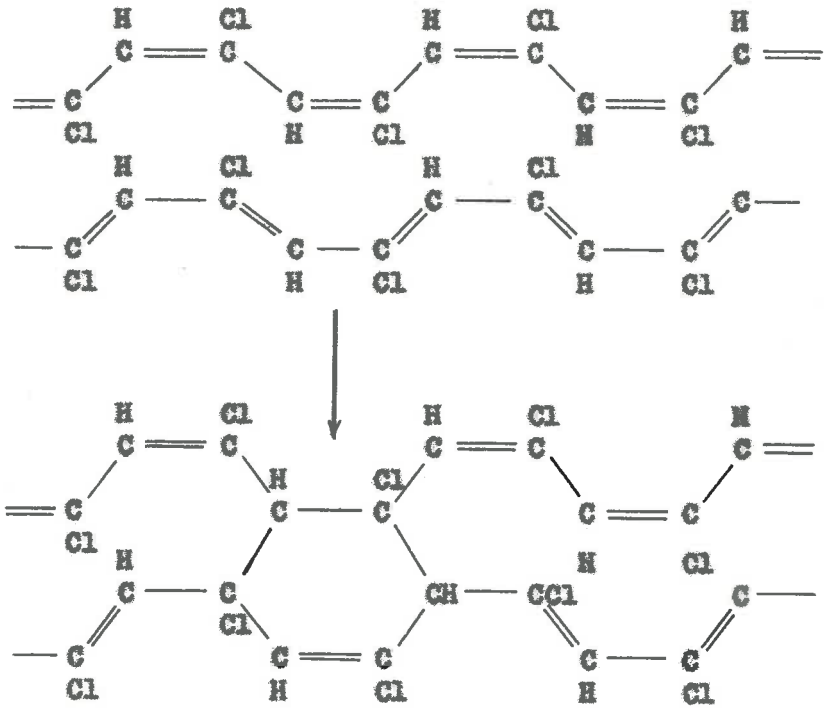

The ring structure then loses hydrogen chloride to form an aromatic ring[47, 48].

X-ray patterns of solid residues[51, 47], heated between 250° and 800°C, are very diffuse and show little change in the degree of ordering of the structure. Indeed, Franklin's[29] X-ray measurements for polyvinylidene chloride carbonized to 1,000°C, revealed that the crystallites are only 16 Å in diameter and two layers thick.

<u>Polyvinyl Chloride</u> Polyvinyl chloride initially decomposes on pyrolysis with a quantitative loss of hydrochloric acid[52] and further heating to 900°C produces gaseous products[53] as shown in Fig. 4(b). The carbonization of polyvinyl chloride is known to be effected by the composition of the atmosphere; under nitrogen

polyvinyl chloride forms a coke, but under oxygen it forms a char[40]. Furthermore the presence of an oxygen atmosphere during pyrolysis markedly increases the yield of solid[53]. It seems likely that possible effects of oxygenation are to cross-link the initial residue and to remove hydrogen. Both of these processes would make it more difficult for fragments to break away from the solid.

According to Winslow et al.[51], thermally stable cross-links develop in polyvinyl chloride only at temperatures above 400°C, hence aromatic regions have more chance to re-order, at least in the critical early stages of pyrolysis. This probably explains why, for a polyvinyl chloride carbon[29], the crystallite dimensions rapidly increase as the temperature is raised above 800°C.

Summary Carbonization of polymers is best summarized under the two headings - thermal degradation and polymerization (room temperature to 500°C) and carbonization (500° to 800°C).

Thermal Degradation and Polymerization From the study of individual polymers it is clear that the initial product of carbonization contains low molecular weight fragments, a proportion of which, by a process of molecular condensation, form a great variety of higher boiling point compounds. As the temperature rises, aromatization of some of these compounds occurs with the development of a system of cross-linked, planar, condensed benzene ring molecules. Further rise in temperature removes unbonded hydrocarbons and the residue rapidly polymerizes and cross-links still further to form a hard mass.

The properties of the final carbon do not appear to be influenced by the capacity of the polymer to form a coke or a char; the main factor seems to be the degree of cross-linking. Mrozowski[55] suggests that, at this stage of development, the carbonaceous mass possesses both the short range order of the groups of

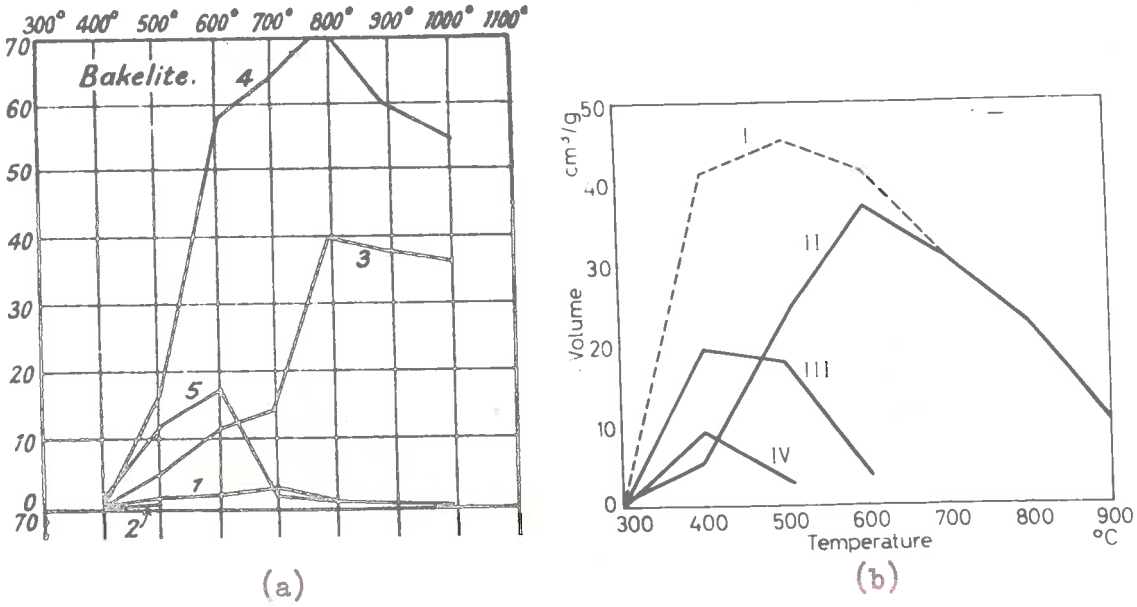

Fig. 4 - Gaseous Products of Carbonization of (a) Phenol-formaldehyde Resin[44] and (b) Polyvinyl Chloride[53]

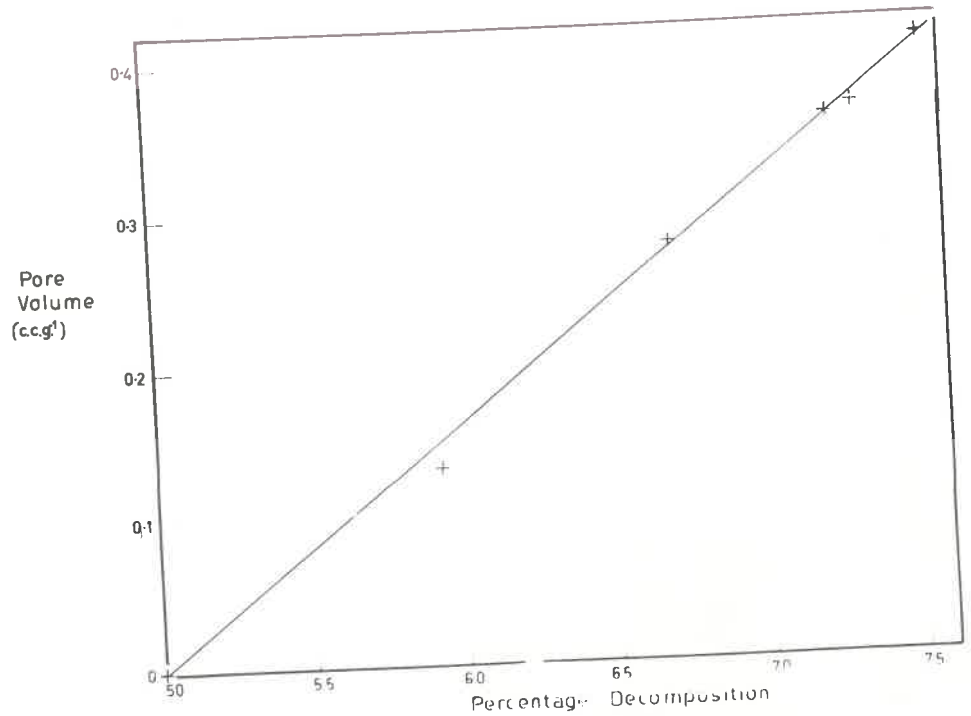

Fig. 5 - Pore Volume Versus the Percentage Decomposition of Polyvinylidene Chloride[48]

aromatic layers and the long range order due to cross-linking between the molecules.

Carbonization Continued condensation and cracking occur with the release of gases such as CO, H_2, CO_2 and CH_4 around the peripheries of aromatic planes. The resulting unsaturated valency causes further bonding and shrinkage with the mass becoming harder and stiffer. Crystal growth occurs mainly in the L_a direction, supposedly by the incorporation of some of the surrounding disorganized material[29].

Porosity continually develops and normally reaches a maximum at approximately 800°C. Fig. 5 shows some results obtained by Dacey and Barradas[48] for a polyvinylidene chloride carbon; the pore volume, calculated from argon adsorption isotherms, is plotted against the percentage decomposition of the polymer.

2.1.3 Heat Treatment of Carbons

In the previous section we have considered the formation of solid carbons with their typical grossly defective structure. Further heat treatment progressively removes lattice and chemical defects, and the structure approaches that of near ideal graphite.

The development of order in the crystal lattice is considered in Section 2.1.3.1, while Sections 2.1.3.2 and 2.1.3.3 deal with the nature and mechanism of crystallite growth, respectively. Associated with heat treatment, of course, is the thermal expansion of crystallites and the bulk specimen; this subject is discussed in Section 2.1.3.4.

2.1.3.1 Development of the Ideal Graphite Lattice

X-ray studies have been mainly responsible for an understanding of the crystallographic changes on heat treatment. Therefore it will be appropriate to follow the changes by reference to a series of typical X-ray intensity curves obtained by

Warren[6], showing the effect of heat treatment on a Spheron carbon black (see Fig. 6). The curve for the un-heat treated sample is typical of diffuse reflections given by carbon pyrolysed to 800°C.

The intense low angle scattering increases rapidly with decreasing angle and is interpreted in terms of voids, cracks and other in-homogenities. Diamond[56], Franklin[29] and others have used this part of the curve to obtain a measure of the size of the pores.

The crystalline (00ℓ) reflection, (002), is normally the most prominent peak and arises from the stacking of aromatic layers. The peaks (11) and (10) are two-dimensional (hk) reflections and are produced by individual graphite layers taking independently all orientations in space[6]. The crystallites develop rather perfectly only in two dimensions, with growth in the third dimension being extremely small. Since the (00ℓ) reflections show there are layers parallel to each other, it is the absence of the (hkℓ) reflections and the presence of (11) and (10) reflections, which show that these layers must be randomly orientated about the normal. The two-dimensional reflections are easily identified from (00ℓ) reflections by the way the former slowly fall off at high angles.

Now as the crystallites grow, the peaks become progressively narrower, and it is basically this change in peak breadth which constitutes the measurement of crystallite dimensions. Heat treatment to 1,500°C considerably sharpens the (00ℓ) peak which indicates an increase in the average number of layers in a parallel layer group. The (10) reflection also sharpens, but still retains its characteristic shape, showing that, although the layer diameter has increased, the layers are still orientated at random about their normal. A further rise in temperature sharpens the reflection still further and a more detailed analysis of the (10) reflection shows the development of modulations corresponding to the layers re-ordering about their normal to form the ideal graphite configuration[6]. Both the (10) and (11) reflections split

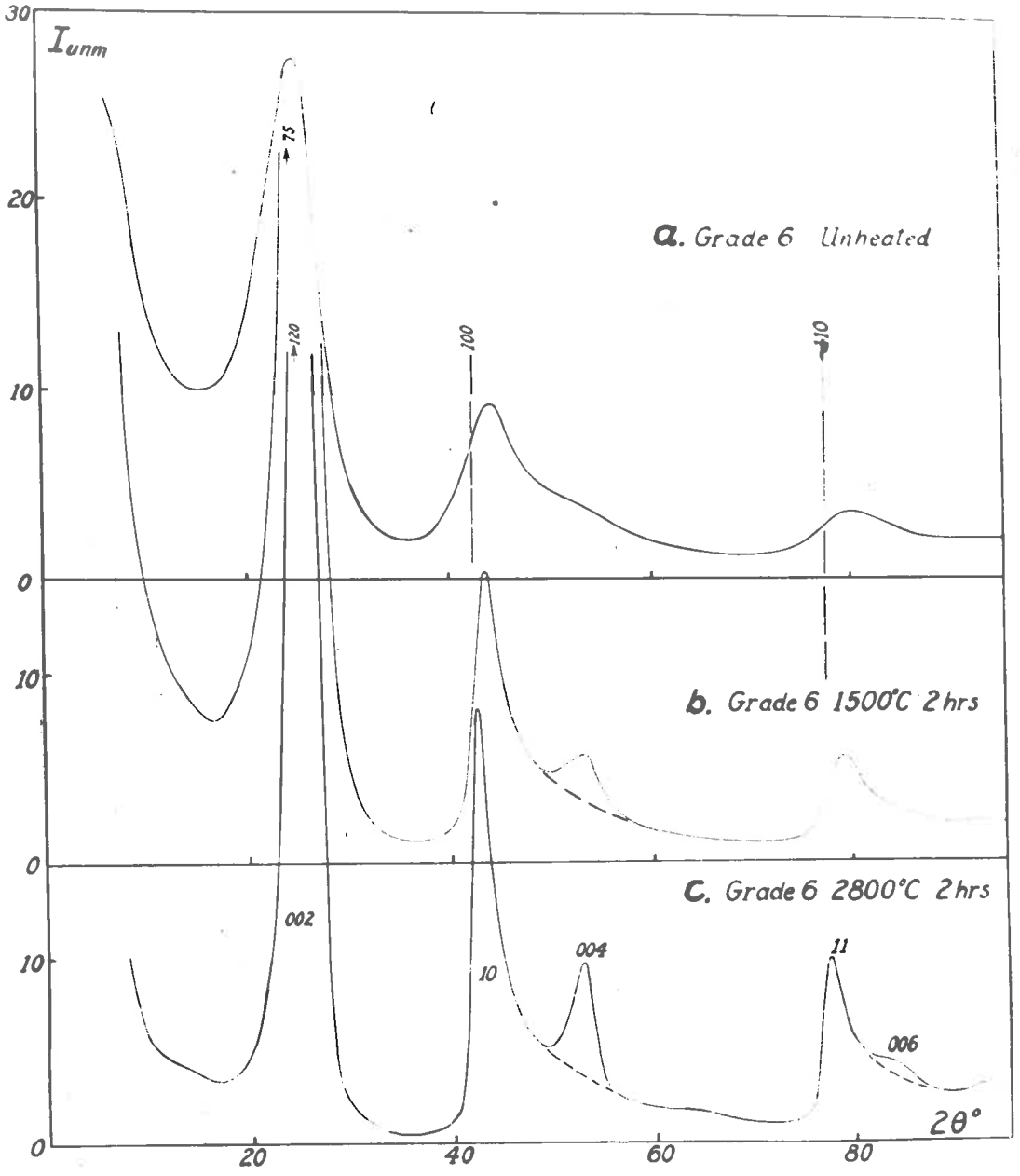

Fig. 6 - X-ray Diffraction Patterns of Heat Treated Spheron Carbon[6]

up and begin to form crystalline three-dimensionally ordered modulations.

2.1.3.2 Crystal Growth

An important result of heat treatment is the increase in size of the crystallites. Franklin[29] investigated a series of heat treated carbons prepared from polyvinyl chloride, polyvinylidene chloride, and a variety of petroleum and coal cokes and suggested that carbons, in relation to their ease of crystallite growth, can be divided into two classes - non-graphitizing and graphitizing. The graphitizing carbons exhibited a rapid growth in both L_a and L_c dimensions in contrast to the non-graphitizing carbons which, even at high temperatures, failed to approach the size of crystallites in graphitizing carbons (see Fig. 7 and 8). Since Franklin's work was published, the sharp division into two classes has been questioned[57] on the evidence of carbon blacks exhibiting intermediate properties. It is still useful, however, to retain this classification as representing the two possible extremes of response to heat treatment.

Apart from the difference in crystallite growth, the two classes of carbons can be further distinguished. For instance, non-graphitizing carbons are hard, porous, and usually formed from substances of either low hydrogen or high oxygen content. Graphitizing carbons on the other hand are soft, compact, and formed from substances rich in hydrogen. There is a strong tendency in graphitizing carbons for crystallites to roughly align; consequently, electron photo-micrographs[58] reveal the existence of a plate-like structure of particles. Non-graphitizing carbons, however, exhibit no fine structure, with the result that particle edges are jagged. The marked difference in response to heat treatment of non-graphitizing and graphitizing carbons has been explained in terms of the rigidity of the low temperature carbon. In a substance such as polyvinylidene chloride, pyrolysis soon results in

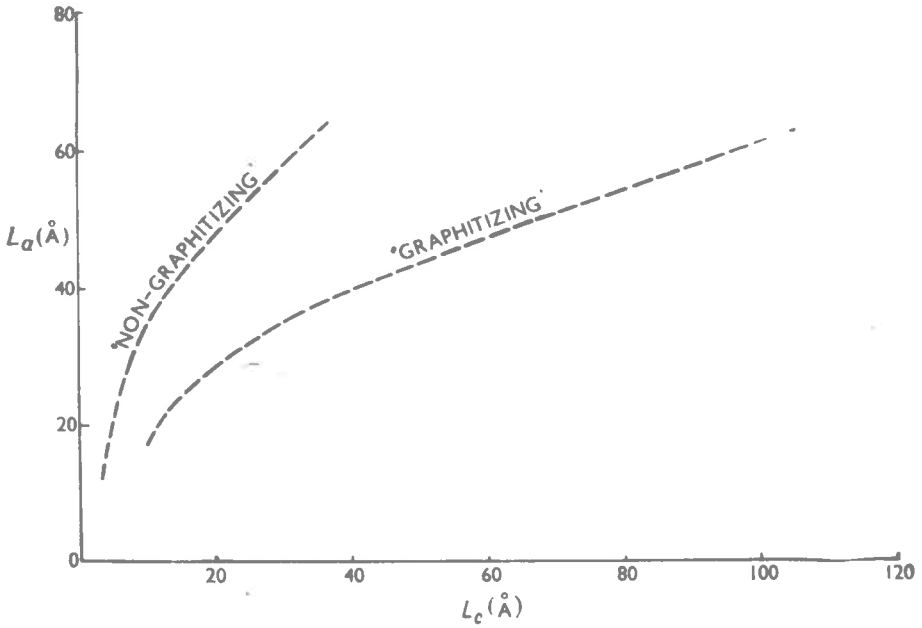

Fig. 7 - Comparison of L_a and L_c Values for Non-graphitizing and Graphitizing Carbons[29c]

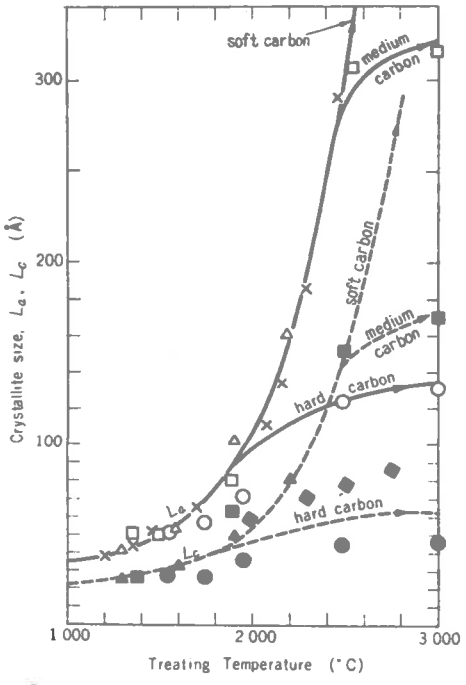

Fig. 8 - Crystallite Growth of Soft and Hard Carbons[71]

the formation of a strongly cross-linked structure which resists any further re-alignment and growth. For graphitizing carbons, however, pyrolysis of, say, polyvinyl chloride, results in a relatively mobile residue with few cross-links. The presence of relatively large amounts of hydrogen tends to destroy cross-links either by reduction or by bonding immediately to the edge carbon atoms, and thus preventing further bonding between carbon atoms. Layer growth and development is then facilitated by partially aligned crystallites with few cross-links.

Observations reveal that crystallite growth is dependent upon the following factors during carbonization: (1) maximum temperature, (2) rate of heating, (3) holding time, (4) the atmosphere above the polymer during pyrolysis, (5) the catalytic nature of container walls, (6) the physical state of the substance, and (7) the chemical structure of the substance.

The maximum temperature of carbonization is the most dominant factor for any particular carbon and is discussed in Sections 2.1.3.1 and 2.1.3.3.

Rates of heating have been found to influence the oxygen content of cellulose chars[59], but it is only for very high heating rates that marked differences occur in the physical properties of chars[30, 60]. On the other hand, for soft cokes, the results of Okada et al.[61] show that rapid heat treatment at the rate of 930°C per min. has little effect on crystalline parameters such as interlayer spacing and crystallite size. A recent study by Hogan et al.[62] has shown that rates of increase in temperature up to 300°C per hr. in the zone 25° to 1,200°C produced no difference in the properties of the graphites investigated.

Kinetic studies[29, 57, 63] show that crystallite growth occurs with measurable speed over the temperature range 800° to 3,000°C and that equilibrium is reached within 15 to 30 min. Mrozowski[30] and Mizushima[63] found that for subordinate parameters such as electrical resistivity, thermal conductivity, and real

density most of the change occurs within 20 min.

A small percentage of oxygen in the atmosphere during the pyrolysis of non-oxygen containing polymers can have a marked effect on the final properties of the carbons. Kipling and Wilson[40] have found that if polyvinyl chloride is carbonized in nitrogen it fuses and the residual carbon takes the shape of the containing vessel. If, however, polyvinyl chloride is carbonized in air, it does not fuse, but chars and retains the outline of the original sample. The explanation offered[40] is that oxygen is taken up at the temperature of the initial decompesition and helps to form cross-links between crystallites, thus resulting in a more rigid structure.

There is evidence that the surfaces of containers effect the pyrolysis reaction. For the thermal decompesition of hexamethylenetetramine, Stanski[64] found that various phase boundaries (glasses, quartz, solid 'hexa') act as catalysts during the initial induction period.

The physical state of the organic compound during pyrolysis can have a marked effect on the ease of graphitization of the carbon[39, 60]. In the liquid state organic compounds such as 9,9-bianthryl or anthracene produce chars at 500°C which readily graphitize at 3,000°C. In the vapour phase, however, a wide variety of organic compounds produce spherical carbon black particles which resist graphitization even at 3,000°C. On the other hand, if the vapours are impinged on solid surfaces at 900° to 1,400°C, graphitizable carbons are produced. In this latter case, it is interesting to note that for high temperatures, the structure of the initial material has little effect on the structure of the carbon formed.

2.1.3.3 Mechanism of Crystal Growth

Observations reveal that crystal growth occurs at a measurable rate over a wide temperature range. This suggests that

any structural change that results must render further development progressively more difficult[29]. This type of mechanism would require a continuously increasing activation energy as the temperature increases. Mizushima[63] has, in fact, found that activation energies for electrical resistance, thermal conductivity, and crystallite growth continually increase in the temperature range 800° to 2,400°C. Furthermore, the mechanism must explain the difference in the rate of growth of crystallites between soft and hard carbons. Fig. 8 is a summary of data on crystallite growth and clearly shows the marked difference between soft and hard carbons.

There is strong evidence against crystal growth occurring by atomic diffusion, i.e. carbon atoms breaking carbon-carbon bonds and migrating from smaller to larger crystallites through the vapour phase or by surface diffusion. Franklin[29] has pointed out that, as this process involves breaking strong carbon-carbon bonds, it would of necessity be a high temperature reaction and occur over a narrow temperature range. If growth did occur by atom migration, then it would not be possible to explain the observed difference in behaviour of various carbons on heat treatment. The mode of aggregation of the crystallites, the degree of cross-linking and the porosity would not effectively inhibit crystal growth. Fieldman et al.[65] and Kanter[66] have shown that for graphites, diffusion of atoms through the bulk phase is negligible at temperatures below 1,800°C.

How then do crystallites grow? It is generally agreed, although not substantially proved, that the initial growth of crystallites occurs by the incorporation of the disorganized phase from the surrounding matrix. Franklin[29] found on heating carbons above 1,000°C, that, along with a decrease in the percentage of disorganized carbon, the crystallites grew mainly in the a direction (see Fig. 7). This growth is said to be facilitated by the fact that most of the hydrogen has already been evolved at 1,000°C

thus allowing the resulting unsaturated carbon atoms around the peripheries of the crystallites to combine with other carbon atoms. When this disorganized phase is exhausted, continued growth must occur at the expense of other crystallites. The data of Franklin[29], for a non-graphitizing polyvinylidene chloride carbon, indicate that this change probably occurs at a temperature greater than 2,000°C; for soft carbons, Mrozowski[30] suggests a temperature of 1,300°C.

It is most unlikely that the incorporation of disorganized material could account for the increased rate of growth for soft carbons at temperatures above 2,000°C. The mechanism proposed by Franklin[29] is that entire layers or even groups of layers coalesce with their neighbours. Electron micrograph and electron diffraction patterns of the sub-structures of soft cokes[67] show that c-axis directions of the crystallites are nearly perpendicular to the grain. Consequently on heat treatment the layers do not have to move far before they become mutually parallel. Diamond's[68] results for carbonized coals support this mechanism, which for coals operates at temperatures above 600°C. It is also possible that a more effective rearrangement is promoted by plastic deformation of the disordered phase. Seal[69] has found direct evidence of carbon-carbon bond deformation at temperatures above 1,800°C. For temperatures above 1,500°C, Mizushima[31] contends that the size of the crystallites for soft carbons is too large to allow displacement and rearrangement. Furthermore, at 1,500°C, most of the hydrogen from around the peripheries has been evolved, so that crystallites are bound to each other through covalent bonds. These suggestions are supported by the fact that at approximately 1,500°C there is a marked change in the rate of change in resistivity. Below 1,500°C, the change in resistivity is completed in several minutes while at 2,100°C the change may take about 15 minutes. For the above reasons Mizushima supposed that crystal growth proceeds by an atomic process.

The final stage in crystallite growth is the re-orientation of the layers about their normal to form the ideal graphite lattice. It has been established by many investigators[29, 6, 70], that this will not occur until the diameter of the layer plane is approximately 100 Å, when it is presumed that there is sufficient decrease in binding energy between the two parallel layers. For reasons already mentioned, Mizushima[31] considered that rotation of such a large layer would be improbable. Instead, reordering would take place through movement of boundaries or arrays of dislocations.

Tsuzuku[71] discussed crystal growth from the standpoint of the dislocation theory. Dislocations can be produced by buckling and twisting as crystallites anistropically expand on heat treatment. On the other hand, stresses formed by anisotropic expansion are expected to promote rearrangement of the crystallites and also crystal growth. This suggests a close connection between crystal growth and the presence of dislocations. Below 1,100°C, crystallites were considered too small to contain dislocations, but as the temperature is raised, gradual growth can generate dislocations at boundaries. At higher temperatures the movement of dislocations tends to relax the thermal stresses, thus forming a more ordered structure.

Recently, Mizushima[63] studied the rate of graphitization by measuring the rate of change of thermal conductivity, electrical conductivity and crystallite size at various temperatures. Calculation of activation energies showed that crystal growth occurs by two rather distinct groups of processes. The first process has an activation energy of 100 k cal. per mole and occurs at approximately 1,400°C, while the second has an activation energy of 200 kcal. per mole at a temperature of approximately 2,200°C. The first process is associated with the healing of the disordered lattice and seems to correspond to the model suggested by Davidson and Losty[33]. The second process is responsible for growth of crystallites mainly in the a direction by the movement of

boundaries between adjacent layer planes. According to Franklin[29] the driving force for layer movement arose from the increased thermal energy as the temperature increased. Mrozowski[30] questioned this theory on the grounds that this energy would be insufficient and suggested that additional energy is available from stresses produced by anisotropic expansion of crystallites. Mrozowski gained some support for this argument from evidence that fine grinding before heat treatment lowered the resultant crystallite growth. The particle size, being of the order of 1 micron, could not impose a limitation on crystal growth, but would probably lower the thermal stress. Tsuzuku[71] concluded that three driving forces could be expected to be effective in producing crystallite growth. These are:

(1) surface tension tending to lower total interfacial energy,

(2) stresses resulting from anisotropic expansion ('graphitization stresses'), and

(3) difference in strain energy between adjacent crystallites.

2.1.3.4 Thermal Expansion

It is important to define the previous history of a specimen when referring to the thermal expansion of carbons. A carbon previously heated to 1,100°C will exhibit reversible expansion up to this temperature on reheating, but, if the carbon is then heated to a higher temperature, it will exhibit irreversible expansion. The irreversible expansion can occur in two ways. Firstly, gases are evolved, even above 1,100°C, so the carbon structure will slightly coalesce - this is known as shrinkage. Secondly, as the temperature rises, the crystallites will tend to expand and, because of interlocking around peripheries, this expansion will be somewhat constrained. It is therefore inevitable that on cooling the crystallites will not freely contract back to

their original position.

Reversible Expansion As mentioned in Section 2.1.1.2, the ideal graphite lattice is markedly anisotropic with regard to thermal expansion, thermal expansion in the c-axis being about 28×10^{-6} per ^{o}C, and in the a-axis about 1×10^{-6} per ^{o}C. The thermal coefficient of polycrystalline carbons, however, is much lower. For instance, the thermal expansion coefficient of a graphitized lamp black[4] is 4×10^{-6} per ^{o}C, and for a reactor graphite[4] 3×10^{-6} per ^{o}C. There is also wide variation in the thermal expansion coefficients from different carbons, the value depending upon various factors such as source of the carbon, method of preparation, presence of binders, etc.

Loch and Austin[72] attempted to explain these problems in two ways. Firstly, it is thought that the low bulk thermal expansion is partly the result of crystallites expanding into pore spaces. Loch and Austin found that for the carbons they investigated, a linear relationship existed between thermal expansion and micro-pore volume; as the micro-pore volume increased, the thermal expansion coefficient decreased. Analysis of the thermal expansion of some reactor graphite by Sutton and Howard[73] showed that accommodation of thermal expansion was associated with the crystal c-axis, some 37% of the c-axis expansion contributing to the bulk expansion. The authors suggested that accommodation can be attributed to cleavage micro-cracks in the reactor graphite. Secondly, it is expected that rigidity of the carbon structure restrains the movement of individual crystallites. The nature of the restraining forces and the consequent formation of lattice strains has been previously discussed in Section 2.1.1.2.

Irreversible Expansion Collins[74] measured dimensional changes of polycrystalline carbons during heat treatment. The data refer to samples made with binders, but are nevertheless worth mentioning. Soft cokes prepared from petroleum coke and a coal tar binder

preheated to 1,100°C showed reversible expansion on reheating to this temperature. With further rise in temperature, expansion was irreversible; shrinkage was observed between 1,100° and 1,400°C and from then on there was a gradual expansion. A hard carbon prepared from phenol-benzaldehyde (using the same resin as a binder) and preheated to 1,100°C exhibited a much smaller reversible expansion than the soft coke on reheating to 1,100°C. From 1,100° to 1,700°C, irreversible expansion was only relatively slight, but after 1,700°C, the carbon showed an appreciable continuing shrinkage.

Davidson and Losty[75] found that the shrinkage in the length of a cellulose carbon on heating from 800° to 1,800°C amounted to less than 2% of the original value.

2.2 Sintering of Carbons and Graphites

Heat treatment of certain carbons above approximately 800°C produces a marked change in the adsorptive capacity and density. A change in the adsorptive capacity has also been observed for graphites subject to severe neutron irradiation. While the circumstances for sintering of graphites and porous carbons appear unrelated, it is possible that a similar mechanism causes sintering in both cases.

2.2.1 The Change in the Adsorptive Capacity of Porous Carbons on Heat Treatment

Until recently, the loss in surface area of porous carbons on heat treatment has been treated as a side issue to the main investigation. Consequently, while some observations extend back over 50 years, there has been little or no work especially directed towards the subject of sintering in carbons.

Whilst investigating the removal of colour and impurities by active carbon, early workers such as Lemon[76] soon established the fact that heating the carbon adsorbent above approximately 800°C decreased the adsorptive power. A similar deduction was

made by Howard and Hulett[77]; they were mainly interested in substantiating the use of helium to measure real densities, but, in the course of their work, discovered that adsorption of nitrogen on their cocenut char was considerably reduced when the char was heated from 900° to 2,000°C; in fact, the amount of nitrogen adsorbed fell from 8.2 to 0.2 c.c. per g.

McBain and Sessions[78] in their early work on porous sugar carbons found that the iodine value, i.e. the quantity of iodine adsorbed per g. of carbon, increased with increased heat treatment to a maximum at 800°C, but rapidly decreased thereafter.

Later, Smith[79], investigating the formation of carbons from various organic materials such as hexachlorobenzene, inositol and barium mellitate found that the surface area, as measured by nitrogen adsorption, reached a maximum at 800°C, but then quickly decreased at higher temperatures.

However, it was not until 1958 that this sintering phenomenon was deemed worthy of further investigation. Boocock and Holdsworth[80], in their extensive review on the carbonization of polymeric materials, noted the case of cellulose in which the micro-porosity increased between 100° and 1,000°C and then decreased to almost zero at 1,600°C. They suggested that closed pores were actually developed in the material during heat treatment.

Later a paper by Wynne-Jones[81] focused attention on the phenomenon of sintering in porous carbons. The results obtained on a cellulose carbon are shown in Fig. 9. There is a sharp drop in surface area from 500 $m.^2$ per g. at 1,000°C to 25 $m.^2$ per g. at 1,500°C; above 1,500°C, however, the surface area remained practically constant. It has been suggested that at temperatures above 1,000°C the decrease in hydrogen content may cause the welding together of crystallites, with a consequent decrease in surface area. In the opinion of Wynne-Jones[81], however, the large drop in surface area must, at least in part, be the consequence of the sealing off of pores, rather than their disappearance as the result

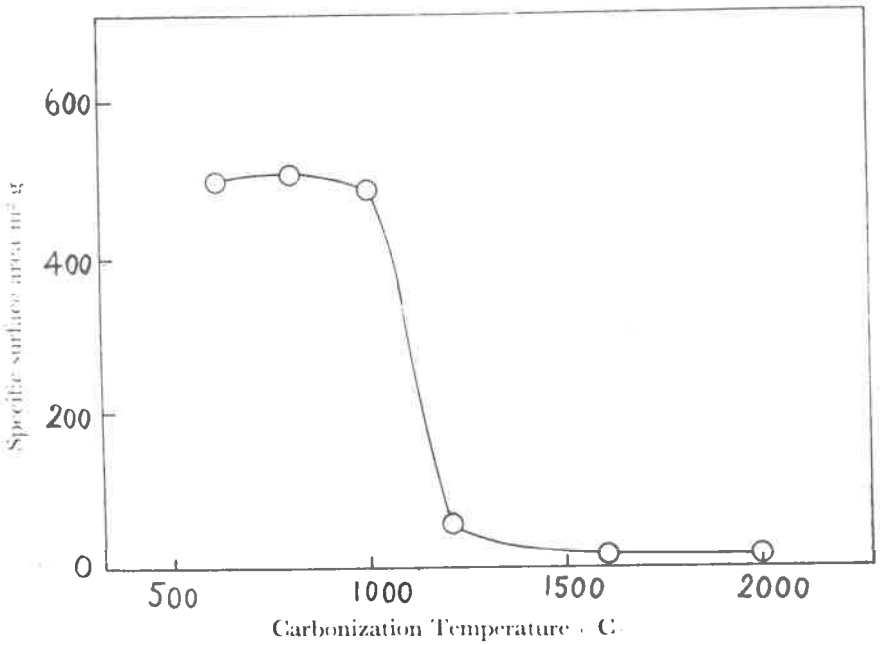

Fig. 9 - The Effect of the Carbonization Temperature on the Surface Area of Cellulose Chars[81]

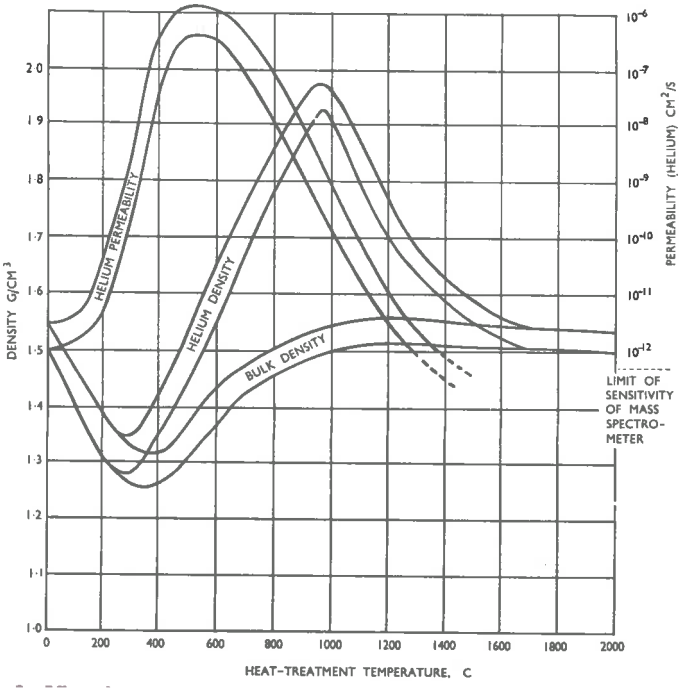

Fig. 10 - Helium Density, Bulk Density and Helium Permeability of Heat Treated Cellulose Carbons[75]

of particles fusing together.

Among the Russian workers in the adsorption field, Kiselev et al.[82, 83, 84] were apparently the first to deliberately measure adsorption on heat treated porous carbons. From adsorption isotherms of nitrogen on carbons, both untreated and heat treated at 1,700°C, they found that at saturation the amount adsorbed had decreased at least by half. They concluded that heating the carbon at 1,700°C destroyed part of its pore structures and so considerably reduced the pore volume.

In more detailed work, Dubinin et al.[85, 86] heat treated activated samples of phenol-formaldehyde (carbon A) and polyvinylidene chloride (carbon C) and then measured crystallite growth and adsorption of benzene, cyclohexane and nitrogen. To the adsorption isotherm, Dubinin et al.[87, 88, 89] fitted linear equations developed from the potential theory[90], the constants of which reflect such structural factors as limiting adsorption, pore volume of micro- and transitional pores and the size of micro-pores. They found that for both carbons, the micro-pore size increased while the macro-pore size decreased, the net result being an overall decrease in the average pore size. The rate of adsorption of benzene on the carbon C heat treated to 1,750°C was extremely slow, so it was difficult for the authors to obtain an equilibrium isotherm. According to Dubinin[86], the change in micro-porous structure of carbon C on heat treatment to 1,750°C was distinguished by a narrowing of micro-pore inlets and decrease in micro-pore volume. In further experiments the liquid phase adsorptive capacity of carbon A was measured for acids and bases. The results indicated that the chemical nature of the surface apparently remained unchanged during heat treatment.

2.2.2 The Change in the Density of Porous Carbons on Heat Treatment

Howard and Hulett[77] were probably the first investigators to measure the effect of heat treatment on the helium density of a

carbon. They observed a change in density from 2.22 to 1.35 g. per c.c. on heat treatment of a coconut charcoal from 1,000° to 2,000°C. This decrease in density clearly indicated that a considerable portion of the pore volume of the heat treated carbon was no longer accessible to helium molecules.

Franklin[91] heat treated various carbonized coals and measured densities in helium and various liquids. She concluded that the accessibility of the pores and inner surfaces to liquids and gases decreased with increasing carbonization temperatures in the range 600° to 1,600°C, and was governed by the width of fine constrictions in the pore system, rather than the mean diameter of the pores.

Later, Franklin[29] measured the densities of some heat treated polymers by the float-sink method, i.e. a liquid density method. For the non-graphitizing carbon, polyvinylidene chloride, the density decreased from 1.59 to 1.19 g. per c.c. on heat treatment from 1,000° to 2,160°C but then increased to 1.38 g. per c.c. when the temperature rose to 3,000°C. For the graphitizing carbon polyvinyl chloride, the density increased from 1.99 to 2.25 g. per c.c. on heat treatment from 1,000° to 3,000°C.

In a recent article by Davidson and Losty[75], helium density, bulk density and helium permeability have been measured on a heat treated cellulose carbon, and the results are summarized in Fig. 10. The interesting point is that the helium density reaches a maximum at 900°C, but then rapidly decreases so that at 1,700°C it equals the bulk density as measured with mercury. Furthermore, it is seen that the helium permeability reaches a very low figure and, in fact, is less than that exhibited by borosilicate and fused silica glasses.

2.2.3 The Change in the Adsorptive Capacity of Graphites on Irradiation

Sintering may be produced by neutron irradiation as well as by heat treatment. Because graphite has been used in various

types of nuclear reactors, its susceptibility to damage from neutron irradiation has been closely examined. Spalaris et al.[92, 93] found for an artificial graphite that surface area, pore size and true density decreased with increasing exposure to radiation. A typical reduction in surface area, as measured by nitrogen adsorption, was between 12 and 40% of the original area. Pore size distributions showed an overall decrease in the average pore size and this was supported by the results of rate measurements, in which the time elapsed for the adsorbed gases to reach equilibrium was three to four times longer for irradiated samples than for non-irradiated samples. Another interesting point was that whereas the crystallite size increased by about 15%, the overall bulk dimension only increased from 0.2 to 0.6%, indicating that crystallites probably expanded into the pores. This suggestion would account for the loss in pore volume and surface area on irradiation. The mechanism of crystallite growth is not fully understood, but it is proposed[93] that neutron irradiation produces a large number of imperfections and defects, which cause the crystallites to expand. Unlike heat induced sintering of porous carbons, neutron induced sintering can be almost entirely removed by annealing at quite moderate temperatures (ca. 600°C). It is interesting to note that charcoal irradiated with 1 MeV electrons showed no change in adsorptive capacity[94].

2.2.4 The Industrial Significance of Sintering in Carbons and Graphites

From an industrial view-point the sintering of carbons can be either a disadvantage or an advantage. For a process depending upon carbons possessing their maximum surface area, sintering is clearly a disadvantage, e.g. adsorption and gasification processes. On the other hand, sintering has been used to advantage in the preparation of low permeability carbons for use in high temperature, gas-cooled, nuclear reactors, as both a canning material for the fuel and as a moderating material.

It has been known for some time that, in the production of a porous carbon from raw materials and also during its revivification, there is a maximum temperature which should not be exceeded if the carbon is to retain its adsorptive capacity[95, 96]. A similar restriction applies to the manufacture of carbons for subsequent gasification. The rate of gasification will depend upon the accessibility of the oxidizing gases to the internal surface of the carbon[97]; therefore, it is important that during the manufacture of carbon the temperature be kept sufficiently low to prevent loss of surface area with the consequent decrease in the accessibility of gases to inner surfaces. For an Australian coal[98], the maximum surface area is developed at a carbonization temperature of 600° C; higher temperatures cause a marked drop in the surface area. Thus, if the coke is to be used for the production of fuels, it is essential that the coking temperature for the preparation of the carbon does not exceed 600°C.

While sintering of porous carbons is normally a disadvantage, Davidson[99] recently proposed a novel use for highly sintered cellulose carbons. A tremendous effort has been made in recent years to make artificial graphite impermeable to gases so that it can be used as a canning material for fuel elements in high temperature gas-cooled nuclear reactors. Most of the research effort was directed towards filling the pores of artificial graphite with an impregnating fluid such as furfuryl alcohol and afterwards carbonizing. The method used by the General Electric Laboratories[8, 75, 99] to produce solid tubes of cellulose involves centrifugal slip-casting followed by carbonization in two stages. In the first stage the cellulose is slowly heated to 1,000°C to allow evolution of gases and tars without disrupting the structure. At the completion of the first stage of heat treatment, the carbon possesses a high porosity with an average pore size of approximately 50 Å. During the second stage the temperature is raised to between 1,500° and 2,000°C and, although still possessing a relatively low

density, the carbon becomes quite impermeable to gases. Davidson[99] suggests that crystallites grow and block the pores at the constrictions and so prevent the flow of gas through the structure.

2.3 The Determination of the Crystallite Structure of Carbons

The three techniques available for investigating the crystal structure of carbons are X-ray diffraction, neutron diffraction and electron diffraction. X-ray methods have been the most useful in elucidating the crystal structure of carbons and graphites, in fact, graphite was one of the first substances to be analyzed by X-rays[2]. X-rays are scattered by electrons and therefore cannot give any information as to the position of impurity atoms such as hydrogen and oxygen in the graphite lattice. Neutrons, however, are scattered by the atom nucleus and not by the electrons and thus thermal neutron diffraction techniques[172] have been helpful in determining the role of impurities in the graphite structure. Electron diffraction[100] has been used in studying the nature of lattice defects in carbon and graphite.

X-ray scattering from carbons may be conveniently divided into three regions[68]:

(1) Scattering at low angles for which

$$s = \frac{2 \sin\theta}{\lambda} < 0.15 \text{ Å}^{-1} .$$

(2) Scattering at medium angles for which

$$0.15 < s < 0.4 \text{ Å}^{-1} .$$

(3) Scattering at high angles for which

$$s > 0.4 \text{ Å}^{-1} .$$

Low angle scattering provides information regarding the porosity and homogeneity of the material; however, the measurement of low angle scattering requires special techniques. The medium and high range angles have been carefully studied and have yielded the bulk of information on the crystalline structure of carbons. Methods of

analysis of high and medium range scattering can be divided into the following:

(a) Radial distribution analysis.

(b) Analysis based on the two-dimensional random layer lattice theory.

(c) Least squares analysis.

These methods all ultimately involve the comparison of a curve derived from experiment with one calculated for a hypothetical structure.

(a) Radial Distribution Analysis

Radial distribution analysis specifies the density of atoms as a function of the radial distance from any reference atom in the system. Debye[2] in 1915 showed that the intensity in electron units scattered by a non-crystalline array of atoms at the angle θ is given by:

$$I = \sum_m \sum_n f_m f_n \frac{\sin s r_{mn}}{s r_{mn}}$$

where $s = \frac{4 \pi \sin \theta}{\lambda}$,

f_m & f_n = respective atomic scattering factors of the mth. and nth. atoms,

r_{mn} = the magnitude of the vector separating these two atoms,

and λ = radiation wavelength.

A structure for the unknown specimen was assumed and the theoretical scattering calculated as a function of s from equation above. This was compared by a trial and error procedure with the observed experimental scattering. The method was tedious and, in fact, not entirely successful. A more direct approach was to convert the experimental scattering to electron units and to invert these data using the Fourier integral theorem. Thus, the radial distribution function of the specimen was obtained without any a priori

assumptions as to its structure[101].

Application of this method to the determination of the structure of carbon does not directly give information concerning the size of the layers, but rather gives the information that atoms are arranged, as in graphite, on a hexagonal net. Franklin[102] analyzed the (10) and (11) reflections of a carbon obtained from polyvinylidene chloride and compared the results with those obtained from the atomic distribution function. While the only direct information was that the carbon contained graphite-like layers, she was able, by approximate methods, to estimate the layer size and the percentage of carbon in graphite-like layers.

(b) Analysis Based on the Two-Dimensional Random Layer Lattice Theory

It was generally recognized that the X-ray patterns of carbon blacks were essentially a 'washed out' graphite pattern[5], but despite radial distribution analysis showing that graphite-like layers were present, the relative arrangement of the layers could still not be uniquely determined. By heat treating some carbon blacks, Biscoe and Warren[5] were able to follow the development of the X-ray pattern to a stage where the pattern definitely indicated a random layer structure, i.e. crystallites consisting of single graphite-like layers stacked equidistant from each other, but with each layer being randomly orientated about the layer normal. The patterns showed the stacking bands (00ℓ) and the two-dimensional bands (hk), but no three-dimensional band such as ($hk\ell$). Warren[103, 104] was then able to derive a general theory for diffraction from randomly orientated layers and developed equations giving both the form and absolute intensity of the (hk) bands in terms of the layer dimension L, and the position s_0, of the related (hk0) reflexion. The analysis procedure involves fitting the theoretical curve to that obtained from experiment. Franklin[102] used this method to determine the structure of a polyvinylidene chloride

carbon and found it yielded more precise information than radial distribution analysis.

Warren also derived a simple equation relating the peak breadth to the layer diameter, viz.

$$L_a = \frac{1.84\ \lambda}{B \cos \theta} \quad . \quad . \quad . \quad (1)$$

where B = peak breadth at half peak height

and θ = Bragg angle.

Except for the numerical coefficient this equation is, in fact, in the same form as the equation for crystallite particle size developed by Scherrer[105].

(c) Least Squares Analysis

Diamond[68, 106] suggested that no single curve of the Warren type would fit the observed curve obtained from a specimen containing a wide distribution of molecular sizes. The larger molecules contribute heavily to the sharp maxima and are principally responsible for the height of each peak, while the smaller molecules tend to produce broadening at the base. To overcome this weakness, Diamond proposed the method of least squares to estimate molecular size distributions in carbons. The principle of the method is to calculate exactly the X-ray scattering from randomly orientated aromatic molecules of particular sizes by the use of the Debye radial distribution function, and then to fit a linear combination of such curves to the observed intensity curve for a particular specimen. The coefficients in such a combination provide an estimate of the molecular size distribution; the distribution is usually presented in histogram form in which the terms represent fractions by weight of material in particular size groups. The utility of the method has been demonstrated by Diamond[56] for the analysis of diffraction data from some carbonized coals, and he has listed seven distinct advantages for using it over the preceding methods[106]. One of the

interesting advantages is that it is possible to take into account scattering from impurities such as oxygen, especially if they can be treated as roentgenamorphous material*.

For the application of radial distribution analysis and two-dimensional layer lattice theory, the experimental curve has to be converted to electron units; herein lies a potential source of error. After correcting the intensities for absorption and polarization, the curve is generally converted to absolute units by equating the experimental intensities at large values of s with the calculated total theoretical independent scattering. The principle of this method is that for non-crystalline materials, interference effects at large angles are negligible, and the observed intensity is then approximately equal to the sum of incoherent and coherent scattering. For carbons[101], interference from bands becomes negligible at s values from 8 to 10. To remove difficulties of working at angles of $2\theta > 90^{\circ}$, a short wavelength radiation such as MoKα is used. A scaling factor is then obtained, which converts the experimentally observed MoKα curve into electron units. As a longer wavelength radiation such as CuKα produces wider bands, some authors[107, 108] then compare similar bands in the MoKα and CuKα traces and so convert the CuKα trace into electron units. Unfortunately, a small error in the scaling factor at high angles, produces a large error in the absolute intensity at low angles. Furthermore, this procedure calls for long range consistency in both theoretical and observational data. In the least squares analysis method of Diamond[106], these errors are avoided as the experimental data have only to be corrected for absorption and polarization.

The choice of diffraction peaks for analysis is important.

* Substances showing no crystalline nature whatever.

For the determination of L_a, one is limited to the (hk) bands (10) and (11). The (10) band is said to be affected over its entire length by the nearby (00ℓ) reflections, (002) and (004). In order to utilize the (10) band to determine two-dimensional ordering it is necessary to correct for the effects of these (00ℓ) reflections. To avoid unnecessary computation, both Franklin[102] and Diamond[106] have used the more remote (11) band. However, as the layers begin to order themselves into the ideal graphite lattice, modulations (the splitting of the two-dimensional reflection bands into the three-dimensional ordered bands, e.g. the (10) band splits into (100) and (101) bands) appear and considerably distort the band shape. Warren[6] has shown how to evaluate the (hk) bands when such modulations occur.

Information concerning stacking of layers in crystallites is obtained from the (00ℓ) reflections such as (002), (004) and (006). There are at present two main methods available for analyzing these bands. The first method proposed by Scherrer[105] is relatively simple and involves only the determination of peak broadening at half-peak height. Substitution of the peak breadth in the equation

$$L_c = \frac{C \lambda}{\beta \cos \theta} \qquad . \quad . \quad . \qquad (2)$$

where C = constant,
λ = wavelength,
θ = Bragg angle, and
β = peak breadth,

yields a value for the height L_c of the crystallites. The second method involves calculation of the intensity of (00ℓ) reflections by the theory of the simple diffraction grating[109].

2.4 The Determination of Surface Area and Pore Size

The first part of this section is concerned with the application of adsorption theories to the determination of the surface area. The second part deals with the computation of average pore size and pore size distribution, molecular screening and other indications of pore size changes.

2.4.1 The Application of Adsorption Theories to the Determination of Surface Area

There are basically two methods of obtaining an estimate of the surface area (Σ) of a solid. The first method involves the determination of the monolayer capacity, i.e. the amount of substance adsorbed to give an even monolayer coverage over the complete surface area. Then, from the area of the adsorbate molecule, one can calculate the surface area of the solid from the equation

$$\Sigma = \frac{V_m}{V} N \sigma_m \qquad \cdot \quad \cdot \quad \cdot \qquad (3)$$

where V_m = monolayer capacity,
V = molecular volume of adsorbate,
N = Avogadro's number, and
σ_m = area occupied by an adsorbed molecule.

The second method yields the surface area directly without having to introduce a value for σ_m.

2.4.1.1 Estimates of the Monolayer Capacity V_m

(a) Langmuir Theory

The assumptions, underlying the derivation of the Langmuir equation[10], have been clearly stated by Fowler[110]: "Necessary and sufficient assumptions . . . . . are that atoms (or molecules) of the gas are adsorbed as wholes on to definite points of attachment on the surface of the adsorber, that each point of attachment can

accommodate one and only one adsorbed atom, and that the energies of the states of any adsorbed atom are independent of the presence or absence of other adsorbed atoms on neighbouring points of attachment". On the basis of a particular kinetic theory, Langmuir obtained the equation

$$V = V_m \frac{bp}{1 + bp} \quad . \quad . \quad . \quad (4)$$

where p = pressure

V = volume of gas adsorbed, and

b = constant for a particular temperature and absorbent.

Later, Fowler[111] derived the same equation by the application of statistical mechanics to the above model.

Equation (4) can be rearranged to give

$$\frac{p}{V} = \frac{p}{V_m} + \frac{1}{bV_m} \quad . \quad . \quad . \quad (5)$$

On plotting p/V versus p, a straight line should be obtained with slope $1/V_m$ and intercept $1/bV_m$. Generally, the equation is a poor fit, except for some systems which exhibit Type I isotherms (Brunauer's[90] classification), e.g. charcoal.

(b) The Point B Method

Emmett and Brunauer[112] investigated a series of Type II adsorption isotherms and considered a number of points on the isotherm which might conceivably correspond to completion of the monolayer. They found that the point at the beginning of the middle linear portion of the isotherm, Point B, gave the most consistent results for a series of different gases and temperatures. Further evidence in favour of using Point B was provided when Emmett and Brunauer[112] found that heat of adsorption for one of their specimens reached a maximum at an amount adsorbed corresponding very closely to the monolayer capacity.

(c) The BET Method

Brunauer, Emmett and Teller[113] generalized Langmuir's treatment to take into account the formation of multi-layers. The adsorbed molecules in the first layer are assumed to act as sites for the adsorption of molecules in a second layer. Similarly the second layer molecules act as sites for the third layer molecules and so on. The concept of localization still prevails for the first layer and must therefore also apply for the rest of the layers. Brunauer, Emmett and Teller were able to derive the following equation by analyzing the kinetics of evaporation and condensation on the above model

$$\frac{p}{(p_o - p)V} = \frac{1}{V_m c} + \frac{c - 1}{V_m c}\frac{p}{p_o} \quad . \quad . \quad . \quad (6)$$

where c = constant

and p_o = the saturation vapour pressure of the pure adsorbate.

It can be seen from equation (6) that a straight line should result from the plot of $\frac{p}{(p_o - p)V}$ versus p/p_o and that values of V_m can be calculated from the slope $(c - 1)/V_m c$ and the intercept $1/V_m c$.

While equation (4) applies for an adsorbed film that is infinitely thick, Brunauer et al.[114] developed an equation for the more general case where adsorption is restricted to n layers, (e.g. for adsorption in small capillaries).

$$V = \frac{V_m cx}{(1 - x)} \left\{ \frac{1 - (n + 1)x^n + nx^{n-1}}{1 + (c - 1)x - cx^{n+1}} \right\} \quad . \quad . \quad . \quad (7)$$

where $x = p/p_o$.

Substitution of $n = \infty$ yields equation (6), while substitution of $n = 1$ yields the Langmuir equation (equation (4)).

While the BET equation, (usually referring to equation (6)), has been used with outstanding success to reduce a variety of isotherm types to straight line plots, it is now generally agreed that the original assumptions are so crude that the equation must be regarded as semi-empiricial in nature. In fact, Halsey[115] suggests that Point B alone has physical significance in V_m determinations, and that the BET equation is merely a convenient graphical method of locating Point B on the isotherm.

(e) Calculation of V_m from rate measurements

The foregoing determinations of surface area have relied upon appropriate theoretical treatment of equilibrium measurements. Jura and Powell[116] have shown how V_m can be obtained from measurement of the rates of gaseous adsorption. The specific rate of adsorption of water vapour on anatase was found to decrease markedly on completion of a monolayer. From a plot of rates of adsorption at various coverages, the value of V_m was obtained from the point where the marked change occurred. The value of V_m obtained by this method was about 20% lower than that obtained by equilibrium measurements.

(f) Estimation of V_m from Adsorption Thermodynamics

Pierce and Smith[117] found that a minimum occurred in the plot of entropy of adsorption versus amount adsorbed. They suggested that the minimum corresponded to completion of a monolayer, when the molecules had reached a state of maximum order and orientation. Hill et al.[118] found that for high values of the BET constant c, the integral entropy gave a minimum which fell near $V = V_m$. The minimum was ascribed to the relatively small number of possible configurations of the system as the first layer was completed. While there have been many examples of the minimum occurring very close to the BET value of V_m, the method is not

sufficiently precise or convenient to be regarded as a practical means of determining V_m. However, it does offer a useful confirmation of BET V_m values.

2.4.1.2 Methods Leading Directly to Surface Area

Direct methods of determining the surface area will not be considered as they have not been used in this project; the reader is referred to the reviews of Connor[119] and Young and Crowell[120].

2.4.1.3 Other Methods of Estimating Surface Area

Of the numerous other methods of determining surface area of solids, only one will be mentioned here, namely, the X-ray method. Details of other methods may be found in the reviews of Connor[119], and Young and Crowell[120].

The X-ray method involves the determination of the average crystallite size from the X-ray pattern, and it is presumed that the calculated surface area of the crystallites is an indication of the true surface area. Arnell and Barss[121] have compared the areas calculated from X-ray diffraction data with those obtained by the normal BET method for a series of progressively activated coconut-shell charcoals. They found the specific X-ray surface area (ca. 2,700 $m.^2$ per c.c.) remained unchanged during activation, but that the BET surface area increased from 1,120 to 2,750 $m.^2$ per c.c. of charcoal. It was suggested then that the specific X-ray surface area represented the potential surface area and that activation progressively removed disordered material from around crystallites. For progressively sintered carbons prepared from phenol-formaldehyde resin, Dubinin et al.[85] obtained the results shown in Table 1.

TABLE I

Surface area values for a Slightly Activated Phenol-formaldehyde Carbon

Temperature of Heat Treatment (°C)	X-ray Surface Area ($m.^2$ per g.)	BET Surface Area ($m.^2$ per g.)
950	2280	1130
1750	1550	610
2000	1230	130
2300	1030	6
3000	740	6

It is clear from the above table that the X-ray surface area is not indicative of the area available to adsorbate molecules.

2.4.1.4 The Selection of Values for the Molecular Area σ_m

For those methods in which V_m is calculated, it is important that a proper selection is made for the molecular area of the adsorbate; σ_m is usually calculated from the density of the bulk liquid adsorbate (d_L) and Emmett and Brunauer[112] used the expression

$$\sigma_m = 1.091 \left(\frac{M}{Nd_L}\right)^{2/3} \quad . \quad . \quad . \quad (8)$$

where M = molar volume of adsorbate

and N = Avogadro's number.

While this equation assumes hexagonal close packing of spherical molecules, other authors (ref. 120 p. 226) have assumed different types of packing with corresponding changes in the packing factor of 1.091. On the other hand, if the measurement of V_m was conducted at temperatures where the normal bulk adsorbate would be in the solid phase, then a value for the corresponding density would be substituted in the above equation. For simple gases such as argon, nitrogen and oxygen, the value of σ_m calculated by the

above method yields consistent results, but for many adsorbates, particularly poly-atomic molecules, the values of σ_m yield unusually low Σ values. To overcome this difficulty some workers (ref. 120 p. 227) have obtained a Σ value by using nitrogen and then by a converse process have obtained a value of σ_m for a poly-atomic molecule, so that the same value of Σ is obtained. This method gives reasonably consistent results and is useful when, (a) the adsorbate molecule presents a different value of σ_m according to its orientation, or (b) when a molecular sieve effect prevents the larger poly-atomic molecules from penetrating into the smallest pores. A helpful selection of σ_m values has been tabulated by Young and Crowell[120].

2.4.2 The Determination of Pore Size

In the calculation of pore size, it is first necessary to adopt a model which is most appropriate for the particular solid. For instance, the simplest model is a pore system of long, non-intersecting, cylindrical capillaries; in this case, calculations yield values for pore diameters. While it is unlikely that solids will possess such a simple structure, it has been assumed that simple models give a 'general picture' of the porous structure. In some instances the picture is completely false[173]. Everett[122] has analyzed a number of geometrical models and considered the problems that arise in trying to identify a particular model with adsorption measurements.

Pore size analyses may be conveniently grouped under the following headings:

(1) Average Pore Size.
(2) Pore Size Distribution.
(3) Pore Size and Molecular Screening Effects.
(4) Other Pore Size Estimates.
(5) Indications of Pore Size Changes.

2.4.2.1 Average Pore Size

The structure of a porous body may be described in terms of (a) total pore volume V_p, (b) surface area $\sum$ and (c) pore size distribution. An indication of the average pore size $\bar{r}_p$, can be obtained from the equation

$$\bar{r}_p = \frac{2V_p}{\sum} \quad . \quad . \quad . \quad (9)$$

The pore volume V_p can be calculated either from density measurements[123] or from the amount adsorbed at the saturation vapour pressure of the adsorbate[124], viz. $p/p_o = 1.0$.

2.4.2.2 Pore Size and the Molecular Screening Effect

Molecules can act as molecular probes for the determination of the size of pores in porous media. An example of this method of determining pore sizes has been given by Breck et al.[125] for a zeolite type A. From sorption measurements they found that the apparent pore size was between 4.2 and 4.75 Å. This was confirmed by X-ray data which suggested that the diameter of "windows" in the zeolite crystal structure was approximately 4.2 Å.

The dimension which controls the entry of a molecule into a pore is called the critical dimension. For a spherical molecule such as argon, the critical dimension is its diameter. Similarly, for symmetrical molecules such as carbon tetrachloride, the critical dimension will be the diameter of the circle circumscribing the triangular base of the molecule. A list of critical diameters for other molecules has been prepared by both Barrer[126] and Breck et al.[125].

Dacey and Thomas[127] have used the method of molecular probes to determine the approximate pore size in polyvinylidene chloride carbons. They found that n-pentane, benzene and nitrogen were adsorbed rapidly and gave approximately the same saturation

volumes; neo-pentane, however, was adsorbed extremely slowly and eventually gave a saturation volume much less than that of n-pentane, etc. This effect was even more marked for the larger molecule tetra-ethyl methane. Dacey and Thomas suggested that the carbon possessed pores that were fine and uniform, slot-like in cross section and between 12 and 15 Å in width at their narrowest dimension.

2.4.2.3 The Calculation of Pore Size Distributions from the Kelvin Equation

The application of the Kelvin equation[128] to adsorption isotherms allows the pore size to be calculated as a function of the relative pressure. Although its application to pores of molecular dimensions has been severely criticized[174], there is, at present, no other method which can give such consistent results. It has long been recognized that capillaries fill according to the combined effects of layer formation and capillary condensation. Hence most applications of the Kelvin equation to desorption isotherms are based on the assumption that desorption occurs from an inner capillary of diameter corresponding to the Kelvin radius r_k, so that an adsorbed layer is left on the walls, i.e. the Kelvin radius $r_k \neq r_p$, the pore radius. Corrections can be applied to allow for the thickness of this layer.

(a) The Corrected Kelvin Equation

Wheeler[130] introduced a composite theory for adsorption which combined the BET multilayer theory and capillary condensation view points. Application of this theory to an experimental isotherm yielded an expression from which the pore distribution could be determined, viz.

$$V_s - V = \int_R^\infty (r - t)^2 L(r)\, dr$$

where V_s = volume of gas adsorbed at saturation,
V = volume of gas adsorbed at pressure p,
$L(r)\ dr$ = total length of pores whose radii fall, between r and (r + dr),
R = corrected Kelvin radius, and
t = multilayer thickness at pressure p.

Wheeler considered the radius of the pores to be equal to the sum of the multilayer thickness calculated from the BET theory and the radius normally calculated from the simple Kelvin equation. It was also suggested that pore size distribution could be approximated by a simple Maxwellian or Gaussian distribution.

Barrett, Joyner and Halenda[131] considered that this assumption of a simple distribution was inadequate and developed a tabular integration of the equation proposed by Wheeler. In this computation (1) the pores are treated as cylinders, (2) the Kelvin equation is applied to the desorption isotherm, and (3) the film thickness remaining on the pore walls after the inner capillary volume has been removed is equated to that adsorbed on a non-porous body at the same relative pressure. This method (known as the BJH method) leads to a pore volume distribution curve which gives the pore volume dV in the pores of radius between r and (r + dr). Pierce[132] has suggested a similar computation except that a value of one of the constants in the BJH method is taken as effectively equal to one. Although slightly less accurate, the calculation is considerably shorter.

Cranston and Inkley[133] developed a more exact method than that of Barrett, Joyner and Halenda, but again used the same principles. The novel features of their method include (1) the cumulative area is almost independent of the BET area, (2) the computation can be applied to either the desorption or adsorption branch of the isotherm, and (3) differences between BET and

cumulative areas are not necessarily ascribed to errors, but rather to the nature of the pores.

For adsorbents possessing the bulk of the pore volume in pores of diameter greater than 25 Å, the cumulative areas derived from the pore size distribution according to the method of BJH, Pierce, and Cranston and Inkley agree very closely with the area calculated from the BET equation.

(b) The Uncorrected Kelvin Equation

Juhola and Wiig[134] have applied the Kelvin equation directly to water isotherms and obtained pore size distributions for a number of active carbons. The molal volume V of the adsorbed water was obtained by helium displacement while the value of $\cos\theta$, referring to the desorption isotherms and used in the Kelvin equation, was taken as 0.49. In a later study, Juhola, Palumbo and Smith[135] found that the above method failed to give consistent results for carbons which exhibited a relatively large amount of water adsorption at low pressures. It has been well established that, because it is a polar compound, the adsorption of water is markedly effected by the chemical nature of the surface. For instance, oxidation of carbon at temperatures at which the pore structure is not altered considerably changes the shape of the water adsorption isotherm[17].

Bierci and Pescetti[136] attributed hysteresis to 'ink-bottle' shaped pores in the adsorbents. Using the Kelvin equation they were able to develop a method (similar to that employed by Bierci and Pescetti in their analysis of magnetic hysteresis) for calculating a pore size distribution in terms of the two radii, r_1 and r_2 of the ink-bottle model, the values of r_1, r_2 and V being presented simultaneously on a three-dimensional plot. The method was applied to the adsorption isotherms of alcohol on a silica gel and water on a sintered charcoal. At present the validity of the procedure has not been confirmed.

2.4.2.4 Other Estimates of Pore Size

Other methods of determining pore size are generally specific for a certain range of pore size. Dubinin[123] has suggested that pore sizes can be divided into three ranges:

(1) macro-pores where $r > 5{,}000$ Å,

(2) transitional pores where $200 > r > 25$ Å, and

(3) micro-pores where $r < 25$ Å.

(a) Microscope Techniques

It is possible for the macro-pores to be examined by means of an optical microscope. A photo micrograph shown in the paper by Dubinin[123] clearly illustrates the presence of pores of a size comparable with that predicted by other methods.

Electron microscope techniques have been used successfully to confirm the presence of pores in the transitional range[123], in fact, for a sample of alumina, the surface area calculated from the pore dimensions agreed very closely with the area derived from the BET equation[137].

(b) Mercury Penetration Measurements

A rapid, convenient and accurate means of determining pore sizes in the macro- and transitional pore ranges is the mercury penetration method suggested by Washburn[138]. This involves the measurement of the pressure required to force a known volume of mercury into the pores. The relationship between the pressure p and the radius of the pores is given by:

$$r = \frac{2\,\gamma \cos\theta}{p} \qquad \ldots \qquad (10)$$

where γ = surface tension

and θ = contact angle.

The measurement of the volume of mercury forced into the porous solid at various pressures enables the cumulative pore volume to be plotted as a function of pore radius.

Ritter and Drake[139] were amongst the first workers to use this method to determine the size of pores in porous materials. Since then it has been widely adopted for pore studies. A typical high pressure porosimeter developed by Ingles[140] can operate at a pressure of 45,000 p.s.i. and is therefore capable of measuring pore diameters down to 50 Å. The largest pore size that can be accurately measured will depend upon the accuracy of the pressure measurement. For the high pressure porosimeter mentioned above, the maximum pore size that can be measured with reasonable accuracy is approximately 40,000 Å. For larger pore sizes a low pressure apparatus capable of measuring pressures below one atmosphere is required.

2.4.2.5 Indication of Pore Size Changes

Dubinin[87-89] has developed an expression - based on the potential theory of Polanyi[90] - by means of which adsorption isotherm data for a variety of carbons may be reduced to straight line plots. From a large amount of experimental evidence, Dubinin[87-89] has shown that changes in certain constants in the equations reflect changes in the pore volume and pore size.

Holmes and Emmett[141] have judged the pore size alteration of activated carbons by the change in shape of low temperature nitrogen adsorption isotherms.

2.5 Kinetics of Adsorption

2.5.1 Transient Flow of Adsorbed Gases in Porous Solids

There are six factors which control the rate of flow of gases through porous media[142]. They are:

(1) the nature and magnitude of the driving forces,

(2) the other gases present in the mixture,

(3) the pore structure of the porous media,

(4) the manner in which each gas interacts with pore walls,

(5) the mean pressure of the system, and

(6) the mean temperature of the system.

If it is assumed that no thermal gradients exist within the porous solid then the two driving forces present will be

(1) normal bulk diffusion resulting from a pressure gradient, and

(2) pressure diffusion resulting from a pressure gradient.

Gas molecules will enter the pore volume of the solid as a result of their random kinetic motions and, if there is no resistance to their flow, molecules will move at the molecular translational velocity of $\sqrt{8\, k_B\, T/\pi m}$, where k_B is Boltzmann's constant and m the mass of the molecule. At normal room temperatures, this velocity is approximately 10^5 cm. per sec. However, there will normally exist two resistances to the movement of gas molecules in a porous body[143]:

(1) molecules will collide with each other, and

(2) molecules will collide with the pore walls.

The first resistance has been described in the usual texts on the kinetic theory of gases. The second resistance is of major importance for flow in porous solids and will be considered in detail.

de Boer[144] has shown that a molecule impinging on a surface can either rebound instantaneously or remain on the surface for time τ before being desorbed. In the former case, the direction of reflection of molecules will depend upon the direction of incidence, but in the latter case, molecules will desorb according to the cosine law. This law states that the number of molecules evaporating from the surface in a certain direction is proportional to the cosine of the angle the direction makes with the normal to the surface. Thus, a molecule will traverse a capillary by a 'random walk' mechanism. de Boer[144] has convincingly demonstrated how this

random walk mechanism can considerably slow down the rate of flow of molecules through a capillary.

It is generally agreed[145] that the two driving forces mentioned previously can produce three distinct diffusion processes, viz.

(a) bulk or ordinary diffusion,

(b) molecular or Knudsen diffusion, and

(c) surface diffusion.

These will now be considered.

(a) Bulk Diffusion

If the mean free path of molecules is considerably less than the pore diameter, then molecules will collide with each other far more often than with pore walls. Hence the diffusion coefficient will be independent of the pore radius and may approach that for normal bulk diffusion.

(b) Knudsen Diffusion

At very low gas pressures or with capillaries of small radius, where the mean free path of gas molecules is many times greater than the pore diameter, the number of collisions of gas molecules with pore walls will greatly exceed the number of collisions amongst themselves. For this type of gas flow, Knudsen[146] showed that the rate of flow of molecules for a particular gas was dependent upon the radius of the capillary, the temperature and the pressure gradient, and independent of the total pressure or concentration in the gas phase.

(c) Surface Diffusion

If the gas molecules are adsorbed to any extent on the surface of the solid, then an additional type of flow pattern may exist. Indeed, the theory of Knudsen diffusion assumes that adsorption takes place, since a molecule must be adsorbed for a finite time τ to undergo a diffuse reflexion. Values of the

Knudsen diffusion coefficient obtained by Clausing and Damkohler[176] for gases adsorbed by porous solids were usually lower than those for gases which were not adsorbed. Simarly Wicke and Voigt[175] found from permeability experiments using diaphragms of sintered glass and charcoal that adsorbed gases frequently gave an enhanced rate of flow. The explanation generally accepted is that along with Knudsen flow, there is a parallel flow due to surface diffusion.

2.5.2 Mathematics of Diffusion

As the rate of physical adsorption on a plane surface may be considered instantaneous[144], it is clear that the rate controlling factor for adsorption in porous media is the diffusion of molecules to adsorption sites. A non-steady state diffusion process may be described by Fick's Second Law in the form

$$\frac{\partial c}{\partial t} = \frac{\partial}{\partial x}\left(D\frac{\partial c}{\partial x}\right) \quad . \quad . \quad . \quad (11)$$

where c = concentration in moles per unit volume of the medium in which the diffusion takes place,

$\frac{\partial c}{\partial x}$ = concentration gradient,

D = diffusion coefficient, and

t = time.

This equation refers to the accumulation of matter in an element of volume dx as a function of time. Unfortunately, the conditions used in the derivation of this equation[147] are not often complied with when the equation is applied to a particular problem. The following points must be kept in mind if this equation is to be solved for values of D.

(1) Equation (11) was derived using the principle of continuity and so is ideally applied only to non-steady state

self-diffusion processes. However, for Knudsen diffusion, where the flow of molecules in either direction is unaffected by the presence of other molecules, it can be expected that the equation will apply.

(2) Equation (11) was derived using a fixed frame of reference for the centre of mass of the system.

(3) There has been some criticism[148, 149] regarding the validity of using concentration as a measure of the driving force for diffusion. While it is generally agreed that chemical potential is a more suitable measurement of driving force, it has yet to be shown that such an equation (it is usually more complex) leads to a better correlation of data[150].

(4) It is first necessary to assume that equation (11) does, in fact, describe the process being investigated; equation (11) will only apply where the rate of flow is proportional to the concentration gradient. Results obtained by Benson and Tompkins[151] for the sorption of ammonia by dehydrated potash alum initially gave indications of obeying Fick's law of diffusion, but further examination of the unusual variation of the diffusion coefficient with concentration, suggested that the diffusion theory was inadequate. Instead, they developed a theory based on the concept of different types of sorption sites.

(5) The diffusion coefficient cannot be simply related to a theoretical diffusion coefficient and must be regarded only as an effective diffusion coefficient D_e. Indeed, Crank[147] has shown that when diffusion is accompanied by an adsorption process governed by Henry's Law, Fick's Second Law becomes, for a constant value of D_e,

$$\frac{\partial c}{\partial t} = \frac{D_e}{K + 1} \cdot \frac{\partial^2 c}{\partial x^2}$$

where K = Henry's Law constant.

The effect of instantaneous adsorption is to slow down the overall diffusion process. For a non-linear adsorption isotherm of the form

$$V = K_1 c^n$$

Crank[147] has shown that the process is formally the same as diffusion governed by a diffusion coefficient, which is not constant, but dependent upon the total concentration of diffusing substance, free and immobile.

(6) If the accumulation of gas is measured as a weight gain, then it is necessary to assume that the weight adsorbed is proportional to the pressure, i.e. Henry's Law should be obeyed.

Equation (11) as it stands is difficult to solve explicitly for D_e. If, however, D_e can be assumed to be independent of concentration, then equation (11) reduces to

$$\frac{\partial c}{\partial t} = D_e \frac{\partial^2 c}{\partial x^2} \qquad . \quad . \quad . \qquad (12)$$

Furthermore even when D_e varies with concentration[147], methods are available for solving the equations.

To solve equation (12) it is first necessary to adopt a suitable model, and standard texts on the mathematics of diffusion[147, 152, 153] give solutions for a variety of geometrical shapes such as cubes, spheres, plane sheets, cylinders, etc.

2.5.3 Experimental Methods

There are several methods of measuring the rate of adsorption. They include:

(1) the constant pressure method,

(2) the constant volume method,

(3) the flow method, and

(4) the frequency response method.

In the first method the pressure is maintained constant and the rate of adsorption followed by weighing the adsorbent. In the second method[154] the volume is maintained constant and the rate of adsorption followed by measuring the change in pressure. In the flow method[155, 156] an inert carrier gas containing a certain partial pressure of adsorbate is flowed past the adsorbent and the rate of uptake of adsorbate measured gravimetrically as in method (1). The frequency response method employs the techniques of automatic control analysis. By measuring the phase lag and attenuation of an induced pressure disturbance, Naphthali and Polinski[157] were able to separate the contributions of fast and slow adsorption rates.

2.5.4 Observations of the Kinetics of Adsorption on Porous Materials

Zeolites are known to possess a very uniform pore structure in comparison with most other porous materials while other porous materials such as charcoals (porous carbons) and silica gels are known to usually possess a broad distribution of pore sizes. Thus, the mechanism of gaseous diffusion in zeolites might be expected to be simpler than that found in porous carbons. It will be convenient to deal with the kinetics of adsorption under two headings:

(a) Zeolites,

(b) Carbons and other Porous Materials.

(a) Zeolites

The earliest recorded investigation[158] of the kinetics of adsorption involved polar molecules such as ammonia and water as adsorbates. Generally, results obtained were difficult to analyze in terms of the diffusion theory. Barrer[158] found that the adsorption of ammonia often took weeks to reach equilibrium and suggested that ammonia chemically reacted with the zeolite. Later Barrer and Ibbitson[159] used non-polar chain molecules such as methane,

propane, butane and iso-butane, and measured the rates of adsorption at constant pressure. The rates of adsorption showed that adsorbates could be divided into three groups, viz.

(1) molecules that were rapidly adsorbed,

(2) molecules that were adsorbed slowly, and

(3) molecules that were excluded.

The rate of adsorption depended mainly upon the size of the molecule; smaller molecules such as methane were rapidly adsorbed, while iso-butane molecules were practically excluded. (See Section 2.4.2.2 for molecular sieve action.)

Barrer and Ibbitson found that the initial part of the rate curve corresponded to the parabolic diffusion law

$$\frac{\Delta V_t}{\Delta V_\infty} = k\sqrt{t} \qquad \ldots \quad (13)$$

Over the later stages of adsorption the relation

$$\frac{\Delta V_t}{\Delta V_\infty} = 1 - e^{-k_1 t} \qquad \ldots \quad (14)$$

was applicable. Barrer[152] was later able to show that equation (13) is an approximate solution to Fick's Second Law and independent of the shape[160] of the adsorbent particles whether cubes, spheres or parallelopipeds.

When $\Delta V_t / \Delta V_\infty$ was plotted against $\sqrt{t}$ it was noticed that for short times, the straight lines failed to pass through the origin and intercepted the $\Delta V_t / \Delta V_\infty$ axis. Barrer used the term 'foot' to describe the intercept value. He suggested that the 'foot' was the result of very rapid van der Waals adsorption upon the external crystal surfaces. The modified form of equation (13) is then[160]

$$\frac{\Delta V_t}{\Delta V_\infty} = k t^{\frac{1}{2}} + \Delta \qquad . \quad . \quad . \quad (15)$$

where Δ represents the 'foot' on the $\Delta V_t / \Delta V_\infty$ axis. Barrer and Brook[160] have used the value of Δ to calculate the external surface area of the zeolite crystals. They found that for certain zeolites, values for the surface area were in reasonable agreement with two other independent methods.

Values of k in equation (13) are a measure of the diffusion coefficient and were found to decrease with increasing concentration of adsorbate. Barrer and Riley[161] suggested that the change in diffusion coefficient should be proportional to the fraction of all available sites occupied. Thus equation (13) becomes

$$\frac{1}{t}\left(\frac{\Delta V_t}{\Delta V_\infty}\right)^2 = k D_1(1 - \theta) \qquad . \quad . \quad . \quad (16)$$

where k = constant depending upon particle size, and $D_1 = D$ when $\theta = 0$. Thus the initial rates of adsorption should decrease linearly with θ. For propane, Barrer and Riley found that a plot of the L.H.S. of equation (16) versus the adsorbate concentration, gave two straight lines, suggesting that there existed two kinds of adsorption sites within the zeolite.

The initial rates of adsorption increase with increase in temperature and when $\Delta V_t / \Delta V_\infty \; / \sqrt{t}$ is plotted against $1/T$, a straight line is obtained[161]. Thus it is apparent that sorption occurs by an activated diffusion process; the diffusion coefficient will then obey the relation

$$D = D_o \quad \exp - E/RT$$

where D_o is an independent temperature factor and E the apparent energy of activation. Because the channels through which the

sorbate molecules move are so narrow, the molecules can be expected to always move in the periodic potential energy field of the crystal. Barrer[162] found that, for a particular zeolite, a linear relationship existed between the activation energy E and the cross-sectional radius of the sorbate molecule; the larger the molecule, the higher the activation energy.

(b) Carbon and other Porous Materials

The diffusion of gases through coal is of fundamental importance in many aspects of coal technology. Maggs[164], and Zwietering et al.[163] showed that results for the adsorption of gases by coals could be explained if the coal material possessed an ultra-fine pore structure and that gases penetrated the material by an activated diffusion process. Zwietering et al.[163] and Joy[165] found that the diffusion rate of methane under conditions far removed from equilibrium, was linearly related to $\sqrt{t}$. Bolt and Innes[166] fitted an exponential equation to their data for the diffusion of CO_2 through coal; then by comparison with the theoretical exponential equation obtained by solving equation (11) for a specific model, they were able to estimate a value for the effective diffusion coefficient.

Dacey and Thomas[127] measured the kinetics of adsorption of molecules of various size such as nitrogen, n-pentane, and neo-pentane (see Section 2.4.2.2) on a carbon prepared from polyvinylidene chloride. Neo-pentane was the only adsorbate which was studied extensively and the activation energy for this molecule was found to vary from $\Delta H/3$ to $\Delta H/2$ where ΔH is the heat of adsorption. This suggested that neo-pentane molecules migrated from site to site in close proximity to the surface, i.e. the pores were probably so small that molecules were continually within the potential energy force fields of the surrounding carbon atoms of the capillary.

Later, Dacey, Young and McDougall[167] measured the rate of adsorption of n-heptane at constant pressure on a non-porous carbon black, Spheron 6 (Σ = 131 m.^{2} per g.). The initial rate of adsorption conformed to the parabolic diffusion law, but the diffusion coefficient obtained from the slopes of the straight lines increased with increased concentration of adsorbate. The calculated activation energy for adsorption was not significantly different from the heat of adsorption, suggesting that the rate determining step involved desorption of n-heptane molecules from the surface. From the size of the Spheron 6 particles and the packing density, the size of the interstices would be about 500 Å, thus allowing Knudsen diffusion to be the predominant flow mechanism.

2.6 Thermodynamics of Adsorption

Heats and entropies of adsorption often provide valuable information concerning the nature of the adsorbent surface and the nature of the adsorbate-adsorbate interactions. However, in the past, these thermodynamic functions have not been clearly defined.

The situation has been clarified by the work of Hill[168, 169] and Everett[170], which has been recently reviewed by Young and Crowell[120].

Young and Crowell have shown that the most useful functions are derived by methods of solution thermodynamics. Consider the two component system consisting of n_A moles of adsorbent and n_S moles of adsorbate in equilibrium with the unadsorbed gas. At a pressure P and temperature T, the internal energy U of the system is given by *

* A modified form of Young and Crowell's[120] notation is used in this thesis to describe the thermodynamic functions. Capital letters ($P, T,$) refer to total thermodynamic functions, small capital letters (s, h) refer to molar quantities and small capital letters with a bar ($\bar{s}, \bar{H},$) refer to differential molar quantities.

$$dU = TdS - PdV + \mu_A dn_A + \mu_S dn_S \quad . \quad (17)$$

where S is the entropy of the system, V is the volume, μ_A is the chemical potential of the adsorbent and μ_S is the chemical potential of the adsorbate. Generally, however, the adsorbent can be regarded as inert and, as Hill[168] has shown, thermodynamic functions of the adsorbate can be separated from equation (17). In the absence of adsorbate, $n_S = dn_S = 0$, and equation (17) reduces to

$$dU_{OA} = TdS_{OA} - PdV_{OA} + \mu_{OA} dn_A \quad . \quad (18)$$

where U_{OA}, S_{OA}, etc. refer to pure adsorbent in the same state of subdivision.

Now if the thermodynamic functions associated with formation of an adsorbed film are defined as

$$U_S = U - U_{OA} \qquad V_S = V - V_{OA}$$

$$S_S = S - S_{OA} \qquad H_S = H - H_{OA}$$

and equation (18) is subtracted from equation (17), then

$$dU_S = TdS_S - PdV_S + (\mu_A - \mu_{OA})\, dn_A + \mu_S dn_S \quad . \quad . \quad . \quad (19)$$

As n_A is proportional to the surface area Σ, equation (19) becomes

$$dU_S = TdS_S - PdV_S - \Phi\, d\Sigma + \mu_S dn_S \quad . \quad . \quad . \quad (20)$$

where ϕ is defined as $(\frac{\partial U}{\partial \Sigma})_{S_S, V_S, n_S}$.

Following the treatment used by Young and Crowell[120], the Gibbs free energy G_S can be defined as

$$G_S = U + PV_S - TS_S \quad . \quad . \quad . \quad (21)$$

Substitution of equation (20) in equation (21) gives

$$dG_S = -S_S dT + V_S dP - \phi \, d\Sigma + \mu_S dn_S . \quad (22)$$

By definition let

$$\bar{s}_S = (\frac{\partial s_S}{\partial n_S})_{P,T,} \quad \text{and} \quad \bar{v}_S = (\frac{\partial V_S}{\partial n_S})_{P,T,}$$

where $\bar{s}_S$ and $\bar{v}_S$ are differential quantities. Therefore, from equation (22),

$$d\mu_S = -\bar{s}_S dT + \bar{v}_S dP - (\frac{\partial \phi}{\partial n_S})_{P,T,} \, d\Sigma +$$

$$(\frac{\partial \mu_S}{\partial n_S})_{P,T,\Sigma} \quad . \quad . \quad . \quad (23)$$

For a change at constant P,T, and n_S, equation (23) reduces to

$$d\mu_S = -\bar{s}_S dT_{n_S,\Sigma} + \bar{v}_S dP_{n_S,\Sigma} \quad . \quad . \quad (24)$$

For the gas phase

$$d\mu_G = -s_G dT_{n_S,\Sigma} + v_G dp_{n_S,\Sigma} \quad . \quad . \quad (25)$$

where μ_g is the chemical potential of the gas phase molecules, and $s_g = \frac{S_g}{n_g}$ and $v_g = \frac{V_g}{n_g}$ are the molar entropy and volume of the gas phase, respectively. At equilibrium, $d\mu_s = d\mu_g$ and assuming that $P = p$ equations (24) and (25) combine to give

$$\left(\frac{\partial P}{\partial T}\right)_{n_g, \Sigma} = \frac{s_g - \bar{s}_s}{v_g - \bar{v}_s} \quad . \quad . \quad . \quad (26)$$

In the usual approximation of a perfect gas, $v_g \gg \bar{v}_s$ and $pv_g = RT$, and equation (26) becomes

$$\left(\frac{\partial \ln P}{\partial T}\right)_{n_g, \Sigma} = \frac{s_g - \bar{s}_s}{RT} \quad . \quad . \quad . \quad (27)$$

This is the equation from which the differential thermo-dynamic functions can be determined from adsorption isotherms.

2.7 Summary and Recommendations

It is evident from the literature review that changes in surface area during heat treatment have been noted for a number of carbons, but little has been achieved towards an understanding of the processes by which the surface area diminishes and the pore structure is altered. Furthermore, there has been no attempt to survey the process of sintering for a number of different types of carbons with the view to establishing whether or not sintering is an isolated phenomenon applying only to the few carbons investigated. While Davidson and Losty[75] have suggested that the growth of crystallites forms constrictions in the pores and so reduce the surface area and pore volume, no definite evidence has been presented for either the formation of constrictions or the inter-relationship between crystallite growth and sintering.

Thus the mechanism of sintering of porous carbons and the

accompanying change in pore structure requires further examination and it is logical to extend the knowledge in this field by studying:

(1) the changes in the physical structure of a series of carbons on heat treatment, and

(2) the effect of sintering on the adsorptive properties and derived thermodynamic quantities.

3. EXPERIMENTAL

3.1 Scope of Experimental Work

The following is a statement of the experimental work planned to implement the recommendations suggested in the previous Section.

1.a. Preparation of carbons from the polymers cellulose acetate, cellulose, phenol-formaldehyde, polyvinylidene chloride and polyvinyl chloride. Carbons prepared from these polymers possess a wide range of surface areas, pore sizes, densities, crystallite growth etc. For instance, the area of a polyvinylidene chloride carbon is extremely high compared with the area of a phenol-formaldehyde carbon; a polyvinyl chloride carbon exhibits a much larger crystallite growth on heat treatment than other polymer carbons. A commercial activated carbon, Cal carbon, made from a high grade coal, was included for purposes of comparison.

b. Steam activation of carbons.

c. Heat treatment of carbons at temperatures between 800° and 3,000°C.

2.a. Measurement of adsorption isotherms and calculation of (i) surface area, (ii) adsorptive capacity, (iii) pore volume, (iv) pore size, (v) pore size distribution, and (vi) heats and entropies of adsorption.

b. Measurement of adsorption isotherms for a series of adsorbates of varying molecular size and shape ('molecular sieve' experiments) to obtain additional information concerning the pore size and shape.

3. Chemical analysis of the original polymer and heat treated carbons.

4. Determination of helium and mercury densities and calculation of pore volumes.

5. Calculation of the pore size distribution by high pressure mercury penetration measurements.
6. Measurement of gas permeability of carbons.
7. Measurement of rates of adsorption on the carbons and the calculation of diffusion coefficients.
8. Determination of the crystallite growth from X-ray diffraction measurements.

3.2 Preparation of Carbon Samples

3.2.1 Raw Materials

The source and physical condition of the polymers used for the preparation of carbons are given below.

Cellulose Acetate

Source: Colonial Sugar Refining Chemicals Pty. Ltd. of Australia.
Physical Condition: flake.

Cellulose

Source: Whatman Ashless Quality powder.
Physical Condition: fibrous-low bulk density.

Phenol-formaldehyde Resin

Source: Monsanto Chemicals (Australia) Ltd.
Physical Condition: solid lumps.

Polyvinylidene Chloride

Source: Dow Chemical Co., U.S.A.; trade name Saran B118.
Physical Condition: fine powder.

Polyvinyl Chloride

Source: Imperial Chemical Industries of Aust. & N.Z. Ltd.
Physical Condition: fine powder.

A sample of an industrial type of activated carbon was included for purposes of comparison.

Cal Carbon

Source: Active Carbon Division[178], Pittsburgh Coke and Chemical Co., U.S.A.

Physical Condition: gramular.

Chemical analysis (see Section 3.3) of the raw materials is given in TABLE 2.

TABLE 2

Chemical Analysis of the Raw Materials

Per Cent by Weight

Raw Material	Carbon	Oxygen	Hydrogen	Chlorine	Ash
Cellulose acetate	48.0	45.0	5.9	-	.07
Cellulose	44.1	49.4	6.1	-	.015
Phenol-formaldehyde resin	76.9	16.1	6.05	-	0.2
Polyvinylidene chloride	26.5	0.6	2.4	70.9	< 0.2
Polyvinyl chloride	39.1	1.0	4.9	54.4	0.3
Cal Carbon	75.9	*	2.3	-	6.5

* The percentage of oxygen was difficult to determine directly because of the large percentage of ash present.

Analysis also revealed that the cellulose acetate polymer was in the form of the tri-acetate with the percentage of acetyl radical equal to 41.5%.

Preparation of the carbons from the above polymers took place in three stages, viz. carbonization, reheat and heat treatment. A sample of polyvinylidene chloride carbon was also steam activated after reheating and prior to heat treatment.

The experimental procedures of carbonization, reheat,

activation and heat treatment will now be discussed in detail.

3.2.2 Carbonization and Reheating

The carbons were prepared by heating the polymers under an inert atmosphere of nitrogen. Except for the preparation of some discs of cellulose carbon, the polymers used for carbonization were in the same physical condition as obtained from the source. The cellulose discs were prepared by pelletizing cellulose powder in a 1" diameter die under a pressure of 10,000 pounds. Details of the apparatus used for carbonization are shown in Appendix I. A polymer was placed in a silica tube and the system evacuated. A flow of 'oxygen free' nitrogen was then passed through the silica tube and the heating cycle commenced. The temperature was gradually raised to the decomposition temperature and held there for a period of at least 4 hours. After this period, the reaction subsided and the temperature was increased to a maximum of 800°C for at least 3 hours. The silica tube was then rapidly cooled to room temperature and the carbon removed and crushed to pass a 16-mesh B.S.S. sieve.

To stabilize the carbons and to remove unwanted reaction products, the carbon samples were reheated to 800°C in a transparent silica tube under high vacuum for 3 hours. Representative samples were then chosen by conventional sampling techniques.

3.2.3 Activation

The steam activation apparatus was similar to that used by Morgan et al.[179], and Culver and Heath[124]. It consisted of a long vertical silica tube heated by two 2.7-kW furnaces mounted in series. The lower half of the silica tube was packed with silica chips, while the upper half contained the carbon sample supported on a fine stainless steel mesh (see Appendix J). A 200-W flash boiler supplied steam to the base of the tube, along with a supply of 'oxygen free' nitrogen to act as a diluent. The system was evacuated to a rough vacuum and then purged with nitrogen while the temperature of the furnace was raised to 900°C. Steam was admitted and the quantity

of nitrogen adjusted to fluidize the bed of carbon and activate it in approximately 10 minutes. Fluidization of the bed was observed through a sight tube at the top of the silica tube and the flow of gases adjusted to give a reasonable degree of mixing of particles in the bed. The degree of activation was measured by the change in weight of the sample before and after activation, e.g. an 80% activation corresponded to an 80% burn-up of the sample. At the completion of activation the sample was cooled to room temperature in a stream of 'oxygen free' nitrogen.

3.2.4 Heat Treatment

The reheated carbon samples were heat treated by one of two different methods, depending upon the maximum temperature required.

(a) Induction Heated Furnace - maximum temperature 1,700°C.

Details of the apparatus are shown in Appendix K. In brief, the carbon samples were loaded into a graphite crucible inside an evacuated transparent silica tube. Surrounding the outside of the silica tube near the graphite crucible were 4 turns of $\frac{1}{4}$" copper pipe supplying the power from the induction heater. The system was evacuated to 10^{-5} mm. of mercury and the temperature raised gradually while the vacuum was maintained throughout the heat treatment cycle. It is known[63] that crystallite growth in carbons is complete in approximately 15 min. and, to ensure attainment of equilibrium, the maximum temperature was held for 30 min. The sample was then cooled under vacuum and stored in a glass jar.

The temperature was measured with a Cambridge Optical Pyrometer which was sighted onto the carbon sample through a hole in the graphite crucible lid. Unfortunately, the power of the induction heater limited the maximum temperature to 1,700°C.

(b) Graphite Furnace - maximum temperature greater than 3,000°C.

This furnace was housed at the Australian Atomic Energy Commission Establishment at Lucas Heights, New South Wales. Details of the furnace and auxiliary apparatus are shown in Appendix I. Briefly, the furnace consisted of a graphite tube element heated by an electric current. The carbon sample was placed in a graphite crucible which was then positioned in the centre of the graphite tube. A stream of dry argon was passed through the tube to remove oxidizing gases and the heating cycle commenced. Temperatures were measured with a Cambridge Optical Pyrometer sighted directly onto the graphite crucible. The maximum temperature was maintained for 30 min.

It will be convenient to designate the carbon samples by the following abbreviations:

Cellulose acetate carbon	CA
Cellulose carbon	CEL
Phenol-formaldehyde carbon	PF
Polyvinylidene chloride carbon	SA
Polyvinylidene chloride carbon (activated)	SAA
Polyvinyl chloride carbon	PVC
Cal carbon	CAL

Numbers after the letters will refer to the heat treatment temperature, e.g. CA-1200 refers to cellulose acetate carbon heat treated to 1,200°C.

3.3 Chemical Analysis of Carbons

Chemical analysis of the samples of polymers and carbons was carried out by the Microanalytical Laboratory, Division of Organic Chemistry, C.S.I.R.O.; the limit of error was stated to be less than 0.3%.

3.4 Weight Loss Measurements

During the reheat stage of the preparation of carbon samples, a considerable amount of gas was evolved in the temperature range 500° to 800°C. It was important to find out whether this quantity of gas altered the adsorptive characteristics of the carbons. The following procedure was used to determine the effect of degassing on the adsorption isotherm of a cellulose acetate carbon.

A sample of carbonized cellulose acetate was placed in a silica bucket on one arm of the microbalance. The operational features of the microbalance are described in Section 3.5; but, for the high temperature measurements, the hard glass balance tubes were replaced with transparent silica tubes of twice the length. Extended suspension wires and suitably placed reflectors prevented the high temperature in the vicinity of the specimen from affecting the normal operation of the balance. While the samples were heated, a pressure of at least 10^{-4} mm. of mercury was maintained in the balance. The following operational sequence was employed:

I The sample was heated for 24 hours under vacuum at 350°C; an argon adsorption isotherm was measured at -196°C; the procedure was repeated twice.

II The sample was heated to 900°C and the weight loss recorded; an argon adsorption isotherm was measured at -196°C; the sample was heated to 900°C, cooled, and exposed to the atmosphere for 24 hours.

III The sample was heated to 900°C and the weight loss recorded; an argon adsorption isotherm was measured at -196°C; the sample was heated to 900°C, cooled and kept in a vacuum of at least 10^{-3} mm. Hg.

IV The sample was heated to 900°C and the weight loss recorded.

3.5 Measurement of Isotherms

3.5.1 Argon and Nitrogen Isotherms

To determine a point on the adsorption isotherm, it is necessary to know the amount of gas adsorbed per gram of adsorbent V at a pressure P and temperature T. The apparatus constructed for this purpose is shown in Fig. 11. The weight of gas adsorbed by the adsorbent was first measured gravimetrically by a silica spiral spring balance and later by a torsion wire null-point microbalance. Pressures were measured by a McLeod gauge F, an oil U-tube manometer G, and mercury U-tube manometers D and E. The temperature of the sample was maintained constant by a cryostat with an operating range of -183° to $-196^{\circ}C$.

(a) Weight Measurement

There are several advantages to be gained by using a gravimetric method to measure the amount of adsorption.

(i) In the gravimetric method, the pressure and amount of adsorbate are determined independently; the sorbate is weighed directly, whereas in volumetric methods, it is calculated indirectly from changes in pressure. Errors in the measurement of pressure cannot influence the readings for the weight of sorbate.

(ii) A sensitive balance can yield more accurate results for the measurement of an adsorption isotherm. Propagation of errors or the accumulation of errors from point to point is eliminated.

(iii) The accuracy is independent of volume, i.e. the volume of the system does not have to be calibrated.

(iv) Adsorption of gases on the inside walls of containers or on lubricants does not interfere with the measurements.

(v) The approach to equilibrium can be measured continuously.

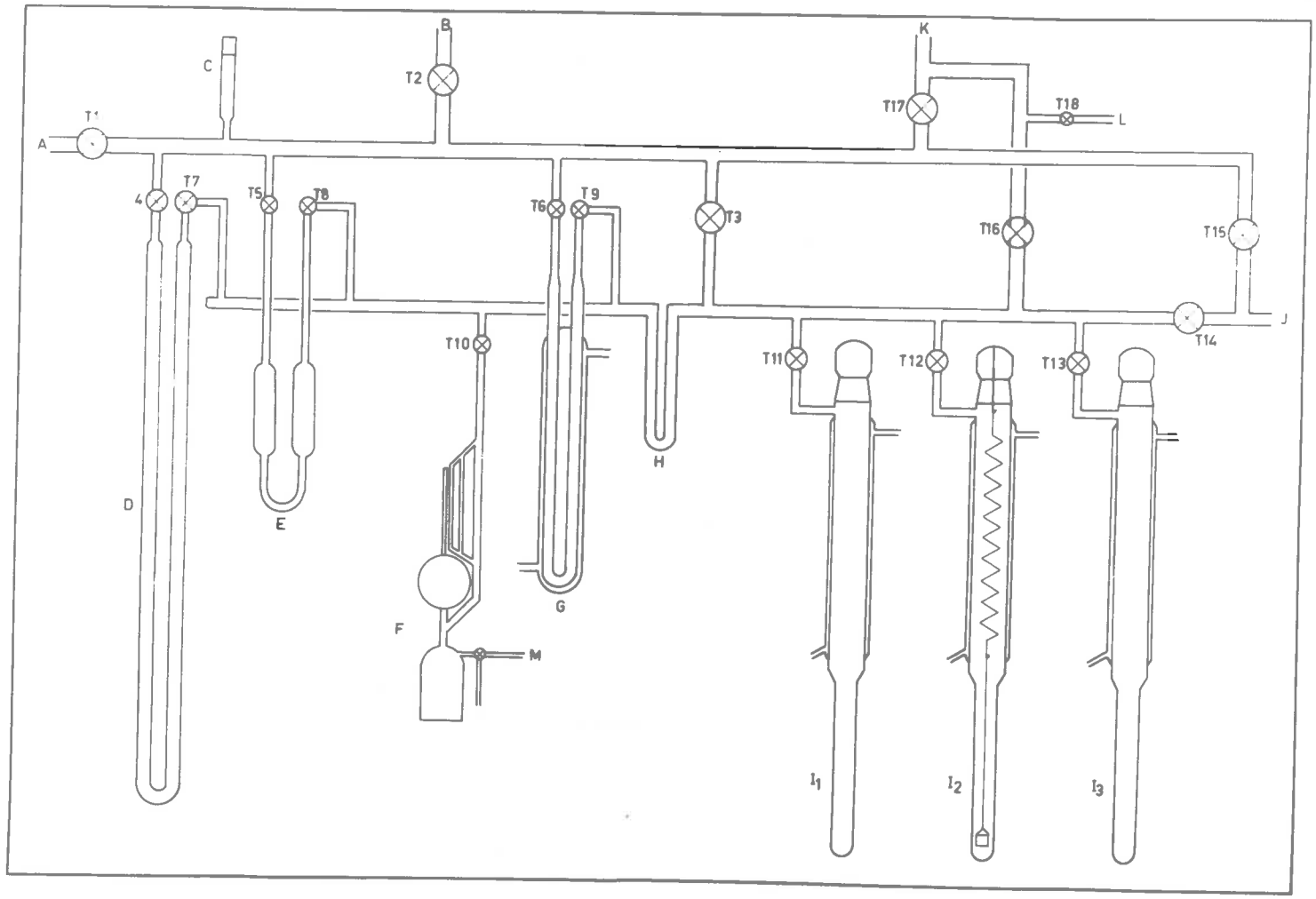

Fig. 11 - Argon/Nitrogen Gravimetric Adsorption Apparatus

KEY TO FIGURE 11

Argon/Nitrogen Gravimetric Adsorption Apparatus

A.	To organic adsorbate adsorption apparatus
B.	To high vacuum pumps
C.	Pirani gauge
D.	Mercury U-tube manometer
E.	Mercury U-tube manometer
F.	McLeod gauge
G.	Oil U-tube manometer
H.	Cold trap
I_1, I_2, I_3.	Balance cases
J.	To microbalance
K.	40 ℓ ballast
L.	From gas purifying train

(vi) Tubes with a large diameter can be used so that the time taken to evacuate the system is considerably reduced.

(vii) More than one balance can be operated simultaneously.

The operation and the characteristics of the silica spring balance and the micro-balance will now be discussed in detail.

Silica Spiral Spring Balance

The bucket containing the adsorbent was suspended from a silica spiral spring by a long quartz fibre and the assembly mounted in a jacketed glass balance case. The linear extension of the spring was calibrated with known weights so a change in the weight of the adsorbent was measured as a change in length of the spring. The extension of the spring was measured by focusing the cross-hairs in the telescope of a cathetometer onto the curved hook at the bottom of the spring. A single quartz fibre, hanging down from the point of suspension of the spring, provided a point of reference.

Most of the silica spiral springs were made[180] in the department, but some were obtained from Thermal Syndicate Limited, England. The sensitivity of the springs lay between 70 and 80 cm. per g. Constant sensitivity of the springs was maintained by water jacketing the balance case; the variations in temperature was $\pm$ 0.1°C. Dell and Wheeler[181] have shown that, if the temperature variation of the spring is kept within these limits, the thermal expansion of the spring is negligible.

On the cathetometer, the normal adjusting screw was replaced with a metric micrometer having a total available extension of 2 cm. For most adsorption isotherms, the total extension of the spring was well within 2 cm., so that the high accuracy of the micrometer could be utilized over the complete adsorption isotherm. With suitable illumination of the hook, the extension of the spring could be measured to $\pm$ 0.001 cm.

Reproducibility of the springs is known to be excellent. McBain and Sessions[182] have tested a series of springs in different organic atmospheres and observed no appreciable permanent stretching even after a period of 20 years.

The buoyancy effect on the bucket and sample - calculated by the method of Dell and Wheeler[181] - was less than the minimum observed weight change, even at atmospheric pressure.

Sartorius Micro Balance

The Electrono I Vacuum Electronic Micro Balance, manufactured by Sartorius-Werke Goettengen, Germany, has several features which make it ideally suited to the measurement of adsorption isotherms and rates of adsorption. The technical details and operation of the balance have been described by Gast et al.[183].

(1) Weighing Principle

The description of the principle of operation is directly quoted from the operating instructions issued with the balance.

"The Electrono operates on the principle of automatic compensation by an electrically induced counter force of a torque moment induced by the load."

The essential element of the balance is shown in Fig. 12.

"Two arms of a quartz beam (1) are fused onto a quartz ring (2) which, by virtue of a wire coil wound around its inside, forms a rotating coil. The ring is suspended on two sides on Platinum-Iridium Torsion wires (3). These also serve as current leads to the coil.

The coil surrounds a cross magnetized ceramic magnet (4) whose lines of force are horizontal in the vicinity of the coil.

The ceramic magnet, of high specific resistance and vacuum equivalent permeability, supports another coil (5) through which circulates a high frequency alternating current. Coil (5) is part of an oscillator circuit which produces a frequency of approximately 480kc. in the regulator. The rotating coil is

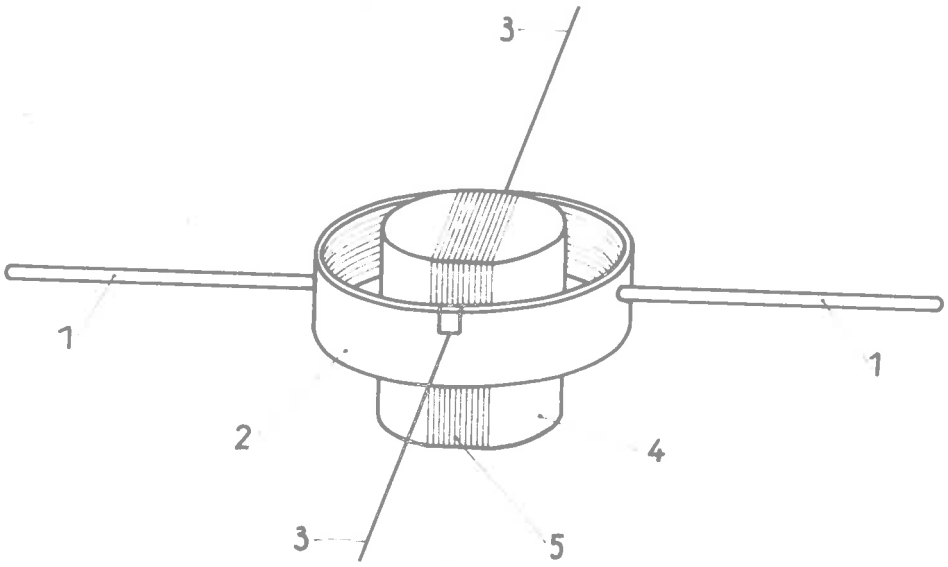

Fig. 12 - Operating Principle of Electrono Microbalance

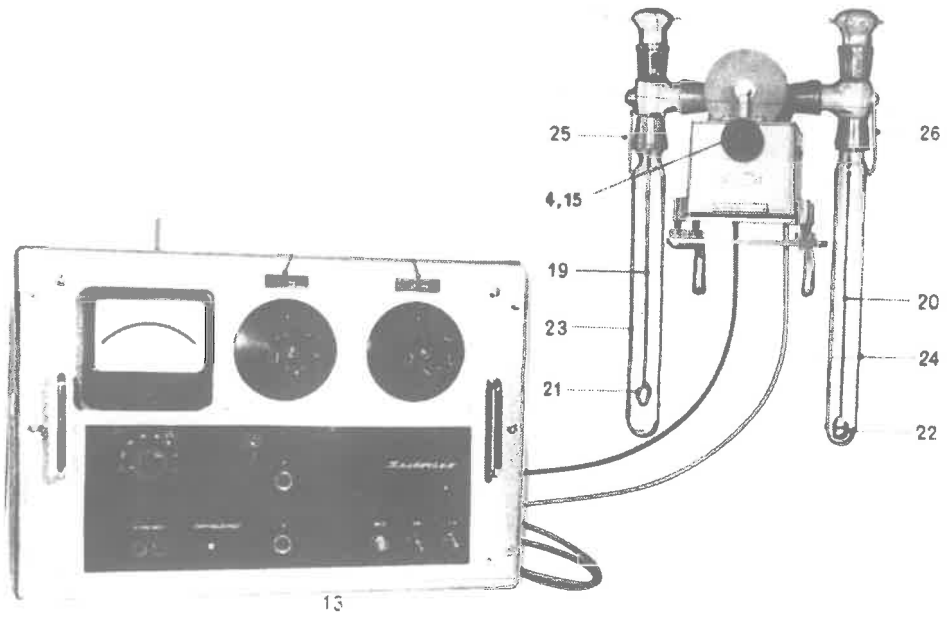

Fig. 13 - Electrono I Vacuum Electronic Microbalance

exposed to this high frequency magnetic field. Superimposed on the latter is the constant magnetic field of the ceramic magnet. In the rest position, i.e. with the balance at equilibrium, the coil is not exposed to the lines of the HF field. If the beam deviates because of an external force (weight change), then a high frequency signal induced by the HF coil originates in the rotating coil. This signal, whose magnitude and polarity depend on the angle of torque, is amplified in the regulator and returned to the rotating coil, after rectification, phase adjustment, and repeated amplification. The counter torque moment thus induced is practically equal to the force applied and returns the beam almost to its rest position. This counter torque moment is proportional to the product of the field intensity H of the ceramic magnet and the current I. Since the intensity of the field of the ceramic magnet is known to be constant, the counter torque moment is strictly proportional to the current I. Thus, the direct current as indicated on the measuring instrument is a measure of the torque acting on the beam, i.e. the weight sought. The weighing is thus converted to an electrical measurement."

(2) Technical Data

The total capacity of the balance was 1 g. on each arm. With a range control adjustment the following ranges and scale divisions were available:

Range	Scale Division
0.2 mg.	0.002 mg.
0.4 mg.	0.004 mg.
1.0 mg.	0.010 mg.
2.0 mg.	0.020 mg.
4.0 mg.	0.040 mg.
10.0 mg.	0.100 mg.
20.0 mg.	0.200 mg.

Fine external taring of the balance was accomplished by applying a small torque to the torsion wires. The motion of the taring knobs was transmitted through the glass wall by multiple polarized disc magnets. The maximum range of the torsion taring system was 4 mg.

With a weight compensation device, maximum sensitivity could be obtained over the entire weight range. The device consisted of two resistance decades which compensated for excess weight and, in effect, provided a suppressed zero.

The 20 mg. weight range was often inadequate to cope with the weight increase for a 1 g. sample. An additional device was fitted to the balance by means of which a rider could be placed on the left hand arm of the balance. The addition of this rider doubled the range capacity of the balance. There was no need to return the rider to the same position on the balance, as the weight of the rider was automatically measured as a weight difference during a run.

The response time of the balance was not stated; however the addition of a small weight to the balance resulted in an almost instantaneous change of reading with no sign of overshoot or hunting.

(3) Factors Interfering with Measurement

Various factors can interfere with the weighing and these either have to be eliminated or accurately known.

Electrostatic Charge There was no evidence of electrostatic charges when the Jena glass balance tubes were employed. However, for temperatures above 500°C, transparent silica tubes were substituted for the Jena glass tubes and there was strong electrostatic reaction between the silica tube and the bucket. This was effectively counteracted by coating the silica tube with a thin layer of platinum chloride and heating the tube to red heat to deposit a layer of platinum on the tube surface.

Radiation Two polished platinum reflectors were suspended at intervals above the bucket to dissipate thermal radiation from external surfaces.

Vibration The balance was placed on the rubber mounted steel platform shown in Appendix O, which reduced the effect of extraneous vibrations on the balance to a minimum.

Temperature The balance was kept in a room air-conditioned to a temperature of $\pm$ 1°C. Radiation onto the balance was eliminated by a sheet of aluminium foil wrapped around the balance case enclosing the beams.

Buoyancy The balance was counterpoised with transparent silica chips of a density comparable with that of a dense carbon (ρ = 2.21 g. c.c.$^{-1}$). However, for the less dense carbons, there was a difference in the volumes of gas displaced by the carbon and the counterpoise. The resultant upthrust was accurately calculated from the density of argon displaced and an appropriate correction applied to the readings.

To test the validity of the calculations, a sample of silica was placed in one pan and counterpoised with platinum foil. The pressure of argon was increased to one atmosphere in steps and the change in weight recorded. As the experiment was conducted at room temperature, the observed weight change could be assumed to be solely due to buoyancy effects. It was found that the calculated buoyancy agreed with the observed buoyancy to within at least 1%.

(b) Pressure Measurement

Pressures from 10^{-5} mm. to 2 mm. of mercury were measured with a calibrated Jena McLeod gauge. The calibration of the gauge was checked against a standard McLeod gauge constructed according to Barr and Anhorn[184].

Higher pressures were measured with the mercury U-tube

manometer D. The manometer was constructed from 2.0 cm. I.D. glass tubing of length approximately 100 cm. With a black-above-white background and a diffuse light source, the levels were read by a cathetometer to an accuracy of $\pm$ 0.02 mm.

Mercury and oil vapours from the manometers were prevented from reaching the sample by a U-tube cold trap H. The use of large diameter tubing throughout the system eliminated the effect of thermal transpiration on the measured pressure.

All pressures were corrected to cm. of mercury at 0°C. The saturation pressures of argon and nitrogen at specific temperatures were obtained from the data of Din (ref. 185 Vol. II) and Armstrong[186], respectively.

(c) Temperature Control

The temperature of the sample was controlled by a cryostat based on the design of Lopez-Gonzalez et al.[187] and shown in Fig. 14. The outer Dewar flask and the inner copper vessel contain either liquid oxygen or nitrogen depending upon the desired temperature. By varying the pressure over the liquid in the Dewar flask the temperature could be maintained at any value between -183° and -196°C. The pressure controller consisted of a small U-tube manometer containing a pair of contacts which operated a solenoid valve between the Dewar flask and a mechanical vacuum pump. Despite the introduction of surge tanks into the vacuum line leading to the Dewar, large pressure fluctuations occurred when the valve was activated, and caused temperature variations of up to 0.5°C. To reduce the pressure fluctuations, the inner copper tube was lagged with glass tape and a heater C (see Fig. 14) placed between the copper tube and the glass tube containing the sample. The heater - in the form of a fine wire mesh screen - was controlled by the oxygen vapour pressure thermometer shown in Fig. 15. A pair of contacts K in one arm of the thermometer and an adjustable mercury level, enabled the temperature to be set at any desired value. A

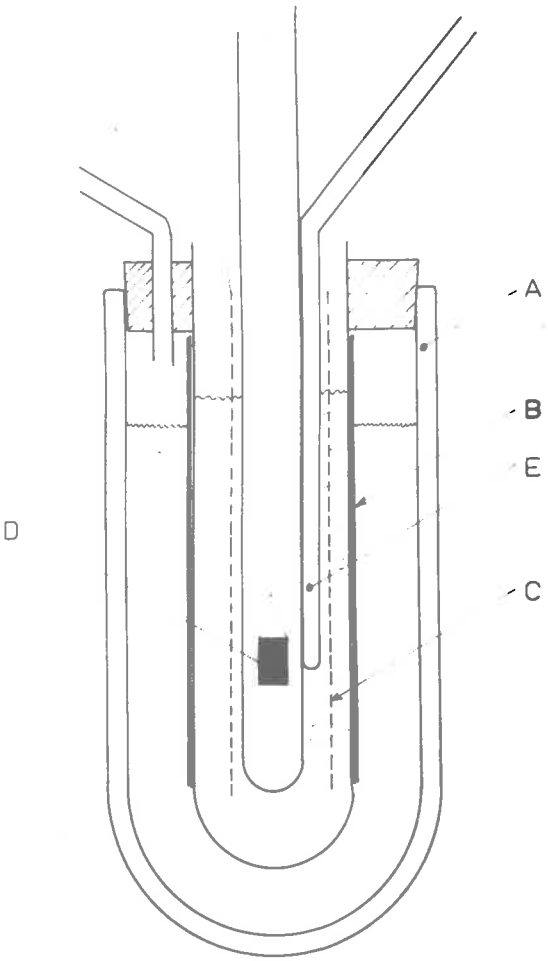

Fig. 14 - Low Temperature Cryostat

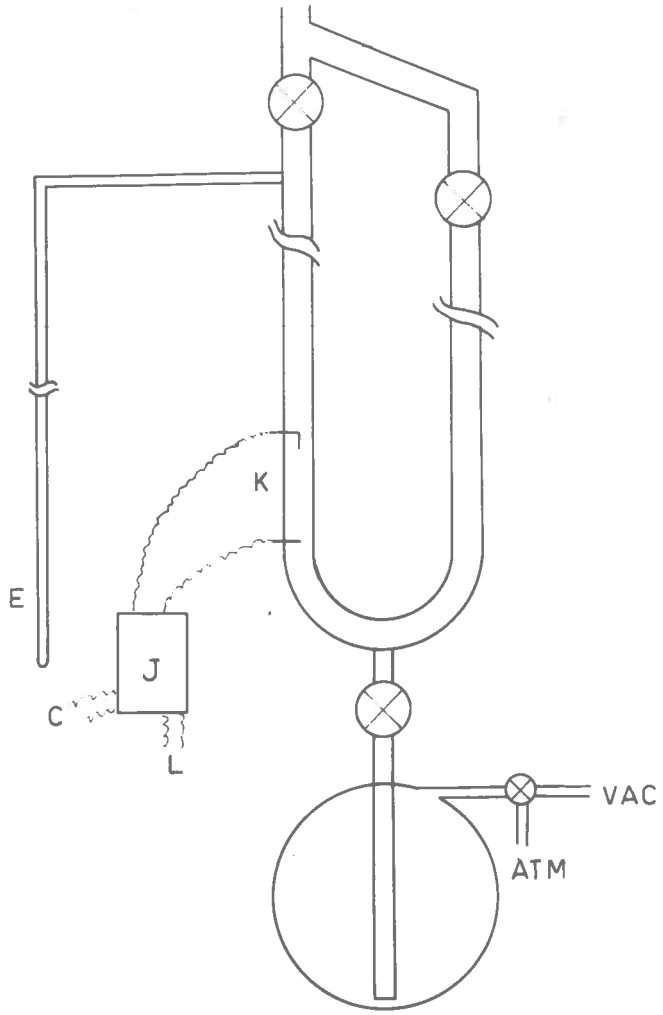

Fig. 15 - Oxygen Vapour Pressure Control Thermometer

KEY TO FIGURE 14

Low Temperature Cryostat

A. Outer Dewar flask

B. Inner copper tube

C. Heater

D. Sample bucket

E. Oxygen vapour pressure thermometer bulb

KEY TO FIGURE 15

Oxygen Vapour Pressure Control Thermometer

J. Thyratron relay

K. Tungsten contacts

L. Power supply

thyratron relay with an adjustable current output was connected to the contacts K and to the heater in such a manner that a fall in temperature broke the circuit and supplied power to the heater.

During the operation of the cryostat the outer bath temperature was kept slightly below the desired sample temperature. The level of mercury in the vapour pressure thermometer was adjusted to the 'set point' and the thyratron relay J switched on. As the oxygen vapour pressure thermometer was very sensitive to temperature changes, the inner bath temperature could be controlled to at least $\pm$ 0.01°C.

For adsorbents requiring a long time to reach equilibrium, it was necessary for the supply of liquid in the outer Dewar to be replenished. To do this a modified liquid level controller[177] sensed the level of the liquid in the outer Dewar. The sensing device was initially filled with oxygen and then partially filled with mercury to the levels shown in Fig. 16. The device was mounted so that when the level of the liquid fell below a certain point, the oxygen in the bulb N expanded and thereby raising the level of the mercury to close the circuit through the contacts Z. The contacts energized a relay R which opened a solenoid valve V above the supply Dewar flask T (see Fig. 17). Liquid was forced over into the outer Dewar flask of the cryostat until the oxygen in the bulb of the sensing device contracted and allowed the mercury to break the circuit.

(d) Temperature Measurement

Temperatures between -183° and -196°C were measured with the oxygen vapour pressure thermometer used to control the bath temperature. The oxygen vapour pressure thermometer was constructed according to Sandersen[188]. The pressure in the manometer was read with a cathetometer to $\pm$ 0.04 mm. of mercury; the resulting temperatures calculated from the oxygen vapour pressure tables of Hoge[189] were accurate to $\pm$ 0.01°C.

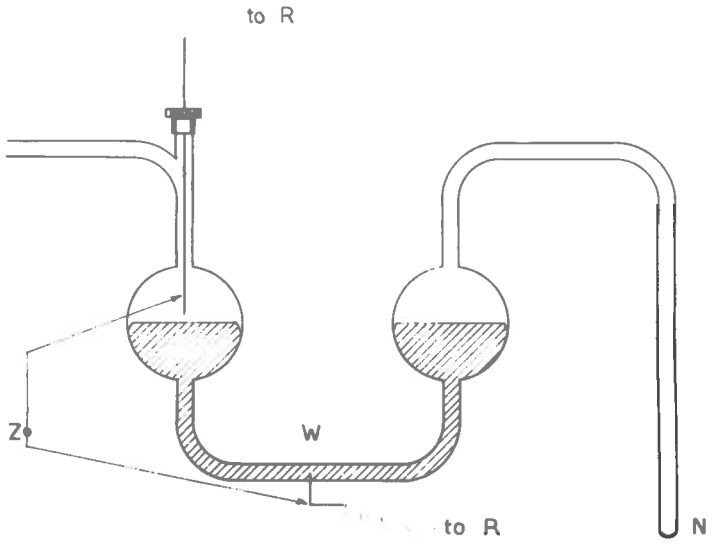

Fig. 16 - Liquid Level Sensing Device

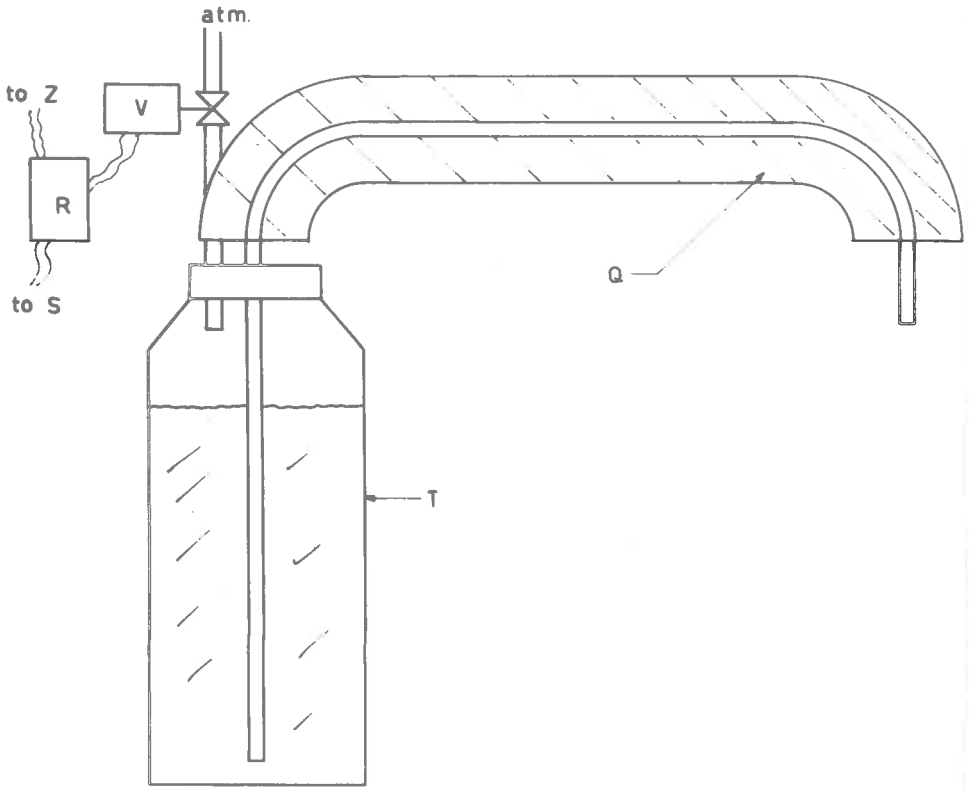

Fig. 17 - Liquid Refrigerant Supply Dewar

KEY TO FIGURE 16

Liquid Level Sensing Device

B. Bulb
R. Relay
W. Mercury
Z. Tungsten contacts

KEY TO FIGURE 17

Liquid Refrigerant Supply Dewar

Q. Urethane insulation
R. Relay
S. Power Supply
T. Supply Dewar
V. Solenoid valve
Z. Tungsten contacts in liquid level sensing device.

(e) Materials

Argon was supplied by Commonwealth Industrial Gases in cylinders and contained 10 p.p.m. of oxygen and 20 p.p.m. of water vapour. From the cylinder, the argon was passed through a cold trap containing copper turnings to remove condensables and then through a tube containing bright copper turnings at 400°C to remove oxygen. The purified argon was stored at atmospheric pressure in four 10 l. ballast tanks.

'Oxygen-free' nitrogen containing 10 p.p.m. of oxygen and 20 p.p.m. of water vapour was purified in the same way and was stored in ballast tanks.

(f) Isotherm Determination

A sample of carbon was weighed and placed in either the platinum bucket of the spiral spring balance or the silica bucket of the microbalance. The system was evacuated and the sample degassed for 24 hr. under a vacuum of at least 10^{-5} mm. of mercury at a temperature of 350°C.

After degassing, the sample was cooled and the cryostat placed around the balance case. The mercury level in the oxygen vapour pressure thermometer was adjusted to the 'set point' and at least 2 hr. allowed for the system to reach a constant temperature. Taps T3, T11, T14, T15, T16, T17 and T18 were closed and gas admitted to the sample (for the spring balance) through Taps T16 and T11. The extension of the spring balance was noted when no further weight increase could be detected. The pressure and temperature were then measured and recorded. Admission of gas in steps was continued until a complete isotherm up to $p/p_o \approx 1.0$ was obtained.

3.5.2 Organic Adsorbate Isotherms

The apparatus used to measure argon and nitrogen isotherms contained greased high vacuum taps and was therefore not suitable for the measurement of organic adsorbate isotherms. The apparatus

constructed (see Fig. 18) contained mercury cut-offs of conventional design[184] and a special greaseless valve for fine control of gas flow (for details of valve see Appendix M). The amount adsorbed was measured with a silica spiral spring balance of the same design as that used in the argon/nitrogen apparatus. The cap F was sealed to the balance case E by a dry ground glass joint immersed in mercury.

(a) Pressure Measurement

The pressure was measured with the mercury U-tube manometer D constructed from glass tubing of 2.0 cm. I.D. The mercury levels were measured with the cathetometer as for the argon/nitrogen apparatus.

An attempt was made to measure pressures below the range of the U-tube manometer, viz. pressures less than 1×10^{-1} mm. Hg. A Puddington[190] manometer capable of measuring pressures as low as 2×10^{-3} mm. Hg. was constructed, but unfortunately it proved to be too delicate to operate continually.

All pressure readings were corrected to mm. of mercury at 0°C. The saturation vapour pressures of the various adsorbates at specific temperatures were obtained from the tables[191] of the American Petroleum Institute Research Project 44.

(b) Temperature Control and Measurement

For the adsorption of benzene and p-cymene, the temperature of the carbon sample was controlled to within $\pm$ 0.05°C in the range 15° to 45°C by a constant temperature water bath surrounding the bottom of the balance case. The bath was in the form of a jacketed vessel through which water at a constant temperature was circulated from an outside bath. For temperatures from 15° to 25°C, the outside bath temperature was cooled at a constant rate by an immersed copper coil connected to a refrigeration unit. The temperature of the adsorbate bulb B was maintained at a constant temperature between 15° and 45°C in a similar manner to the sample.

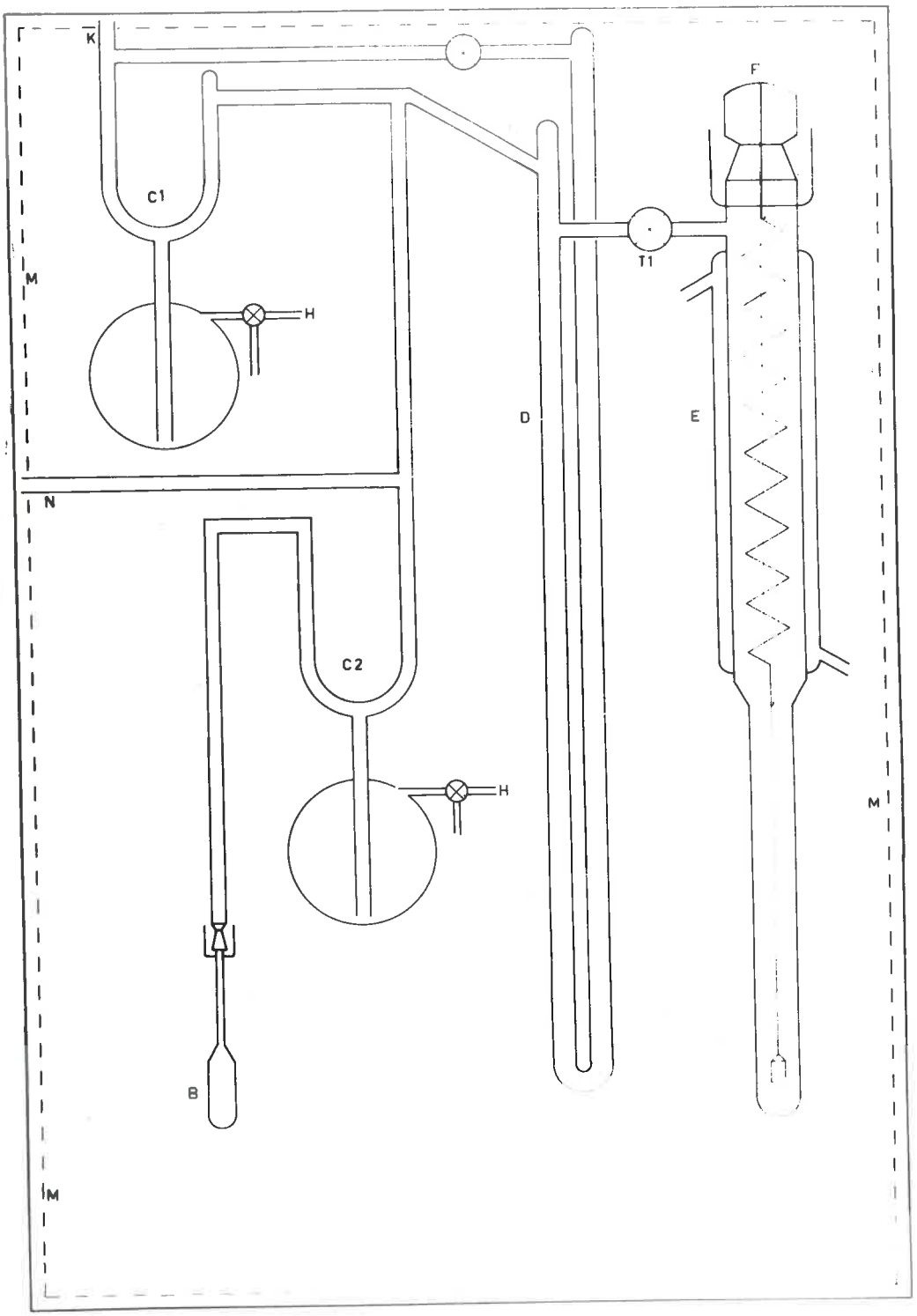

Fig. 18 - Organic Adsorbate Gravimetric Adsorption Apparatus

KEY TO FIGURE 18

Organic Adsorbate Gravimetric Adsorption Apparatus

B.	Adsorbate bulb
C1, C2.	Mercury cut-offs
D.	Mercury manometer
E.	Balance case
F.	Balance case cap
H.	Rough vacuum line
K.	High vacuum line
M.	Constant temperature enclosure
N.	Gas introduction device
T1.	Greaseless fine control vacuum valve

The water from the outside bath circulated first through the vessel surrounding B and then through the vessel surrounding the carbon sample.

For the adsorption of n-butane and neo-pentane, the carbon sample was maintained at 0°C by a stirred ice/slush bath in a Dewar flask.

To enable the saturation vapour pressure to be obtained for benzene and p-cymene at temperatures higher than room temperature, it was necessary to enclose the complete apparatus in an air thermostat controlled at a temperature 0.5°C higher than that of the bulb B. The apparatus was enclosed in a hard-board box, the front panel being a sheet of clear 'Perspex' with suitable small doors for manipulation of taps inside the box. A Jumo mercury-in-glass thermo-regulator, operating through a Jumo relay, controlled the power input to a domestic 'Turbo-fan' room heater. By coupling an outside variable resistance to the resistance winding in the 'Turbo-fan' heater, the power input could be adjusted to minimize variations in the air temperature. An additional high capacity circulating fan installed within the box provided sufficient air turbulence to enable the temperature to be controlled to $\pm$ 0.05°C.

Temperatures were measured with mercury-in-glass thermometers with calibrated ranges of 15° to 30°C and 30° to 48°C spread over a stem length of 20" in 0.02°C divisions. The thermometers were standardized against similar thermometers calibrated at the National Physical Laboratory, England, to an accuracy of $\pm$ 0.02°C.

(c) Materials

The organic adsorbates used were benzene, p-cymene, n-butane and neo-pentane. The purity, preparation and source of the samples are given below.

Benzene Benzene (A.R. Grade) was supplied by The British Drug Houses Ltd. The impurities were stated to be:

Non-volatile matter	0.002 %
Thiophen	0.0002 %
Sulphur compds.	0.0003 %
Water	0.05 %

To remove water the benzene was dried over sodium in bulb B under vacuum for several weeks.

p-Cymene p-Cymene (M.A.R. Grade) was supplied by The British Drug Houses Ltd. The impurities were stated to be less than 0.05%.

n-Butane and neo-Pentane Both these gases (labelled Pure Grade) were obtained from the Phillips Petroleum Company in one quart cylinders. The gases were stated to have a minimum purity of 99% and contain less than 0.005% sulphur.

The liquids benzene and p-cymene were placed in bulb B and thoroughly degassed under vacuum by alternate freezing and boiling. The gases n-butane and neo-pentane were fed from the cylinders through a low pressure diaphragm regulator to a gas introduction device[129] shown in Appendix N. Following a preliminary flushing and evacuation of the device, the introduction of the gases to the high vacuum system could be simply and easily controlled.

(d) Isotherm Determination

If benzene or p-cymene was used as an adsorbate, it was placed in bulb B and degassed. If n-butane or neo-pentane was used, the gas introduction device was flushed and evacuated.

The sample of carbon was loaded into the balance and degassed according to the procedure adopted for the argon or nitrogen isotherm determination. The temperatures of the carbon sample, adsorbate and air in the box were set and the apparatus

allowed to come to equilibrium. Tap T1 and mercury cut-off C1 were closed and adsorbate vapour allowed to enter the system from either bulb B or the gas introduction device M. When the desired pressure had been obtained, the tap T1 was slowly opened and the vapour allowed into the balance case. At equilibrium the spring balance reading was recorded along with the pressure and the temperature. By appropriate increments of vapour, the complete isotherm up to $p/p_o \approx 1.0$ was obtained for benzene and p-cymene; in order to conserve the gases n-butane and neo-pentane, which were available in small quantities only, pressure measurements were limited to $p/p_o \approx 0.3$.

3.6 Helium Density Determination

The helium density of a substance is calculated from the volume of helium displaced by a known weight of substance.

3.6.1 Apparatus

The volumetric apparatus is shown in Fig. 19. The sample bulb B is connected by a capillary manifold to a gas burette G and a constant volume mercury manometer M. The volume of the system could be varied by raising or lowering the mercury in the gas burette G. By measuring the pressure of a gas in the system at each expansion or contraction, the volume in bulb B could be calculated by application of the ideal gas laws.

The constant volume mercury manometer was constructed according to the method of Joyner[184]. The mercury in the right hand arm was always adjusted to the same level with the aid of a 'magic eye' indicator[184]. When the mercury reached the top tungsten contact, a circuit was completed, energizing the 'magic eye' indicator. This enabled the level to be reset to $\pm$ 0.01 mm. (or to less than $\pm$ 0.001 cm^3. volume variation). The level in the left hand arm of the manometer was measured with a cathetometer to an accuracy of $\pm$ 0.002 cm.

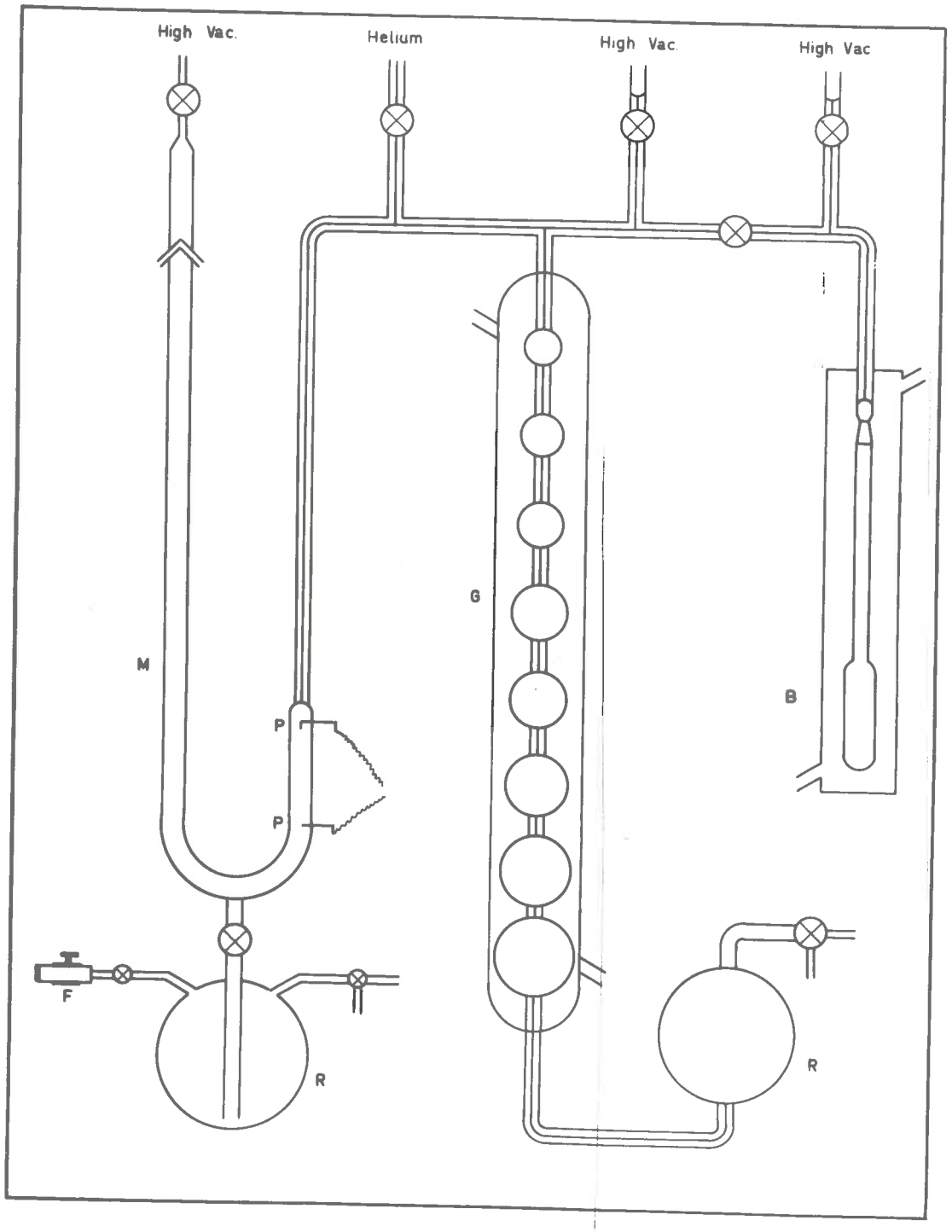

Fig. 19 - Helium Density Apparatus

KEY TO FIGURE 19

Helium Density Apparatus

B. Sample bulb (volume V_B)

E. 'Magic Eye' indicator

F. Fine adjustment control

G. Gas burette (volume V_S)

M. Mercury manometer

P. Tungsten reference point and contacts

R. Mercury reservoirs

Volume Calibration It was necessary to first calibrate the volumes of the gas burette V_S, the free space V_F and the bulb volume V_B.

Gas Burette Volume V_S Values of the cumulative bulb volume from the top mark of the gas burette to successive marks between the bulbs were

2.638	c.c.
6.536	c.c.
13.002	c.c.
19.590	c.c.
32.183	c.c.
44.521	c.c.
73.856	c.c.
104.883	c.c.

These volumes were calibrated[124] directly with mercury before the gas burette was attached to the apparatus. Errors involved in the measurements amounted to less than 0.005 c.c.

Free Space Volume V_F This volume was contained in the capillary tube between the top of the bulb B_9 the manometer and the first mark at the top of the gas burette. As this volume had to be calibrated indirectly and was subject to ambient temperature variations, it was kept to a minimum.

The volume was measured by admitting helium to the system and determining the pressure for a series of expansions obtained by lowering the mercury level in the gas burette to successive marks. From the ideal gas laws

$$\frac{p V_S}{T_S} + \frac{p V_F}{T_A} = \text{constant},$$

where T_S and T_A refer to the temperature of the burette jacket and the ambient temperature, respectively. A plot of $\frac{p V_S}{T_S}$ versus

p/T_A yielded a straight line of slope V_F = 8.34 c.c.

Temperature Control and Measurement The gas burette and adsorbant bulb were water jacketed to a constant temperature of 30$\pm$ .02°C. An air-conditioning unit maintained the ambient temperature of the room to approximately $\pm$ 1°C. Temperatures were measured with mercury in glass thermometers.

3.6.2 Experimental Procedure

The carbon sample was loaded into bulb B and degassed at 350°C under a pressure of less than 10^{-5} mm. of mercury for approximately 24 hours. The sample was then cooled and bulb B surrounded by a water jacket.

The dead space volume V_D, or the volume of the bulb apart from the volume taken up by the carbon sample, was determined by a series of gas expansions and pressure measurements. From the ideal gas law

$$\frac{p V_S}{T_S} + \frac{p V_F}{T_A} + \frac{p V_D}{T_B} = \text{constant.}$$

Thus a plot of $\left(\frac{p V_S}{T_S} + \frac{p V_F}{T_A} \right)$ against p/T_B yields a straight line of slope $-V_D$. Subtraction of V_D from V_B yields the volume of the carbon sample as measured by the displacement of helium.

It was also necessary to accurately determine the true weight of the carbon sample. Under normal atmospheric conditions, a carbon of high surface area was found to adsorb up to one third of its weight of water vapour from the atmosphere. Hence at the completion of a density run, the bulb (containing the sample) was quickly transferred to a balance and weighed. Knowing the weight of the empty bulb B and assuming that the weight of helium in the bulb was negligible, the true weight of the carbon sample could be

obtained by difference.

3.7 Mercury Density Determination

The mercury density of a substance is determined from the volume of mercury displaced by a known weight of substance. Mercury possesses a high surface tension and a contact angle greater than 90° for carbon; hence it should only outline the particle shape of the carbon at atmospheric pressure. However, Juhola and Wiig[134] observed that the interstices between particles were not completely filled with mercury at atmospheric pressure. A pressure of 900 mm., for example, was required to effectively outline 30 mesh smooth glass spheres with mercury.

3.7.1 Apparatus

An apparatus similar to that used by Juhola and Wiig[134] was built to measure the amount of mercury forced into a bulb containing the carbon under a pressure of 0 to 120 cm. of mercury. A diagram of the apparatus is shown in Fig. 20. The main feature of this apparatus is the use of diaphragm taps manufactured by Springham Ltd., England. The diaphragm is made of Viton A rubber which does not contaminate the mercury. These taps provided an excellent seal for mercury and allowed fine control of the movement of mercury during the experiment.

3.7.2 Experimental Procedure

The reservoir F was initially filled with freshly distilled and degassed mercury. The adsorbent was loaded into bulb B and evacuated at a temperature of 350°C under high vacuum for approximately 4 hours. On cooling to room temperature, tap 1 was closed and mercury allowed to flow from the reservoir into the rest of the system up to the level of the marks C and A. Tap 4 was closed and mercury allowed to slowly flow through tap 2 to enter the bulb B. The pressure at G and H was increased so that the average pressure in the bulb B was 900 mm. The volume of mercury entering

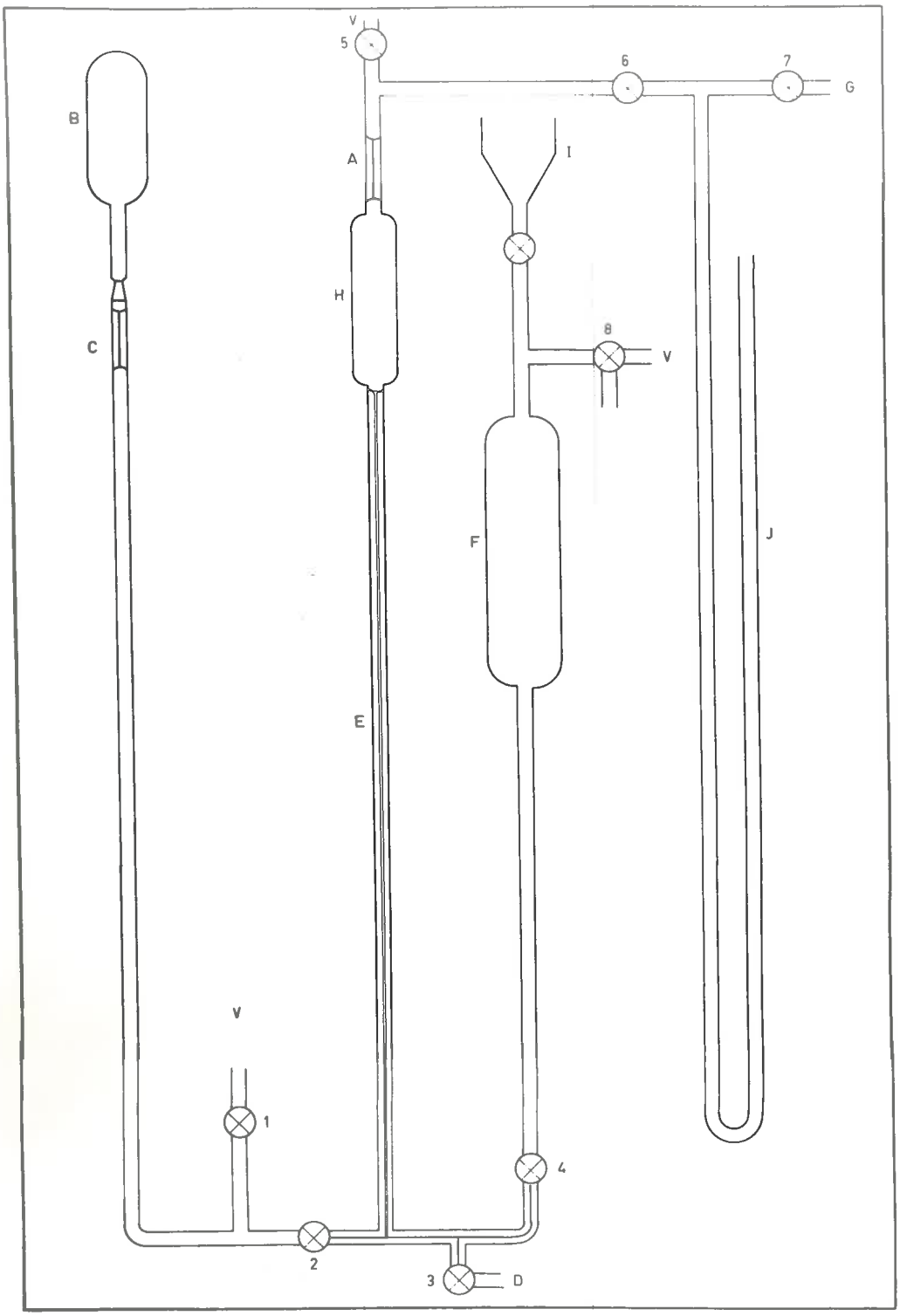

Fig. 20 - Mercury Density Apparatus

KEY TO FIGURE 20

Mercury Density Apparatus

A. Calibrated capillary with set point
B. Adsorbent bulb with socket joint
C. Capillary with set point
D. Mercury outlet
E. Long calibrated capillary
F. Mercury reservoir
G. Connection to high pressure cylinder
H. Calibrated mercury reservoir
I. Mercury filling funnel
J. Mercury manometer
V. Connection to high-vacuum line

Taps 1.2.3.4. - Springham One-Way Diaphragm
Taps 6.7. - Pyrex One-Way
Taps 5.8. - Pyrex Two-Way

the bulb B was measured by the change in level in the capillary burette E. Using a cathetometer to detect this change in level, the amount of mercury entering the bulb B could be estimated to an accuracy of at least 0.001 cm. The bulk volume of the adsorbent was calculated as the difference between the volume of the empty bulb B and the volume of mercury that entered the bulb B containing the adsorbent.

Some dimensions of the apparatus are:

Volume of the bulb B	$\sim$10 c.c.
Volume of reservoir H	$\sim$7 c.c.
Diameter of capillaries C and A	= 0.75 mm.
Diameter of capillary E	= 1.5 mm.

3.8 High Pressure Mercury Penetration Measurements

The measurements were performed on the high pressure mercury porosimeter at the Australian Atomic Energy Commission Establishment at Lucas Heights, New South Wales. This particular instrument is similar in design to that of Ingles[140] in which pressures up to 40,000 p.s.i. are applied to a carbon specimen immersed in mercury by a high pressure ram through the medium of silicone oil (DC.200). The carbon specimen is immersed in mercury contained in the glass bulb B shown in Fig. 21. A precision glass syringe, comprising barrel and plunger, is attached to the glass bulb via a ground glass joint. As the mercury is forced into the pores, the syringe plunger SP moves down and is followed by the soft iron rod SF. The movement of SF induces a change in the voltage across the linear variable differential transformer, so that the movement of SP can be calibrated as a function of the voltage reading on a multi-range galvanometer. The syringe and bulb are located in a brass housing after which the assembly is placed in a high tensile steel cylinder.

A sample of carbon was placed in the glass bulb, the

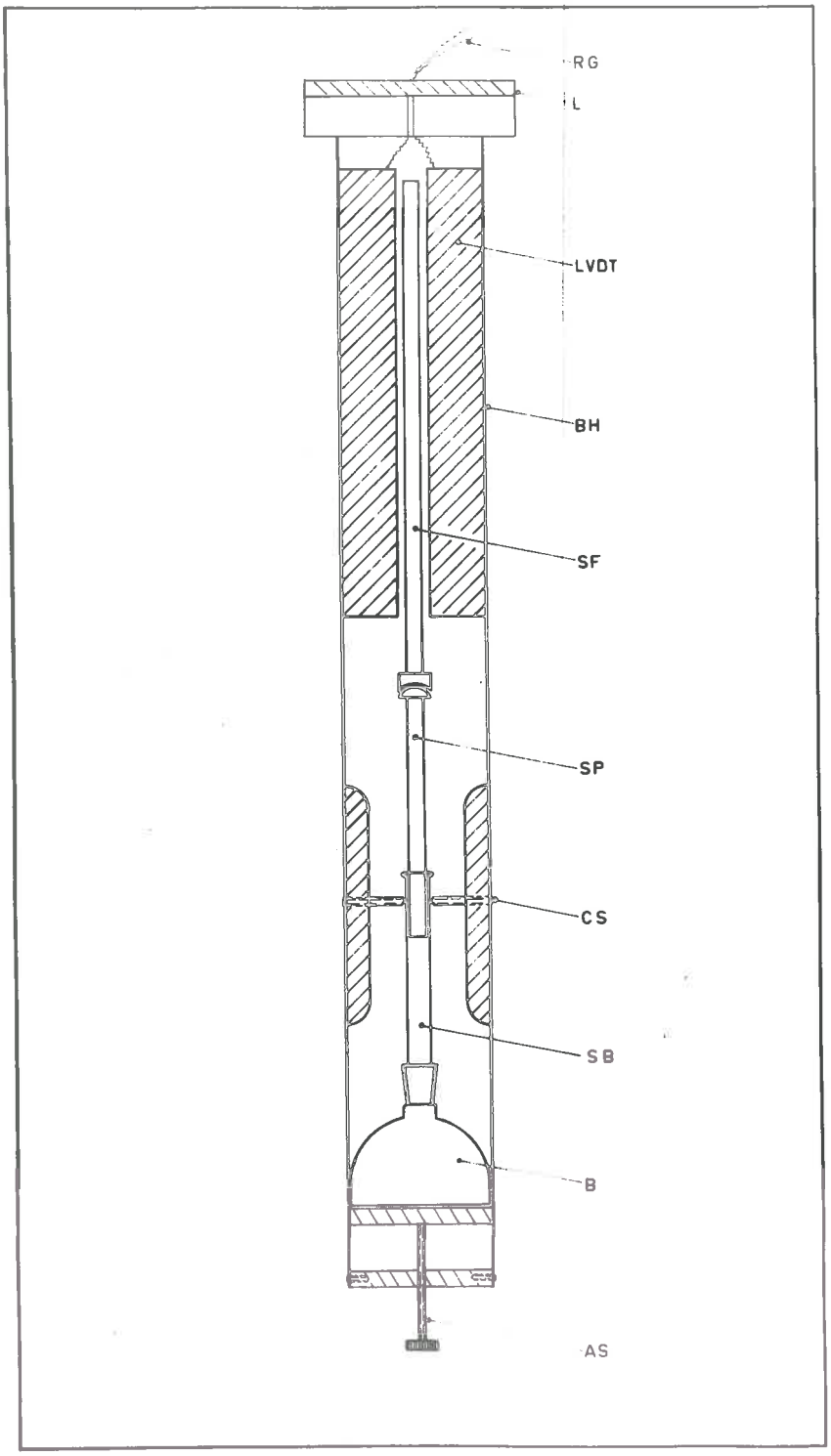

Fig. 21 - Brass Housing and Assembly for the High Pressure Mercury Porosimeter

KEY TO FIGURE 21

Brass Housing and Assembly for the High Pressure Mercury Porosimeter

B.	Glass bulb
SB.	Syringe Barrel
SP.	Syringe plunger
CS.	Centering screws
SF.	Steel follower
LVDT.	Linear variable differential transformer
BH.	Brass housing
RG.	Rubber gasket
L.	Leads from LVDT
AS.	Height adjusting screws

syringe barrel attached and the sample pumped under a vacuum of 10^{-5} mm. of mercury at a temperature of approximately 350°C for at least 12 hours. After cooling to room temperature, degassed mercury was syphoned into the glass bulb to a level near the top of the syringe barrel. The glass bulb and syringe barrel were then removed from the vacuum system and the plunger carefully inserted into the barrel. The bulb and syringe were then centred in the brass housing and the assembly placed in the high tensile steel cylinder. The zero reading on the galvanometer was noted and the pressure increased in steps up to a maximum of 40,000 p.s.i. In this manner measurements were obtained for the cumulative pore volume at various pressures. Generally, equilibrium was reached within at least 30 minutes.

3.9 Influence of Particle Size on the Adsorptive Capacity of Sintered Carbons

Samples of cellulose acetate carbon CA-800 and CA-1700 were ground in an agate mortar to pass a 200-mesh sieve. Argon adsorption isotherms were then measured at liquid nitrogen temperatures on these samples by the methods already outlined in Section 3.5.1.

3.10 Measurement of the Permeability of Sintered Carbons

As compressed cellulose discs retain their shape on carbonization, it was initially hoped that the carbonized discs could be suitably mounted to allow measurement of the permeability.

Experimental Procedure

A carbonized cellulose disc was carefully mounted in a recess in the end of a steel tube with Apiezon wax W. This method of mounting, although crude, has been very successfully used in the department for low temperature - low pressure permeability experiments with graphite.

The results of preliminary permeability measurements immediately indicated the presence of large pores and an examination

of the discs under a microscope revealed a number of peripheral cracks directed towards the centre of the disc. Further discs were slowly carbonized over a period of two days, but despite careful preparation, it was apparent that stresses produced during carbonization had again been relieved by the formation of peripheral cracks. This line of investigation was therefore discontinued.

3.11 Measurement of Rates of Adsorption

The rate of adsorption of argon on the heat treated carbons was measured gravimetrically using the Sartorius Microbalance described in Section 3.5.1. The uptake of argon was measured at constant pressure and temperature.

(a) Weight Measurement

The change in weight was recorded by a Leeds and Northrup potentiometric chart recorder directly connected to a take-off point on the Microbalance. The characteristics of the recorder were:

(1) Speed of response : 1 sec. for full scale deflection.
(2) accuracy rating : ± 0.3% of span.
(3) range : 10 mV.
(4) dead band : 0.15% of span.
(5) chart width : 10"
(6) chart speed : 60" per hr.

(b) Pressure Control and Measurement

The balance and the adsorbent were connected to a 40 ℓ. ballast so the decrease in pressure during a run was practically negligible. Large diameter glass tubing of 15 to 20 mm. bore connected the ballast to the balance so that the pressure change in the balance case reached the equilibrium value very soon after opening tap T14 (see Fig. 11).

The pressure was measured by a McLeod gauge and U-tube mercury manometer, as for adsorption isotherms. A cold trap

between the manometer and the balance case prevented back diffusion of mercury into the balance.

(c) Temperature Control and Measurement

The following constant temperature baths were employed:

(1) dry-ice / acetone mixture; temp. approx. -81°C.
(2) liquid oxygen ; temp. approx. -183°C.
(3) liquid nitrogen ; temp. approx. -196°C.

The temperature coefficient of the rates of adsorption was fairly low so that very accurate control of the bath temperatures was unnecessary. The temperature of the well-stirred dry-ice / acetone mixture did not vary by more than ± 0.5°C over the 30 minute period of the rate run. The variation in the temperature of the liquid oxygen bath was ± 0.1°C over a 1 to 4 hour period, and the corresponding variation of the liquid nitrogen bath was ± 0.2°C.

The choice of temperature was dictated by the adsorptive capacity of the carbon. For cellulose acetate carbons, the adsorptive capacity at 0°C was so low that accurate rate measurements could not be obtained. Similarly, for polyvinylidene chloride carbons, the adsorptive capacity was too low for measurements above -183°C.

The temperatures of the liquid oxygen and liquid nitrogen baths were measured with the oxygen vapour pressure thermometer used to measure temperatures for adsorption isotherms. The temperature of the dry-ice / acetone mixture was measured with a pentane thermometer to an accuracy of ± 0.5°C.

(d) Experimental Procedure

The sample was initially outgassed at 350°C under high vacuum for 24 hr. Constant temperature baths were then placed around both balance tubes to maintain them at the same temperature. The sample was allowed to reach the bath temperature over a period of one hour. The ballast pressure was adjusted to a predetermined

value for the first step, the connecting tap quickly opened and the recorder chart started. Usually the pressure fluctuation only affected the balance reading for the initial 30 seconds. When equilibrium was reached, the connecting tap was closed and a slightly higher pressure built up in the ballast. The above procedure was then repeated. In this manner a series of adsorption steps were obtained corresponding to the pressure steps $p_1 - p_2$, $p_2 - p_3$, $p_3 - p_4$, etc. Crank[147] has termed this procedure "the progressive sorption experiment".

The size of a step pressure change was determined by the smallest amount adsorbed that could be accurately recorded. Usually the total weight change was restricted to 200 or 400 μg. However, for purposes of analyzing the rate process, considerably larger steps were made in some experiments.

Rates of desorption were also measured in several experiments. The same techniques were used except that the ballast pressure was reduced before the beginning of each step.

3.12 X-ray Diffraction Measurements on Carbons

It has been suggested that crystallite growth on heat treatment was in some manner responsible for loss in surface area[99]. It was, therefore, important to measure the increase in the crystallite dimensions of carbon on heat treatment.

3.12.1 X-ray Diffraction Apparatus

Investigations of carbon black structures by Alexander and Sommer[107], Austin[36], and Warren[6], have shown that X-ray diffractometer measurements can equal or surpass the accuracy of the older method of X-ray powder photograph measurement. A Philips X-ray generator, type PW1009, equipped with interchangeable copper and molybdenum targets and their respective nickel and zirconium filters provided the source of Cu$K\alpha$ and Mo$K\alpha$ radiation. A para-focusing goniometer (radius 10"), manufactured by Crystal Structures Ltd., was used with the normal sets of vertical slits and horizontal

Soller slits. A beam collimator with a slit width of 1° and a detector slit width of 0.25° provided sufficient intensity. The detector for the CuKα radiation was a Philips proportional counter and for the MoKα radiation a General Electric scintillation counter. A pulse height analyzer helped considerably to filter out undesired pulses, such as those resulting from circuit noise and background radiation. The intensity was recorded as a function of the diffractometer angle on a strip chart recorder with a 1 second response time. A goniometer scanning speed of 22° 2θ per hour gave an 8" trace on the chart recorder. The time constant and the count rate were adjusted to suit the peak breadth and intensity of each specimen. Most of the specimens gave broad peaks and the lag in recorder trace was found by experiment to be insignificant.

3.12.2 Specimen Preparation

Carbon has a very low coefficient of absorption of X-rays and it is therefore important to have a sufficiently thick sample to fully absorb the incident beam. The thickness of the sample for maximum intensity is given by[101]

$$t \geqslant \frac{3.2\rho}{\mu\rho'} \sin\theta$$

where ρ = density of the solid material,

ρ' = density of the powdered material, and

μ = linear absorption coefficient of the solid material.

The sample was finely ground in an agate mortar and packed into a rectangular cavity of dimensions 2 x 0.8 x 0.4 cm. in a flat steel holder, the procedure for packing and mounting of the specimen being very similar to that used by McCreery[192]. Alexander and Sommer[107] have already shown theoretically and experimentally that the use of thick samples does not appreciably alter the position or breadth of diffraction lines.

3.12.3 Calibration of Diffractometer

Specimens of pure tungsten and sodium chloride were used to obtain values of instrument broadening as a function of $2\theta^{\circ}$. The line broadening due to the unresolved $K\alpha$ doublet was neglected, thus line broadening at specific angles could be obtained by interpolation. In addition, the tungsten and sodium chloride specimens provided a check on the accuracy of the angular marker on the goniometer. Despite the rather poor design of this angular marker, angles could be interpolated from the chart to an accuracy of $\pm 0.05^{\circ}$ 2θ.

4. RESULTS

4.1 Chemical Analysis of Carbons

Results of the chemical analysis of the carbons are shown in Fig. 22.

For the polyvinyl chloride carbon, the quantities of hydrogen and chlorine are soon reduced to less than 0.1%, while, for the other carbons, these impurities are apparently much harder to remove. The other interesting point is that at 800°C, both the polyvinylidene chloride and the polyvinyl chloride carbons contain, respectively, 16 and 3 % of oxygen, despite the original polymers being oxygen free and the carbonization being carried out under nitrogen. As suggested by Kipling[40], the carbons must react with the oxygen when they are exposed to the atmosphere at room temperature.

4.2 Weight Loss Measurements

The amount of gas evolved in g. per g. of carbon is shown in Fig. 23, for the three heat treatment steps II, III and IV, Section 3.4. The curves are labelled according to the experimental procedure mentioned in Section 3.4. The argon isotherms obtained in steps I and II are shown in Fig. 24 and are labelled accordingly.

The results of the preliminary experiments in step I, involving cycling the carbon at 350°C and measuring the argon adsorption isotherms, gave no evidence of any change in the amount adsorbed. This confirms the generally accepted view[120] that heating a carbon to 350°C provides a stable surface for adsorption measurements.

The argon isotherms for the samples degassed at 350° and 900°C, respectively, (Fig. 24) show that the amount of gas evolved has little effect on the adsorptive capacity.

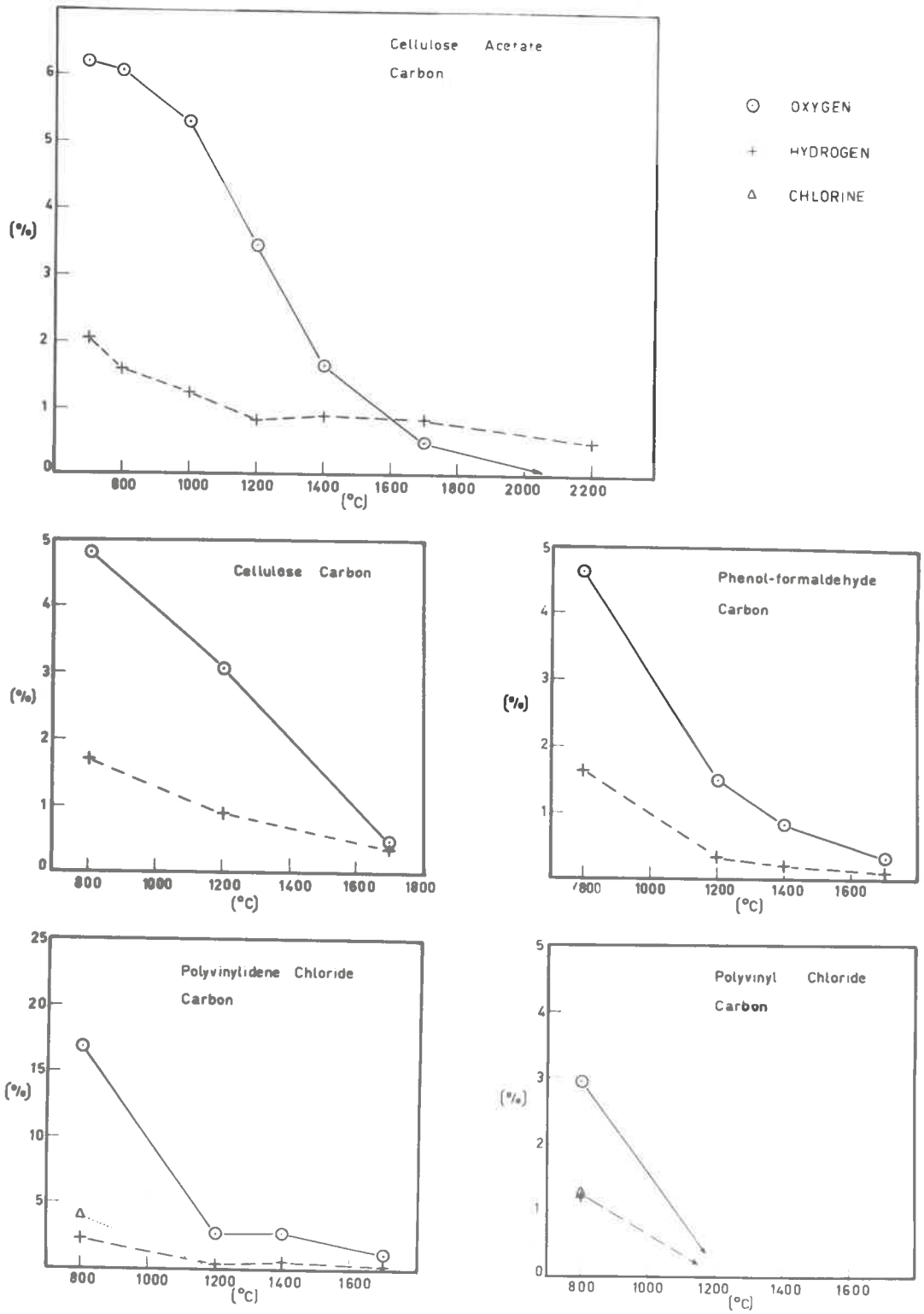

Fig. 22 - Chemical Composition of Heat Treated Carbons

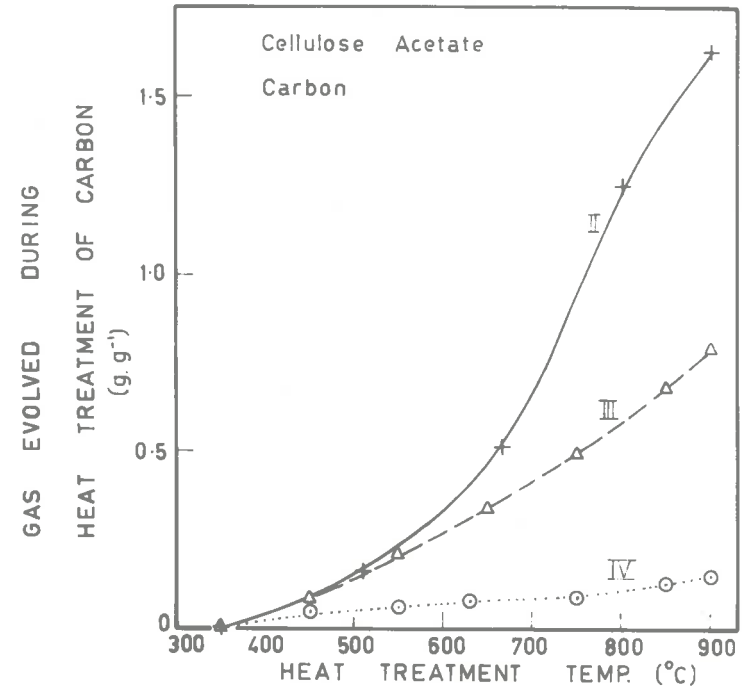

Fig. 23 - Evolution of Gases During the Heat Treatment of Cellulose Acetate Carbons

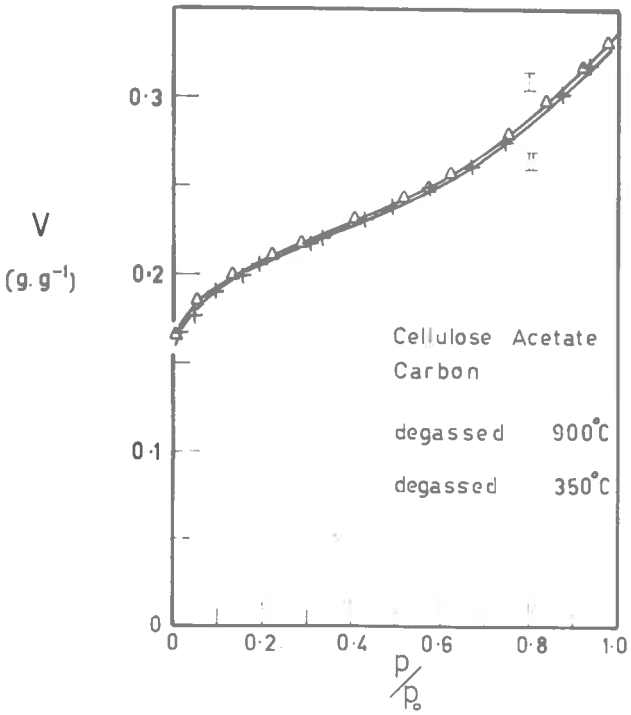

Fig. 24 - Argon Isotherms on Cellulose Acetate Carbons Degassed at 350° and 900°C

4.3 Isotherm Data

All the isotherm data refer to one particular sample of carbon, e.g. only one sample of CA-800 was used for the determination of isotherms using various adsorbates at various temperatures. For the same sample, reproducibility of the isotherms was 0.25%.

(a) Argon and Nitrogen

Argon and nitrogen isotherms for the carbons

(1) CA-700, CA-800, CA-1000, CA-1200, CA-1400, CA-1700, CA-2200, CA-2600 and CA-2700,

(2) CEL-800, CEL-1200 and CEL-1700,

(3) PF-800, PF-1200, PF-1400 and PF-1700,

(4) SA-800, SA-1200, SA-1400, SA-1700 and SA-2200,

(5) SAA-900 and SAA-1700,

(6) PVC-800, PVC-1200 and PVC-1700, and

(7) CAL-original and CAL-1700

at -196°C are shown in Fig. 25 to 31, and the data are tabulated in APPENDIX C.1. For SA-1400 the rate of adsorption was so slow that only a few points on the isotherm were obtained.

For the cellulose acetate carbons CA-800, CA-1200 and CA-1700, the data for argon adsorption isotherms at temperatures between -183° and -196°C are tabulated in APPENDIX C.1.

(b) Organic Adsorbates

Isotherms for the adsorption of benzene on the cellulose acetate carbons CA-800, CA-1200 and CA-1700 at 40°C are shown in Fig. 32. Data for isotherms on these carbons at temperatures between 15° and 45°C are tabulated in APPENDIX C.2. Isotherms for the adsorption of n-butane, neo-pentane and p-cymene on CA-800, CA-1200 and CA-1700 are shown in Fig. 33 to 35, and the data are listed in APPENDIX C.3 to C.5.

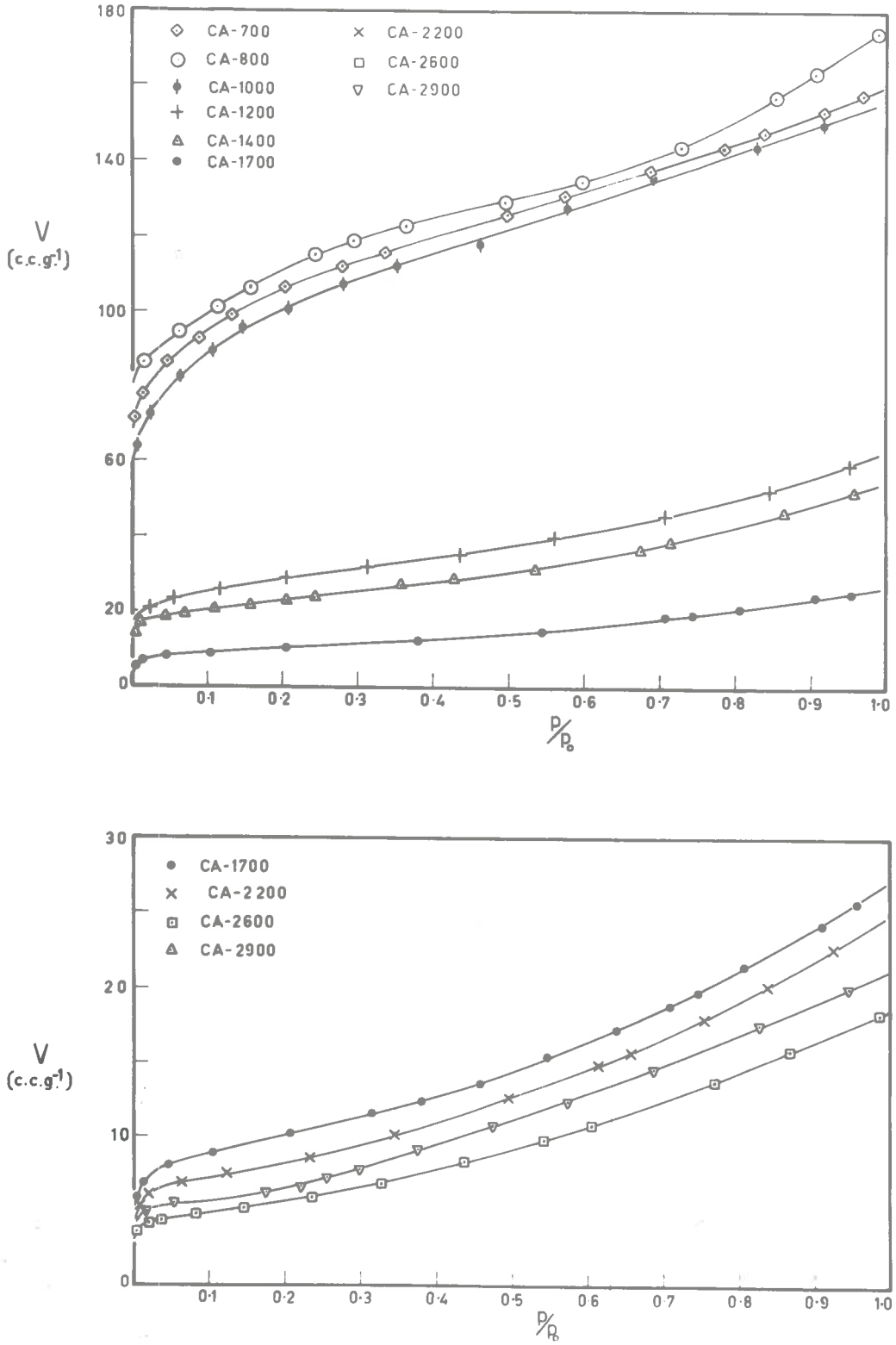

Fig. 25 - Argon Isotherms on Heat Treated Cellulose Acetate Carbons

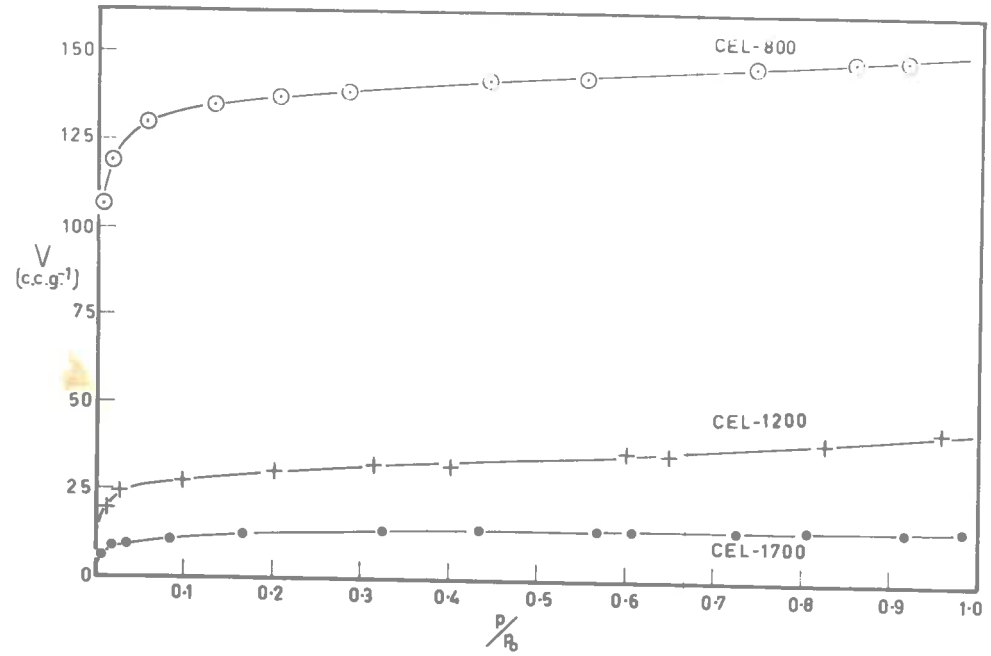

Fig. 26 - Nitrogen Isotherms on Heat Treated Cellulose Carbons

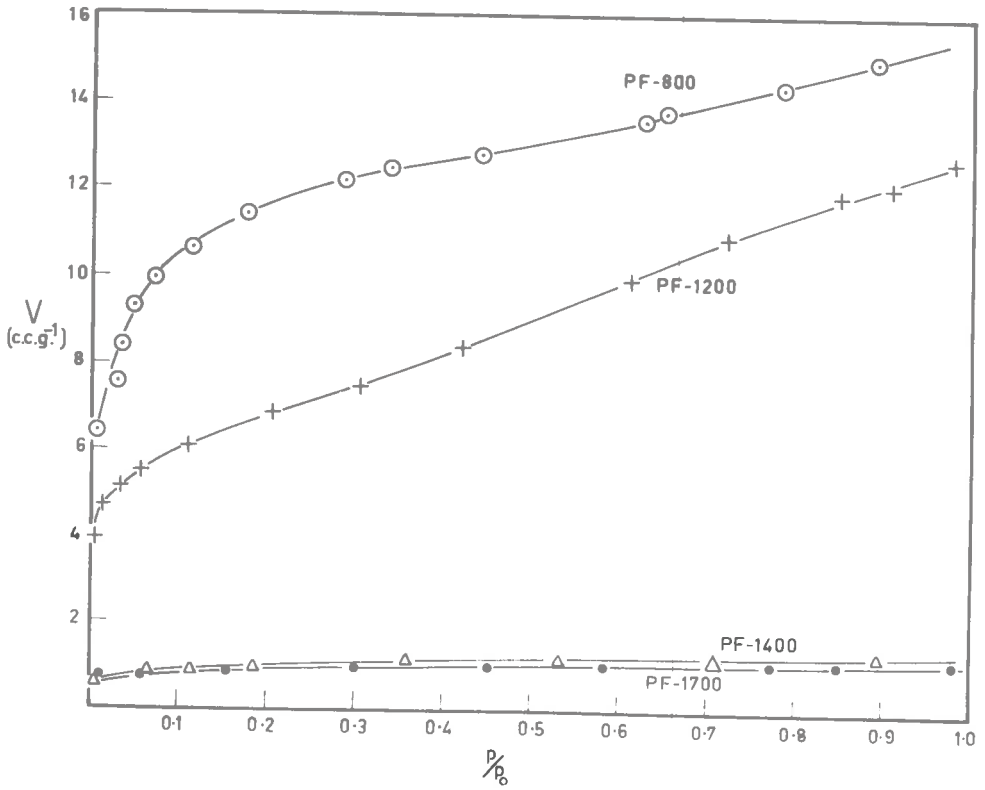

Fig. 27 - Argon Isotherms on Heat Treated Phenol-formaldehyde Carbons

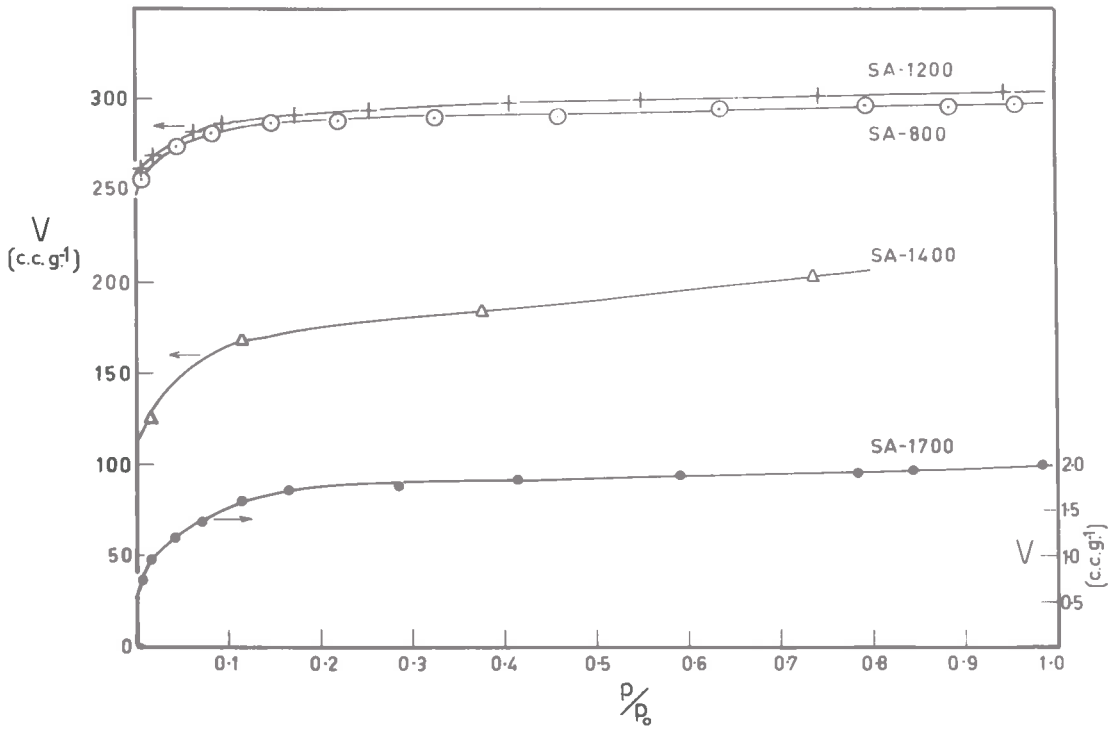

Fig. 28 - Argon Isotherms on Heat Treated Polyvinylidene Chloride Carbons

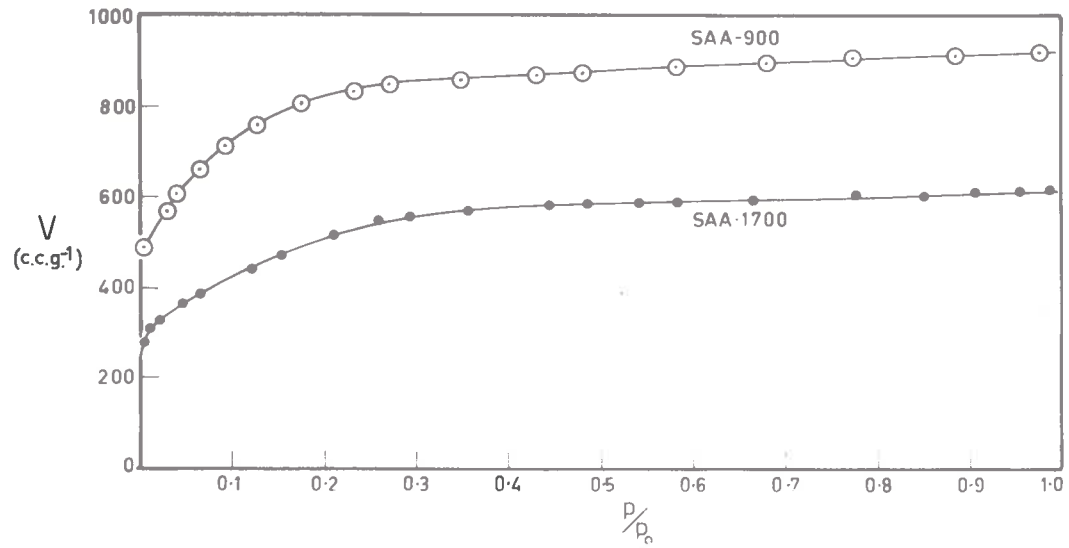

Fig. 29 - Argon Isotherms on Heat Treated Activated Polyvinylidene Chloride Carbons

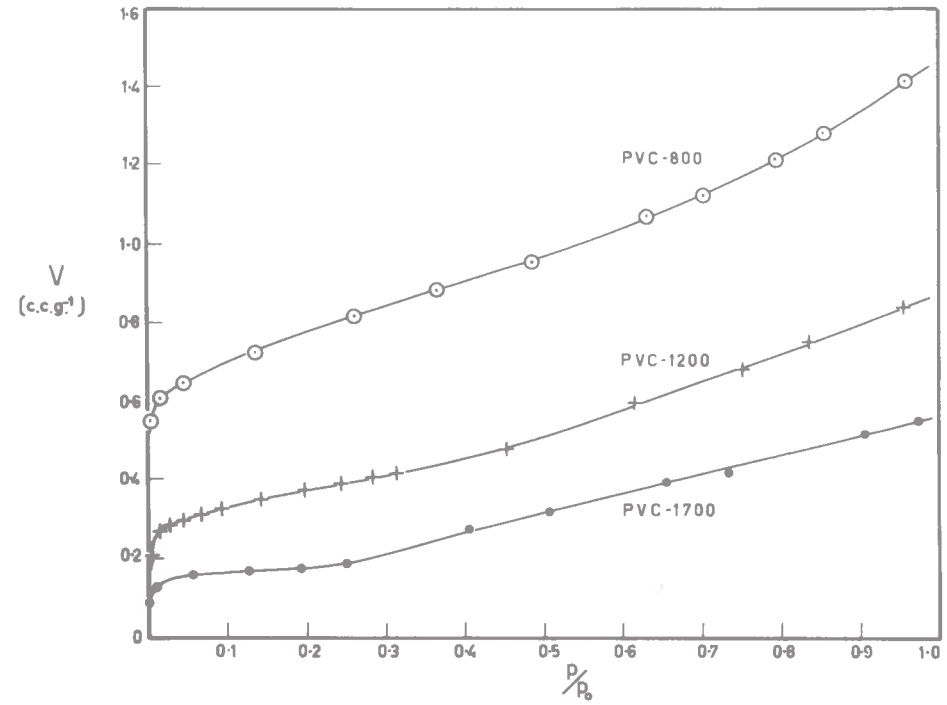

Fig. 30 - Argon Isotherms on Heat Treated Polyvinyl Chloride Carbons

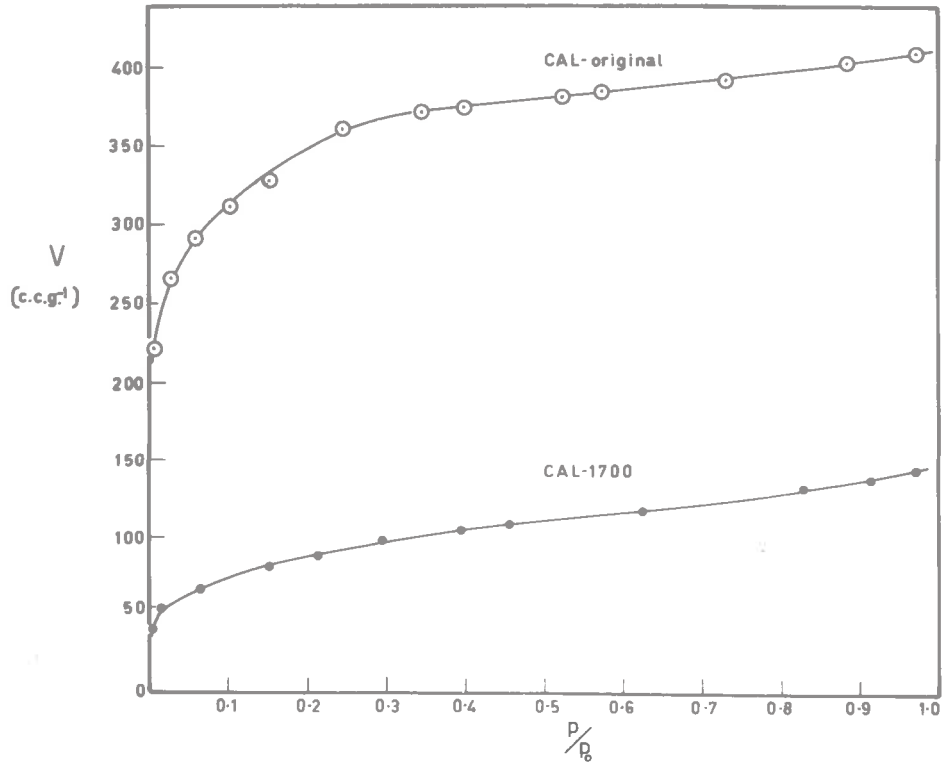

Fig. 31 - Argon Isotherms on Heat Treated Cal Carbons

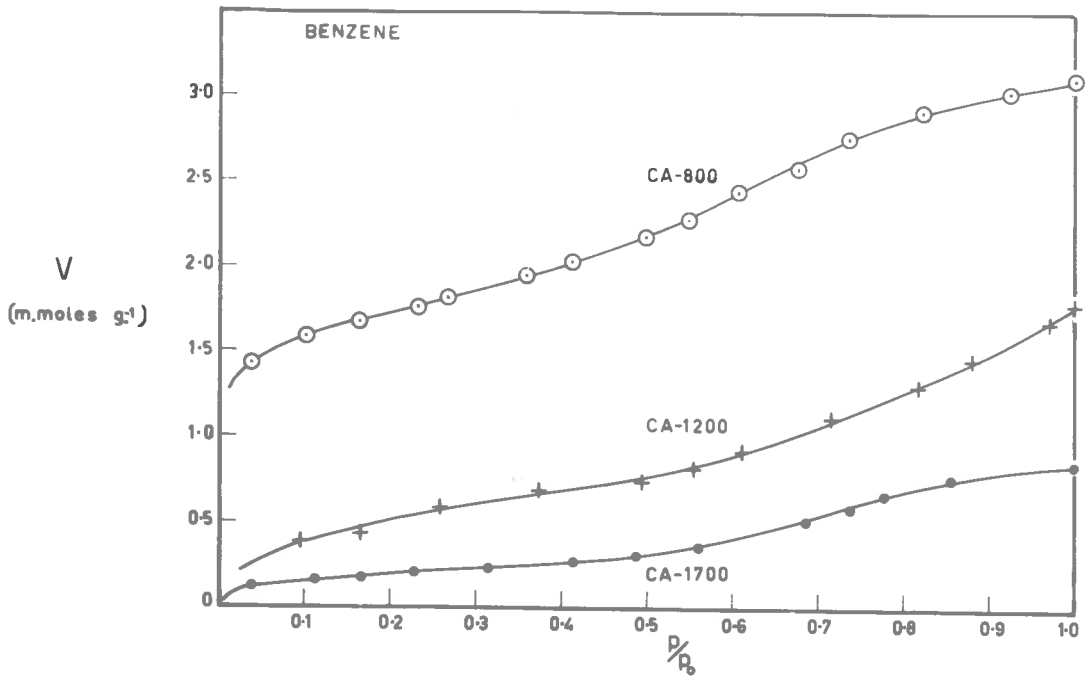

Fig. 32 - Benzene Isotherms at 40°C on Heat Treated Cellulose Acetate Carbons

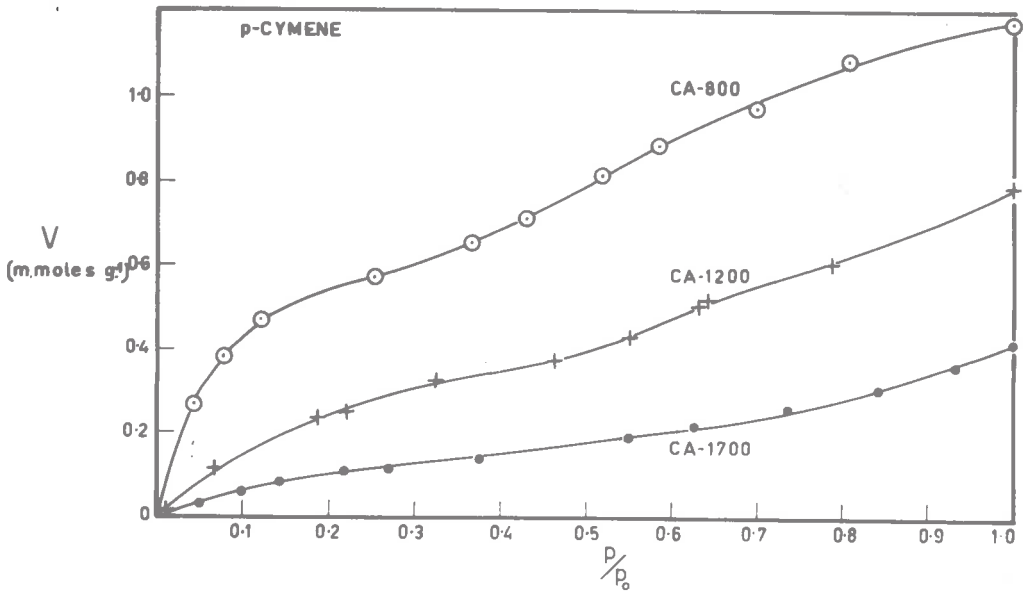

Fig. 33 - p-Cymene Isotherms at 45°C on Heat Treated Cellulose Acetate Carbons

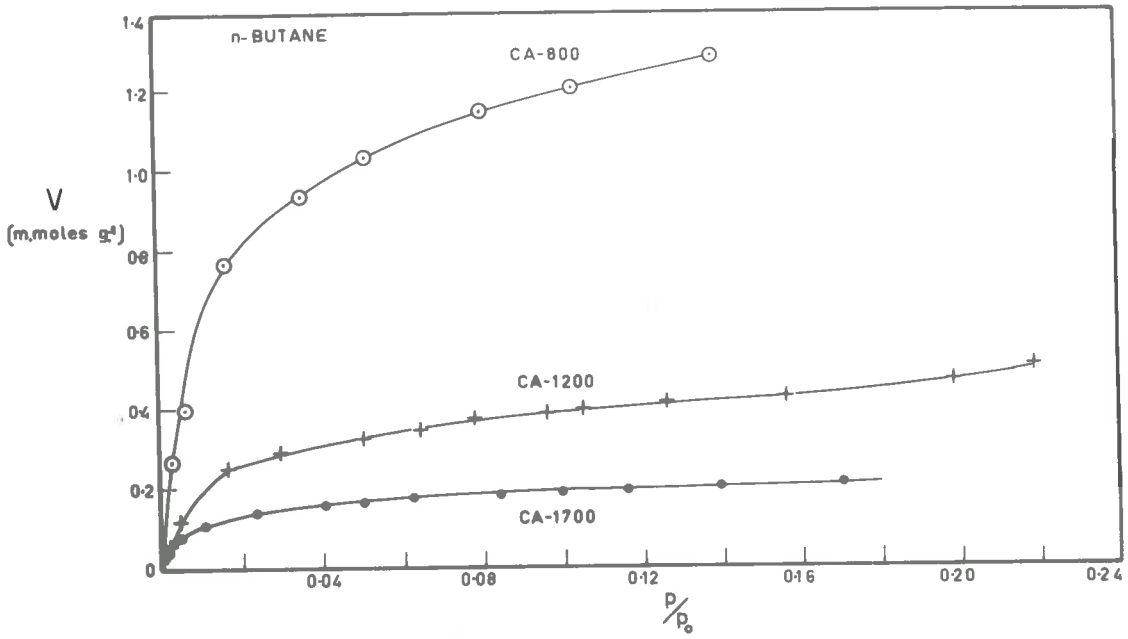

Fig. 34 - n-Butane Isotherms at 0°C on Heat Treated Cellulose Acetate Carbons

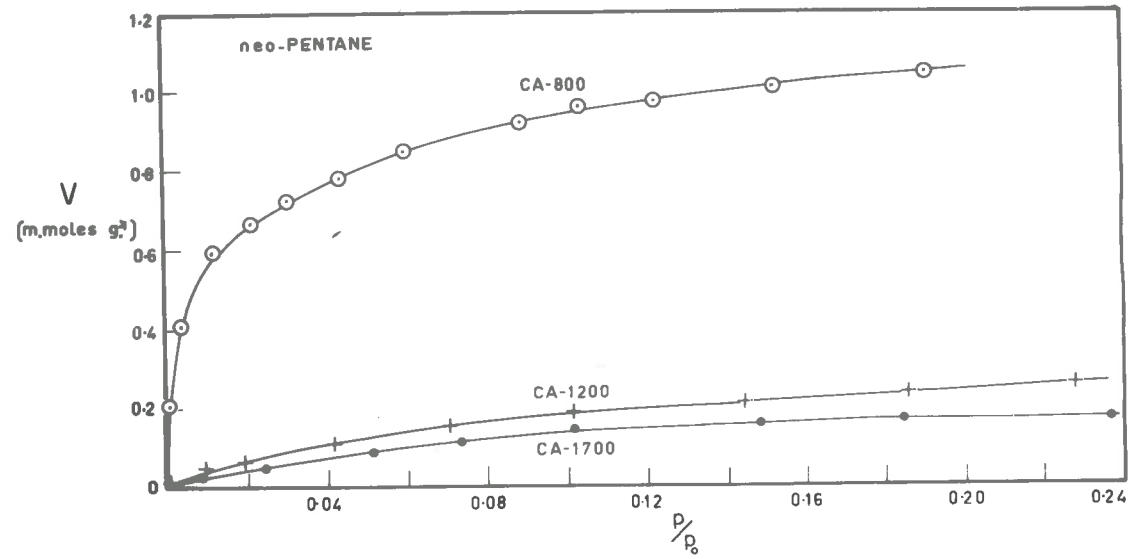

Fig. 35 - neo-Pentane Isotherms at 0°C on Heat Treated Cellulose Acetate Carbons

4.4 Surface Area Values

The data used for the calculation of monolayer capacities and surface areas were obtained from the argon and nitrogen isotherms at -196°C.

For the cellulose acetate, cellulose, phenol-formaldehyde and polyvinyl chloride carbons, the monolayer capacity V_m was determined from the normal form of the BET equation (equation (6)). However, the carbons possessing a high adsorptive capacity such as the polyvinylidene chloride carbons SA-800, SA-1200, SA-1400, SAA-800 and SAA-1700, and the Cal carbons CAL-800 and CAL-1700, all failed to yield reasonable straight lines for the plot of equation (6). Culver and Heath[124] attempted to fit equation (7) to the nitrogen isotherms of activated polyvinylidene chloride carbons, but found that the results were inconclusive and that the monolayer capacity was best obtained from the selection of Point B on the isotherms. Hence, for these high surface area carbons, the monolayer capacity was determined by the Point B method.

The values of the molecular area, σ_m, were those calculated from equation (8) using the density of the bulk liquid adsorbate at -195.8°C. The values of σ_m are

Argon : $\sigma_m = 14.0$ Å^2

Nitrogen : $\sigma_m = 16.2$ Å^2

The monolayer capacities and surface areas for the various carbons are collected in TABLE 3.

TABLE 3

Monolayer Capacities and Surface Areas of Sintered Carbons

Sample	Monolayer Capacity V_m ($c.c.g.^{-1}$)	Surface Area Σ ($m^2 g^{-1}$)
CA-700	84	316
CA-800	92	346
CA-900	91	342
CA-1000	81	304
CA-1200	23.5	91.5
CA-1400	18.2	68.5
CA-1700	8.0	30.4
CA-2200	6.5	24.2
CA-2600	4.5	17.0
CA-2900	5.5	20.8
CEL-800	130	565
CEL-1200 *	25.2	110
CEL-1700	7.61	32.9
PF-800	8.78	33.0
PF-1200	5.10	19.2
PF-1400	0.79	2.94
PF-1700	0.70	2.62
SA-800	285	1070
SA-1200	290	1090
SA-1400	170	639
SA-1700	1.75	6.6
SA-2200	0.20	0.75
SA-2600	0.03	0.1
SA-2900	0.03	0.1

Sample	Monolayer Capacity V_m (c.c.g.$^{-1}$P)	Surface Area Σ (m^2g^{-1})
SAA-900	860	3240
SAA-1700	560	2100
PVC-800	0.62	2.32
PVC-1200	0.28	1.04
PVC-1700	0.15	0.56
CAL-original	276	1000
CAL-1700	69.9	262

* Isotherm measured with nitrogen

4.5 Density Values

Helium Density As mentioned in Section 3.6, the helium density was obtained from the slope of the plot of $^{p}V_S/T_S + {}^{p}V_F/T_A$ against $^{p}/T_B$. Conventional graphical methods of determining the slope, however, were too inaccurate so a least squares method of analysis was used.

Values for the helium density for cellulose acetate, phenol-formaldehyde, polyvinylidene chloride, activated polyvinylidene chloride and polyvinyl chloride carbons are presented in TABLE 4 and the results plotted versus the heat treatment temperature in Fig. 36 to 39.

The estimated accuracy for any one determination was $\pm$ 0.005 g. c.c.$^{-1}$ while the results for any one carbon were reproducible to $\pm$ 0.01 g. c.c.$^{-1}$.

Mercury Density Values of the mercury density for cellulose acetate, phenol-formaldehyde, polyvinylidene chloride, activated

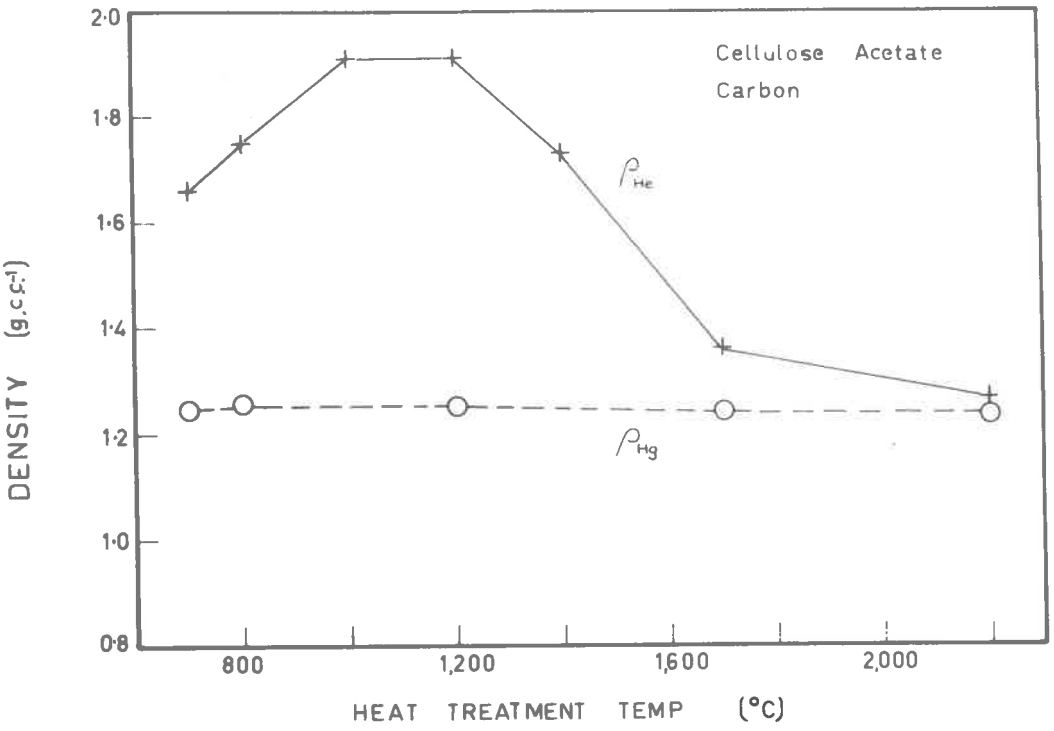

Fig. 36 - Helium and Mercury Densities on Heat Treated Cellulose Acetate Carbons

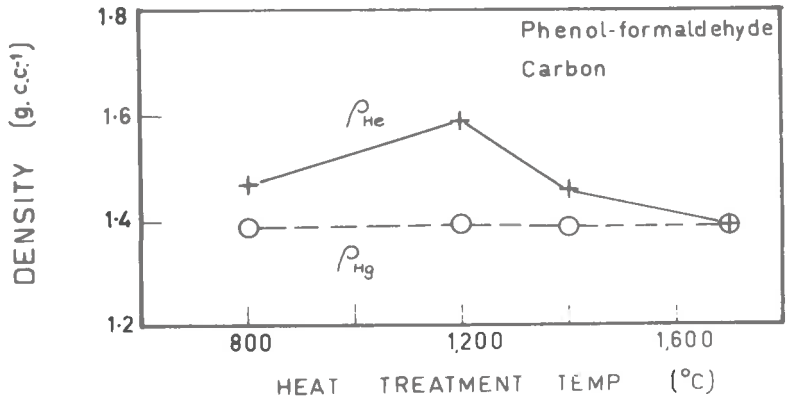

Fig. 37 - Helium and Mercury Densities on Heat Treated Phenol-formaldehyde Carbons

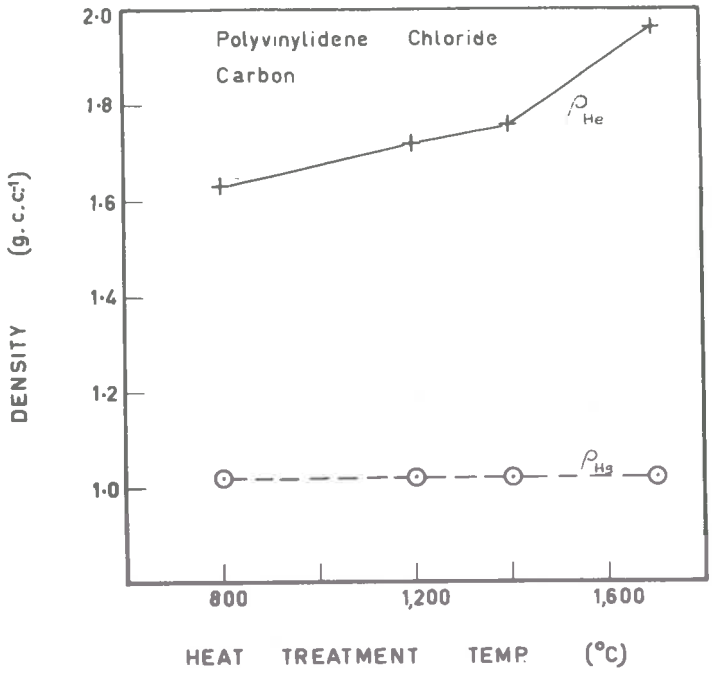

Fig. 38 - Helium and Mercury Densities on Heat Treated Polyvinylidene Chloride Carbons

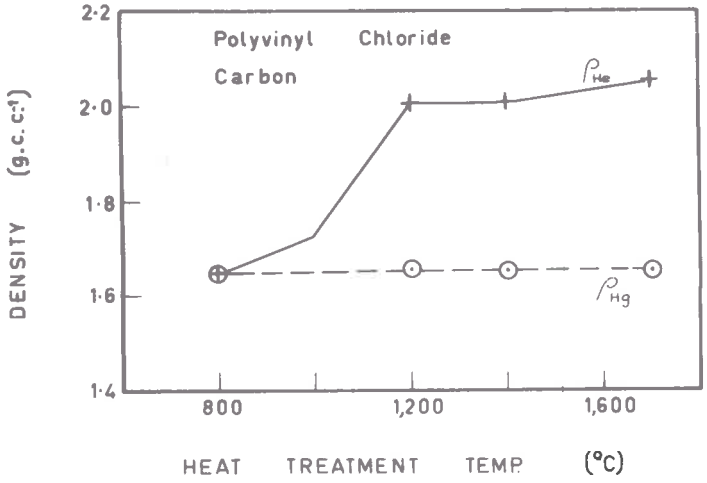

Fig. 39 - Helium and Mercury Densities on Heat Treated Polyvinyl Chloride Carbons

polyvinylidene chloride and polyvinyl chloride carbons are presented in TABLE 4, and the results plotted versus the heat treatment temperature in Fig. 36 to 39.

The estimated accuracy for any one determination was $\pm$ 0.001 g. c.c.$^{-1}$ while the results for any one carbon were reproducible to $\pm$ 0.005 g. c.c.$^{-1}$.

TABLE 4

Helium and Mercury Densities

Sample	Helium Density ρ_{He} (g. c.c.$^{-1}$)	Mercury Density ρ_{Hg} (g. c.c.$^{-1}$)
CA-700	1.66	1.250
CA-800	1.75	1.260
CA-1000	1.91	-
CA-1200	1.91	1.253
CA-1400	1.73	-
CA-1700	1.36	1.245
CA-2200	1.27	1.238
CA-2600	1.31	-
CA-2900	1.29	-
PF-800	1.47	1.392
PF-1200	1.59	1.397
PF-1400	1.46	1.388
PF-1700	1.39	1.390
SA-800	1.63	1.021
SA-1200	1.66	1.020
SA-1400	1.76	1.020
SA-1700	1.96	1.020

Sample	Helium Density ρ_{He} (g. c.c.$^{-1}$)	Mercury Density ρ_{Hg} (g. c.c.$^{-1}$)
SAA-900	2.24	0.635
PVC-800	1.65	1.660
PVC-1000	1.73	-
PVC-1200	2.01	1.655
PVC-1400	2.01	1.653
PVC-1700	2.05	1.654

4.6 Pore Volumes

The pore volume was calculated by two methods. Firstly, a value of V_p for the pore volume can be obtained from the equation

$$V_p = \frac{1}{\rho_{Hg}} - \frac{1}{\rho_{He}} \quad . \quad . \quad . \quad (28)$$

One of the main difficulties with this method is that the subtraction of two very similar figures is involved, so the total error now becomes the sum of the individual errors. In addition, because a mercury density determination does not allow the sample to be recovered uncontaminated, different samples of the carbon under investigation have to be used for the mercury and helium density determinations. The total error under these conditions could amount to $\pm$ 0.02 c.c. g.$^{-1}$.

The second method of calculating the pore volume assumes that at $p/p_o = 1.0$ on the adsorption isotherm the adsorbate completely fills the pore volume in the form of capillary condensate. Using the density of liquid argon at the temperature of the isotherm, the volume of liquid argon adsorbed can be calculated; this yields the value for the pore volume V_{SL}.

Values of V_p and V_{SL} for cellulose acetate, cellulose, phenol-formaldehyde, polyvinylidene chloride, activated polyvinylidene chloride, polyvinyl chloride and Cal carbons are listed in TABLE 5. Values of V_p and V_{SL} for cellulose acetate and phenol-formaldehyde carbons are plotted against the heat treatment temperature in Fig. 40 and 41.

TABLE 5

Pore Volumes calculated from Density and Isotherms Measurements

Carbon	V_p (c.c. $g.^{-1}$)	V_{SL} (c.c. $g.^{-1}$)
CA-700	0.20	0.195
CA-800	0.22	0.210
CA-900	-	0.203
CA-1000	0.27	0.191
CA-1200	0.27	0.078
CA-1400	0.22	0.067
CA-1700	0.06	0.033
CA-2200	0.01	0.030
CA-2600	0.03	0.022
CA-2900	0.02	0.026
CEL-800	-	0.236
CEL-1200	-	0.067
CEL-1700	-	0.023

Carbon	V_p (c.c. g.$^{-1}$)	V_{SL} (c.c. g.$^{-1}$)
PF-800	0.04	0.019
PF-1200	0.07	0.016
PF-1400	0	$0.017.10^{-1}$
PF-1700	0	$0.015.10^{-1}$
SA-800	0.36	0.361
SA-1200	0.38	0.371
SA-1400	0.41	0.255
SA-1700	0.47	$0.237.10^{-2}$
SA-2200	-	$0.240.10^{-3}$
SAA-900	1.13	1.12
SAA-1700	-	0.741
PVC-800	0	$0.180.10^{-2}$
PVC-1000	0.02	-
PVC-1200	0.11	$0.107.10^{-2}$
PVC-1400	0.11	-
PVC-1700	0.12	$0.693.10^{-3}$
CAL-original	-	0.376
CAL-1700	-	0.176

4.7 Pore Size Calculations

4.7.1 Average Pore Radius

Assuming that the pores are cylindrical, an average pore radius $\bar{r}_p$ can be calculated from the equation

$$\bar{r}_p = \frac{2 V_{SL}}{\sum} \qquad \cdot \quad \cdot \quad \cdot \qquad (29)$$

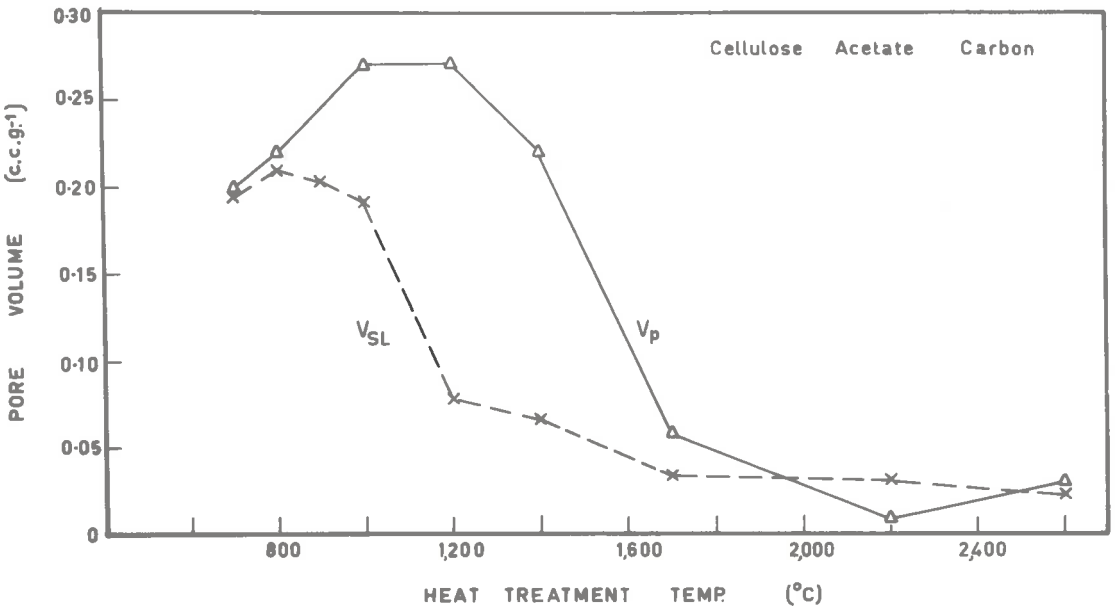

Fig. 40 - Pore Volumes V_p and V_{SL} for Heat Treated Cellulose Acetate Carbons

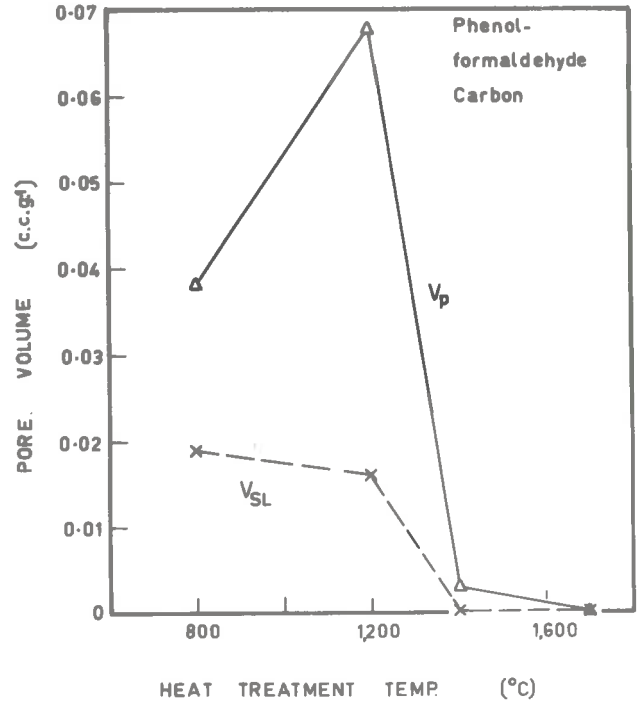

Fig. 41 - Pore Volumes V_p and V_{SL} for Heat Treated Phenol-formaldehyde Carbons

Values of $\bar{r}_p$ for cellulose acetate, cellulose, phenol-formaldehyde, polyvinylidene chloride, activated polyvinylidene chloride, polyvinyl chloride and Cal carbons are listed in TABLE 6.

TABLE 6

Average Pore Radii

Sample	Surface Area $\sum$ ($m.^2\ g.^{-1}$)	Pore Volume V_{SL} ($c.c.\ g.^{-1}$)	Average Pore Radius $\bar{r}_p$ (Å)
CA-700	316	0.195	12.6
CA-800	346	0.210	12.1
CA-1000	304	0.191	12.5
CA-1200	91.5	0.078	17.05
CA-1400	68.5	0.067	19.5
CA-1700	30.4	0.033	21.8
CA-2200	24.2	0.030	25.1
CA-2600	17.0	0.022	25.8
CA-2900	20.8	0.026	24.9
CEL-800	565	0.236	8.4
CEL-1200	110	0.067	12.1
CEL-1700	32.9	0.023	14.0
PF-800	33.0	0.019	11.5
PF-1200	19.2	0.016	16.2
PF-1400	2.94	$0.017.10^{-1}$	11.5
PF-1700	2.62	$0.015.10^{-1}$	11.2

Sample	Surface Area $\sum$ ($m.^2 g.^{-1}$)	Pore Volume V_{SL} ($c.c. g.^{-1}$)	Average Pore Radius $\bar{r}_p$ (Å)
SA-800	1070	0.361	6.75
SA-1200	1090	0.371	6.8
SA-1400	639	0.255	8.0
SA-1700	6.60	$0.237.10^{-2}$	7.2
SA-2200	0.75	$0.240.10^{-3}$	6.4
SA-2600	< 0.1	—	—
SA-2900	< 0.1	—	—
SAA-900	3240	1.12	6.9
SAA-1700	2100	0.741	7.05
PVC-800	2.32	$0.180.10^{-2}$	15.5
PVC-1200	1.04	$0.107.10^{-2}$	20.6
PVC-1700	0.56	0.693.10-3	24.6
CAL-original	1000	0.376	7.5
CAL-1700	262	0.176	13.4

4.7.2 Pore Size Distributions

From Nitrogen Isotherms From the nitrogen isotherms measured at -196°C on CA-800 and CA-1700, the pore size distribution was calculated using the method of Cranston and Inkley[133]. The results of the calculations (see Appendix D.1) are plotted in Fig. 42 as the cumulative pore volume versus the pore diameter. Differentiating the curves in Fig. 42 with respect to the pore diameter D, yields the pore volume distribution shown in Fig. 43. The value dV/dD indicates the pore volume V required to fill all pores between D and (D + dD). Hence a plot of dV/dD versus D shows the extent to

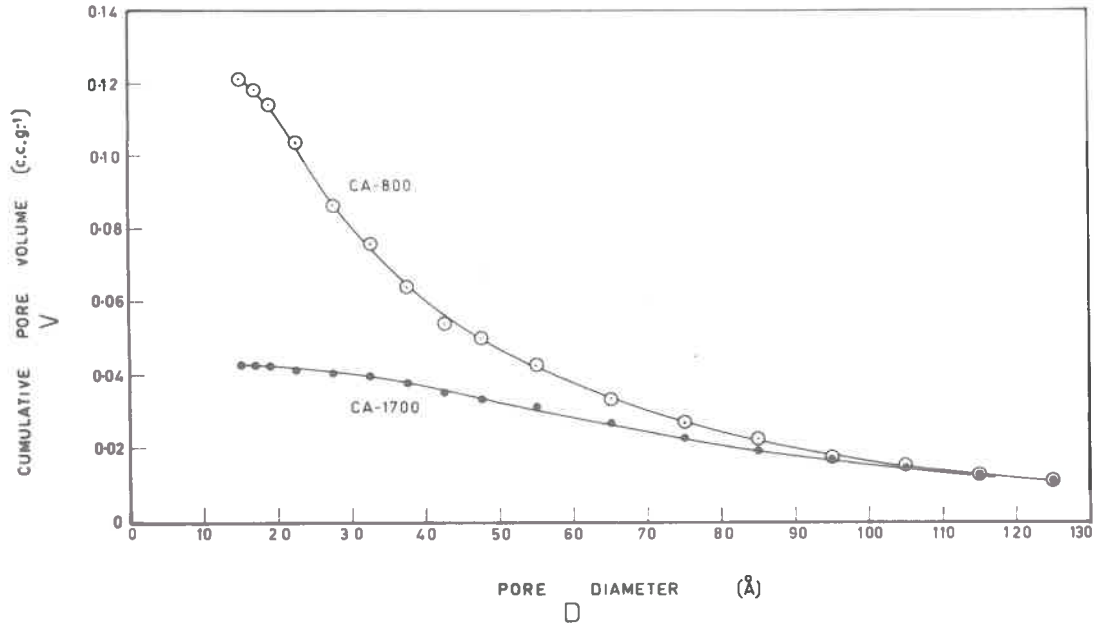

Fig. 42 - Pore Size Distribution for Heat Treated Cellulose Acetate Carbons

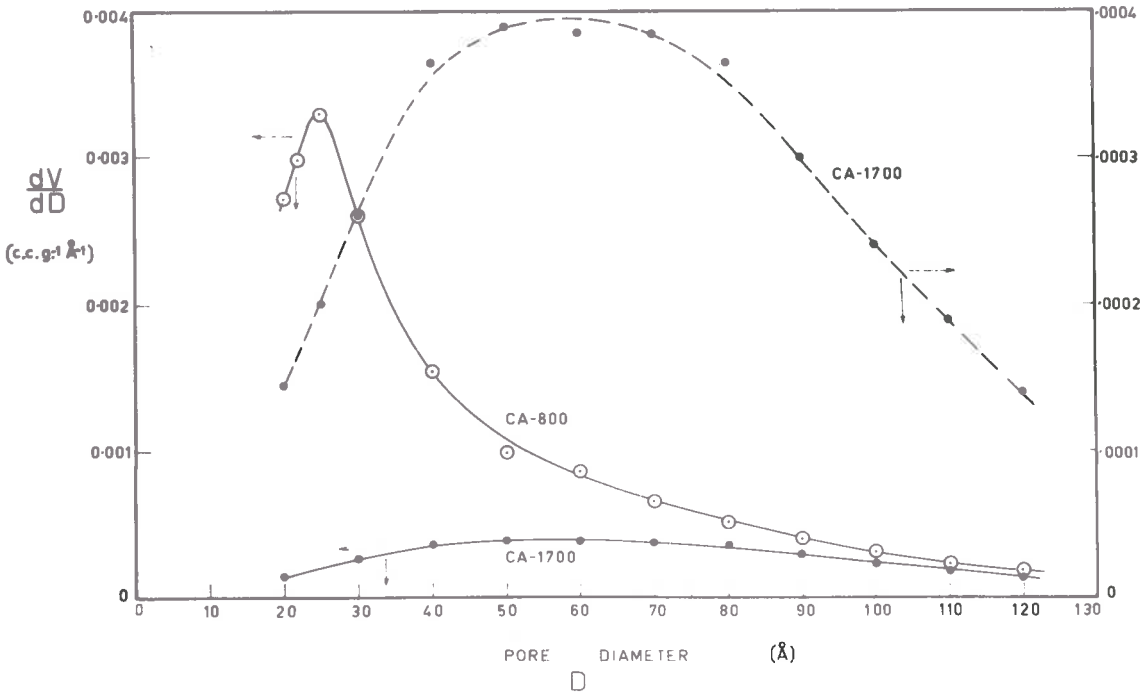

Fig. 43 - Differential Pore Size Distribution for Heat Treated Cellulose Acetate Carbons

which pores of a given diameter contribute to the total pore volume.

From High Pressure Mercury Penetration Measurements From the relationship

$$r = \frac{2 \gamma \cos \theta}{p} , \qquad . \quad . \quad . \qquad (10)$$

the pore radius can be calculated. The generally accepted value of the contact angle θ is 140°. Substituting a value of 480 dynes per cm. for the surface tension γ of mercury, the above equation reduces to

$$r = \frac{75,000}{p}$$

where r is in Å and p in atmospheres. Thus, knowing the volume of mercury forced into the pores at each pressure, the cumulative pore volume can be plotted as a function of r.

The samples tested were:

(1) cellulose acetate carbons heat treated at temperatures of 800°, 1,200°, 1,400° and 1,700°C,

(2) polyvinylidene chloride carbon prepared at 800°C, and

(3) polyvinyl chloride carbon prepared at 800°C.

Plots of cumulative pore volume versus pore radius are shown in Fig. 44 and 45. The results were reproducible to within ± 0.5 %. Unfortunately, time did not permit measurements to be made on heat treated carbons other than CA-800, CA-1200, CA-1400 and CA-1700.

4.8 Influence of Particle Size on the Adsorptive Capacity of Sintered Carbons

Argon isotherms for the unground and finely ground samples are shown in Fig. 46 and 47. Values for the monolayer capacity and surface area are listed in TABLE 7.

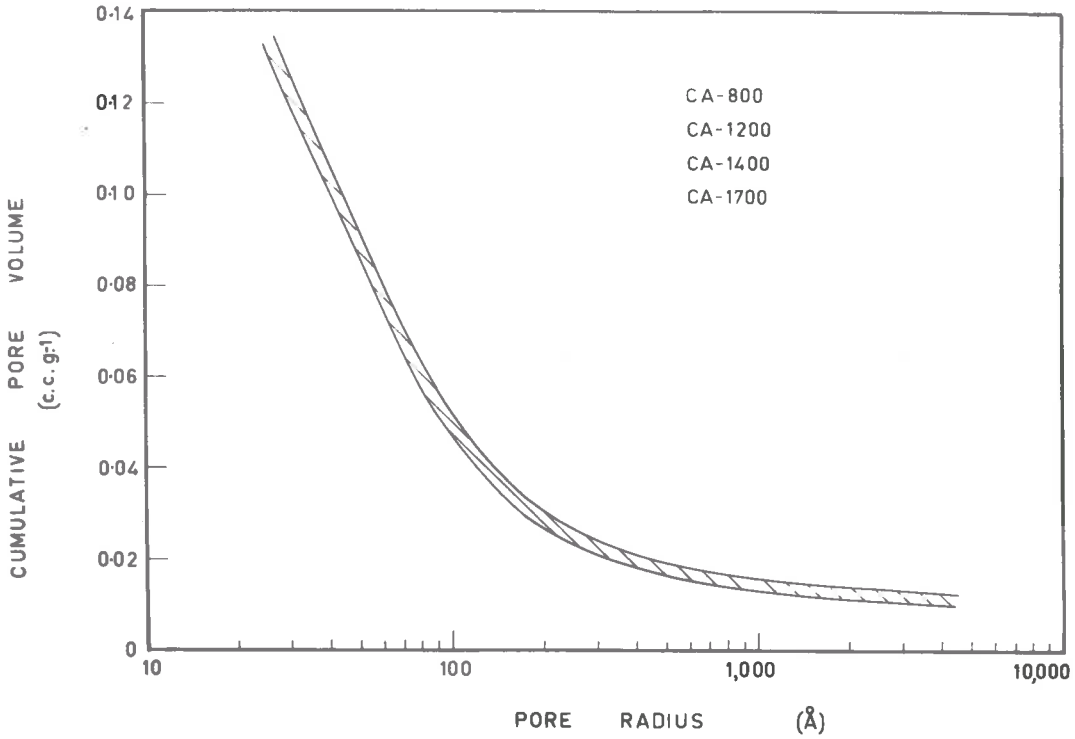

Fig. 44 - Pore Size Distribution for Heat Treated Cellulose Acetate Carbons (Mercury Porosimeter Measurements)

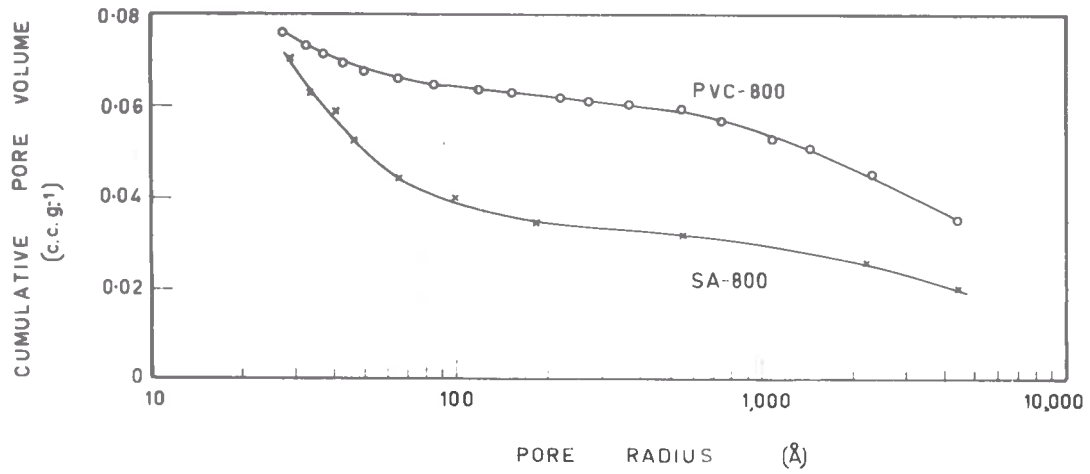

Fig. 45 - Pore Size Distribution for Carbons SA-800 and PVC-800 (Mercury Porosimeter Measurements)

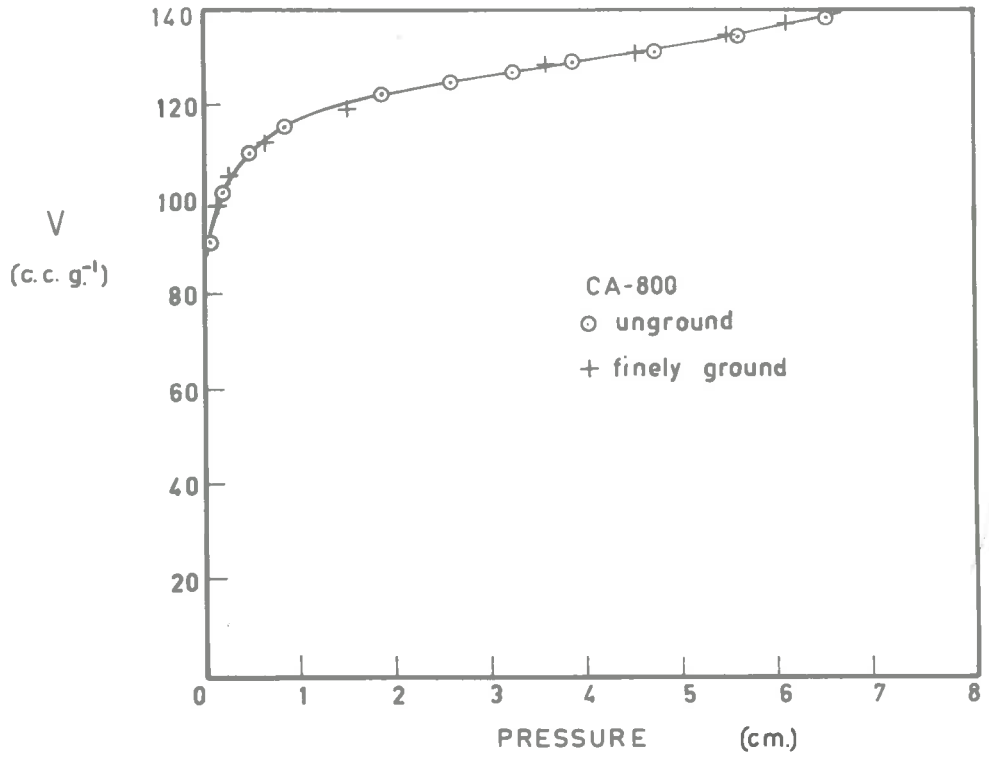

Fig. 46 - Influence of Particle Size on the Adsorptive Capacity of CA-800

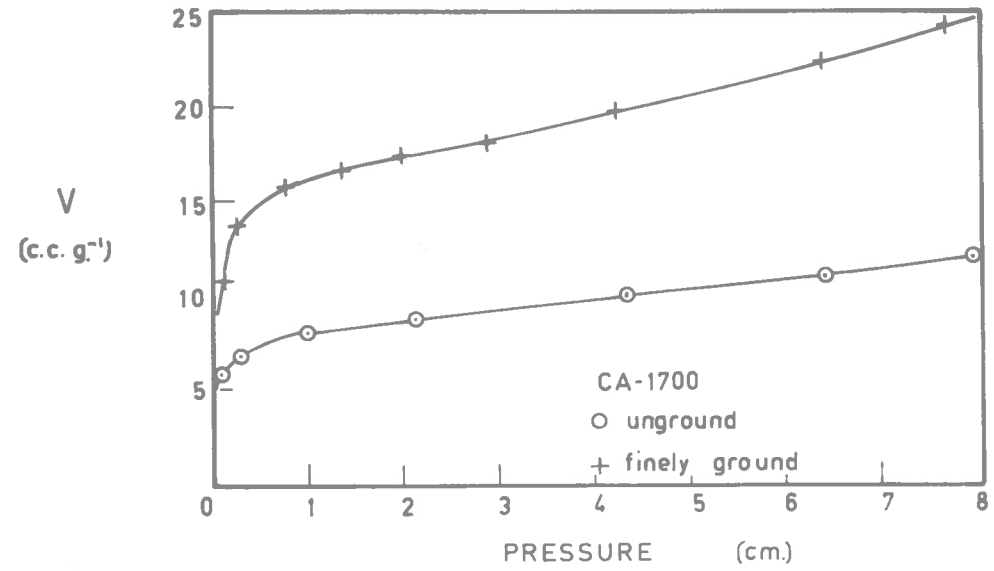

Fig. 47 - Influence of Particle Size on the Adsorptive Capacity of CA-1700

TABLE 7

Monolayer Capacities and Surface Areas

		V_m c.c. $g.^{-1}$	$\sum$ $m.^2 g.^{-1}$
Cellulose Acetate Carbon			
800	unground	118	444
800	finely ground	118	444
1700	Unground	8.0	30.4
1700	finely ground	14	52.6

The sample of cellulose acetate carbon CA-800 used in this experiment came from a different batch from that used in the rest of the project and exhibited a slightly larger adsorptive capacity. The reason for this variation is not known but the sample may have become slightly activated by air leaking into the apparatus during reheating.

4.9 Kinetics of Adsorption

The results for the rate measurements were plotted as $V_t - V_o / V_\infty - V_o$ versus $t^{\frac{1}{2}}$, where V_o, V_t and V_∞ are, respectively, the weight adsorbed at time zero, time t and infinite time. The rates of adsorption of argon on CA-800 at $-81^\circ C$ are shown in Fig. 48, where the curves refer to adsorption, in steps, at progressively increasing pressures. Within experimental error, the curves for CA-800 were coincident and similarly for the other carbons. This meant that, over the total pressure range studied, one curve represented the rate of adsorption of argon on a particular carbon. Thus the comparison of the rates of adsorption for the various heat treated carbons was considerably simplified.

Plots of $V_t - V_o / V_\infty - V_o$ versus $t^{\frac{1}{2}}$ for (a) cellulose acetate carbons CA-800, CA-1200 and CA-1700 at -81°, -183° and

-196°C, and (b) polyvinylidene chloride carbons SA-800, SA-1200, SA-1400 and SA-1700 at-196°C, are shown in Fig. 49 to 52 respectively.

The maximum pressure was deliberately kept well below the relative pressure corresponding to the monolayer capacity of the carbon, so that transport processes associated with multilayer formation, such as capillary flow, could not complicate the flow pattern in the capillaries.

Ratios of bed depth to bed diameter from 0.3 to 2 were used in several rate measurements and the results indicated that the rates of adsorption were unaffected.

The accuracy of the rate measurements depended mainly upon (1) the accuracy of the time reading obtained from the chart recorder, (2) the accuracy of the weight reading obtained from the chart recorder, and (3) the initial delay during the opening of the tap between the balance and the ballast tubes. The time was read from the chart to within $\pm$ 3 sec. while the accuracy of the time base of the recorder was approximately $\pm$ 0.5 % at the end of a 30 min. period. The weight was read from the chart to $\pm$ 2 μg. while the accuracy of the chart reading was $\pm$ 0.3 % of span. The time required for the tap leading to the balance to be turned from the shut to the fully open position was approx. 5 sec. Thus the value of the time t obtained from the rate measurements over the initial stages of the run was accurate to $\pm$ 8 sec. while the weight V was accurate to $\pm$ 4 μg.

In the light of the experience gained, it appears that for carbons exhibiting fast rates of adsorption an experimental technique similar to that employed by Winfield and Sutherland[193] might be adopted to advantage. With this technique transient pressure changes are measured with a high sensitivity - fast response diaphragm, acting as a tuned condenser and coupled to a recording oscilloscope.

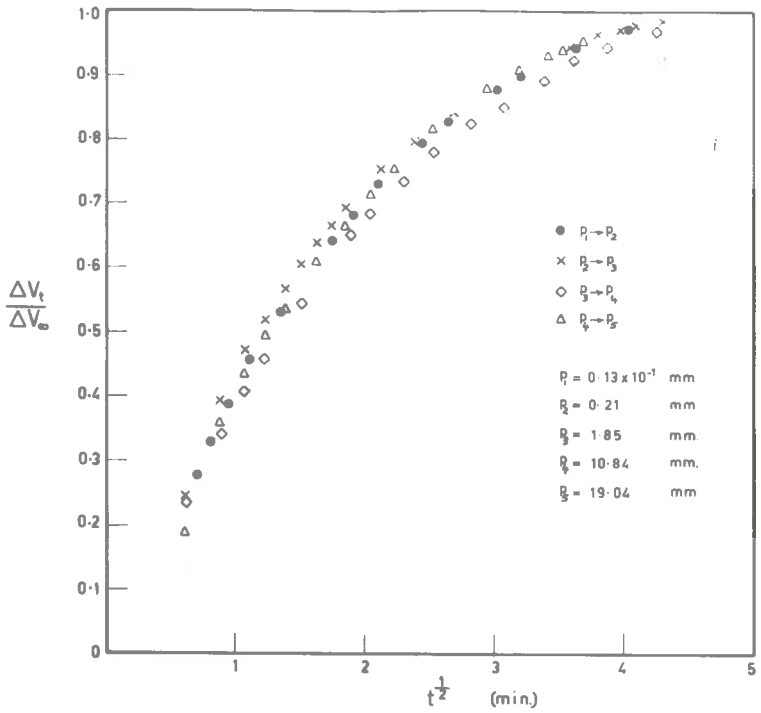

Fig. 48 - Rate of Adsorption of Argon on CA-800 at -81 °C for a Series of Pressure Steps

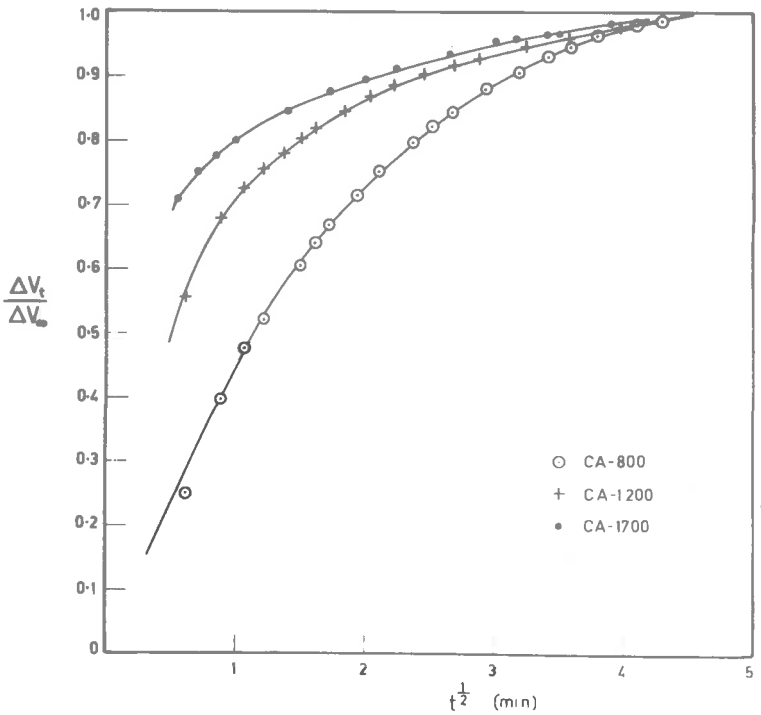

Fig. 49 - Rate of Adsorption of Argon on CA-800, CA-1200 and CA-1700 at -81 °C

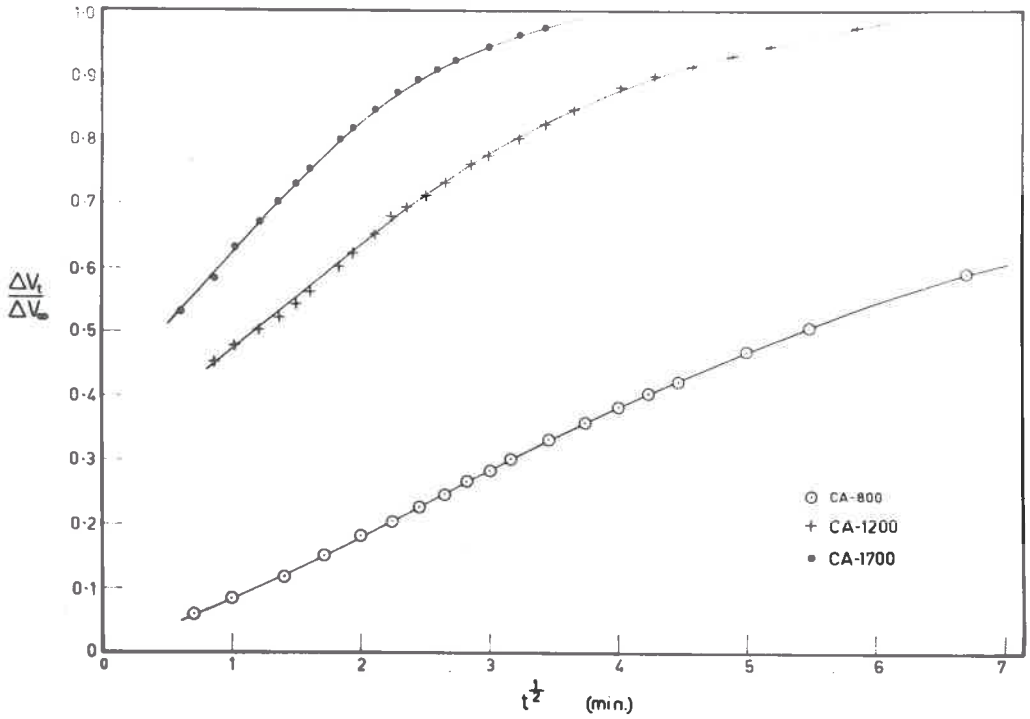

Fig. 50 - Rate of Adsorption of Argon on CA-800, CA-1200 and CA-1700 at -183°C

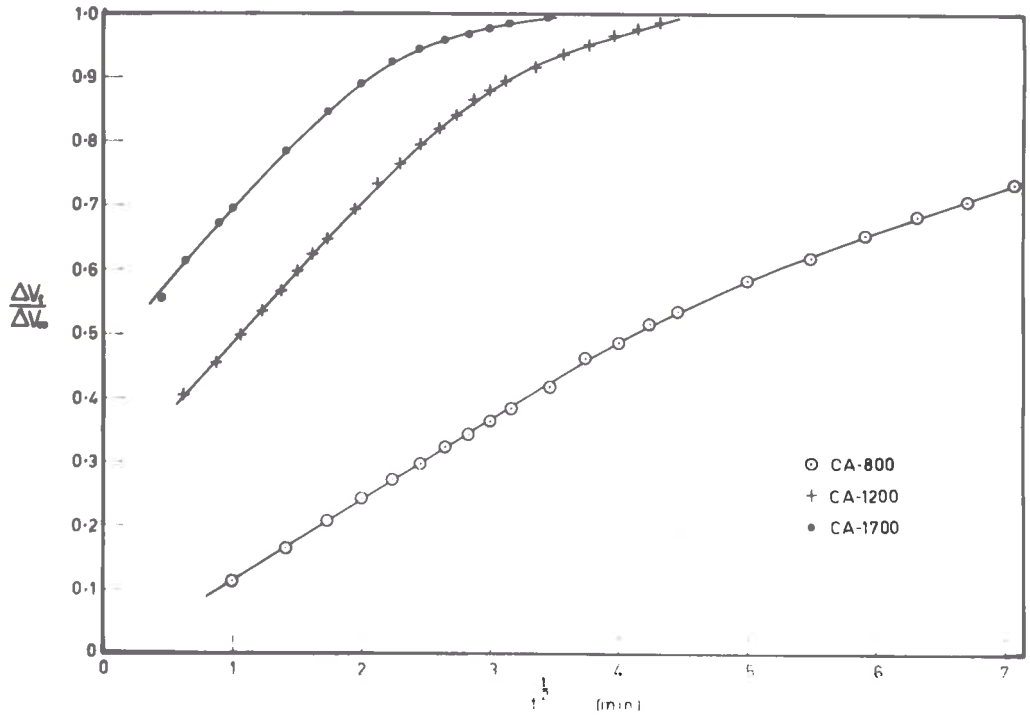

Fig. 51 - Rate of Adsorption of Argon on CA-800, CA-1200 and CA-1700 at -196°C

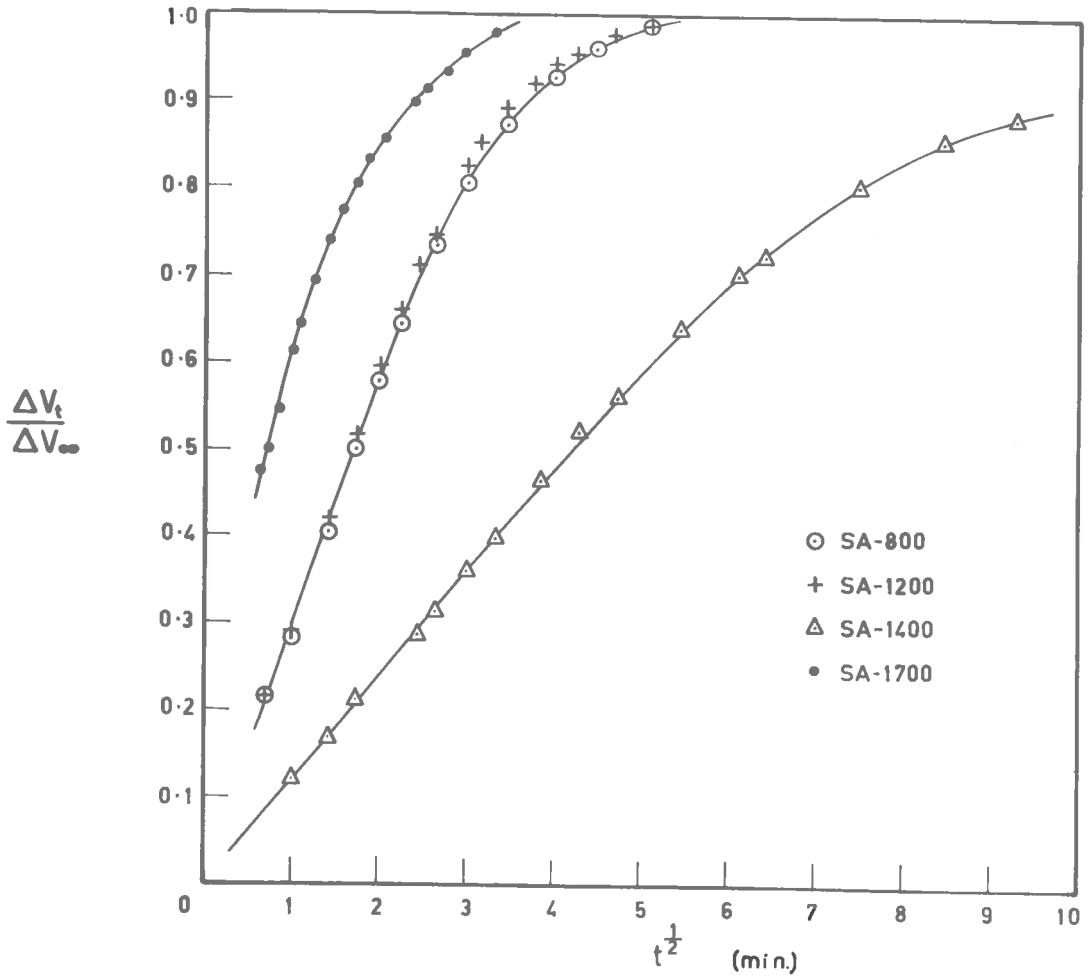

Fig. 52 - Rate of Adsorption of Argon on SA-800, SA-1200, SA-1400 and SA-1700 at -196°C

4.10 Differential Molar Heats and Entropies of Adsorption

(a) Differential Molar Heats of Adsorption

The isothermal adsorption of dn_s moles of adsorbate will be accompanied by the transfer of an amount of heat dQ. Depending upon the path of the adsorption process, various differential heats of adsorption can be defined by

$$q = \frac{dQ}{dn_s}$$

If the adsorption process is conducted at constant pressure and temperature, then q_{st}, the isosteric heat of adsorption, is defined as $\bar{s}_g - \bar{s}_s$. Thus, the isosteric heat of adsorption may be defined as the heat evolved in transfering one mol of adsorbate from the gas at the equilibrium pressure P to an infinite surface at constant surface coverage, P and T being kept constant. Substituting q_{st} in equation (27) gives

$$\left(\frac{\partial \ln p}{\partial T}\right)_{n_s,\Sigma} = \frac{q_{st}}{RT^2} \qquad \cdot \quad \cdot \quad \cdot \qquad (30)$$

The isosteric heat of adsorption and other derived thermodynamic quantities will be referred to the standard gas state of unit pressure.

Values of the isosteric heat of adsorption were obtained from the slope of the plots of ln p versus $1/T$. For argon, q_{st} was plotted as a function of V/V_m and the results are shown in Fig. 53. For benzene, the value of V_m was uncertain so that q_{st} values were plotted versus $V/\bar{V}_s$ (see Fig. 54), where $\bar{V}_s$ is the average saturation capacity of the carbons at the various temperatures.

For argon, the estimated accuracy of the heat of adsorption

below $V/V_m = 0.9$ is $\pm$ 100 cal. mole^{-1} and above $V/V_m = 0.9$, $\pm$ 10 cal. mole^{-1}. For benzene, the estimated accuracy over the range of V/V_s values shown in Fig. 54 is $\pm$ 50 cal. mole^{-1}. The method of determining these accuracies is given in APPENDIX G.2.

(b) Differential Molar Entropy of Adsorption

The isosteric heat of adsorption can be expressed in terms of the entropy of the gas phase in equilibrium with the adsorbate at temperature T, s_g^T, and the differential entropy of the adsorbate[194], $\bar{s}_S$, viz.

$$\frac{q_{st}}{T} = s_g^T - \bar{s}_S$$

or
$$\bar{s}_S = s_g^T - \frac{q_{st}}{T} \quad . \quad . \quad . \quad (31)$$

For argon, the entropy of the gas phase can be calculated from the equation

$$s_g^T = R \ln \frac{kT}{p} + R \ln \frac{(2\pi mkT)}{h^3} + \frac{5}{2} R \quad . \quad (32)$$

where R = 1.98 cal. mole^{-1} deg.$^{-1}$,
k = Boltzmann's constant,
m = mass of the atom and
h = Planck's constant.

Combination of equations (31) and (32) allows $\bar{s}_S$ to be calculated from experimentally determined quantities. For the adsorption of argon on cellulose acetate carbons, the plots of the entropy $\bar{s}_S$ versus V/V_m are shown in Fig. 55.

For benzene, the entropy of the gas phase can be calculated from the equation[194]

$$s_G^T = s_G^0 + \int_{T^0}^{T} \frac{C_p\, dT}{T} + R \ln \frac{p^0}{p} - \alpha p \qquad . \quad . \quad . \quad (33)$$

where s_G^0 = molar entropy of the ideal gas at a standard pressure p^0 and temperature T^0,

T = temperature of the experiment,

C_p = heat capacity of the gas at constant pressure

and α = correction for non-ideality of the gas phase.

The standard pressure p^0 was chosen as 760 mm. of mercury and the standard temperature as 25°C. The correction for non-ideality, α, was calculated from Berthelot's equation of state

$$\alpha = \frac{27}{32} \frac{R T_c^3}{P_c T^3}$$

where T_c = critical temperature of the bulk phase

and P_c = critical pressure of the bulk phase.

For benzene, T_c = 288.5°C and P_c = 47.7 atm. At the temperature and pressure encountered in the measurement of benzene isotherms, the value of the correction term, αp, was negligible.

The value for the heat capacity at constant pressure was calculated from the equation

$$C_p = a + bT + cT^2$$

where $a = -0.283$,

$b = 77.936 \times 10^{-3}$

and $c = -262.96 \times 10^{-7}$. (ref. 191)

Over the range of temperature of approximately 30°C used in the measurement of the isotherms, the value of C_p could be regarded

as constant.

The value of s_G^0 for benzene at 25°C (ref. 191) was taken as 68.34 cal.mole^{-1}deg.$^{-1}$.

Thus equation (33) now becomes

$$s_G^T = 68.34 + C_p \ln \frac{T}{298} + R \ln \frac{760}{p} \quad . \qquad (34)$$

Combination of equations (31) and (34) allows $\bar{s}_g$ to be calculated. The values of $\bar{s}_g$ for benzene adsorption on the cellulose acetate carbons are shown in Fig. 56 as a function of $V/\bar{V}_g$.

The estimated accuracy of the entropy of adsorption of argon below $V/V_m = 0.9$ is $\pm$ 1 cal. mole^{-1} deg.$^{-1}$ and above $V/V_m = 0.9$, $\pm$ 0.1 cal. mole^{-1} deg.$^{-1}$. For benzene the estimated accuracy of the entropy of adsorption is $\pm$ 0.2 cal. mole^{-1} deg.$^{-1}$.

4.11 X-ray Diffraction Measurements on Carbons

The recorded intensities were corrected for polarization by the factor $(1 + \cos^2 2\theta)/2$, giving the experimental data in corrected arbitary units. Unfortunately, the (11) line, for most of the low temperature carbons, was too diffuse for accurate analysis. An attempt was then made to analyze the remaining two prominent peaks (002) and (10) by a method similar to that used by Alexander and Sommer[107]. This first required the conversion of the data into electron units. The usual normalization procedure of obtaining a scaling factor by comparison of the MoKα curve at high angles with the theoretical total independent scattering curve, failed to give reasonable results. It soon became apparent that the normalizing procedure was sensitive to minor variations in experimental conditions. Although some effort was made to account for these variations, it was clear that a disproportionate amount of time would have to be allotted to obtaining information on the reaction of the diffraction pattern to variations in experimental conditions.

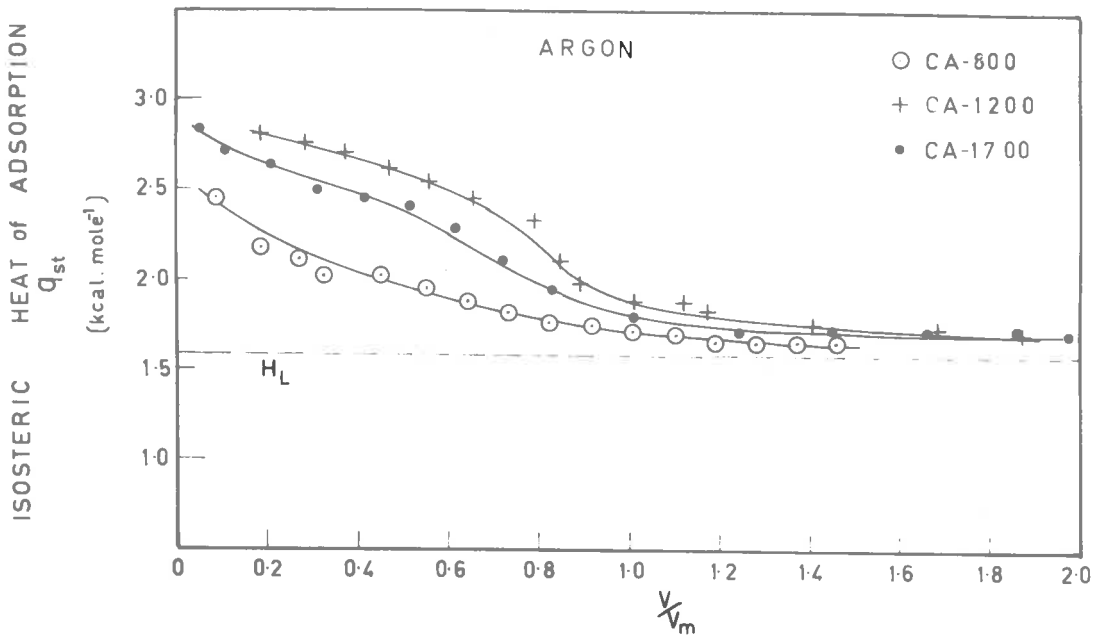

Fig. 53 - Isosteric Heats of Adsorption of Argon on CA-800, CA-1200 and CA-1700

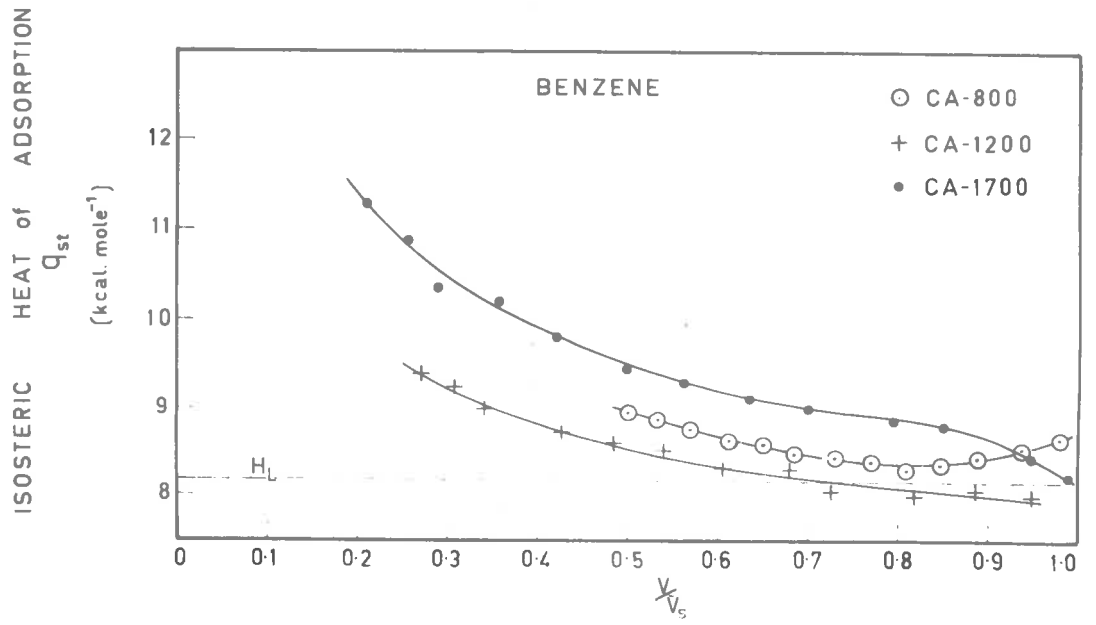

Fig. 54 - Isosteric Heats of Adsorption of Benzene on CA-800, CA-1200 and CA-1700

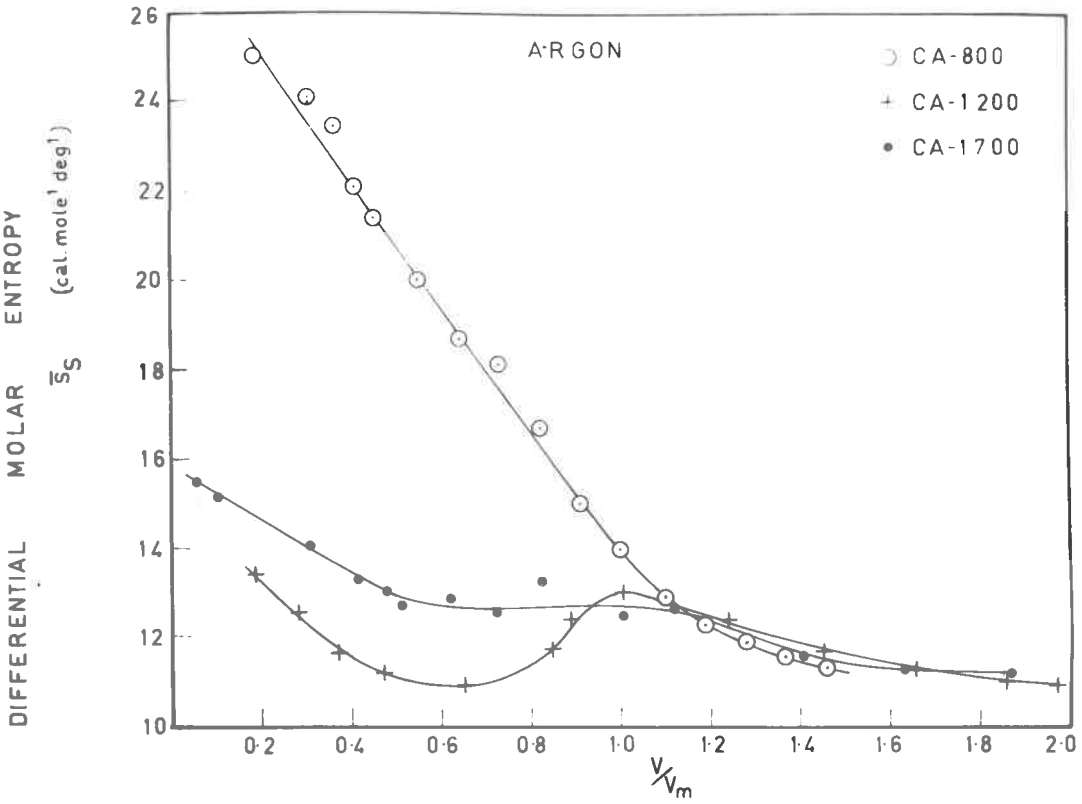

Fig. 55 - Differential Molar Entropy of Adsorption of Argon on CA-800, CA-1200 and CA-1700

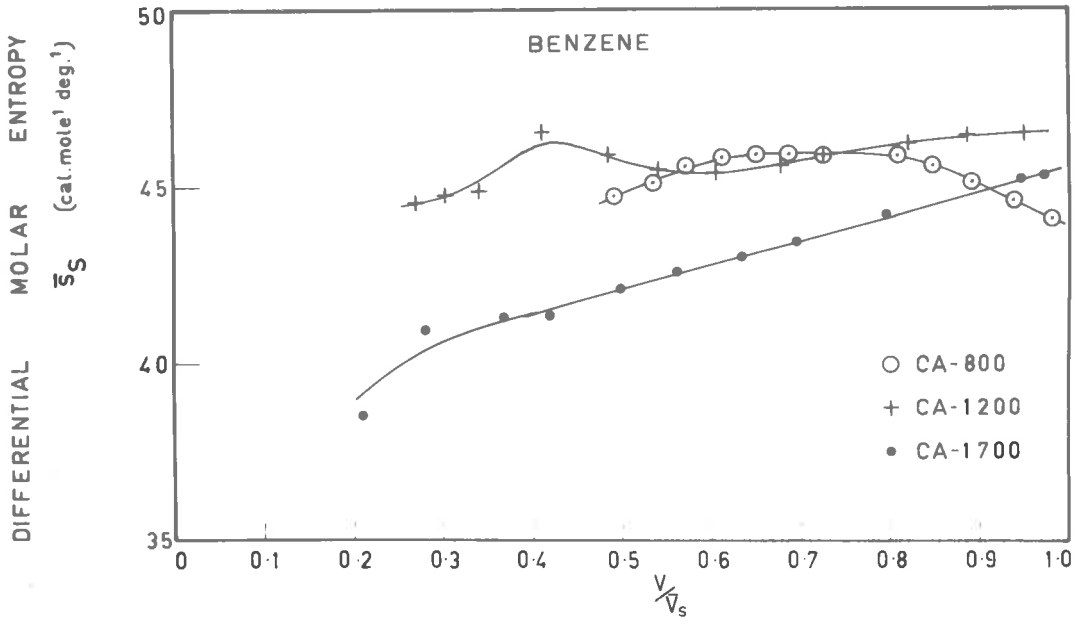

Fig. 56 - Differential Molar Entropy of Adsorption of Benzene on CA-800, CA-1200 and CA-1700

It is interesting to note that after this work on the determination of crystallite sizes had been completed, a paper by McKinstry and Short[195] was published which pointed out the limitations in the experimental procedure. McKinstry and Short[195] have made it clear that many authors have failed to recognise the importance of clearly understanding the influence of certain experimental variables on the X-ray diffraction pattern, especially those variables associated with use of X-ray diffractometers. McKinstry and Short were concerned with developing a satisfactory X-ray diffractometer technique for use with Diamond's least squares method[106] for the determination of crystal size distribution in turbostratic carbons. They found that the position of the filter in the secondary beam considerably altered the distribution of molecular sizes and changed some values of the weighted distribution from negative to positive values. They also found that the Soller slits in the secondary beam, as supplied by the manufacturer, were not wide enough laterally to pass all of the reflected beams and that their removal resulted in a useful gain in intensity without any impairment to accuracy. Variation in adsorption corrections and scattering factors produced significant alterations in the molecular size distributions, but not necessarily in the average crystallite size.

After considerable delay it was decided to revert to the simpler method of determining crystallite size from measurement of the peak breadth. L_a was determined by applying Warren's[5] two-dimensional particle equation

$$L_a = \frac{1.84\,\lambda}{\beta \cos\theta}$$

to the (hk) bands (10) and (11). The L_c dimension was determined from the (002) band using Scherrer's[105] equation

$$L_c = \frac{K \lambda}{\beta \cos \theta}$$

and Jones'[196] value of K = 1.0. The broadening of a peak is caused by the combination of diffraction from small crystallites and machine factors. Neglecting the broadening due to the unresolved $K\alpha$ doublet, the experimental broadening at half-peak height is termed B and the broadening by the machine factor, b. By using Jones'[196] correction curve for the 'new type' spectrometer which plots β/B against b/B a value of β can be obtained which is free of machine broadening.

Graphs of the experimental intensity as a function of the goniometer angle 2θ are shown in Fig. 57 to 63. The double peak for the (112) and (006) reflections of PVC-2900 are the result of the separation of the incident radiation into its component wavelengths α_1 and α_2.

Graphs of the crystallite dimensions L_a and L_c as a function of the heat treatment temperature are shown in Fig. 64, and the data are summarized in APPENDIX H. For the polyvinyl chloride carbons, line broadening of the reflections due to crystallite size at temperatures above 1,700°C closely approached that of line broadening due to instrument factors so that values of L_c and L_a could not be evaluated to an acceptable degree of accuracy.

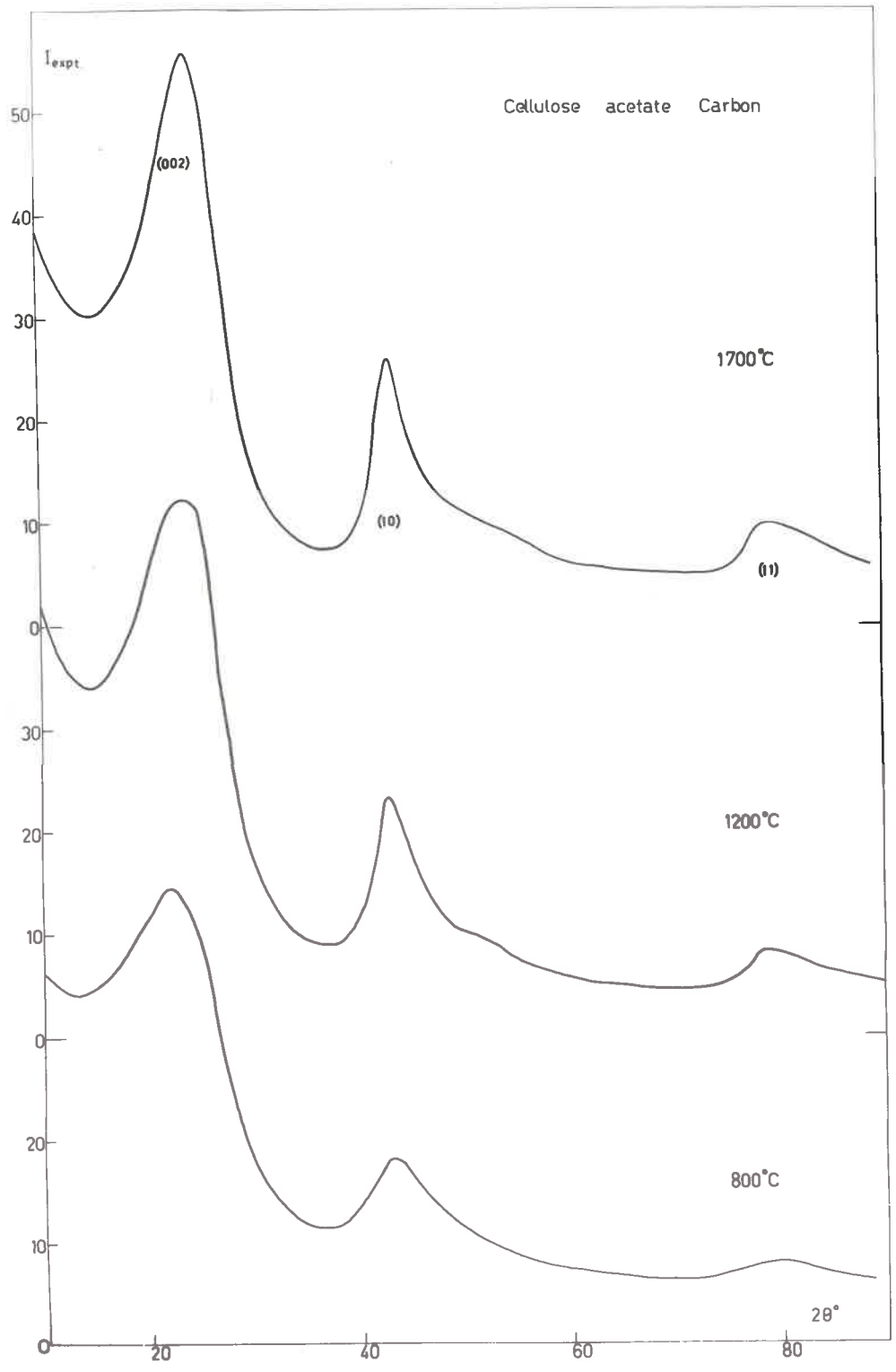

Fig. 57 - X-ray Diffraction Pattern of Heat Treated Cellulose Acetate Carbons CA-800, CA-1200 and CA-1700

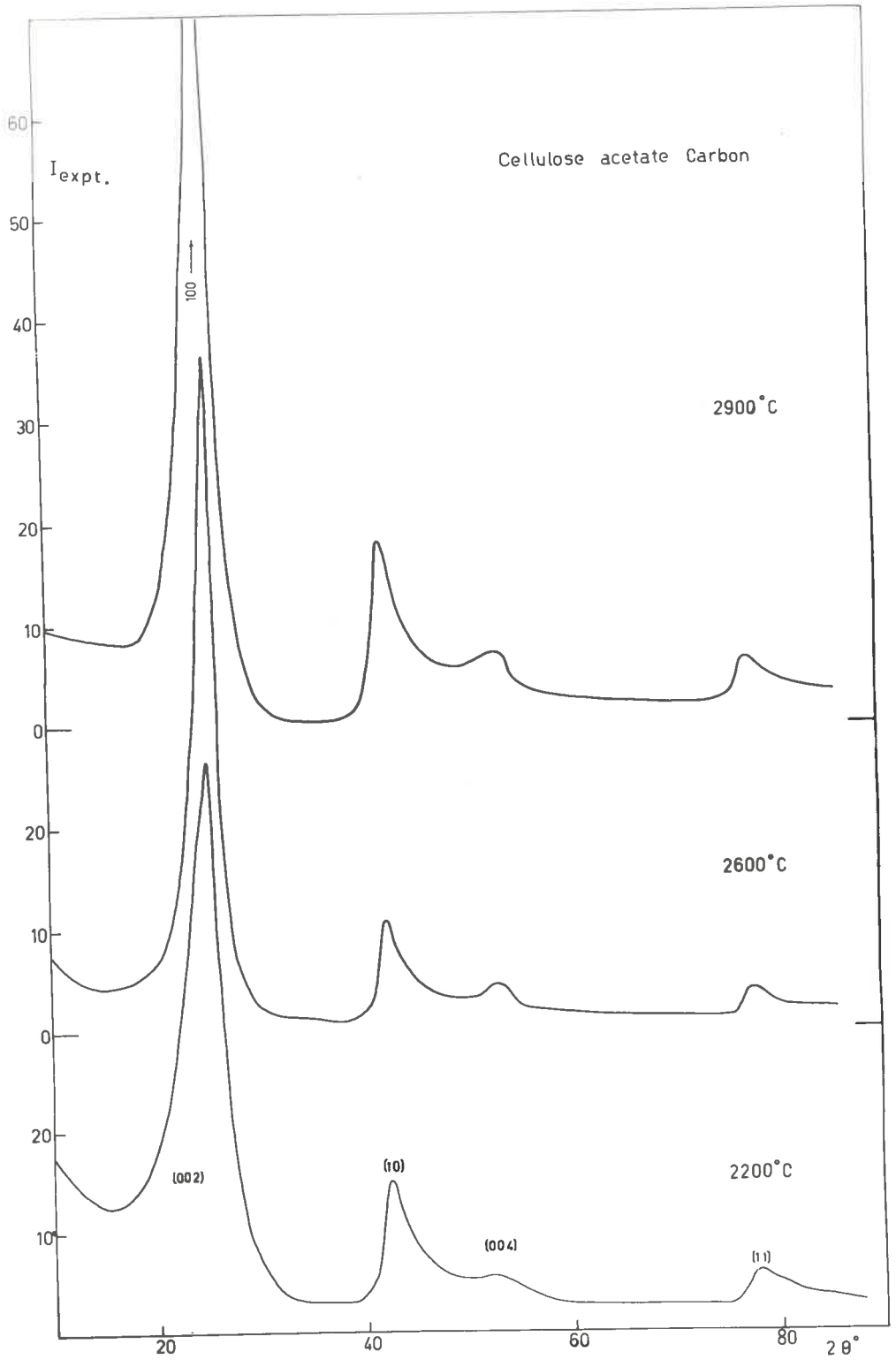

Fig. 58 - X-ray Diffraction Pattern of Heat Treated Cellulose Acetate Carbons CA-2200, CA-2600 and CA-2900

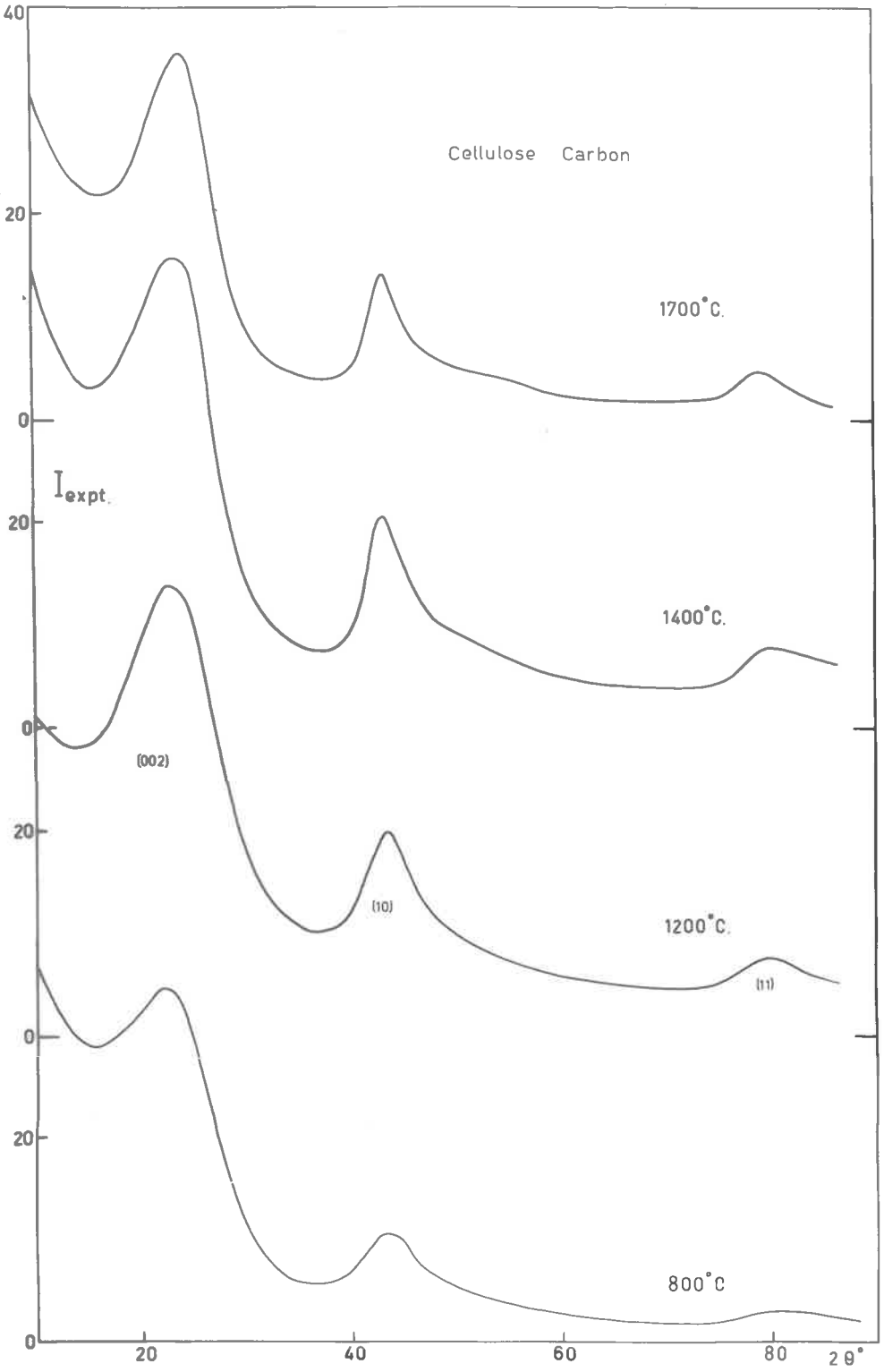

Fig. 59 - X-ray Diffraction Pattern of Heat Treated Cellulose Carbons CEL-800, CEL-1200, CEL-1400 and CEL-1700

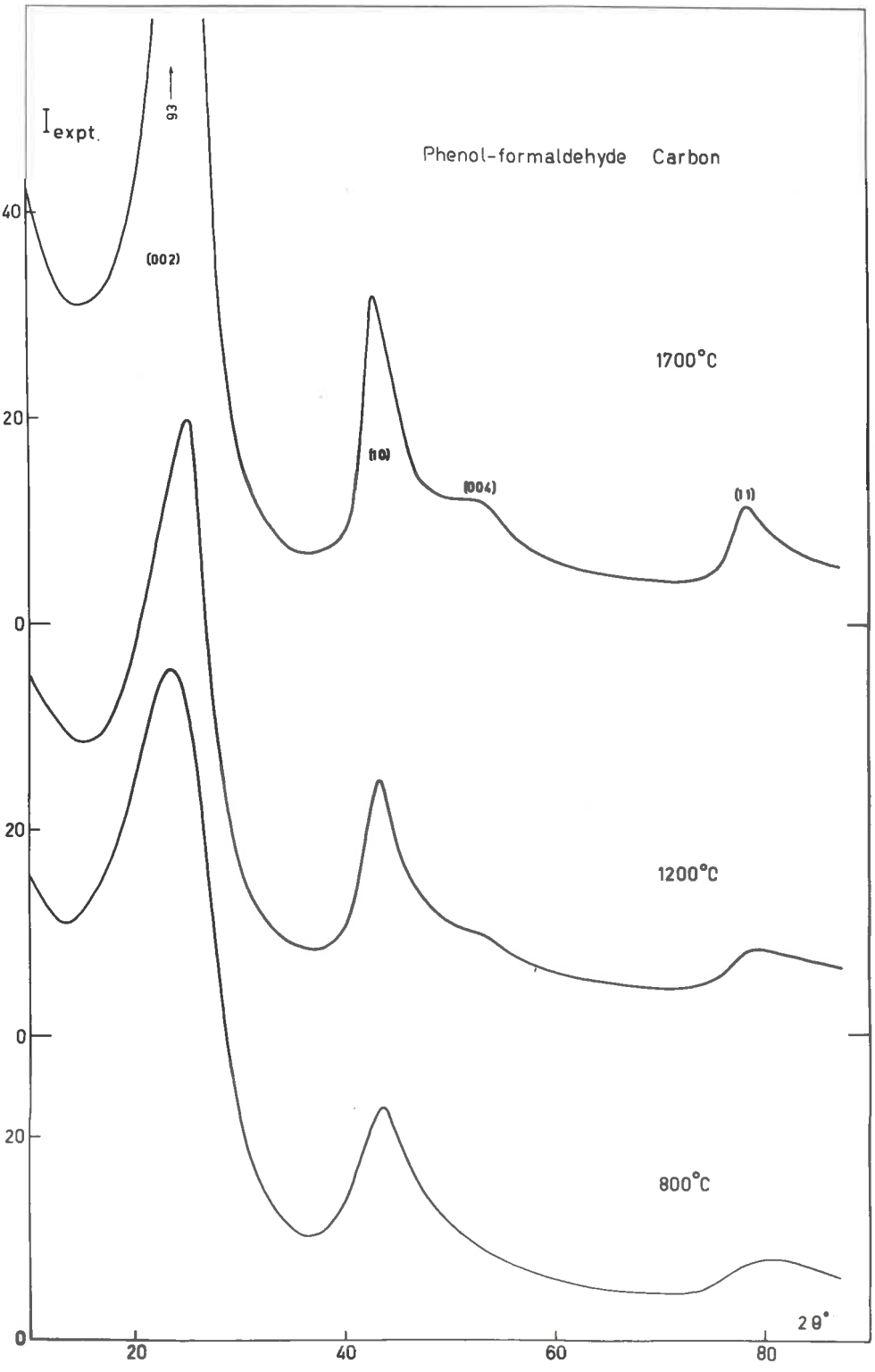

Fig. 60 - X-ray Diffraction Pattern of Heat Treated Phenol-formaldehyde Carbons PF-800, PF-1200 and PF-1700

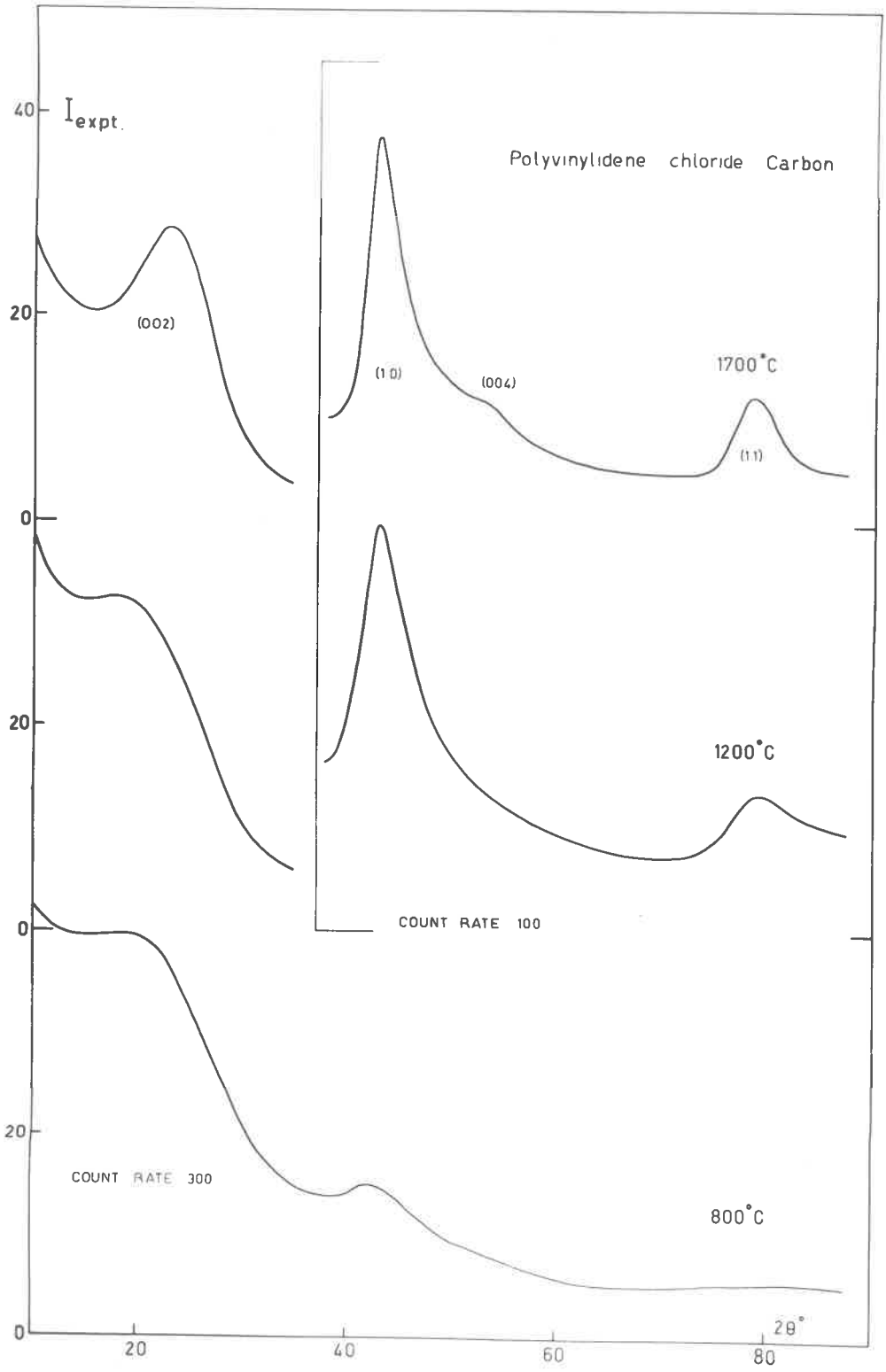

Fig. 61 - X-ray Diffraction Pattern of Heat Treated Polyvinylidene Chloride Carbons SA-800, SA-1200 and SA-1700

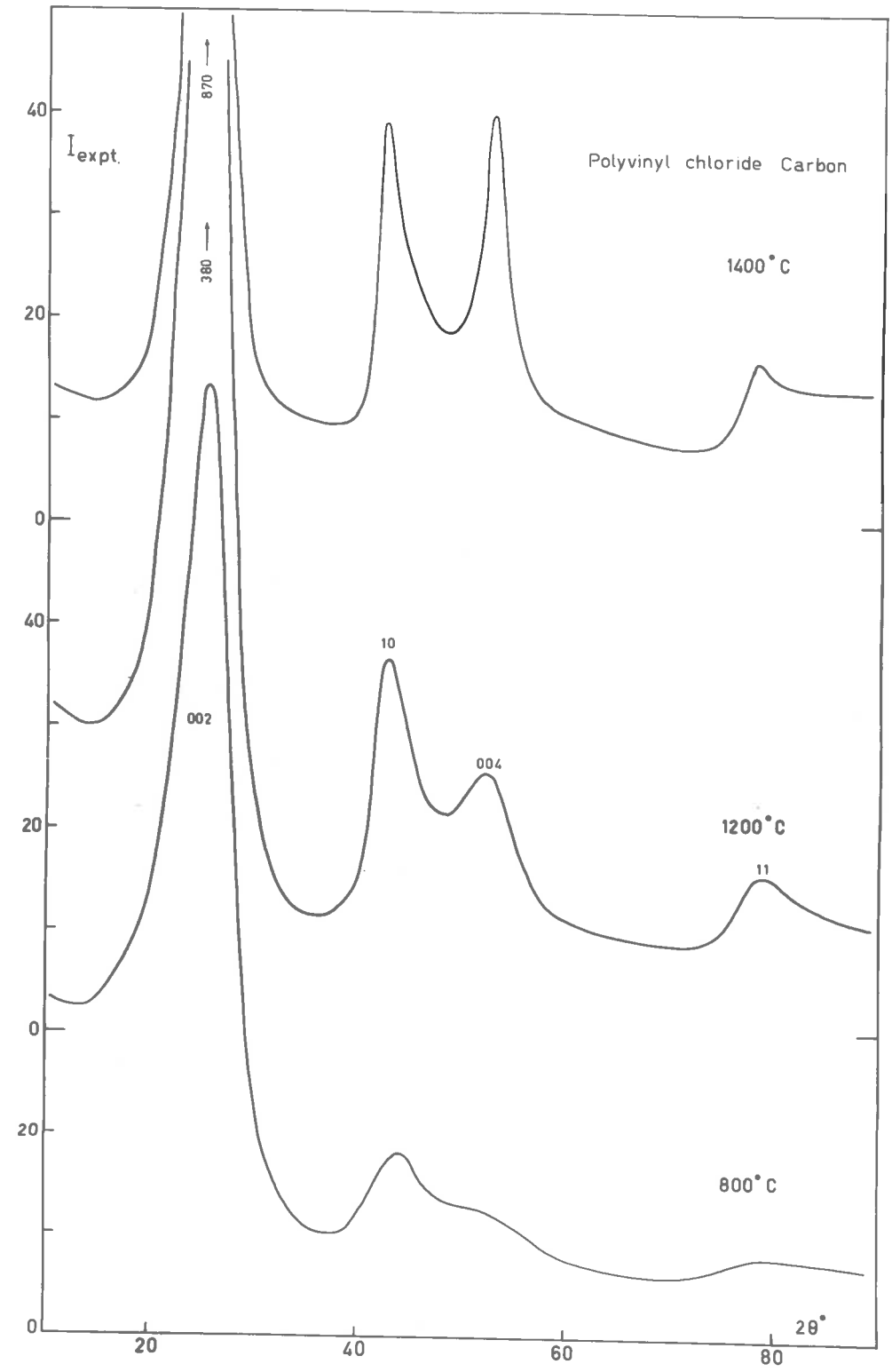

Fig. 62 - X-ray Diffraction Pattern of Heat Treated Polyvinyl Chloride Carbons PVC-800, PVC-1200 and PVC-1400

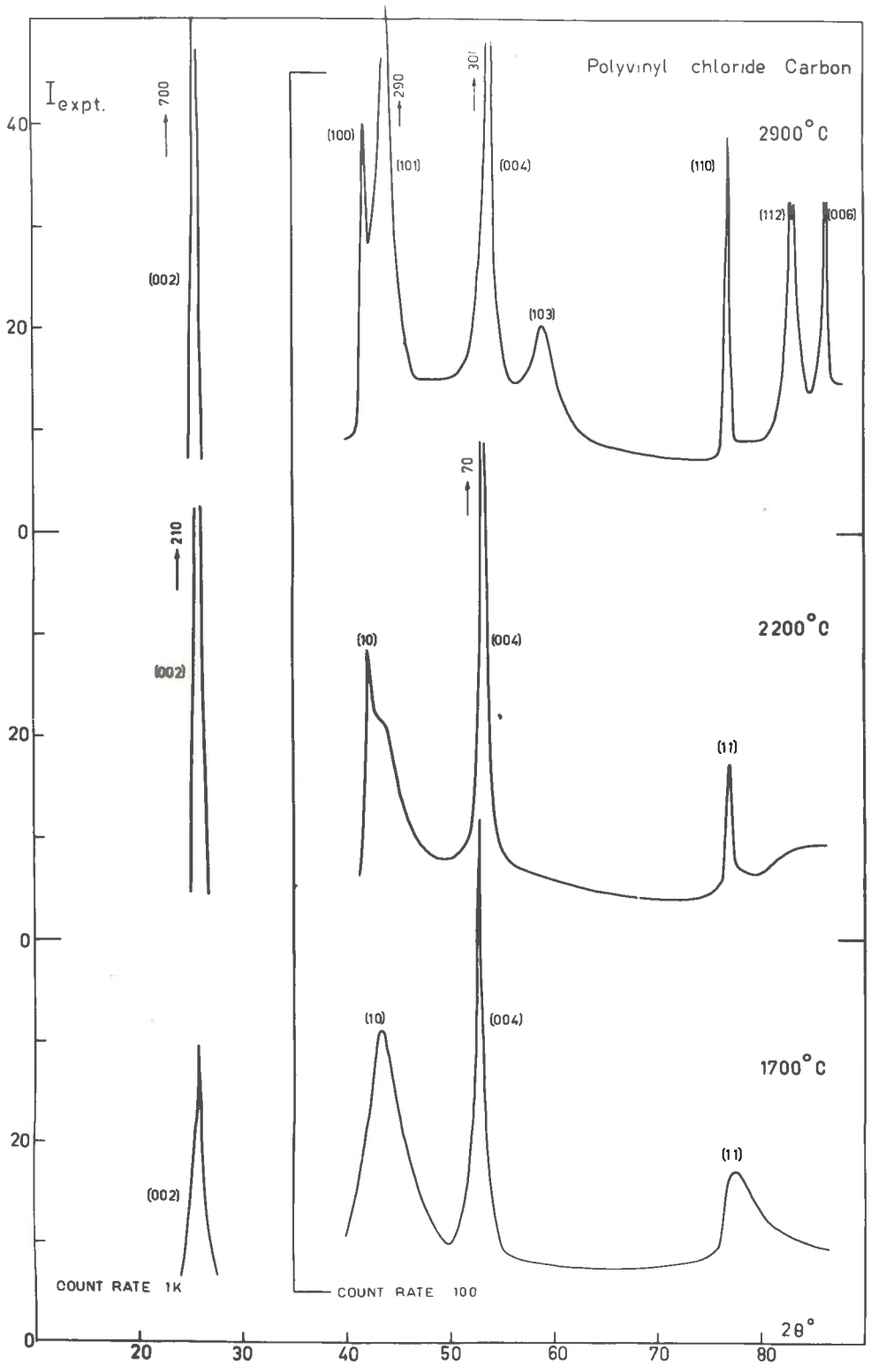

Fig. 63 - X-ray Diffraction Pattern of Heat Treated Polyvinyl Chloride Carbons PVC-1700, PVC-2200 and PVC-2900

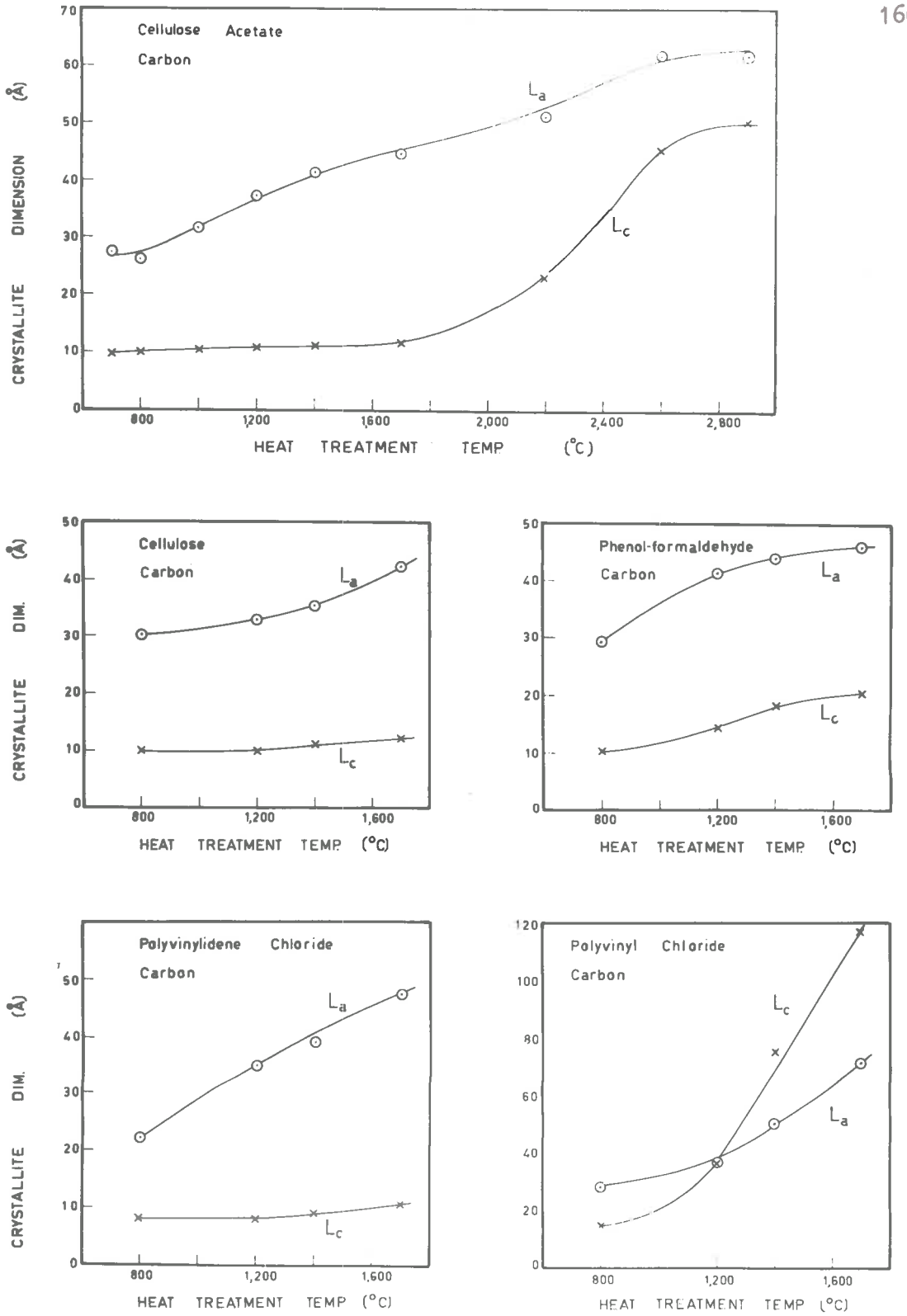

Fig. 64 - Crystallite Growth of Heat Treated Carbons

5. DISCUSSION

5.1 Sintering of Porous Carbons

5.1.1 Adsorptive Capacity and Surface Area

For most of the carbons, heat treatment produced a marked decrease in both the adsorptive capacity and the surface area (see Fig. 25 to 35 and TABLE 3). There are, however, significant differences in the degree of sintering exhibited by the carbons which will be considered in turn.

Cellulose Acetate Carbons The adsorptive capacity reached a maximum at a heat treatment temperature of 800°C and then generally decreased with increasing temperature. The carbon heated to 2,900°C adsorbed slightly more argon than the carbon heat treated to 2,600°C. This was probably due to the fact that at 2,900°C the carbon was so reactive that it was slightly activated by oxygen present as an impurity in the inert gas being flushed through the furnace. With this particular carbon the surface was much blacker than for other samples heat treated at lower temperatures and activated carbons generally possess a blacker surface than unactivated carbons.

The change in the surface area with heat treatment temperature follows a similar pattern to that obtained by Wynne-Jones[81] for a cellulose carbon (see Fig. 9). Fig. 65 shows that for cellulose acetate the largest change in surface area occurs from 900° to 1,200°C.

Cellulose Carbons The sintering behaviour is very similar to that exhibited by cellulose acetate.

Phenol-formaldehyde Carbons Although non-graphitizing carbons normally possess a large surface area, it was not surprising to find that the surface area of the phenol-formaldehyde carbon PF-800, was relatively low. The granules of phenol-formaldehyde carbon were hard, the surface was glassy and there was no external

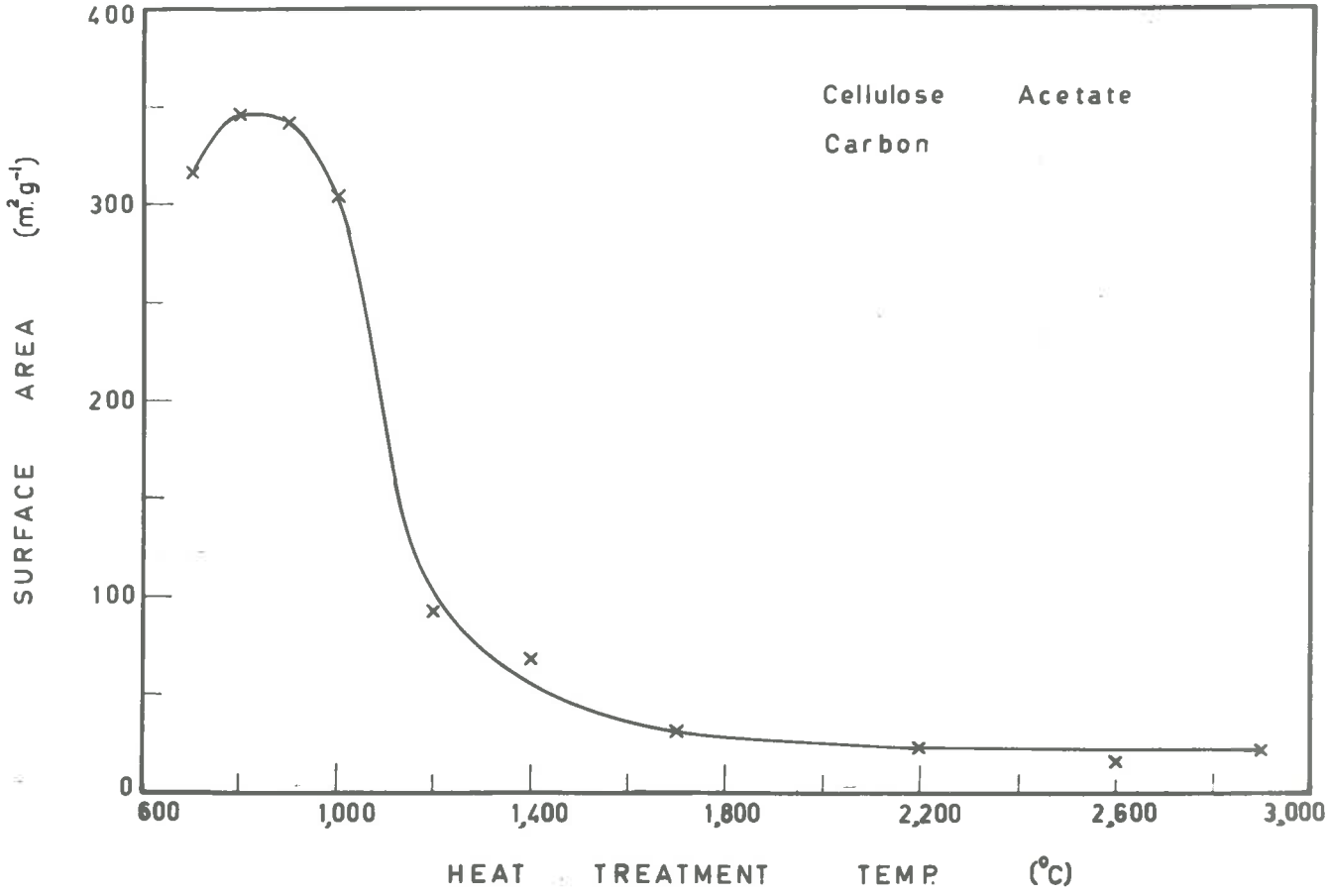

Fig. 65 - The Effect of the Heat Treatment Temperature on the Surface Area (Σ) of Cellulose Acetate Carbons

evidence of a fine pore structure.

A large change in adsorptive capacity occurred in the temperature range 800° to 1,400°C, corresponding to a 91% reduction in the surface area.

Polyvinylidene Chloride Carbons The sintering behaviour of this carbon displayed some interesting differences when compared with other carbons. The carbon, on heat treatment at 1,200°C, actually exhibited a slight increase in adsorptive capacity and surface area. Dubinin et al.[85, 86] obtained a similar result for a slightly activated polyvinylidene chloride carbon heat treated to 1,300°C. The observed slight increase in surface area may be the result of two opposing factors. Sintering leads to a reduction in area, but an increase in area may also be expected since large amounts of impurities are removed at the same time; chemical analysis of the carbon before and after heat treatment at 1,200°C reveals a 14% decrease in oxygen content and a 2% decrease in hydrogen content.

The isotherm for the 1,400°C carbon could not be measured accurately because of the very long time required for equilibrium to be reached. The points shown in Fig. 28 were obtained from the rate measurements (Section 4.9) and must be considered as approximate only. Dubinin et al.[85] encountered similar difficulties with a partially activated polyvinylidene chloride carbon heat treated to 1,750°C, where the adsorbate used was benzene.

The adsorptive capacity of the carbon heat treated to 1,700°C was extremely low; in fact, compared with the carbon heat treated at 800°C, there was a 99.4% reduction in the amount adsorbed at saturation. Even lower values were obtained for temperatures above 1,700°C where the amounts adsorbed for the carbons heat treated to 2,600° and 2,900°C were less than 0.03 c.c. per g.

Polyvinylidene Chloride Carbons (Activated) There is a three fold increase in the adsorptive capacity on activation, but heat treatment

at 1,700°C reduces it by approximately one third. It is interesting to note that this amount is comparable with the adsorptive capacity of an unactivated polyvinylidene chloride carbon heat treated at the same temperature.

Polyvinyl Chloride Carbons It is evident from Fig. 30 that, although polyvinyl chloride carbons possess only a very low initial surface area and are renowned as graphitizing carbons, the sintering behaviour is similar to that shown by most of the other carbons.

Cal Carbon The original Cal Carbon possesses a high adsorptive capacity and surface area. Sintering to a temperature of 1,700°C reduces the surface area by approximately 74%.

5.1.2 Densities and Pore Volumes

In this section, changes in the mercury and helium densities during heat treatment of various carbons will be discussed and pore volumes calculated from these densities will be compared with pore volumes calculated from isotherm data.

In general, values for the mercury density remained practically constant for increasing temperatures of heat treatment. As distinct from the steam activation of carbons, there is no erosion of the surface or enlargement of the pore volume[197] of a carbon on heat treatment. The helium density of a carbon, however, changes with the temperature of heat treatment and this change is by no means consistent for carbons prepared from different sources.

One of the main reasons for determining helium and mercury densities is the calculation of pore volumes. However, the size of the pores to which this pore volume refers is often overlooked. The density obtained by helium displacement measurements refers to all pores which can be penetrated by helium atoms, i.e. pores with diameters greater than approximately 2.0 Å, the critical diameter of the helium atom. Now, for the mercury density, the size of pores penetrated will depend upon the pressure. The pressure

chosen for this series of experiments was 900 mm. of mercury, corresponding to pores of diameter greater than 130,000 Å. Thus, the pore volume, calculated from the difference between the helium and mercury densities, will refer to pores of diameter ranging from 2.0 Å to 130,000 Å.

An alternative value for the pore volume can be calculated from the saturation value of the isotherm at $p/p_o = 1.0$. The value obtained, however, is influenced by:

(1) the critical diameter of the adsorbate molecule relative to the size of the pores,

(2) the packing density, and

(3) the possibility that at $p/p_o = 1.0$ the larger pores may not have completely filled.

The critical diameter of the argon atom is approximately 3.8 Å, so it will not penetrate pores of diameter less than this figure. Furthermore, it is possible that in pores of molecular dimensions, the packing density will be less than the normal liquid density. This would have the affect of reducing the value of V_{SL}, the saturation capacity expressed in c.c. of liquid per g. Lastly, there is evidence[198] that even at a value of $p/p_o = 1.0$, the larger macro-pores are not completely filled by capillary condensate.

The results obtained for densities and pore volumes will now be considered for cellulose acetate, phenol-formaldehyde, polyvinylidene chloride and polyvinyl chloride carbons.

Cellulose Acetate Carbon The trend in the helium density values with heat treatment (Fig. 36) is very similar to that obtained by Davidson and Losty[75] (Fig. 10) for cellulose carbons. At first, the helium density increases, but then, at heat treatment temperatures above 1,200°C, the helium density decreases and ultimately approaches the mercury density. The overall decrease in density may be attributed to the exclusion of helium atoms from the pore volume. The initial increase in density, however, is more

difficult to explain and is probably the net result of several factors.

Firstly, as the crystallites grow with heat treatment, the disorganized phase surrounding the crystallites is incorporated into the crystal lattice[29]. As the density of the disorganized phase is likely to be less than that of the crystallites, the removal of the disorganized phase will increase the overall density.

Secondly, the decrease in the interplanar spacing d_{002} which follows the growth of crystallites during heat treatment will increase the density ρ, since d_{002} and ρ are interrelated by the expression[85]:

$$\rho = \frac{z A m}{\underline{a}\,\underline{b}\,\underline{c}} = \frac{7.627}{d_{002}} \text{ g. c.c.}^{-1}$$

where z = 4, the number of carbon atoms in the elementary cell,
A = 12, the atomic weight of carbon,
m = 1.66×10^{-24} g., the mass of the hydrogen atom,
$\underline{a}$ = $\underline{b}$ = 2.456 Å, constants of the crystal lattice of graphite for the elementary plane,
$\underline{c}$ = $2\,d_{002}$, the dimension of the elementary cell along the $\underline{c}$ axis,
and d_{002}, the interplanar spacing in Å.

Dubinin et al.[85] have shown that heat treatment of a polyvinylidene chloride carbon from 750° to 1,750°C increased the crystallite density by approximately 0.2 g. c.c.$^{-1}$.

Thirdly, there is some evidence[48, 102, 199] that during the density determination helium tends to adsorb onto graphite surfaces. Therefore, as the crystallite size increases, it is possible that more helium will be adsorbed, giving the false impression that the density is increasing.

Pore volumes calculated from density and isotherm measurements are compared in Fig. 40. These results support the

view that heat treatment produces constrictions in pores, the pore volumes behind the constrictions eventually becoming inaccessible to helium. Initially, the pores contain few constrictions, allowing argon and helium atoms to penetrate the pore volume to the same extent, with the results that V_p is only slightly greater than V_{SL}. However, as the temperature of heat treatment is increased, the growth of constrictions begins to markedly influence the relative penetration of helium and argon, i.e. the carbons act as a molecular sieve. Thus when carbons are heat treated above 800°C, Fig. 40 shows that argon atoms no longer penetrate the same pore volume, so V_{SL} decreases. For helium, the maximum in V_p is reached for heat treatment temperatures between 1,000° and 1,200°C, but V_p decreases rapidly thereafter. For carbons heat treated at 2,000°C, V_p and V_{SL} are once again practically the same. This suggests that, at this temperature, the constrictions have grown to such an extent that the proportion of micro-pores in the total pore volume is quite small. Thus, the bulk of the pore volume is contained in larger pores, which are equally accessible to both argon and helium atoms.

For heat treatment temperatures between 800° and 2,000°C, the difference between V_p and V_{SL} is probably due to the 'sieving' of helium and argon atoms. Bearing in mind the particular pore sizes to which V_p and V_{SL} refer, the difference between V_p and V_{SL} will be the pore volume residing in pores of diameter 2.0 to 3.8 Å, plus the pore volume in macro-pores not taken into account in V_{SL}. This can be expressed as

$$V_p - V_{SL} = V_H + V_{MAC} \quad . \quad . \quad . \quad (35)$$

where V_H = pore volume not accessible to argon but accessible to helium,

and V_{MAC} = pore volume in those macropores not taken into account in V_{SL}.

Now, as $V_p = V_{SL}$ at 800°C, it is likely that for cellulose acetate V_{MAC} is negligible. Thus equation (35) reduces to

$$V_p - V_{SL} = V_H$$

where V_H increases from zero at 800°C to a maximum of 0.19 c.c. $g.^{-1}$ at 1,200°C, and then decreases to zero again at approximately 2,000°C.

Phenol-formaldehyde Carbon Similar results were obtained for the heat treated phenol-formaldehyde carbons except that the values of V_p and V_{SL} were much lower than those for the cellulose acetate carbons.

Polyvinylidene Chloride Carbon The results obtained for this carbon differ from those for cellulose acetate and phenol-formaldehyde carbons in that the density increased with the heat treatment temperature up to 1,700°C. Thus it appears that the effect of heat treatment up to 1,700°C is to render the pores more accessible to helium atoms.

While the pore volumes V_p and V_{SL} are equal for the carbon SA-800 (see TABLE 5), the values rapidly diverge as the carbon is heat treated at temperatures above 800°C.

Polyvinyl Chloride Here again the helium density increased with the temperature of heat treatment up to 1,700°C, signifying an opening up of pores. This may be due to extensive crystallite growth on heat treatment (see Section 4.11) and the development, to a limited extent, of a three-dimensionally ordered lattice. The resulting densification of the crystallites would be expected to be more marked than for other carbons.

For the carbons prepared from polyvinylidene chloride and phenol-formaldehyde, as seen from Fig. 36 and 37, the shape of the

helium density curves depends largely upon the value determined for the carbons heat treated to 1,700°C, i.e. if the helium densities for the carbons were grossly in error then the upward trend of the curves might be reversed. However, to avoid human error the helium densities of the carbons prepared at 1,700°C were repeated several times with the value in TABLE 4 for the carbons SA-1700 and PVC-1700 being the average of three separate determinations.

5.1.3 Pore Sizes

(a) Average Pore Size

The average pore size may be calculated from the relationship

$$\bar{r}_p = \frac{2\,V_p}{\Sigma} \qquad \cdot \quad \cdot \quad \cdot \qquad (9)$$

where $\bar{r}_p$ = radius of a cylindrical capillary. However, as carbons consist of small irregularly shaped crystallites, it is most unlikely that the capillaries will be cylindrical in shape. To allow for other shapes, Everett[122] has introduced the numerical factor γ into equation (9) to account for the detailed geometry of the system. Equation (9) now becomes

$$\bar{r}_p = \frac{1}{\gamma}\left(\frac{2\,V_p}{\Sigma}\right) \qquad \cdot \quad \cdot \quad \cdot \qquad (36)$$

For example, $\gamma = 1$ for a cylinder and $\bar{r}_p$ refers to the radius of the cylinder; for packed spheres where $\bar{r}_p$ refers to the radius of the sphere, $\gamma = 0.613$. Now all the suggested models of the crystallite structure of carbons (see Section 2.1.1.2) suggest that pores are formed as a result of irregular packing of crystallites, the shape of the pores being best represented as parallel-sided fissues. For this model Everett has suggested that $\gamma = 1$ and that $\bar{r}_p$ refers to the distance apart of the walls. Accordingly, the values of $\bar{r}_p$ calculated from the

experimental results all refer to a constant value of $\gamma = 1$.

The various carbons and their values of $\bar{r}_p$ can be divided into the two groups:

(1) carbons where $\bar{r}_p$ increases, and

(2) carbons where $\bar{r}_p$ remains constant.

Cellulose acetate carbon is typical of those in the first group, where $\bar{r}_p$ increases with increasing temperature of heat treatment. For a heat treatment temperature of 2,600°C, $\bar{r}_p$ reaches a value twice that for the carbon prepared at 800°C. Similarly, cellulose carbon, polyvinyl chloride carbon and Cal carbon all exhibit a marked increase in $\bar{r}_p$ with the temperature of heat treatment. As the pore volume is proportional to the square of the pore radius, it would at first sight appear as though the results for $\bar{r}_p$ contradict the value of the pore volume V_L obtained from the adsorption isotherms. However, if sintering destroys or closes up micro-pores, the proportion of large pores will increase, or in other words, it can be expected that $\bar{r}_p$ will increase.

Polyvinylidene chloride, activated polyvinylidene chloride and phenol-formaldehyde carbons correspond to the second group where the value of $\bar{r}_p$ remains practically constant as the temperature of heat treatment increases. Pore size estimates support the view that the bulk of the pore volume of polyvinylidene chloride carbons lies within a narrow pore size range[127]. If this is so, closing up the micro-pores would only slightly increase the average pore size.

For the activated polyvinylidene chloride carbon, it is interesting to note that there is only a small increase in the average pore radius on activation despite the large increase in pore volume and surface area. An extensive study by Culver and Heath[197] on the activation of polyvinylidene chloride carbons, showed that about half the measured increase in pore volume was due to an increase in $\bar{r}_p$, while the remainder was due to the creation of new pores. Sintering at 1,700°C produced only a slight increase

in $\bar{r}_p$.

(b) Pore Size Distribution

From Nitrogen Adsorption Isotherms Although the methods of Barrett, Joyner and Halenda[131], and Cranston and Inkley[133] have been criticized on several points[122], the method of analysis is the only one available for determining the pore size distribution in the micropore range. For adsorbents with relatively large pore sizes, this method is known to give consistent results. For instance, Cranston and Inkley[133] analyzed the nitrogen adsorption isotherm for a silica-alumina gel and found that the cumulative surface area, calculated by their pore size distribution analysis, agreed to within 1.5% of the value of the surface area obtained by the normal BET method.

For both the cellulose acetate carbons CA-800 and CA-1700, the method of analysis of Cranston and Inkley applied to nitrogen adsorption isotherms, came to a forced stop at a pore diameter of 14 Å; below this figure the calculation involved invalid negative values of the pore volumes. Calculated BET surface areas and total pore volumes are shown in TABLE 8 together with cumulative surface areas and pore volumes obtained from the pore size distribution analysis.

TABLE 8

Surface Areas and Pore Volumes for Cellulose Acetate Carbons

	CA-800	CA-1700
BET Surface Area ($m.^2 g.^{-1}$)	473	47.8
Cumulative Surface Area ($m.^2 g.^{-1}$)	148	27.5
Total Pore Volume ($c.c.\ g.^{-1}$)	0.261	0.0527
Cumulative Pore Volume ($c.c.\ g.^{-1}$)	0.122	0.0428

For CA-800, only 31% of the surface area is accounted for in the pore size distribution analysis compared with 58% for CA-1700. For the pore volumes, the agreement is somewhat better, with 46% of the pore volume taken into account for CA-800 and 81% for CA-1700.

The cumulative pore volumes are shown in Fig. 42 as a function of the pore size. Below a pore diameter of 130 Å, the cumulative pore volume becomes negligible as the pore diameter approaches 300 Å. The marked drop in pore volume as a result of heat treatment to 1,700°C, is mainly associated with those pores of diameter less than 60 Å.

Differentiating the curves in Fig. 42 yields the differential pore size distribution shown in Fig. 43. The pore size distribution for CA-800 is narrow and yields a maximum at a pore diameter of 25 Å, a value in close agreement with the average pore diameter calculated from equation (9). For CA-1700, the distribution is broader and the maximum appears at 50 Å.

On the basis that the observed loss of surface area and pore volume on heat treatment of carbons could be attributed to growth of constrictions into micro-pores, the effect of sintering was examined for selected geometrical models with a view to determining the resulting change in pore size distribution. In the first model constrictions were presumed to form in pores and act as a barrier to the passage of molecules through the pores. Starting with the experimentally observed pore distribution for CA-800, a constriction of length 10 Å was assumed to have developed in all the pores, reducing the effective pore diameter by 10 Å and thus altering the pore size distribution to that given by curve II in Fig. 66. Similarly, curve III resulted from the development of a constriction of length 25 Å. The second model involved the growth of a circular constriction which occupied pore volume proportional to the area of the constriction.

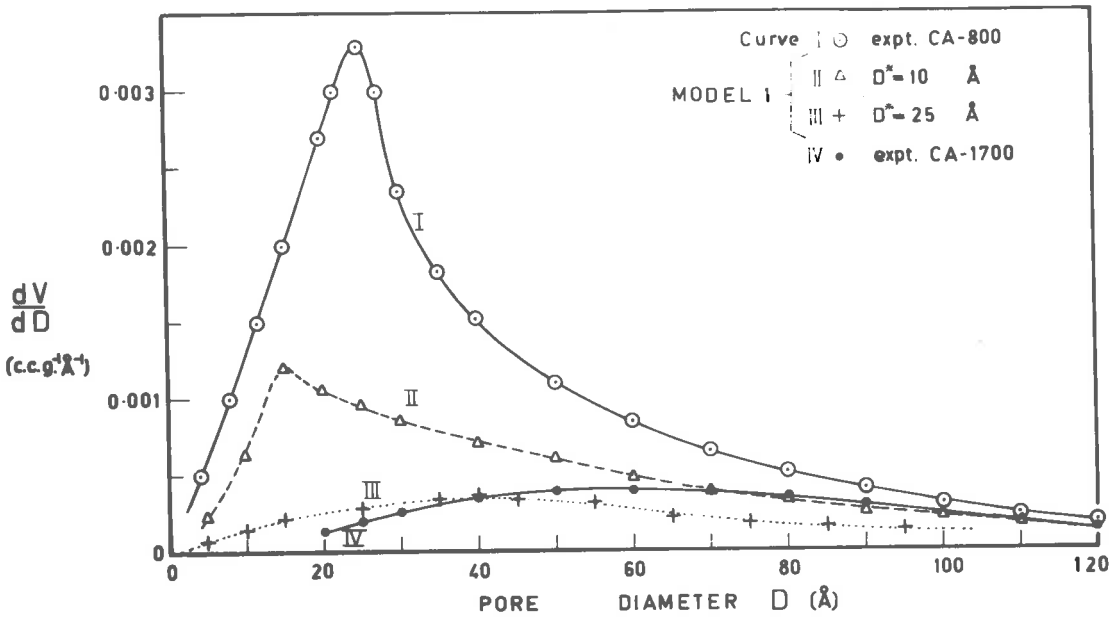

Fig. 66 - Change in the Differential Pore Size Distribution for Different Values of the Constriction Diameter D^* - MODEL 1

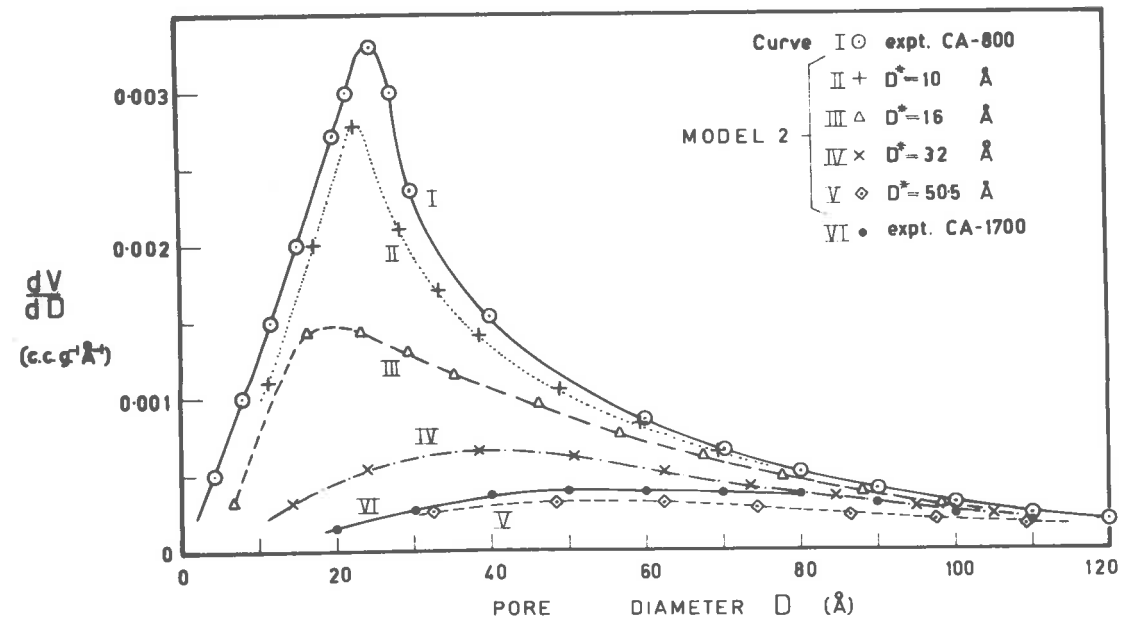

Fig. 67 - Change in the Differential Pore Size Distribution for Different Values of the Constriction Diameter D^* - MODEL 2

The size of the constrictions and the resulting pore size distribution curves are shown in Fig. 67. Calculations appear in APPENDIX D.2.

The models chosen probably represent the two extreme types of constriction. In the first model, the constriction acts only as a gate and no account is taken of the pore volume it occupies; the end result is a relatively severe reduction in pore volume. For the second model, the same growth of constriction has much less effect on the pore volume than in the first model. Comparison of the theoretical and experimental pore size curves for CA-1700, indicates that, for the first model, a constriction of approximately 25 Å is appropriate and, for the second model a constriction of 40 to 50 Å. In both cases the fit of the theoretical and experimental curves is imperfect over the complete pore size range, and it is likely that the mechanism of sintering involves some combination of both models.

High Pressure Mercury Penetration Measurements Although Thurstan and Wall[200] have shown that there are several corrections that must be applied to the results to allow for the compression of the mercury, the glass and the carbon sample, it is unlikely that these corrections would vary between experiments. Thus, for a qualitative analysis of the results these corrections can be ignored.

For cellulose acetate carbons, the results shown in Fig. 44 indicate that the bulk of the pore volume lies in pores of radii less than 100 Å. The slopes of the curves at pore radii less than 100 Å, indicate that a large amount of pore volume is contained in pores of radii less than 30 Å. It is also clear that heat treatment has little effect on the cumulative pore volume over the range of pore radii 30 to 10,000 Å.

The results for polyvinylidene chloride carbon are typical of a finely porous carbon, where the bulk of the pore volume lies in pores of radius less than 30 Å. Clearly polyvinylidene chloride

carbons possess a much narrower pore size distribution than cellulose acetate carbons.

For the polyvinyl chloride carbon PVC-800, the pore size distribution curve resembles that of the polyvinylidene chloride carbon. However, from a comparison of the measured pore volume with that obtained from isotherm measurements, polyvinyl chloride carbons would not be expected to possess a large pore volume in pores less than the 30 Å radius.

The pore volume calculated from mercury porosimeter data for the cellulose acetate carbon CA-1700 is considerably greater than the corresponding saturation value obtained from the adsorption isotherm. There are two factors which could explain this discrepancy. Firstly, the mercury penetration data refer to the diameter of the constriction[139] in a pore rather than to the average pore diameter. Accordingly, the pore diameter generally obtained will be too small, or correspondingly, the pore volume at a specific pore diameter will be too large. This would mean that the plots shown in Fig. 44 and 45 should be shifted towards larger values of the pore diameter if appropriate corrections could be made. Meyer[201] has suggested a method of correcting the results, but unfortunately the method is long and tedious. The failure of the bulk of the mercury to move out of the pores when the pressure was reduced at the conclusion of a run is additional evidence for the presence of constrictions in the pores of cellulose acetate, polyvinylidene chloride and polyvinyl chloride carbons, i.e. these carbons exhibited considerable hysteresis.

Secondly, Holmes and Emmett[141] have shown that even when nitrogen isotherms are extended to very high relative pressures, corresponding pore volumes are much lower than those obtained from mercury penetration methods. Emmett[202] has suggested that values of the pore volume obtained from nitrogen isotherms are much more likely to represent minimum values. Bangham and Razouk[198] found

that, even at a relative pressure of unity, large pores would not fill with capillary condensate; only immersion of the solid in the liquid caused the large pores to fill.

(c) Estimation of Pore Size from Molecular Sieve Data

Saturation values V_s obtained from the isotherms at $p/p_o = 1.0$ for cellulose acetate are presented in TABLE 9; the isotherms for n-butane and neo-pentane were not measured to saturation pressure so it was necessary to use the value V_s' at $p/p_o = 0.10$ in subsequent calculations. The V_s values have been converted from c.c. of gas adsorbed to c.c. of liquid using the density of the liquid adsorbate at the temperature of the isotherm[191].

TABLE 9

Comparison of Saturation Values for Cellulose Acetate Carbons

Cellulose Acetate Carbon	Saturation Values V_s (c.c. $g.^{-1}$)		$100. \frac{V_s(N_2) - V_s(Ar)}{V_s(N_2)}$
	Nitrogen	Argon	
CA-800	0.270	0.210	22
CA-1200	0.116	0.075	34
CA-1700	0.044	0.033	25
	Benzene	p-Cymene	$100. \frac{V_s(B) - V_s(C)}{V_s(B)}$
CA-800	0.280	0.190	32
CA-1200	0.165	0.125	24
CA-1700	0.077	0.065	13
	n-Butane	neo-Pentane	$100. \frac{V_s'(Bu) - V_s'(P)}{V_s'(Bu)}$
CA-800	0.143	0.113	21
CA-1200	0.038	0.022	43
CA-1700	0.018	0.017	8

Values for the critical diameter[126] of the adsorbates are: N_2 = 3.0 Å, Ar = 3.84 Å, C_6H_6 = 6.0 Å, p-cymene = 6.0 Å, n-butane = 4.9 Å and neo-pentane = 6.2 Å. While benzene and p-cymene molecules both have approximately the same critical diameter, the molecules of p-cymene have a minimum thickness of 4.4 Å compared with benzene which has a thickness of approximately 2.5 Å.

The data have been arranged so that saturation values for similar species of molecules can be compared, e.g. nitrogen - argon, benzene - p-cymene, and n-butane - neo-pentane. The percentage differences in saturation values are shown in column 4 of TABLE 9. Less argon is adsorbed than nitrogen, less benzene is adsorbed than p-cymene and less n-butane is adsorbed than neo-pentane throughout the carbon series, but there is some inconsistency in the percentage difference in saturation values. The percentage difference in saturation values for benzene and p-cymene decreases with increasing temperature of heat treatment which indicates that the available pore volume is becoming more accessible to the larger molecule - p-cymene.

The results, while of interest, do not permit any definite conclusions to be drawn regarding the effect of heat treatment on the mean pore size of the carbons. It is clear that carbons with a relatively wide pore size distribution such as cellulose acetate carbon, cannot function as molecular sieves and yield consistent results. As Emmett[202] has pointed out, the packing density and the number of integral layers of adsorbate that can fit into a pore may, in certain instances, override the influence of the ratio of the critical diameter of the adsorbate to the pore diameter.

(d) Indications of Pore Size Changes

Using the method of Holmes and Emmett[141] for estimating changes in pore size in carbons on activation, the following qualitative deductions can be made from the change in shape of the adsorption isotherms for the sintered carbons.

The adsorption isotherms of argon on the various carbons (see Fig. 25 to 31) all show a decrease in the total adsorption below $^{p}/_{p_o} = 0.4$, indicating a reduction in the volume of micropores (D 40 Å) present in the carbon. The slope of the middle portion of the isotherms from $^{p}/_{p_o} = 0.4$ to 0.7 decreases slightly signifying a small decrease in the volume of the pores in the

intermediate range (D = 40 to 100 Å). Similarly, there is only a minor change in the slope of the final section from $^{p}/_{p_o}$ = 0.7 to 0.99, corresponding to pores of diameter from 100 to 600 Å.

The decrease in the volume of micro-pores can be more clearly illustrated by calculating the ratio R of pore volume above $^{p}/_{p_o}$ = 0.1 to the pore volume below $^{p}/_{p_o}$ = 0.1. TABLE 10 summarizes the values of R obtained from the isotherms of nitrogen, argon, benzene and p-cymene on the cellulose acetate carbon series.

TABLE 10

Pore Volume Ratio R for Heat Treated Cellulose Acetate Carbons

Heat Treatment Temperature °C	Ratio R			
	Nitrogen	Argon	Benzene	p-Cymene
700	-	0.68	-	-
800	0.44	0.76	0.95	1.39
1000	-	0.77	-	-
1200	1.11	1.61	3.34	4.42
1400	-	1.75	-	-
1700	1.54	2.23	4.77	5.78
2200	-	2.50	-	-
2600	-	2.71	-	-
2900	-	2.56	-	-

In each case (except for CA-2900) the ratio R increased with increased temperature of heat treatment; this indicates that the proportion of pore volume in the large pores increases with increasing temperature of heat treatment.

5.1.4 Influence of Particle Size on the Adsorptive Capacity of Sintered Carbons

According to TABLE 7 variations in particle size have very little effect on the adsorptive capacity and surface area of the cellulose acetate carbon CA-800. The increase in external surface area resulting from the decrease in particle size, is negligible in comparison with the internal surface area. However, for the sintered carbon cellulose acetate CA-1700, there is a marked increase in both adsorptive capacity and surface area when the particle size is reduced. The increase in surface area of about 50% is probably due to previously blocked pores becoming available for adsorption. In agreement with this theory, Franklin[91] found that the helium density for a series of heat treated carbonized coals noticeably increased as the particle size was reduced. This evidence suggests that heat treatment produces constrictions in the pores, thus preventing the transport of molecules into the pore volume behind the constrictions.

Supporting evidence that constrictions in the pores largely determine the available pore volume, has been obtained by Dacey and Thomas[127] from experiments on the adsorption of neo-pentane on a polyvinylidene chloride carbon. They found that grinding the carbon to a fine powder increased the rate of adsorption of neo-pentane by a factor of at least 100. Cameron and Stacy[203] finely ground cokes and chars from coals and discovered that the surface area was considerably increased.

5.2 Kinetics of Adsorption

It has been shown that if the rates of adsorption are plotted as $\frac{V_t - V_o}{V_\infty - V_o}$ versus a function of time then, for a specific carbon and temperature, the curves are practically coincident. Now it is desirable to examine the rate controlling step for the rate of adsorption as represented by the curves in Fig. 48 to 52. The rate controlling step could be:

(1) the rate of adsorption of gas molecules from the gas phase to the adsorbed phase,

(2) the rate of heat transfer from the adsorbent to the surrounding isothermal bath, or

(3) the rate of diffusion of gas molecules through the porous structure to positions adjacent to final equilibrium adsorption sites.

There is substantial evidence[144] to show that the rate of adsorption from the gas phase to the adsorbed phase is extremely fast (see Section 2.5).

With regard to the rate of heat transfer, the heat evolved during adsorption ($q_{st} \approx 2{,}000$ cal.mole^{-1}) will cause the temperature of the specimen to rise in the absence of heat transfer between the sample and its surroundings. As calculated by the procedure of Deitz et al.[204], the maximum temperature rise of the carbon sample, assuming no heat transfer, would be approx. 5^{o}K. This would not markedly affect the rate of adsorption, the temperature coefficient for the adsorption of argon being fairly small (see Section 5.2.1). However, there is strong experimental evidence for the rate of adsorption being independent of the rate of heat transfer. Firstly, for a particular sample and temperature, the rate of adsorption curves for successive pressure increments are coincident, despite at least a thousand-fold change in the pressure or a hundred-fold change in the amount adsorbed. If heat transfer was the rate controlling factor in the adsorption process the disposition of the rate curves would be expected to depend upon the total pressure and the amount adsorbed. Secondly, rates of desorption measured for several runs were found to be nearly the same as the rates of adsorption. As desorption is an endothermic process and adsorption an exothermic process, this would only occur if the rate of adsorption or desorption was unaffected by the rate of heat transfer.

The remaining rate controlling factor to be considered is

the rate of diffusion of gas molecules into the porous structure. To investigate the possibility that the rate of adsorption is controlled by this factor, a geometrical model of the adsorbent was assumed and the solution of the relevant diffusion equations compared with the experimental results.

5.2.1 Mathematics of Diffusion

For a diffusion process, Fick's Second Law can be assumed to be the governing relationship, provided the following criteria are satisfied:

(1) the mode of gaseous transport is Knudsen flow, and

(2) the flux is proportional to the gaseous concentration gradient.

Firstly, the mode of transport of the gas molecules depends upon the ratio of the mean free path of the molecules to the pore diameter. At atmospheric pressure, the mean free path of the adsorbate molecules is approximately 1,000 Å. This figure greatly exceeds the mean pore diameter of the carbons, which may be of the order of 25 to 50 Å, based on results obtained with the mercury porosimeter (Section 5.1.3). Hence Knudsen flow should be the predominant mode of transport of gas molecules.

With regard to the second criterion, as Benson and Tompkins[151] have shown, it is necessary to examine the trends in the constants and diffusion coefficients derived from the solution of Fick's Second Law. Thus assuming that, a priori, the flux is proportional to the concentration gradient, Fick's Second Law can be written in the form

$$\frac{\partial c}{\partial t} = \frac{\partial}{\partial x}\left(D_e \frac{\partial c}{\partial x}\right) \qquad \cdot \quad \cdot \quad \cdot \qquad (37)$$

where D_e is the effective diffusion coefficient and $\frac{\partial c}{\partial x}$ the concentration gradient of molecules in the gas phase. Now the rate of adsorption at a given temperature on a particular sample has been

found to be independent of the total pressure and concentration so the diffusion coefficient must be independent of concentration. Under these conditions equation (37) can be written

$$\frac{\partial c}{\partial t} = D_e \frac{\partial^2 c}{\partial x^2} \quad \cdot \quad \cdot \quad \cdot \quad (38)$$

Furthermore, for adsorption on carbons at -183°C and -196°C where small increments of pressure of approximately 0.1 cm. were employed, the concentration of the adsorbate on the surface can be assumed to be proportional to the pressure without serious error. Even at -81°C, where the pressure steps were of the order of 1 cm., Henry's Law was obeyed to a good approximation up to a pressure of 20 cm. Thus, the parameter measured in the rate of adsorption experiments, viz. the rate of weight change of the adsorbent $\frac{\partial V}{\partial t}$ can be substituted for the rate of change of the gas phase concentration $\frac{\partial c}{\partial t}$.

An appropriate geometrical model for the particles of carbon is a sphere of radius r_o since the granules of carbon are approximately spherical in shape. Solutions of equation (38) for this model are[147, 150]:

$$\frac{V_t - V_o}{V_\infty - V_o} = 1 - \frac{6}{\pi^2} \sum_{n=1}^{\infty} \frac{1}{n^2} \exp\left(-\frac{Dn^2 \pi^2 t}{r_o^2}\right) \quad \cdot \quad (39)$$

$$\frac{V_t - V_o}{V_\infty - V_o} = 6 \left(\frac{Dt}{r_o^2}\right)^{\frac{1}{2}} \left[\pi^{-\frac{1}{2}} + 2 \sum_{n=1}^{\infty} \text{ierfc } n \left(\frac{Dt}{r_o^2}\right)^{-\frac{1}{2}}\right] - \frac{3Dt}{r_o^2} \quad \cdot \quad \cdot \quad (40)$$

The series in equation (39) converges rapidly for large values of $(Dt/r_o^2)^{\frac{1}{2}}$, while the series of equation (40) converges rapidly for small values of $(Dt/r_o^2)^{\frac{1}{2}}$. A numerical solution of these equations

is shown in Fig. 68 in terms of the dimensionless parameter $(Dt/r_o^2)^{\frac{1}{2}}$ (ref. 147 p. 90 Fig. 6.4, curve for zero fractional exhaustion).

Values for the diffusion coefficient have been calculated by three methods assuming a priori that the process is diffusion controlled. Method A assumes that the diffusion process is described by equation (38). Methods B and C involve certain approximations which reduce equations (39) and (40) to linear forms.

Method A - Calculation of the Diffusion Coefficient by Comparison of the Experimental Curve with the Theoretical Curve.

A numerical solution of equation (40) can be calculated in terms of the dimensionless parameters $(Dt/r_o^2)^{\frac{1}{2}}$ and $\frac{V_t-V_o}{V_\infty-V_o}$. The plot of this solution is shown in Fig. 68 while the data are listed in APPENDIX F.4. For arbitary values of $\frac{V_t-V_o}{V_\infty-V_o}$, the theoretical values of $(Dt/r_o^2)^{\frac{1}{2}}$ were compared with the experimental value of $t^{\frac{1}{2}}$ allowing the determination of values of $\frac{D^{\frac{1}{2}}}{r_o}$ as a function of $\frac{V_t-V_o}{V_\infty-V_o}$.

Method B - Calculation of the Diffusion Coefficient for Large Values of $(Dt/r_o^2)^{\frac{1}{2}}$.

If it is assumed that the terms after n=1 in the summation are negligible, equation (39) reduces to

$$\frac{V_t-V_o}{V_\infty-V_o} = 1 - \frac{6}{\pi^2} \exp\left(-\frac{D\pi^2 t}{r_o^2}\right) \quad \cdot \quad \cdot \quad (41)$$

or,

$$\frac{V_t-V_\infty}{V_o-V_\infty} = \frac{6}{\pi^2} \exp\left(-\frac{D\pi^2 t}{r_o^2}\right) \quad \cdot \quad \cdot \quad (42)$$

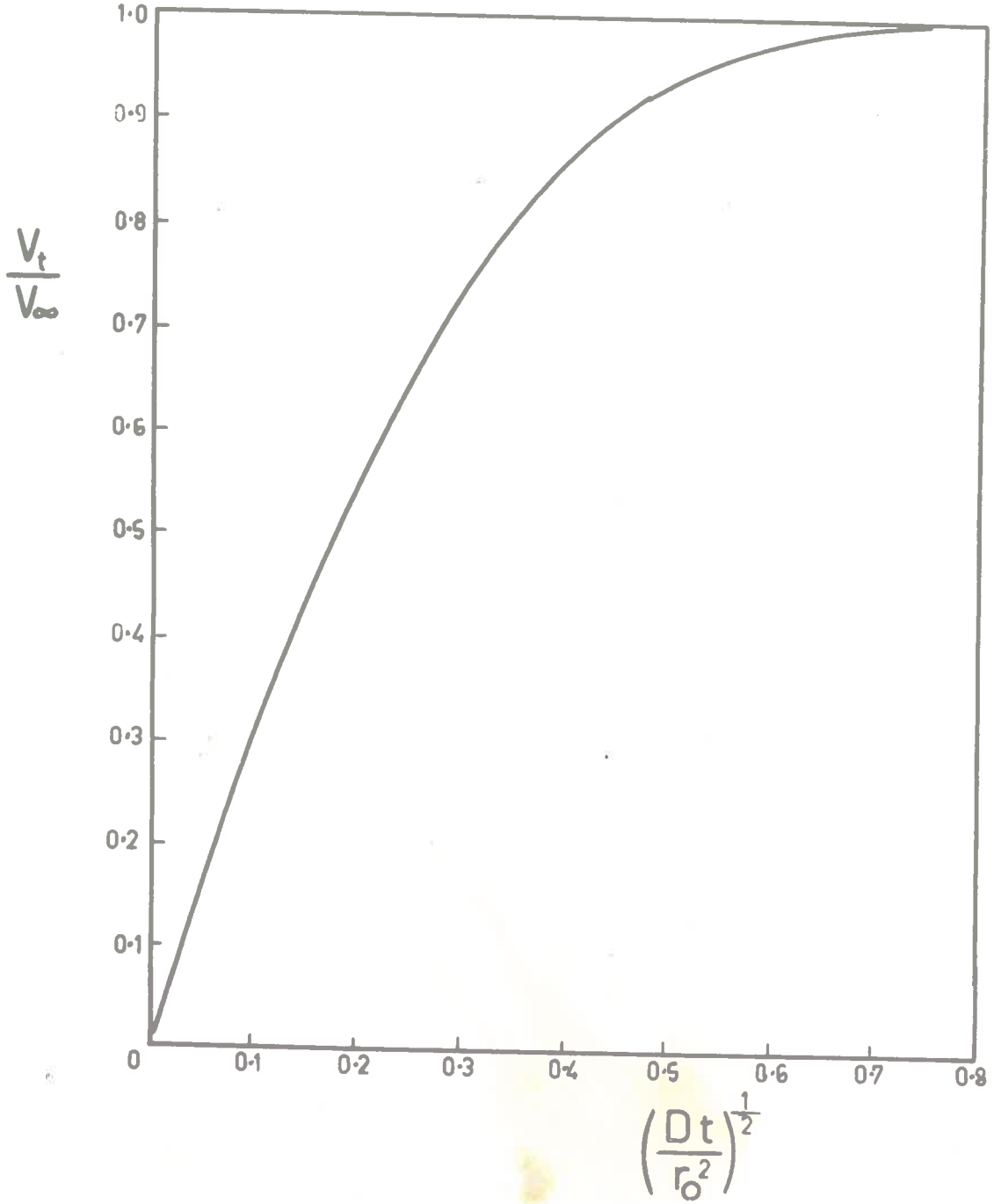

Fig. 68 - Theoretical Curve for the Diffusion Into a Sphere of Radius r_o (ref.147 p.90)

Taking logarithms,

$$\log\left(\frac{V_t-V_\infty}{V_o-V_\infty}\right) = \log\frac{6}{\pi^2} - \frac{1}{2.303}\,\frac{D\pi^2 t}{r_o^2} \qquad (43)$$

Thus a plot of $\log\left(\frac{V_t-V_\infty}{V_o-V_\infty}\right)$ versus t should yield a straight line of slope $-\frac{1}{2.303}\,\frac{D\pi^2}{r_o^2}$.

Method C - Calculation of the Diffusion Coefficient for Small Values of $(Dt/r_o^2)^{\frac{1}{2}}$.

For small values of $(Dt/r_o^2)^{\frac{1}{2}}$, the ierfc terms behind the summation in equation (40) are negligible (ref.147, p.326, TABLE 2.1). Thus equation (40) reduces to

$$\frac{V_t-V_o}{V_\infty-V_o} = 6\left(\frac{Dt}{r_o^2}\right)^{\frac{1}{2}}\pi^{-\frac{1}{2}} - \frac{3\,Dt}{r_o^2} \qquad (44)$$

This equation can be reduced to a linear form by one of the following procedures:

(1) by differentiating with respect to t or $t^{\frac{1}{2}}$, or

(2) assuming that the last term is negligible.

In the first procedure it matters little to the final value of the diffusion coefficient whether equation (44) is differentiated with respect to t or $t^{\frac{1}{2}}$. Differentiating equation (44) with respect to t, gives

$$d\left(\frac{V_t-V_o}{V_\infty-V_o}\right)/dt = \frac{1}{2}\,\frac{6}{\pi^{\frac{1}{2}}}\,\frac{D^{\frac{1}{2}}t^{-\frac{1}{2}}}{r_o} - 3\frac{D}{r_o^2} \qquad (45)$$

Thus a plot of the left hand side versus $t^{-\frac{1}{2}}$, should yield a straight

line of slope 1.69 $D^{\frac{1}{2}}/r_o$ and intercept 3 D/r_o^2.

For the second procedure equation (44) reduces to

$$\frac{V_t-V_o}{V_\infty-V_o} = \frac{6}{\pi^{\frac{1}{2}}} \left(\frac{Dt}{r_o^2}\right)^{\frac{1}{2}} \quad . \quad . \quad . \quad (46)$$

Thus a plot of $\frac{V_t-V_o}{V_\infty-V_o}$ versus $t^{\frac{1}{2}}$, should yield a straight line of slope $\frac{6}{\pi^{\frac{1}{2}}} \frac{D^{\frac{1}{2}}}{r_o}$.

Application of the above equations to the experimental results and the calculation of the diffusion coefficients will now be discussed.

Cellulose Acetate Carbons

Plots of $\frac{V_t-V_o}{V_\infty-V_o}$ versus $t^{\frac{1}{2}}$ for the cellulose acetate carbons CA-800, CA-1200 and CA-1700 at -81°, -183° and -196°C are shown in Fig. 49 to 51 Section 4.9.

(a) Temperature : -81°C.

Values of $D^{\frac{1}{2}}/r_o$ were computed for CA-800, CA-1200 and CA-1700 by Method A and are listed in TABLE 11.

For long times, i.e. for large values of $(Dt/r_o^2)^{\frac{1}{2}}$ or $\frac{V_t-V_o}{V_\infty-V_o}$, values of $D^{\frac{1}{2}}/r_o$ were obtained by Method B for CA-800, CA-1200 and CA-1700. The graphs of log $\left(\frac{V_t-V_\infty}{V_o-V_\infty}\right)$ versus t for CA-800, CA-1200 and CA-1700 are shown in Fig. 69.

Values of $D^{\frac{1}{2}}/r_o$ for short times were obtained by Method C from equation (45) for CA-800. The straight line plot of

$d\left(\frac{V_t-V_o}{V_\infty-V_o}\right)/_{dt}$ versus $t^{-\frac{1}{2}}$ is shown in Fig. 70. There were insufficient data for CA-1200 and CA-1700 at low values of $\frac{V_t-V_o}{V_\infty-V_o}$ to apply this method successfully.

Values of $D^{\frac{1}{2}}/r_o$ obtained by the above methods are summarized in TABLE 11.

TABLE 11

Diffusion Coefficients for the Adsorption of Argon on Cellulose Acetate Carbons at -81°C

Method of Calculation	$\frac{V_t-V_o}{V_\infty-V_o}$	$\frac{D^{\frac{1}{2}}}{r_o}$ (min.$^{-\frac{1}{2}}$)		
		CA-800	CA-1200	CA-1700
Method A - by comparison of experimental curve with the theoretical	0.162	0.14	-	-
	0.235	0.15	-	-
	0.310	0.15	-	-
	0.442	0.16	-	-
	0.560	0.15	0.35	-
	0.662	0.15	0.32	-
	0.750	0.15	0.28	0.55
	0.880	0.14	0.23	0.34
	0.920	0.14	0.18	0.20
Method B - for large values of $(\frac{Dt}{r_o^2})^{\frac{1}{2}}$ -	> 0.7	0.13	0.12	0.13

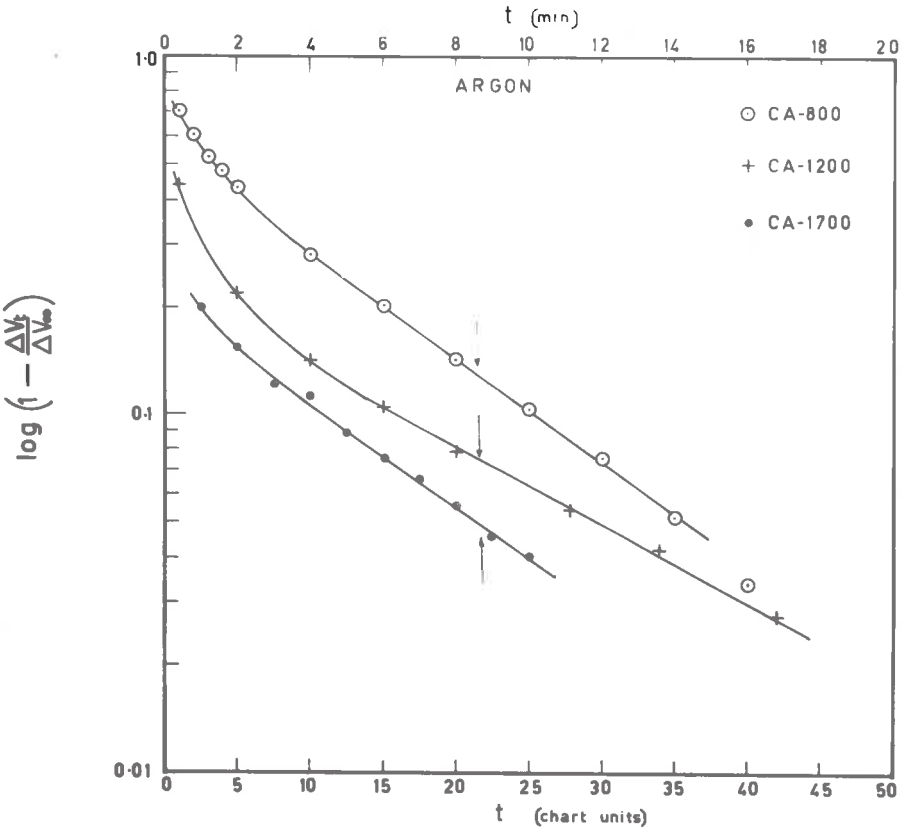

Fig. 69 - Plot of log $(^{1-\Delta V}t/\Delta V_{\infty})$ versus t for CA-800, CA-1200 and CA-1700

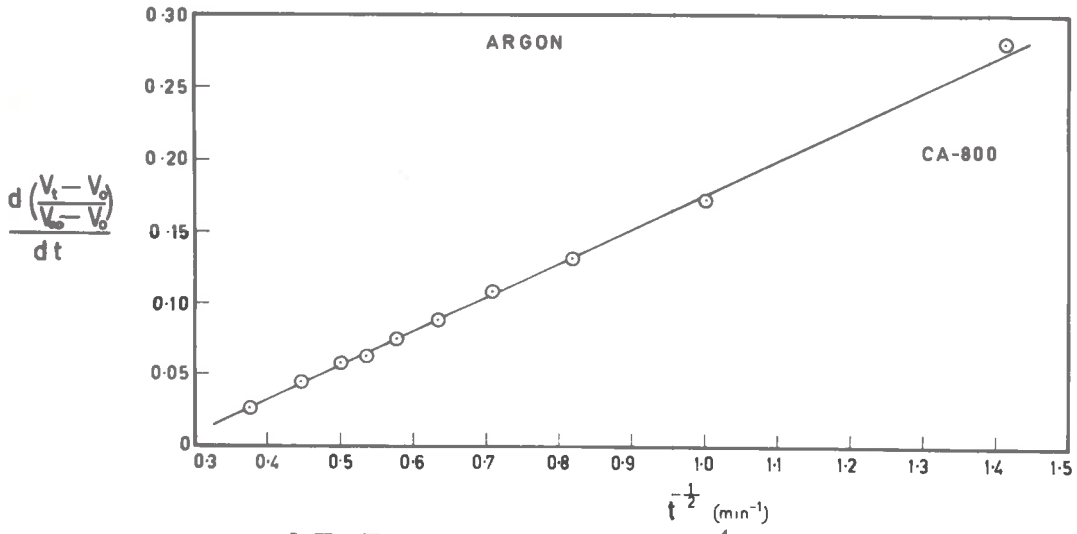

Fig. 70 - Plot of $^{d(V_t-V_o/V_\infty-V_o)}/_{dt}$ versus $t^{-\frac{1}{2}}$ for CA-800 at -81°C

Method of Calculations	$\frac{V_t-V_o}{V_\infty-V_o}$	$\frac{D^{\frac{1}{2}}}{r_o}$ ($min.^{-\frac{1}{2}}$)		
		CA-800	CA-1200	CA-1700
Method C - for small values of $(\frac{Dt}{r_o^2})^{\frac{1}{2}}$ - equation (45)	< 0.7	0.14	-	-

The values of $D^{\frac{1}{2}}/r_o$ obtained by Method A for CA-800 are approximately constant over the complete range of adsorption; this lends support to the assumption that the adsorption process is correctly described by Fick's Second Law. Also, as seen in TABLE 11, the values of $D^{\frac{1}{2}}/r_o$ for CA-800 obtained by Methods B and C are in reasonable agreement with those obtained by Method A. However, values of $D^{\frac{1}{2}}/r_o$ for CA-1200 and CA-1700 obtained by Methods A and B do not agree and will be considered along with the corresponding data obtained at -183° and $-196^\circ C$.

(b) Temperatures : -183° and $-196^\circ C$.

There is a marked change in the shape of the plots of $\frac{V_t-V_o}{V_\infty-V_o}$ versus $t^{\frac{1}{2}}$ at -183° and $-196^\circ C$ compared with the plots at $-81^\circ C$ due, essentially, to slower rates of adsorption at the lower temperatures. Thus for CA-800 at $-183^\circ C$, the plot is approximately linear up to values of $t=20$ min., while, for CA-800 at $-81^\circ C$, the graph begins to depart from a straight line at $t=0.75$ min. Inspection of Fig. 68 however, shows that this behaviour is to be expected and the departure of the plot from a straight line relationship depends upon the range of $\frac{V_t-V_o}{V_\infty-V_o}$ values measured. Thus, the graph for CA-800 at $-81^\circ C$ is, in fact, approximately straight

over the same range of $\frac{V_t-V_o}{V_\infty-V_o}$ values as for CA-800 at -183°C.

The plots of $\frac{V_t-V_o}{V_\infty-V_o}$ versus $t^{\frac{1}{2}}$ for CA-1200 and CA-1700 at -183° and -196°C are distinguished by the presence of a 'foot'. When extrapolated, the linear portion of the CA-1200 and CA-1700 plots cuts the $\frac{V_t-V_o}{V_\infty-V_o}$ axis at some positive value. The presence of a 'foot' in such curves is not unusual and has been ascribed to an 'instantaneous' van der Waals adsorption on the external surfaces of the particles[160,162]. TABLE 12 shows values of the 'foot', Δ, for the carbons CA-800, CA-1200 and CA-1700 at -81°, -183° and -196°C.

TABLE 12

Values of the Instantaneous Adsorption, Δ, (g_o/g_o)

Carbon	Temperature (°C)		
	-81	-183	-196
CA-800	0	0	0
CA-1200	0.1+	0.30	0.27
CA-1700	*	0.40	0.47

* indeterminate

\+ estimate only

The results are not very accurate, but, in general, the values of Δ for CA-1200 and CA-1700 appear to decrease with increasing temperature. This trend has been previously reported for the adsorption of $n\text{-}C_4H_{10}$, CH_2Cl_2 and $(CH_3)_2NH$ on various zeolites[160].

Clearly the presence of the 'foot' must be taken into

account when calculating diffusion coefficients by readjusting the scale on the $\frac{V_t - V_o}{V_\infty - V_o}$ axis to read from 0 to 1.0 over the interval from Δ to 1.0. Under these conditions the calculated diffusion coefficient refers to the adsorption process following the 'instantaneous' adsorption. Values of $D^{\frac{1}{2}}/r_o$, so calculated, for carbons CA-800, CA-1200 and CA-1700 are listed in TABLE 13.

TABLE 13

Diffusion Coefficients for the Adsorption of Argon on Cellulose Acetate Carbons at -183° and -196°C

Method of Calculation	$\frac{V_t - V_o}{V_\infty - V_o}$	$\frac{D^{\frac{1}{2}}}{r_o}$ (min.$^{-\frac{1}{2}}$)		
		CA-800	CA-1200	CA-1700
Method A - by comparison of experimental curve with the theoretical -183°C	0.162	0.025	-	-
	0.235	0.028	0.079	0.11
	0.310	0.032	0.074	0.12
	0.442	0.032	0.081	0.12
	0.560	0.032	0.085	0.13
	0.662	0.032	0.087	0.14
	0.750	0.032	0.088	0.13
	0.822	0.032	0.088	0.14
	0.880	0.032	0.087	0.14
	0.921	0.032	0.086	0.14
	0.954	0.032	0.087	0.14

Method of Calculation	$\frac{V_t - V_o}{V_\infty - V_o}$	$\frac{D^{\frac{1}{2}}}{r_o}$ ($min.^{-\frac{1}{2}}$)		
		CA-800	CA-1200	CA-1700
-196°C	0.162	0.036	-	-
	0.235	0.039	0.10	0.14
	0.310	0.039	0.10	0.14
	0.442	0.041	0.10	0.14
	0.560	0.042	0.11	0.15
	0.662	0.041	0.11	0.16
	0.750	0.041	0.12	0.16
	0.822	0.041	0.12	0.17
	0.880	-	0.12	0.17
	0.921	-	0.12	0.17
	0.954	-	0.13	0.17
Method C - for small values of $(\frac{Dt}{r_o^2})^{\frac{1}{2}}$ - equation (46)				
-183°C	< 0.7	0.029	0.074	0.12
-196°C	< 0.7	0.037	0.090	0.13

Again the consistency of the results lend support to the assumption that the adsorption process is correctly described by Fick's Second Law equation (38).

The discrepancy between $D^{\frac{1}{2}}/r_o$ values for CA-1200 and CA-1700 calculated by Methods A and B can be explained in terms of the presence of a 'foot' in the rate of adsorption curves. Although the value of the 'foot' should be lower at -81°C than at -183° or -196°C, its presence would undoubtedly upset the calculation

of the values of $D^{\frac{1}{2}}/r_o$. Unfortunately, there are insufficient data to accurately extrapolate the rate curves back to the $\Delta V_t/\Delta V_\infty$ axis to obtain a value for Δ.

The change in the diffusion coefficient with temperature indicates that the temperature coefficient is positive between -81° and -183°C, and negative between -183° and -196°C. The temperature coefficient is generally positive[126], as it is associated with an activated diffusion process whereby molecules move down a capillary through the periodic potential energy field of the surrounding crystals. Barrer[126, 162], however, has reported negative temperature coefficients for the rates of adsorption of nitrogen and argon on certain zeolites. He suggested that this could be expected where a rise in temperature reduced the interstitial density of sorbate molecules more than it accelerated their diffusion.

It is interesting to note that the assumption of a particular geometrical model, viz. a sphere, for the carbon particles is not critical, if the value of $D^{\frac{1}{2}}/r_o$ is obtained from the slope of the initial straight line portion of the plot of $\frac{V_t-V_o}{V_\infty-V_o}$ versus $t^{\frac{1}{2}}$. Barrer[160] and Fender[155, 160] have shown that the same result is obtained for a cube, sphere, parallelopiped or a plane sheet.

Polyvinylidene Chloride Carbons

Diffusion coefficients were calculated for the polyvinylidene chloride carbons at -196°C by similar procedures. For the carbon SA-1700, there was evidence of a 'foot' so the scale on the $\frac{V_t-V_o}{V_\infty-V_o}$ axis was adjusted for the calculation of diffusion coefficients. Values for $D^{\frac{1}{2}}/r_o$ are collected in TABLE 14.

TABLE 14

Diffusion Coefficients for the Adsorption of Argon on Polyvinylidene Chloride Carbons at -196°C

Method of Calculation	$\frac{V_t - V_o}{V_\infty - V_o}$	$\frac{D^{\frac{1}{2}}}{r_o}$ (min.$^{-\frac{1}{2}}$)			
		SA-800	SA-1200	SA-1400	SA-1700
Method A - by comparison of experimental curve with the theoretical	0.162	0.091	0.091	0.037	0.132
	0.235	0.094	0.094	0.038	0.150
	0.310	0.095	0.095	0.039	0.154
	0.442	0.098	0.098	0.040	0.167
	0.560	0.104	0.104	0.042	0.167
	0.662	0.109	0.109	0.044	0.167
	0.750	0.112	0.112	0.045	0.163
	0.822	0.113	0.113	0.045	0.154
	0.921	0.115	0.115	0.044	-
Method C - small values of $(\frac{Dt}{r_o^2})^{\frac{1}{2}}$ - equation (46)	< 0.7	0.087	0.087	0.036	0.144

5.2.2 Rates of Adsorption and Pore Distribution of Heat Treated Carbons

Cellulose Acetate Carbon Values of the diffusion coefficient show that the rate of adsorption of argon at -81°, -183° and -196°C increased with the temperature of heat treatment of the carbon. This indicates that heat treatment either reduced the average length of the pores through which the gas molecules diffused or increased the mean pore size by shifting the maximum in the pore size

distribution to higher values of pore diameter. As suggested in Section 5.1, the formation of constrictions in the pores is the most likely explanation for the alteration in the pore size distribution. In this event, changes in pore length or diameter would occur concurrently and be mutually indistinguishable.

The change in the pore size distribution with heat treatment also provides a satisfactory explanation for the 'foot' in the rate of adsorption curves. For CA-800, the 'instantaneous' adsorption on the external surfaces and in the macro-pores represents only a small proportion of the total adsorptive capacity; hence a 'foot' is not apparent on the rate of adsorption curve. However, for CA-1700, where the adsorptive capacity of the micro-pores has been greatly reduced, the adsorption on the external surfaces and large macro-pores comprises a considerable proportion of the overall adsorptive capacity.

An analogous series of data has been obtained by Breck et al.[125] (see Fig. 71). In this series of rate measurements the same zeolite was used in all the runs with five adsorbates, viz. CO_2, C_2H_4, C_2H_6, N_2 and C_3H_6 having critical diameters of 2.8, 4.25, 4.2, 3.0 and 4.89 Å, respectively. X-ray and equilibrium adsorption measurements indicated that the openings in the zeolite structure were from 4.2 to 4.75 Å in diameter. Although several other factors, apart from the critical diameter, may have influenced the rate of adsorption to some extent, viz. temperature and relative pressure, clearly the smaller molecule, CO_2, diffused through the zeolite framework at a much faster rate than some of the larger molecules such as C_3H_6. Thus changes in the ratio of critical molecular diameter to pore diameter are reflected in the rates of adsorption on a zeolite as they are in heat treated carbons.

Polyvinylidene Chloride Carbons The rates of adsorption of argon on the heat treated polyvinylidene chloride carbons are shown in Fig. 52. The isotherms for SA-1200 and SA-800, are almost identical,

as are the rate of adsorption curves. However, for SA-1400, the rate of adsorption was much lower than for SA-800 or SA-1200, with the straight line relationship between $D^{\frac{1}{2}}/r_o$ and $t^{\frac{1}{2}}$ extending to a value of t of approximately 40 min. In fact, the rate was so slow, that the final equilibrium value was difficult to obtain with accuracy. The trend was reversed with carbon SA-1700 which exhibited a faster rate of adsorption than that of SA-800 and SA-1200. Extrapolation of the initial straight line portion of the SA-1700 curve cut the $\frac{V_t - V_o}{V_\infty - V_o}$ axis at 0.24, i.e. the 'foot' = 0.24.

According to Dacey and Thomas[127] polyvinylidene chloride carbons are characterized by a narrow pore distribution, the pores being uniform, slot-like in cross-section, and from 12 to 15 Å across their narrowest dimension. Supporting evidence for this type of structure is provided by the pronounced rectangular shape of the isotherms at -196°C and the estimates of mean pore size. Using the terminology of Dubinin[87-89], the pore size distribution of polyvinylidene chloride carbon would be described as monomode. Now the rates of adsorption for SA-800 and SA-1200 are relatively fast, as would be expected when the ratio of pore diameter to adsorbate diameter ratio is approximately 3.9 (assuming that the critical diameter of the argon molecule is 3.84 Å). However, for SA-1400, the argon molecules apparently encounter considerable resistance in entering the pore structure which indicates that the growth of constrictions has reduced the pore diameter to molecular dimensions. This behaviour can be explained in terms of changes in pore distribution which are represented diagramatically by Fig. 72. Here the height of the vertical lines represent the value of the pore volume at a certain pore size. (It is realized that the actual distribution will show a Gaussian type curve, but for the sake of clarity this diagram will suffice.) For SA-1700, the bulk of the micro-pores have been reduced to a size smaller than the argon

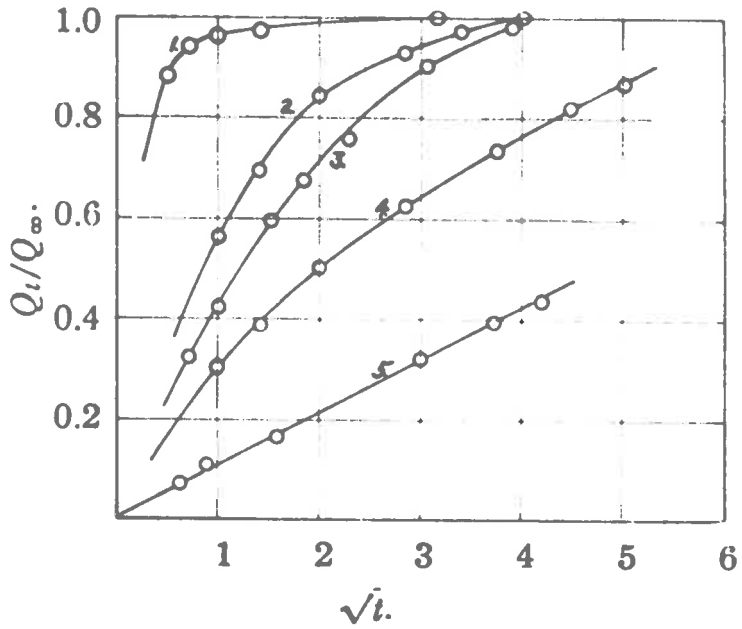

Fig. 71 - Rate of Adsorption on Zeolite A[125]: 1, CO_2 at 1 atm., 25°C; 2, C_2H_4 at 1 atm., 25°C; 3, C_2H_6 at 1 atm., 25°C; 4, N_2 at 1 atm., -78°C; 5, C_3H_6 at 1 atm., 25°C

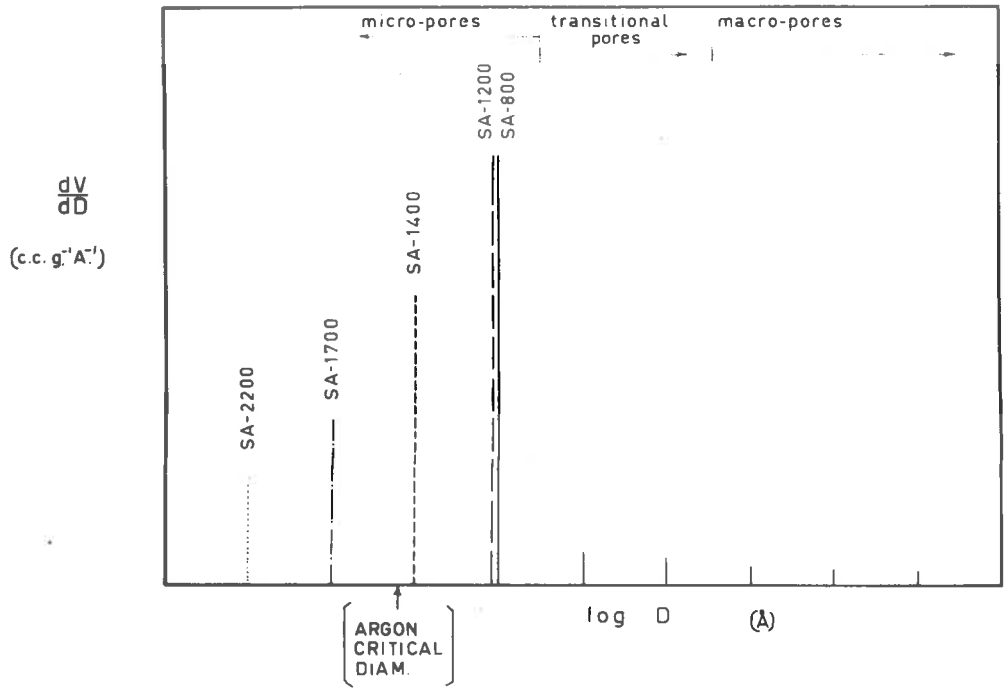

Fig. 72 - Hypothetical Differential Pore Size Distribution of Heat Treated Monomode Polyvinylidene Chloride Carbons

molecule so that the adsorptive capacity is very low. The appearance of the 'foot' on the rate of adsorption curve is in accord with the above model, where the comparatively few transitional and macro-pores account for a major proportion of the total adsorptive capacity.

5.3 Thermodynamics of Adsorption

In this section the differential heat of adsorption (isosteric heat of adsorption) and the differential entropy of adsorption of argon and benzene on the various heat treated cellulose acetate carbons will be discussed.

5.3.1 Differential Heat of Adsorption (Isosteric Heat of Adsorption)

In Fig. 53 and 54 are shown plots of the isosteric heat of adsorption versus the surface coverage for argon and benzene, respectively, on the cellulose acetate carbons CA-800, CA-1200 and CA-1700.

The heat of adsorption curves for argon and benzene are similar and typical of high surface area, porous, solids where the heats of adsorption decrease with increased surface coverage[205]. However, the arrangement of the curves with respect to the heat treatment temperature does not follow any simple pattern. Furthermore the arrangement of the curves differs for argon and benzene.

How the characteristic shape and arrangement of the curves must depend upon (a) the interaction between adsorbate molecules, and (b) the heterogeneous nature of the surface[206]. Roberts et al.[207], Everett,[170] Miller[208] and Barrer et al.[158, 194] have calculated that the contribution to the heat of adsorption from the interaction between the adsorbate molecules is negligible below $p/p_o = 0.9$ to 1.0. Thus, the shape of the heat of adsorption curves at $p/p_o < 0.9$ is largely determined by the heterogeneous nature of the surface.

The observed high heat of adsorption at low coverages is

attributed to high energy sites residing in pores, or surface imperfections[205]. As the high energy sites are gradually occupied by adsorbate molecules, the heat of adsorption decreases and approaches the latent heat of condensation of the adsorbate at surface coverages greater than the monolayer capacity.

There is some evidence to show that pores are associated with high heats of adsorption. From a comparison of heats of adsorption on porous and non-porous materials, Barrer[210] has argued that the occlusion of adsorbate molecules by crystal atoms does not necessarily give rise to high heats of adsorption. However, Barrer[158], and de Boer and Custers[209] have calculated heats of adsorption in pores of such dimensions that molecules experienced attractive forces from the two walls; they found that the heat of adsorption was several times that of adsorption on a plane surface. Even for pores of diameter several times that of the adsorbate molecule, it has been suggested[209] that the co-operative attractive forces from the two walls can still affect adsorption. It follows that the shape of the heat of adsorption curves, at least at low coverages, should be governed by the pore size distribution. Culver and Heath[197] have used this argument to support their contention that steam activation of polyvinylidene chloride carbons increased the mean pore size.

Surface imperfections arise from depressions, dislocations and growth steps. Frank[23] has shown that crystallite growth invariably follows the formation of dislocations. Where a dislocation emerges from the surface, a growth step is formed. Thus, even though a crystal may be annealed to remove heterogeneities, it is most likely that the surface will contain growth steps. As mentioned in Section 2.1.1.2 electron microscope investigations of the surface topography of graphites reveal the presence of large numbers of dislocations and growth steps. For carbons containing small crystallites and a disorganized phase, one would expect an even

larger number of surface imperfections than for graphite. Field et al.[211] have suggested that growth steps could act as favourable adsorption sites, since an adsorbed molecule will be in contact with surfaces on two sides (see Fig. 73) and be subject to binding forces stronger than those from a single surface.

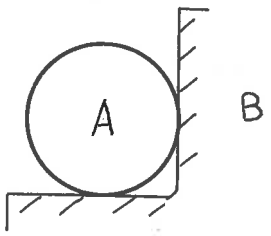

A = adsorbed molecule
B = surface of adsorbent

Fig. 73 Growth Step and Adsorbed Molecule

Considering the arrangement of the curves, evidence obtained from Section 5.1.3 points to the fact that the pore size distribution of cellulose acetate carbons moves to larger pore diameters with increased temperature of heat treatment. If the heat of adsorption at low coverages was solely dependent upon the pore size distribution, then the heat of adsorption should decrease with increased temperature of heat treatment. However, Fig. 53 and 54 show that this arrangement of the curves is not followed. It appears, therefore, that the observed heats of adsorption are more readily accounted for in terms of surface imperfections, such as an increase in the number of growth steps which may or may not reside in pores.

The arrangement of the heat of adsorption curves differ for argon and benzene. This is not unexpected and there are several possible reasons for this difference in adsorptive behaviour between the two molecules.

(1) A benzene molecule has the shape of a flat disc of thickness 2.5 Å and width 6 Å, whereas an argon atom is spherical and of radius 1.92 Å. Thus benzene would be adsorbed into a slightly different set of pores than argon. This is borne out by the V_{SL} values of the carbons CA-800, CA-1200 and CA-1700

for benzene and argon (see TABLE 9, Section 5.1.3).

(2) Benzene, although non-polar possesses an uneven distribution of π-electrons and is therefore sensitive to the presence of surface complexes[212]. Argon, on the other hand, has an uneven distribution of electrons and is therefore unperturbed by the presence of surface complexes.

5.3.2 Differential Molar Entropy of Adsorption

By comparing the value of the experimental entropy of adsorption with the entropy calculated for theoretical models of the adsorbed phase, it was possible to specify the state of the adsorbed phase. For a monatomic gas, the limiting states of the adsorbed atoms are[194],

(1) 3v,
(2) 2v, 1t,
(3) 1v, 2t,

where t and v signify the translational and vibrational components, respectively. For a polyatomic molecule the number of limiting states[217] will be increased as the rotational components become affected by the attractive surface forces. For a monatomic gas, adsorption may restrict movement to such an extent that the normal three translational degrees of freedom possessed by the atoms in the gas phase are replaced by three degrees of freedom of vibration of the atoms against the solid. Similarly, depending upon the force of attraction between the adsorbed atoms and the solid, the atoms may lose only two or perhaps one degree of translational freedom. The differential entropy of the adsorbed atoms for the states (1), (2) and (3) are, respectively

$$\bar{s}_S = \bar{s}_3 + \bar{s}_{th} \quad . \quad . \quad . \quad (47)$$

$$\bar{s}_S = {}^1\bar{s}_T + \bar{s}_{th}' \quad . \quad . \quad . \quad (48)$$

$$\bar{s}_S = 2\bar{s}_T + \bar{s}_{th}' \qquad \cdot \quad \cdot \quad \cdot \qquad (49)$$

Equation (47) corresponds to localized monolayer adsorption. $\bar{s}_c$ is the configurational entropy and arises from the number of distinguishable arrangements of N molecules on N_A uniform adsorption sites and is given by

$$\bar{s}_c = R \ln\left(\frac{1}{\theta - 1}\right)$$

where θ = fraction of adsorption sites occupied. The thermal entropy $\bar{s}_{th}$ for a monatomic gas includes the entropy mainly originating from the vibration of the atoms about their mean position.

Equation (48) corresponds to non-localized adsorption with one degree of translational freedom. The differential translation entropy may be shown to be[218]

$$1\bar{s}_T = R \ln(\pi)^{\frac{1}{2}} l + \ln\left(\frac{1}{\theta - 1}\right) - 1/(1/\theta - 1) + \tfrac{1}{2} + \ln(2\pi k/N_o h^2)^{\frac{1}{2}}$$

$$\cdot \quad \cdot \quad \cdot \qquad (50)$$

where M = molecular weight,
k = Boltzmann's constant,
h = Planck constant,
R = gas constant and
l = co-length of adsorbed atom.

The thermal $\bar{s}_{th}'$ should possess a value corresponding to the entropy arising from two degrees of vibration freedom.

Equation (49) corresponds again to non-localized adsorption, but in this case, the translational entropy for two degrees of freedom is[218]

$$2\bar{s}_T = R \ln MTa + \ln\left(\frac{1}{\theta - 1}\right) - (1/1/\theta - 1) + 1 + \ln(2\pi k/N_o h^2)$$

$$\cdot \quad \cdot \quad \cdot \qquad (51)$$

where a = co-area of adsorbed atoms. The thermal entropy $\bar{s}_{th}''$ is the entropy arising from one degree of vibrational freedom.

All three models require that the surface be homogeneous or, in other words, the heat of adsorption should be independent of the surface coverage. An inspection of the heat of adsorption curves for both argon and benzene (Fig. 53 and Fig. 54) reveals that all surfaces are heterogeneous to some extent. Empirical methods[170] of dealing with heterogeneous surfaces have been developed for the localized monolayer, but highly accurate heat of adsorption data ($\pm$10 cal.mole^{-1}) are required if the calculations are to be of value. However, the system argon/CA-800 approximately satisfies the condition that the surface should be uniform, and to a lesser extent the systems argon/CA-1700 and argon/CA-1200. Accordingly, values for $\bar{s}_0$, $_1\bar{s}_T$, $_2\bar{s}_T$, $\bar{s}_{th}$, $\bar{s}_{th}'$ and $\bar{s}_{th}''$ have been calculated for these systems in APPENDIX G.3. Considering the results obtained, it appears that in the system argon/CA-800 the adsorbed phase can be described by the non-localized model possessing one degree of freedom. This corresponds to an atom being constrained to move through a pore only slightly larger than itself. The other two degrees of translational freedom normally possessed by argon atoms are converted to 'loose' vibrations against the enclosing solid.

The relative disposition of entropy curves (Fig. 55 and 56) gives some indication of the change in the state of the surface of the carbon with heat treatment. The decrease in differential entropy observed with increasingly heterogeneous surfaces has been discussed by Drain and Morrison[220], and Everett[170] has examined the effect of heterogenity on the configurational and thermal entropy in some detail. Firstly, when the adsorbed phase is localized, heterogenity will reduce the configurational entropy. Secondly, as Everett has pointed out, surface heterogenity affects the thermal entropy. If a molecule is strongly attracted to the surface it

lies in a 'deep potential well' and consequently its contribution to the thermal entropy is low. As the overall entropy of adsorption can be considered as the sum of the configurational and thermal entropy*, the effect of surface heterogenity is to reduce the overall entropy of adsorption. As the surfaces of CA-800 and CA-1700 are not homogeneous over a wide range of coverage, the data for the two systems are not strictly comparable. However, it is tempting to infer from the results obtained from both the argon and benzene systems, that the carbon CA-1700 possesses a more heterogeneous surface than CA-800.

Comparison of Fig. 55 and Fig. 56 reveals a marked contrast between the shape of the entropy curves for argon and benzene. For argon, the entropy generally decreases with increasing surface coverage while for benzene, the entropy generally increases. These results, however, are not unlike those obtained by Drain and Morrison[220] for the entropy of adsorption of argon and nitrogen on rutile; for argon, the entropy generally decreased with increasing surface coverage whereas it increased for nitrogen. Everett[170] associated the low initial entropy of the adsorption of nitrogen with the high initial heat of adsorption. By similar reasoning the increase in entropy with surface coverage observed for the adsorption of benzene may be accounted for in terms of surface heterogenity.

* Hill[219] has pointed out that for heterogeneous surfaces, the separation of $\bar{s}_s$ into $\bar{s}_c$ and $\bar{s}_{th}$ must be treated with caution.

5.4 Crystallite Growth in Carbons

This discussion is concerned with the development of the ideal graphite lattice from the turbostratic crystal structure during heat treatment and the differences that exist between the crystallite growth of the various carbons.

In this section, it will be convenient to divide the carbons into two groups - non-graphitizing and graphitizing. As will be shown later, the crystal growth of graphitizing carbons is markedly different from that of non-graphitizing carbons.

5.4.1 Development of the Ideal Graphite Lattice

Non-Graphitizing Carbons These include carbons prepared from cellulose acetate, cellulose, phenol-formaldehyde, polyvinylidene chloride and sucrose. Non-graphitizing carbons are characterized by relatively limited development of the ideal three dimensionally ordered graphite lattice. Amongst the non-graphitizing carbons, however, there is very little difference in the development of the crystal structure up to 1,700°C. The X-ray patterns for these carbons (see Fig. 57 to 61) all exhibit the two prominent peaks (002) and (10), the (11) peak being considerably smaller. These patterns are typical of turbostratic packing of the crystallites. Even for the cellulose acetate carbon heat treated at 2,900°C, there is no indication of three dimensional ordering of the crystal lattice.

The polyvinylidene chloride carbons yield a very low value for the peak height to background ratio for both the (002) and (10) peaks. Franklin[29] has suggested that the high intensity background scattering at low angles is a result of the reflection of X-rays from inhomogenities in the structure, such as pores. The Fourier transform[102, 213] of the low angle scattering for the carbons heated from 1000° to 3000°C revealed that the size of the pores lay between 10 and 20 Å.

Graphitizing Carbons For the polyvinyl chloride carbon there is a rapid development of the crystal structure on heat treatment. At 2,200°C, a noticeable modulation in the (10) peak represents the beginning of the separation of the (10) reflection into the reflections (100) and (101). This means that between 1,700° and 2,200°C the crystallite layers are beginning to reorientate themselves into the three-dimensionally ordered graphite-like lattice. At 2,900°C, the (100) and (101) peaks have become quite distinct. Also, at 2,900°C, the two dimensionally ordered reflection (11) has separated into the three-dimensionally ordered (110) and (112) reflections.

5.4.2 Crystal Growth

Values of L_a and L_c for cellulose acetate, cellulose, phenol-formaldehyde, polyvinylidene chloride and polyvinyl chloride carbons are plotted against the heat treatment temperature in Fig. 74 and 75.

Non-Graphitizing Carbons The crystallite growth in the L_a direction is very similar for all non-graphitizing carbons. This is remarkable when it is realized that considerable differences exist among the properties of these carbons such as porosity, surface area and hardness. For instance, the phenol-formaldehyde carbon PF-800 is hard, glassy, and possesses a surface area of 33 $m.^2 g.^{-1}$, while polyvinylidene chloride carbon SA-800 is much softer, dull in appearance, and possesses a surface area of 1,070 $m.^2 g.^{-1}$, i.e. approximately 30 times that of PF-800. Similarly, for an activated polyvinylidene chloride carbon, the crystal growth on heat treatment is the same as that for the unactivated polyvinylidene chloride carbon, despite a considerable overall increase in surface area. Thus crystallite growth appears to be independent of porosity. These results are contrary to those obtained by Franklin[29] whose low angle scattering results for a polyvinylidene chloride carbon indicated that parallel layers were co-extensive with particle size. It follows that growth of layers

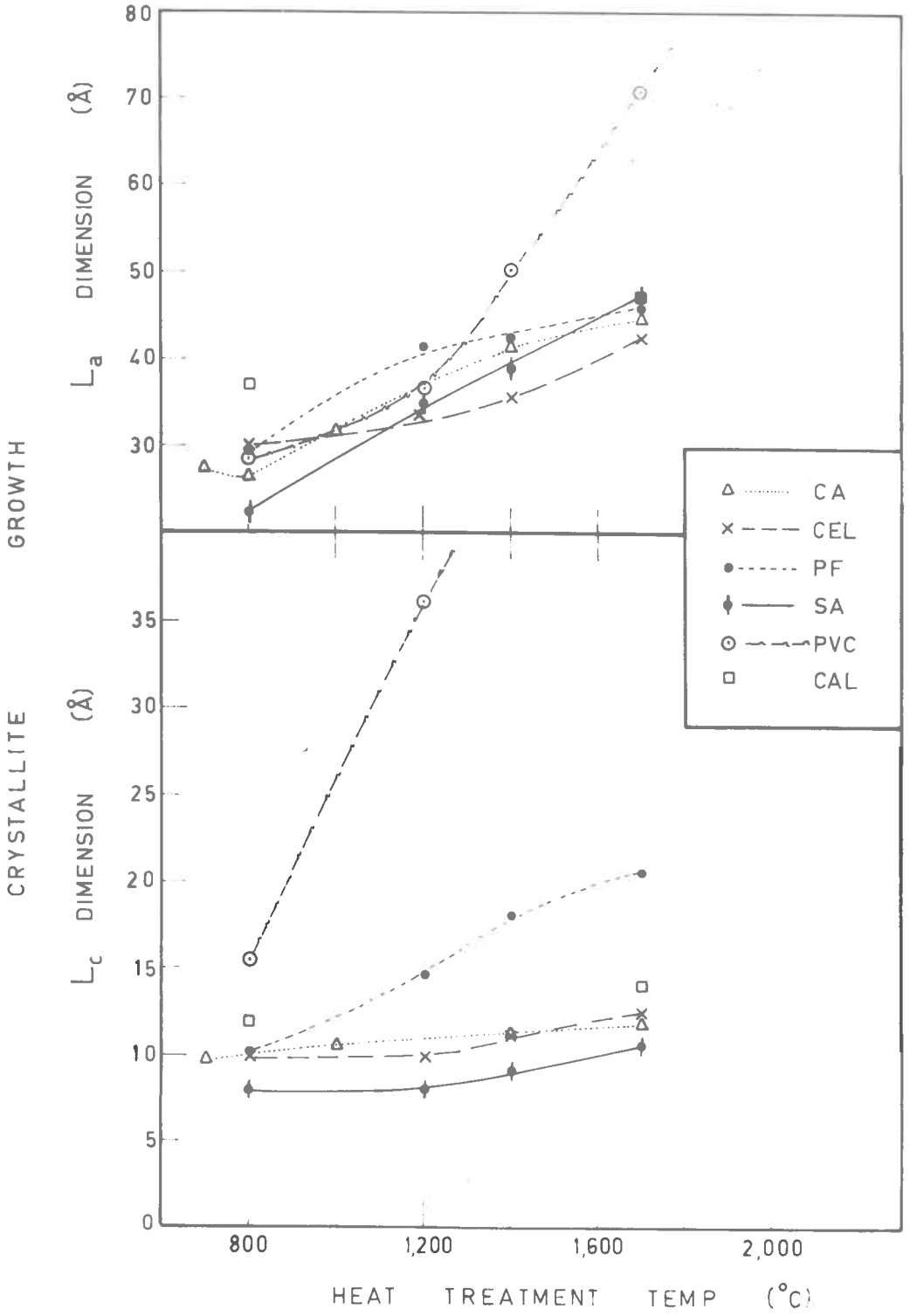

Fig. 74 and 75 – Increase in the Crystallite Dimensions L_a and L_c of Heat Treated Carbons

is limited by the growth of the particles and that the non-graphitizability of the carbon is related to its finely porous structure.

While, for the non-graphitizing carbons, the size of crystallites in the L_c direction is approximately the same at 800°C, there is a divergence in L_c values as the heat treatment temperature increases. Again, however, comparison of the change in surface area with the growth of crystallite size does not reveal any relationship between crystal growth and porosity.

The independence of crystal growth from the porosity of the carbons can be simply and most satisfactorily explained by the crystallite growth mechanism proposed by Franklin[29]. In this mechanism the disorganized phase lying between the crystallites is gradually incorporated into the crystallite lattice. The carbon atoms of the disorganized phase attach themselves more readily to the layer edges atom by atom rather than to the basal planes in groups of atoms because the edge carbon atoms have a greater free valence than the carbon atoms in the centre of the layer[11, 171]. This suggestion would explain why the crystallites grow preferentially in the L_a direction rather than the L_c direction. Furthermore, the incorporation of the atoms of the disorganized phase by the crystallites would be independent of the porosity of the carbon.

As mentioned above, rapid crystallite growth in the L_c direction could probably only occur by the addition of groups of carbon atoms or even whole layer planes. The ability to do this would depend upon the degree of alignment amongst the crystallites and the ease with which a complete crystallite could move into a position parallel to its neighbour. The disorganized phase probably consists of cross-links between the crystallites and these would restrain any movement of a complete crystallite. This could be one reason why crystallites in non-graphitizing carbons are reluctant to grow in the L_c direction. For instance, heat treatment of a

polyvinylidene chloride carbon, from 800° to 1,700°C, only adds one layer in the L_c direction.

Graphitizing Carbons Between 800° and 1,200°C the growth of crystallites in the L_a direction is very similar to that for the non-graphitizing carbons. Above 1,200°C, however, there is a marked increase in growth in the L_a direction. According to Mrozowski[30], the disorganized phase becomes exhausted at a temperature of approximately 1,300°C. Thus at temperatures above 1,300°C, the encumbering disorganized phase has now been removed, so that layers or even whole crystallites can more easily orientate themselves into a position to coalesce with their neighbours. Furthermore, electron micrographs of the structure of carbons[58] reveal that crystallites of graphitizing carbons are much more favourably aligned than those of non-graphitizing carbons. In this manner there is a rapid increase in the growth of crystallites in both the L_a and L_c directions as they coalesce.

Crystallite growth by coalescence must be preceded by the elimination of foreign atoms. Data on the chemical composition of carbons at various temperatures (Fig. 22) reveal that the proportion of foreign atoms present in non-graphitizing carbons is greater than that for graphitizing carbons. At 1,700°C, the proportion of foreign atoms such as hydrogen, oxygen and chlorine in the non-graphitizing carbons is approximately 1% compared with less than 0.1% in graphitizing carbons. For polyvinyl chloride the approach in the proportion of foreign atoms to zero coincides with the beginning of the marked increase in the crystallite growth in the L_a direction.

5.5 Mechanism of Sintering

It has been shown that heat treatment of carbons at temperatures above 800°C has a marked effect on the porous structure. Furthermore, it has been proposed that the sintering process involves

the closing off or destruction of micro-pores by the growth of constrictions into the pore space. The mechanism by which these constrictions are formed will now be discussed.

Firstly, it will be helpful to briefly review the mechanism of sintering that occurs during the heat treatment of ceramic materials and silica gels, and during the neutron irradiation of graphites.

The sintering of ceramic materials has been investigated quite extensively[214]. The particles of ceramic materials are roughly spherical, the pore volume comprising the volume between the particles. Sintering is usually achieved by the application of pressure and temperature and the particles aggregate by flowing together at the points of contact, thus reducing the pore volume and surface area.

Modified silica gels used as catalysts in the petroleum industry show a marked drop in surface area with heat treatment[215], e.g. for a silica xerogel of surface area 810 $m.^2 g.^{-1}$, heat treatment to a temperature between $1,000^{\circ}$ and $1,100^{\circ}C$, reduced the surface area to less than 10 $m.^2 g.^{-1}$. Ries[215] attempted to explain this decrease in area by suggesting that the elementary particles of the silica were in the form of platelets. An idealized picture of the silica structure is shown in Fig. 76 top row (I). The two sets of platelets were presumed to fuse together during sintering. This reduced the specific surface area and pore volume of the silica xerogel while the pore diameter remained constant (row (II)). Another possibility was that the two inner plates fused to the two outer plates so that the specific pore volume remained constant, the specific surface area decreased and the pore diameter increased (row (III)). These processes have been represented on a macro-scale but Ries suggested that in practice sintering could take place by either surface diffusion or crystal growth.

For neutron irradiated graphites, the loss in surface area

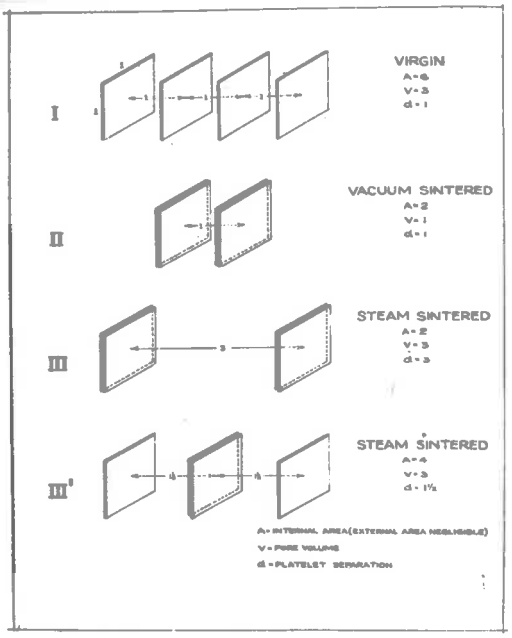

Fig. 76 - Schematic Representation of Silica Structure and Mechanism of Sintering (ref.215 p.110)

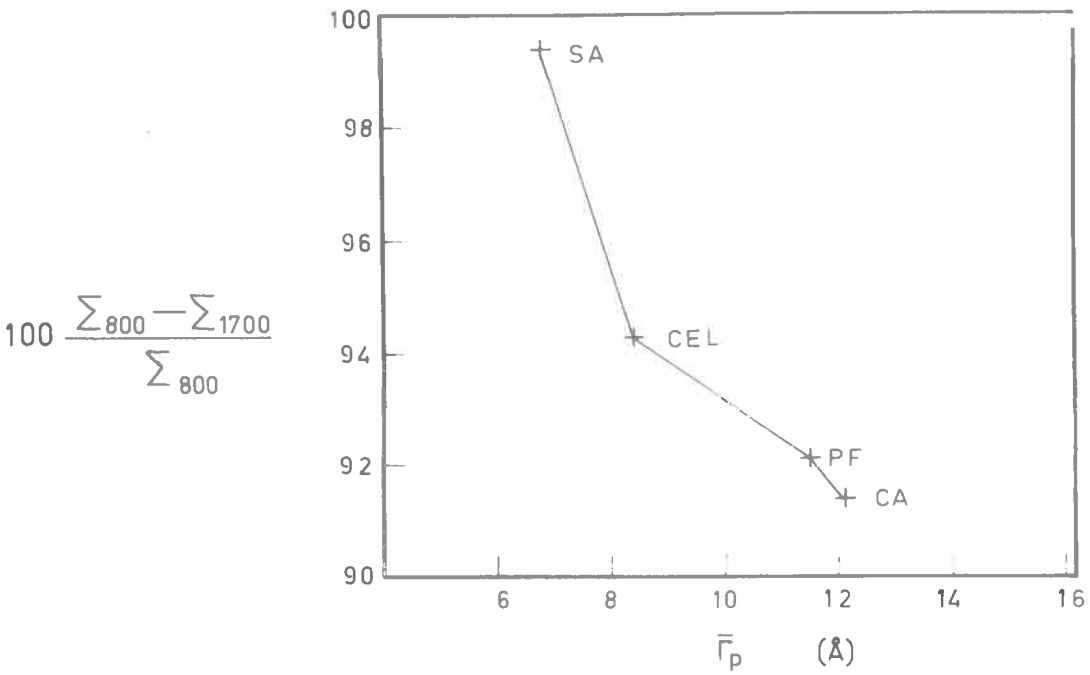

Fig. 77 - Percentage Decrease in Surface Area Compared with the Average Pore Radius

and pore volume occurs as the result of the formation of a large number of defects and imperfections in the crystallites (see Section 2.2.3). This causes the crystallites to expand into the pore volume and form constrictions. A feature of neutron induced sintering[92, 93] in graphites is that the original surface area and pore volume can be restored by heating the sintered graphite to a temperature of approx. 600°C.

A comparison of the sintering characteristics of heat treated porous carbons, with those for ceramics, silica gels, and neutron irradiated graphites, suggests that a different mechanism of sintering must be postulated for porous carbons. Porous carbon particles do not tend to fuse together, the temperature of sintering is comperatively low, the mode of aggregation of crystallites and the stability of the structure is different from that of silica gels, and the process of sintering is irreversible in contrast with the reversible neutron induced sintering of graphites.

For porous carbons there are at least three possible mechanisms by which sintering occurs during heat treatment. They are:

(1) closing of cracks or sealing of wedge-shaped blind-end pores,

(2) irreversible expansion of crystallites into the pore volume, and

(3) growth of crystallites to form constrictions in pores.

These mechanisms will now be considered.

Permeability measurements by Davidson and Losty[75] on cellulose carbons (see Fig. 10) clearly show that heat treatment to 1,700°C markedly reduces the permeability. This would not occur if sintering only effected wedge-shaped pores or cracks.

It is possible that crystallites expand into the pores during heat treatment, but are prevented from contracting on cooling. Loch and Austin[72] have shown that the reversible expansion

of crystallites in graphites is accommodated in the pore volume. They showed that a relationship exists between the bulk thermal expansion of graphites and the porosity - the higher the porosity, the lower the bulk thermal expansion. Accommodation of the thermal expansion of the crystallites in the pore volume caused the overall thermal expansion of the graphite specimens to be much less than the theoretical value. However, for porous carbons, it is unlikely that irreversible thermal expansion can account for the formation of constrictions. Consider a crystallite in a pore of diameter 15 Å with the layers of the crystallite parallel to the pore wall to give the maximum thermal expansion. The coefficient of thermal expansion[4] in the direction perpendicular to the layers $\alpha_{\perp}$ is 300 x 10^{-7} per °C. For a carbon heat treated from 800° to 1,700°C, the temperature rise to be considered is 900°C. The expansion into the pore required to partially block the pore would be, say, 10 Å. Therefore, the size of the crystallite necessary to give this thermal expansion is

$$L_c = \frac{\Delta L}{\alpha_{\perp} \Delta t} = 333 \text{ Å}$$

where ΔL = 10 Å, the crystallite expansion,

L_c = size of the crystallite in the c direction,

and Δt = 900°C, the temperature rise.

Clearly a value of L_c = 333 Å does not agree with the results obtained for non-graphitizing carbons heat treated at 1,700°C, viz. $L_c \backsim$ 12 Å. If the size of crystallite is taken as L_c = 12 Å, then 333/12, or approximately 30 crystallites would have to act together to produce an expansion of 10 Å. In view of the rigid nature of the carbon structure of non-graphitizing carbons, this mechanism must be considered as unlikely.

In contrast to thermal expansion, crystallite growth over the temperature range 800° to 1,700°C, or even 800° to 1,200°C, is

sufficiently large to considerably reduce the size of the pores. TABLE 16 lists the increments in the L_a dimension during crystallite growth from 800° to 1,200°C and from 800° to 1,700°C for the series of carbons, along with the average pore radius for the carbons prepared at 800°C.

TABLE 16

Increments in the L_a Dimension of Crystallites for Carbons Heat Treated to 1,200° and 1,700°C and the Average Pore Radius for Carbons Prepared at 800°C

Carbon Sample	L_a (Å)		$\bar{r}_p$ (Å)
	800°-1,200°C	800°-1,700°C	
Cellulose acetate	11	19	12.1
Cellulose	3	12	8.4
Phenol-formaldehyde	11	16	11.5
Polyvinylidene chloride	13	25	6.8
Polyvinyl chloride	9	42	15.5
Cellulose*	3	9	-

* (ref. 216)

Remembering that $\bar{r}_p$ is an average pore radius, it is clear from TABLE 16 that crystallite growth is generally sufficient to partially or totally constrict the pores. This mechanism explains the sudden decrease in the surface area for most carbons at a heat treatment temperature of approximately 1,200°C. For instance, cellulose

acetate carbons exhibit a marked decrease in surface area at a heat treatment temperature of 1,200°C. Apparently a crystallite growth of 11 Å constricts or blocks off a major proportion of the smallest pores. Depending upon the pore size distribution, further crystallite growth will generally become less effective in reducing the surface area as the pores remaining are relatively large. At a temperature of 2,200°C the pores contributing to the surface are so large that crystallite growth into the pores has little effect in reducing the surface area.

For cellulose carbon, the crystallite growth at 1,200°C appears to be insufficient to constrict the pores. However, while the value of 3 Å for the increase in crystallite growth agrees with the data of Blayden et al.[216], it is possible that this figure is in error by 2 Å. In this event, a value of 5 Å for the crystallite growth could be considered more effective in reducing the surface area by 81% at 1,200°C.

If it is accepted that crystallite growth is responsible for sintering, then the decrease in surface area with heat treatment should depend upon the amount of crystallite growth in relation to the size of the pores. If the crystallite growth for a series of carbons is approx. the same, then the greatest decrease in surface area should occur for carbons possessing the smallest pores. Fig. 77 shows the plot of the percentage decrease in surface area on heat treatment from 900° to 1,700°C against the average pore size of the carbons prepared at 800°C. While there is some variation in the crystallite growth amongst the carbons, the general trend confirms the above argument.

Now it has been postulated that a crystallite in the wall of a pore grows in the a direction and constricts the pore. However, the nature of the growth of the crystallites into the pore space is difficult to account for. During sintering, if the crystallites grow out into the pore, then carbon atoms must be

transferred to the leading edges of the crystallite through the vapour phase or by surface or solid diffusion. As the vapour pressure of carbon becomes appreciable only at temperatures greater than 2,400°C (ref. 4 p.52), it is most unlikely that at 1,200°C a sufficient number of carbon atoms in the vapour phase could be transported to give a crystallite growth of 10 Å. Similarly, as pointed out in Section 2.1.3.3, there is no evidence[29, 65, 66] for solid state diffusion in carbon until the temperature exceeds 1,800°C. Little is known about surface diffusion apart from the fact that it would probably require less activation energy than solid state diffusion.

It is possible, however, that growth occurs only on the edge imbedded in the carbon matrix. Under these conditions, the crystallite would be pushed out into the pore, the crystallite growth being accommodated in the pore space as for reversible thermal expansion.

6. CONCLUSIONS AND RECOMMENDATIONS

(1) Heat treatment of cellulose acetate, cellulose, phenol-formaldehyde, polyvinylidene chloride, activated polyvinylidene chloride, polyvinyl chloride and Cal carbons produced a marked drop in their surface area. These results taken together with those for other carbons reported in the literature, suggest that the loss in surface area with heat treatment may be a universal phenomenon for porous carbons. The porous carbons susceptible to sintering have been prepared from such diverse carbonaceous materials as coal, coco-nut, organo-metallic compounds and organic polymers. Although activation increases the surface area, sintering the active carbons still reduces the surface area by an amount comparable to that for unactivated carbons. A marked drop in surface area occurs at temperatures between 1,000° and 1,200°C for all carbons except that prepared from polyvinylidene chloride. For the polyvinylidene chloride carbon, it is suggested that the evolution of a large quantity of impurities at 1,200°C 'opens up' sufficient surface area to counteract the reduction in the surface area due to sintering. However, heat treatment of this carbon above 1,700°C produces a large reduction in surface area.

(2) Heat treatment of the porous carbons produced little change in the mercury density, indicating a correspondingly small change in the bulk volume. The change in the helium densities, however, indicates that for cellulose acetate and phenol-formaldehyde carbons, heat treatment alters the pore structure so that ultimately helium atoms penetrate no further into the pore volume than mercury atoms. In other words, the carbons are beginning to behave as low density, non-porous materials. The decrease in helium density and surface area with increased heat treatment temperature,

suggests that constrictions form in the pores and eventually block them off. For the polyvinylidene chloride and polyvinyl chloride carbons, however, the rise in the helium density with the heat treatment temperature implies that the growth of constrictions into the pores has been insufficient to exclude helium atoms from the pore volume. The rise in helium density for polyvinylidene chloride and polyvinyl chloride carbons is attributed to the reduction in the interlayer spacing of the crystallites accompanying crystallite growth and the possibility that helium atoms may be adsorbed onto the crystallite surfaces.

(3) The value of the pore volume calculated from the mercury and helium densities for cellulose acetate and phenol-formaldehyde carbons generally decreased with heat treatment temperature above 1,000°C, and substantiated the argument that heat treatment closes off or destroys the available pore volume. The pore volume calculated from argon isotherm data differed from that calculated from mercury and helium densities, but the difference can be attributed to the carbon acting as a molecular sieve. At 1,700°C, the two pore volumes were approximately equal, suggesting that the pores remaining in the carbon were equally accessible to both argon and helium atoms.

(4) Heat treatment produced an increase in the average pore size (estimated from the pore volume and surface area) for cellulose acetate, cellulose, polyvinyl chloride and Cal carbons, while the average pore size remained constant for polyvinylidene chloride, activated polyvinylidene chloride and phenol-formaldehyde carbons. These results at first sight appear to contradict the previous findings that the surface area and pore volume of the carbons generally decrease with increased temperature of heat treatment. However, if a

carbon possessed a wide pore size distribution, the formation of constrictions in the smallest pores would shift the average pore size to larger pore diameters. On the other hand, if the carbon possessed a narrow pore size distribution, the average pore size would not be greatly altered.

(5) Pore size distribution analysis of the nitrogen adsorption isotherms of heat treated cellulose acetate carbons extended the results obtained for the change in the average pore size quoted above. The analysis revealed that sintering moved the maximum in the pore size distribution to larger values of the pore diameter. High pressure mercury penetration measurements showed that there was no change in the pore size distribution for pores of diameters from 60 to 20,000 Å. Similar qualitative deductions were made from molecular sieve measurements and from an analysis of the change in shape of the adsorption isotherms.

(6) The kinetics of adsorption of argon on the heat treated cellulose acetate and polyvinylidene chloride carbons were successfully described by a solution of Fick's Second Law assuming that the carbon particles were spherical and that Knudsen diffusion was the dominant mode of transport in the gas phase. This is the first time to the author's knowledge that a complete solution of Fick's Second Law has been successfully fitted to the rates of adsorption of a gas in a porous carbon over a range of pressures and temperatures. The diffusion coefficients evaluated from Fick's Second Law for a particular carbon and temperature were constant for pressures below that corresponding to the monolayer capacity. The results for the cellulose acetate carbons showed that sintering actually increased the rate of adsorption. Again these results would appear to be anomalous until it is realized that the effect of the growth of

constrictions is to block the smallest pores and shift the pore size distributions to larger pore diameters, so decreasing the resistance to gas flow into the pores. A similar result was obtained for the rates of adsorption on all heat treated polyvinylidene chloride carbons except for the sample heat treated to 1,400°C. For this particular carbon, the rate of adsorption was slower than for the other members of the series. This behaviour is ascribed to the narrow pore size distribution possessed by the polyvinylidene chloride carbon. During heat treatment a point was reached where the growth of constrictions narrows the pore size to such an extent that the argon molecules only enter the pores with difficulty. Further heat treatment above 1,400°C increased the rate of adsorption - the rate of adsorption for the carbon heat treated to 1,700°C being faster than the carbon heat treated to 800° or 1,200°C.

(7) The change in the heat of adsorption for the series of heat treated carbons was most readily accounted for in terms of surface imperfections. Rather than heat treatment producing a more homogeneous surface, it was suggested that heat treatment encouraged the growth of surface imperfections such as growth steps. This conclusion was supported by corresponding changes in the differential molar entropy with heat treatment. Comparison of the differential molar entropy of argon on CA-800 with several theoretical models of the adsorbed state, suggested that adsorbed argon molecules possessed one degree of translational freedom along with two degrees of vibrational freedom.

(8) The crystallite size measurements clearly demonstrated the marked difference that exists between the crystallite growth of the non-graphitizing carbons prepared from cellulose

acetate, cellulose, phenol-formaldehyde, polyvinylidene chloride and the graphitizing carbon prepared from polyvinyl chloride. Comparison of the crystallite growth of the non-graphitizing carbons with their porosity and surface area values, showed that crystallite growth is apparently independent of the pore structure. Furthermore, this observation agrees with the suggestion by Franklin[29] that crystallites of non-graphitizing carbons grow by a process independent of the porosity, e.g. an increase in the L_a dimension of the crystallite arises from the incorporation of the surrounding disorganized material.

(9) Several possible sintering processes were examined such as sealing of cracks or the irreversible thermal expansion of the crystallites into the pores. However, the only process which can account for the bridging of pores approx. 15 Å in diameter, involves the growth of crystallites into the pore space to form constrictions. This process satisfactorily explained both the sudden decrease in the surface area for most porous carbons at heat treatment temperatures between 1,000° and 1,200°C and also why the reduction in surface area depended upon the average pore size. A detailed analysis of the mechanism of crystallite growth revealed that the crystallites must grow from the edge imbedded in the carbon matrix and not from the leading edge protruding into the pore space. In other words, the crystallite growth is accommodated in the pore space in much the same manner as for reversible thermal expansion.

These conclusions suggest the following investigations might be of interest:-

(1) In view of the unexpected trend in the helium density for heat treated polyvinylidene chloride carbons measurements should be extended to carbons heat treated above 1,700°C. It is likely that the helium density for polyvinylidene chloride

carbons will begin to decrease[29] at heat treatment temperatures above 1,700°C and conform to the pattern of helium densities for other non-graphitizing carbons.

(2) The possible industrial applications of sintered cellulose carbons has been mentioned by Davidson and Losty[75]. The remarkable properties of this carbon suggests that a careful survey should be made of the properties of carbons prepared from various polymers. For instance, the carbon prepared from polyvinylidene chloride possesses a relatively low bulk density (approx. 1.0) and a high crushing strength. If this carbon could be prepared in a machinable form, it would be an excellent low density structural or insulation material. Unfortunately the carbonization of most polymers excepting a few such as cellulose, proceeds through a fluid stage so that particular shapes cannot be prepared in a machinable form.

(3) Rates of adsorption on a polyvinylidene chloride carbon heat treated to 1,400°C show that the pore volume is not readily accessible to adsorbate molecules. As polyvinylidene chloride carbons possess a very narrow pore size distribution, the correct selection of the heat treatment temperature could produce a carbon that would act as an efficient molecular sieve.

(4) Electron micrographs of heat treated porous carbons may provide complementary evidence for the formation of growth steps and constrictions. Previous electron microscope investigations have been mainly concerned with the surface topography of graphite crystals.

APPENDICES

DATA

APPENDIX A

Chemical Analysis of Carbons

A CHEMICAL ANALYSIS OF CARBONS

Carbon Sample	Percentage by weight of element				
	C	O	H	Cl	Ash
Cellulose Acetate					
CA-700	91.7	6.2	2.1		1.3
CA-800	90.6	6.1	1.6		0.9
CA-1000	90.9	5.3	1.3		1.0
CA-1200	96.2	3.5	0.9		0.3
CA-1400	97.1	1.7	0.9		0.2
CA-1700	99.2	0.5	0.9		0.2
CA-2200	98.8	0.2	.5		-
Cellulose					
CEL-800	89.3	4.8	1.7		0.3
CEL-1200	96.1	3.1	0.9		0.2
CEL-1700	100	0.4	0.5		Nil
Phenol-formaldehyde					
PF-800	93.7	4.6	1.7		0.2
PF-1200	98.9	1.5	0.3		0.2
PF-1400	98.6	0.9	0.2		-
PF-1700	98.9	0.3	0.1		0.2
Polyvinylidene chloride					
SA-800	75.6	16.9	2.3	4.0	0.2
SA-1200	96.6	2.8	0.5	Nil	0.2
SA-1400	96.1	2.3	0.6	-	-
SA-1700	99.0	1.2	0.3	Nil	-
Polyvinyl chloride					
PVC-800	95.0	2.9	1.2	1.3	0.2
PVC-1200	99.8	trace	0.5	0.2	Nil
PVC-1700	99.9	trace	0.5	Nil	-

APPENDIX B

Weight Loss Measurements - Isotherm Data

ISOTHERM DATA: ARGON ON CA-800 DEGASSED AT 350°C AND DEGASSED AT 900°C

CA-800 Degassed 350°C Tav = -195.6°C		CA-800 Degassed 900°C Tav = -195.6°C	
V ($g.g.^{-1}$)	P/P_o	V ($g.g.^{-1}$)	P/P_o
0.166	0.015	0.165	0.006
0.176	0.042	0.185	0.053
0.189	0.097	0.199	0.134
0.198	0.151	0.210	0.220
0.204	0.191	0.217	0.289
0.217	0.305	0.232	0.411
0.220	0.330	0.247	0.519
0.230	0.429	0.257	0.623
0.237	0.491	0.280	0.754
0.259	0.635	0.297	0.825
0.274	0.742	0.317	0.920
0.302	0.871	0.332	0.979
0.317	0.928		

APPENDIX C

Isotherm Data

C.1 Argon, Nitrogen on

(i) CA-700, CA-800, CA-1000, CA-1200, CA-1400, CA-1700, CA-2200, CA-2600, and CA-2900

(ii) CEL-800, CEL-1200 and CEL-1700

(iii) PF-800, PF-1200, PF-1400 and PF-1700

(iv) SA-800, SA-1200, SA-1400, SA-1700 and SA-2200

(v) SAA-900 and SAA-1700

(vi) PVC-800, PVC-1200 and PVC-1700

(vii) CAL-original and CAL-1700

at -196°C.

C.2 Benzene on CA-800, CA-1200 and CA-1700 at temperatures between 15° and 45°C.

C.3 p-Cymene on CA-800, CA-1200 and CA-1700 at 45°C.

C.4 n-Butane on CA-800, CA-1200 and CA-1700 at 0°C.

C.5 neo-Pentane on CA-800, CA-1200 and CA-1700 at 0°C.

ISOTHERM DATA

C.1 ARGON ON CA-700 and CA-800

CA-700 Tav = -195.7°C		CA-800 Tav = -195.8°C	
V (c.c. $g.^{-1}$)	P (mm.)	V (c.c. $g.^{-1}$)	P (mm.)
71.57	9.0×10^{-1}	0.21	1×10^{-4}
78.12	2.6×10^{-1}	0.64	4×10^{-4}
86.96	9.4	1.23	5×10^{-4}
92.76	17.6	2.24	8×10^{-4}
99.21	26.6	3.68	1×10^{-3}
106.4	40.6	4.85	1.5×10^{-3}
112.0	54.6	8.47	2.3×10^{-3}
116.1	75.0	11.8	3.5×10^{-3}
125.8	99.4	17.1	5.5×10^{-3}
131.1	114.5	25.9	1.2×10^{-2}
137.9	137.2	33.6	2.8×10^{-2}
143.8	157.0	48.4	7.5×10^{-2}
148.0	167.2	59.0	2.55×10^{-1}
154.1	183.1	72.0	1.00
158.2	193.4	79.0	1.87
		86.6	3.30
		101.2	22.51
		115.1	48.43
		118.7	58.52
		122.8	72.67
		129.2	99.06
		134.3	119.5
		144.0	145.0
		157.5	170.3
		164.0	181.3
		174.5	197.1

ISOTHERM DATA

C.1 ARGON ON CA-1000

CA-1000 Tav = -195.7°C		CA-1200 Tav = -195.7°C	
V (c.c. g.$^{-1}$)	P (mm.)	V (c.c. g.$^{-1}$)	P (mm.)
63.91	1.0	4.95	1.5×10^{-2}
72.31	4.8	15.19	6.4×10^{-1}
81.65	12.6	20.80	4.33
89.74	21.4	23.31	10.81
95.61	29.0	25.62	23.23
103.4	41.4	29.05	41.47
107.30	55.8	31.92	61.43
112.5	70.1	34.93	85.01
118.3	92.1	39.91	110.3
127.5	115.2	45.82	138.5
136.4	138.7	52.56	165.0
144.3	165.5	59.72	187.2
150.3	183.7		

ISOTHERM DATA

C.1 ARGON ON CA-1400 and CA-1700

CA-1400

Tav = -195.6°C

V (c.c. $g.^{-1}$)	P (mm.)
0.91	1×10^{-4}
1.21	1×10^{-3}
2.43	4×10^{-3}
5.93	5.5×10^{-2}
7.15	1.0×10^{-1}
11.52	4.6×10^{-1}
14.13	1.10
17.11	3.89
18.62	8.66
19.54	13.70
20.42	20.16
21.71	31.38
22.80	40.50
23.70	47.70
26.84	70.64
28.83	84.32
31.77	101.5
36.55	132.4
39.10	140.5
47.21	169.9
52.34	188.5

CA-1700

Tav = -195.6°C

V (c.c. $g.^{-1}$)	P (mm.)
0.32	5×10^{-3}
0.74	14×10^{-2}
1.27	3.5×10^{-2}
2.22	1.0×10^{-1}
3.38	2.1×10^{-1}
5.81	9.2×10^{-1}
6.76	2.80
8.03	9.91
8.87	21.30
10.14	43.04
12.25	79.42
13.61	95.96
15.33	113.4
17.15	133.1
18.69	148.9
19.67	156.4
21.43	168.9
24.23	191.5
25.66	200.1

ISOTHERM DATA

C.1 ARGON ON CA-2200 and CA-2600

CA-2200

Tav = -195.8°C

V (c.c. $g.^{-1}$)	P (mm.)
0.04	3 x 10^{-4}
0.13	5 x 10^{-4}
0.29	2 x 10^{-3}
0.52	7 x 10^{-3}
0.83	1.8 x 10^{-2}
1.22	3.5 x 10^{-2}
2.32	1.0 x 10^{-1}
2.94	2.1 x 10^{-1}
4.25	4.5 x 10^{-1}
5.41	1.66
6.02	4.16
6.83	13.75
7.48	24.89
8.55	47.11
10.01	70.04
12.63	101.0
14.81	124.2
15.65	133.5
17.73	153.7
20.20	170.3
22.64	188.5

CA-2600

Tav = -195.7°C

V (c.c. $g.^{-1}$)	P (mm.)
0.10	7 x 10^{-4}
0.25	7 x 10^{-3}
0.47	2.2 x 10^{-2}
1.04	8 x 10^{-2}
3.37	5.8 x 10^{-1}
4.21	3.85
4.45	7.64
4.80	16.54
5.22	29.71
5.89	47.93
6.86	66.77
8.33	88.27
9.90	109.7
10.84	122.6
13.76	155.7
15.71	175.4
18.23	199.5

ISOTHERM DATA

C.1 ARGON ON CA-2900

CA-2900

$T_{av} = -195.6^{\circ}C$

V ($c.c.\ g.^{-1}$)	P (mm.)
0.32	8×10^{-4}
0.49	5×10^{-3}
0.75	1×10^{-2}
0.86	2.5×10^{-2}
2.06	1.5×10^{-1}
4.13	0.50
5.05	2.87
5.59	10.33
6.62	35.74
7.02	44.81
7.37	51.65
7.87	60.49
9.02	76.62
10.75	96.71
12.34	116.5
14.45	139.2
17.49	167.1
20.01	191.3

ISOTHERM DATA

C.1 NITROGEN ON CA-800 and CA-1700

CA-800		CA-1700	
Tav = -193.7°C		Tav = -194.1°C	
V (c.c. g.$^{-1}$)	P (mm.)	V (c.c. g.$^{-1}$)	P (mm.)
0.54	1.5×10^{-3}	6.51	4.45×10^{-1}
9.81	2.8×10^{-3}	8.62	1.57
50.08	2.5×10^{-2}	10.73	8.35
92.15	2.37	11.11	26.57
100.3	8.64	12.67	79.84
106.1	18.06	13.42	133.3
110.5	31.35	14.34	207.0
114.6	53.22	15.43	311.6
119.0	119.4	16.28	380.4
123.4	182.1	18.64	519.3
129.5	259.1	19.44	546.5
132.8	344.5	21.81	645.7
138.4	484.6	24.95	718.3
145.3	567.1	26.82	742.4
151.5	711.1	30.00	832.6
156.5	805.6	34.71	923.5
163.0	935.6		
167.5	1040		

ISOTHERM DATA

C.1 NITROGEN ON CELL-800, CELL-1200 and CEL-1700

CELL-800 Tav = -192.1°C		CELL-1200 Tav = -193.1°C	
V (c.c. $g.^{-1}$)	P (mm.)	V (c.c. $g.^{-1}$)	P (mm.)
45.82	4.5×10^{-3}	18.12	10.1
107.2	4.06	27.70	96.2
118.7	16.37	30.53	199.3
130.9	65.41	30.26	312.0
135.1	151.1	30.24	400.6
137.4	234.	37.63	601.3
139.7	323.4	36.98	646.5
143.2	509.9	40.10	825.7
144.6	633.7	43.01	956.2
147.0	862.5		
149.8	990.3		
150.6	1050.1		

Cont'd.

ISOTHERM DATA

C.1 Nitrogen on CELL-800, CELL-1200 and CELL-1700 (Cont'd.)

CELL-1700

$T_{av} = -192.2^{\circ}C$

V (c.c. $g.^{-1}$)	P (mm.)
6.20	5.8
8.30	19.7
11.56	98.5
12.06	191.5
13.11	376.6
13.75	503.7
14.02	656.0
14.10	704.1
14.67	842.3
15.05	932.0
15.04	1065
15.21	1140

ISOTHERM DATA

G.1 ARGON ON PF-800 and PF-1200

PF-800

Tav = -195.7°C

V (c.c. $g.^{-1}$)	P (mm.)
2.86	1.6×10^{-2}
3.36	5.5×10^{-2}
4.70	1.9×10^{-1}
6.38	0.93
7.78	5.55
8.41	6.81
9.93	14.03
10.61	24.93
11.42	34.95
12.20	57.00
12.56	67.45
12.82	88.65
13.61	125.2
13.78	130.6
14.39	156.9
15.01	177.9

PF-1200

Tav = -195.7°C

V (c.c. $g.^{-1}$)	P (mm.)
1.57	9.5×10^{-2}
2.92	3.8×10^{-1}
3.92	1.13
4.70	2.64
5.15	6.72
5.54	11.43
6.03	22.35
6.82	40.61
7.47	61.21
8.36	84.34
9.95	122.4
10.97	144.2
11.91	163.4
12.12	181.6
12.75	196.0

ISOTHERM DATA

C.1 ARGON ON PF-1400 and PF-1700

PF-1400 Tav = -195.6°C		PF-1700 Tav = -195.6°C	
V (c.c. $g.^{-1}$)	P (mm.)	V (c.c. $g.^{-1}$)	P (mm.)
0.04	8×10^{-4}	0.28	2.5×10^{-2}
0.14	5.5×10^{-3}	0.34	7.5×10^{-2}
0.29	3×10^{-2}	0.39	3.1×10^{-1}
0.41	1.3×10^{-2}	0.56	1.52
0.60	1.15	0.73	11.40
0.70	4.32	0.84	31.45
0.90	23.38	0.95	60.80
0.95	37.46	1.01	90.52
1.11	75.02	1.02	116.5
1.17	108.3	1.03	154.5
1.20	144.1	1.04	169.8
1.34	182.2	1.06	195.8

ISOTHERM DATA

C.1 ARGON ON SA-800 and SA-1200

SA-800

Tav = -195.6°C

V (c.c. $g.^{-1}$)	P (mm.)
2.26	1×10^{-5}
12.23	1×10^{-4}
45.21	7×10^{-4}
81.57	1.2×10^{-3}
169.5	1.2×10^{-2}
223.0	1.3×10^{-1}
256.1	1.47
273.5	9.10
282.0	16.65
287.0	29.24
287.9	44.67
289.6	66.20
292.4	93.39
294.9	128.8
297.0	161.5
297.5	180.0
298.0	194.3

SA-1200

Tav = -195.7°C

V (c.c. $g.^{-1}$)	P (mm.)
1.82	1×10^{-5}
14.01	2×10^{-4}
33.94	3×10^{-4}
118.8	4.5×10^{-3}
126.9	6×10^{-3}
157.7	1.5×10^{-2}
195.7	6×10^{-2}
214.5	2.35×10^{-1}
244.2	9×10^{-1}
248.9	1.17
262.0	1.42
269.1	4.09
282.2	12.61
286.3	19.31
291.0	35.15
293.8	51.46
297.5	82.60
299.8	111.8
302.2	150.6
304.4	191.6

ISOTHERM DATA

C.1 ARGON ON SA-1400, SA-1700 and SA-2200

SA-1400

Tav = -196°C

V (c.c. $g.^{-1}$)	P (mm.)
125	3
167	23
183	75
202	147

SA-1700

Tav = -195.6°C

V (c.c. $g.^{-1}$)	P (mm.)
0.30	2×10^{-2}
0.40	2×10^{-1}
0.78	.93
0.95	2.77
1.18	8.36
1.38	16.48
1.60	23.01
1.71	33.84
1.77	58.03
1.83	84.06
1.89	12.12
1.91	15.92
1.96	17.15
2.01	19.99

SA-2200

Tav = -195.6°C

V (c.c. $g.^{-1}$)	P (mm.)
.11	7.56
.20	11.41

ISOTHERM DATA

C.1 ARGON ON PVC-800 and PVC-1200

PVC-800

Tav = -195.6°C

V (c.c. $g.^{-1}$)	P (mm.)
0.41	1.1×10^{-2}
0.46	4×10^{-2}
0.50	1.6×10^{-1}
0.55	6.5×10^{-1}
0.61	3.02
0.65	9.32
0.73	26.60
0.82	51.90
0.89	72.62
0.96	97.03
1.08	125.9
1.13	139.7
1.22	153.5
1.29	170.6
1.42	191.5

PVC-1200

Tav = -195.6°C

V (c.c. $g.^{-1}$)	P (mm.)
0.02	2.5×10^{-3}
0.05	8×10^{-3}
0.07	1.7×10^{-2}
0.09	4×10^{-2}
0.11	1.0×10^{-1}
0.15	2×10^{-1}
0.20	.50
0.27	2.85
0.29	5.60
0.30	9.09
0.31	13.40
0.32	17.83
0.35	29.41
0.38	39.80
0.39	48.46
0.40	56.10
0.42	62.65
0.44	75.87
0.48	90.35
0.60	123.1
0.68	150.3
0.76	167.5
0.85	190.7

ISOTHERM DATA

C.1 ARGON ON PVC-1700

PVC-1700

$T_{av} = -195.5^{\circ}C$

V (c.c. $g.^{-1}$)	P (mm.)
0.02	2×10^{-2}
0.04	1.1×10^{-1}
0.09	4.8×10^{-1}
0.13	1.9
0.16	11.24
0.17	25.48
0.18	38.52
0.19	50.17
0.28	81.03
0.32	101.2
0.40	131.5
0.52	181.0
0.56	194.7

ISOTHERM DATA

C.1 ARGON ON SAA-900 and SAA-1700

SAA-900

Tav = -195.6°C

V (c.c. $g.^{-1}$)	P (mm.)
28.95	9 x 10^{-4}
300.8	1.7 x 10^{-1}
340.2	2.8 x 10^{-1}
405.0	.66
430.4	.93
490.1	2.15
565.5	5.41
600.5	7.81
665.7	13.11
711.8	18.25
761.3	25.51
804.4	35.12
831.7	46.18
844.2	54.00
858.7	69.40
868.9	86.12
874.7	96.02
883.7	116.4
892.7	135.9
900.6	154.5
910.6	174.8
920.1	195.1

SAA-1700

Tav = -195.5°C

V (c.c. $g.^{-1}$)	P (mm.)
2.21	1 x 10^{-4}
13.22	3.5 x 10^{-4}
58.23	5 x 10^{-3}
72.61	1 x 10^{-2}
87.67	1.6 x 10^{-2}
116.9	3 x 10^{-2}
117.4	9 x 10^{-2}
221.8	2.3 x 10^{-1}
276.6	.87
307.1	2.20
327.0	3.95
363.4	9.07
388.4	13.23
439.8	24.00
471.5	30.56
519.2	42.05
544.6	51.45
559.1	58.26
570.7	70.78
582.1	88.27
585.3	96.71
588.0	108.3

Cont'd.

ISOTHERM DATA

C.1 Argon on SAA-900 and SAA-1700 (Cont'd.)

SAA-1700

Tav = 195.5°C

V (c.c. g.$^{-1}$)	P (mm.)
594.7	116.5
594.7	132.5
602.8	155.1
600.1	170.0
608.2	181.2
610.3	191.0
614.9	200.1

ISOTHERM DATA

C.1 ARGON ON CAL-original and CAL-1700

CAL-original Tav = -195.7°C		CAL-1700 Tav = -195.6°C	
V (c.c. g.$^{-1}$)	P (mm.)	V (c.c. g.$^{-1}$)	P (mm.)
1.12	1×10^{-4}	1.63	3×10^{-4}
6.09	3×10^{-4}	9.52	7.5×10^{-3}
35.81	2×10^{-3}	22.81	6×10^{-2}
99.00	3×10^{-2}	41.67	.47
157.1	1.7×10^{-1}	49.08	1.34
183.4	4.1×10^{-1}	54.10	2.95
221.7	1.6	66.22	13.28
256.0	5.48	80.64	30.68
292.5	11.12	89.18	43.15
312.3	20.71	97.91	60.11
328.4	30.82	105.2	80.42
361.2	49.93	108.8	92.74
372.9	69.86	117.5	126.4
375.0	80.60	132.2	168.2
382.5	105.7	137.0	185.1
385.5	116.4	143.6	194.9
405.6	179.1		
410.3	197.0		

ISOTHERM DATA

C.2 BENZENE ON CA-800

Tav = 14.6°C		Tav = 19.9°C	
V ($g.g_o^{-1}$)	P (mm.)	V ($g.g_o^{-1}$)	P (mm.)
adsorption		adsorption	
0.1092	1.57	0.1174	6.00
0.1344	8.19	0.1269	10.05
0.1383	14.77	0.1362	15.30
0.1719	25.04	0.1528	25.06
0.2236	41.67	0.1738	36.34
0.2384	47.22	0.1955	45.62
0.2511	57.87	0.2250	57.14
desorption		0.2459	75.11
0.2452	39.90		
0.2403	35.57	desorption	
0.2188	22.90	0.2416	67.32
0.1993	16.29	0.2380	59.46
0.1535	9.94	0.2324	48.31
0.1383	3.28	0.2266	41.97
		0.2090	30.81
		0.1813	23.19
		0.1376	8.81

ISOTHERM DATA

C.2 BENZENE ON CA-800

Tav = 24.8°C		Tav = 29.95°C	
V ($g.g_o^{-1}$)	P (mm.)	V ($g.g_o^{-1}$)	P (mm.)
adsorption		adsorption	
0.1074	2.94	0.1185	8.01
0.1296	11.77	0.1364	22.01
0.1467	25.63	0.1480	34.30
0.1643	39.20	0.1630	50.38
0.1871	53.29	0.1855	66.30
0.2094	63.16	0.2126	82.26
0.2349	77.29	0.2304	93.98
0.2476	94.29	0.2454	117.91
desorption		desorption	
0.2423	68.77	0.2378	89.02
0.2292	49.36	0.2325	78.65
0.2032	31.12	0.2271	69.59
0.1493	15.71	0.2183	58.01
0.1313	3.96	0.2124	53.09
		0.1995	44.49
		0.1799	33.47
		0.1530	21.89

ISOTHERM DATA

C.2 BENZENE ON CA-600

Tav = 35.0°C

V ($g.g.^{-1}$)	P (mm.)
adsorption	
0.1165	6.74
0.1279	14.45
0.1349	21.98
0.1480	39.64
0.1565	50.34
0.1745	70.54
0.1842	79.41
0.1972	90.26
0.2061	97.36
0.2222	109.57
0.2365	122.38
0.2470	146.59
desorption	
0.2419	108.61
0.2325	86.78
0.2157	65.41
0.1662	41.07
0.1413	15.96
0.1284	5.01

Tav = 39.3°C

V ($g.g.^{-1}$)	P (mm.)
adsorption	
0.1117	6.03
0.1234	17.23
0.1303	27.89
0.1377	39.71
0.1425	46.10
0.1520	62.05
0.1581	70.94
0.1697	86.12
0.1786	94.71
0.1915	104.30
0.2013	116.69
0.2159	127.23
0.2280	142.21
0.2365	160.32
0.2420	173.12
desorption	
0.2404	155.61
0.2296	112.51
0.2081	76.68
0.1587	49.15
0.1305	10.31

ISOTHERM DATA

C.2 BENZENE ON CA-1200

Tav = 14.1°C

V ($g.g.^{-1}$)	P (mm.)
adsorption	
0.0248	1.57
0.0415	11.10
0.0479	18.21
0.0563	22.59
0.0665	28.33
0.0772	32.83
0.0990	40.59
0.1045	44.37
0.1221	47.67
0.1362	52.16
0.1503	56.36
desorption	
0.1190	41.72
0.1057	31.64
0.0814	17.44
0.0383	4.59
0.0321	1.90

Tav = 19.9°C

V ($g.g.^{-1}$)	P (mm.)
adsorption	
0.0290	4.55
0.0420	16.67
0.0487	24.41
0.0608	34.70
0.0719	41.11
0.0810	46.46
0.0963	53.43
0.1146	62.14
0.1207	65.00
0.1514	75.03
desorption	
0.1243	60.54
0.1013	39.45
0.0650	17.97
0.0364	5.52

ISOTHERM DATA

C.2 BENZENE ON CA-1200

Tav = 25.5°C

V ($g.g._{-1}$)	P (mm.)
adsorption	
0.0117	.391
0.0312	2.60
0.0381	6.62
0.0481	17.15
0.0553	26.52
0.0664	39.44
0.0695	49.17
0.0807	57.54
0.0938	60.37
0.1125	77.05
0.1334	82.33
0.1626	94.92
desorption	
0.1407	80.71
0.1305	77.12
0.1163	66.79
0.1087	56.51
0.0962	41.86
0.0686	24.73
0.0535	16.56

Tav = 29.75°C

V ($g.g._{-1}$)	P (mm.)
adsorption	
0.0312	9.81
0.0385	21.19
0.0457	31.74
0.0506	41.89
0.0571	51.63
0.0663	62.05
0.0760	71.39
0.0965	88.22
0.1089	94.75
0.1319	109.94
0.1481	117.22
desorption	
0.1309	102.45
0.1051	71.44
0.0947	56.09
0.0705	36.01
0.0435	18.25
0.0324	4.46

ISOTHERM DATA

C.2 BENZENE ON CA-1200

Tav = 34.8°C

V ($g.g.^{-1}$)	P (mm.)
adsorption	
0.0231	4.02
0.0354	18.77
0.0424	34.93
0.0520	54.63
0.0663	77.24
0.0859	98.23
0.1087	117.93
0.1218	129.18
0.1308	135.41
0.1407	141.74
0.1471	145.57
desorption	
0.1281	125.22
0.1151	105.34
0.1008	78.51
0.0764	45.43
0.0415	18.09
0.0327	5.60

Tav = 39.7°C

V ($g.g.^{-1}$)	P (mm.)
adsorption	
0.0291	17.21
0.0336	29.53
0.0397	45.69
0.0475	66.03
0.0574	87.27
0.0638	98.07
0.0713	108.44
0.0875	127.26
0.1009	145.56
0.1146	156.34
0.1312	172.11
0.1402	177.79
desorption	
0.1119	132.13
0.1027	112.82
0.0872	82.63
0.0722	66.55
0.0499	51.43
0.0418	37.79
0.0344	16.53

ISOTHERM DATA

C.2 BENZENE ON CA-1700

Tav = 15.0°C

V ($g.g.^{-1}$)	P (mm.)
adsorption	
0.0144	3.54
0.0197	10.70
0.0230	17.48
0.0265	22.71
0.0307	26.64
0.0398	33.58
0.0471	37.99
0.0553	41.85
0.0640	46.65
0.0694	50.33
0.0755	58.90
desorption	
0.0719	47.78
0.0660	38.42
0.0617	32.27
0.0514	23.99
0.0377	18.73
0.0252	14.22
0.0202	10.74
0.0142	1.80

Tav = 20.0°C

V ($g.g.^{-1}$)	P (mm.)
adsorption	
0.0114	3.42
0.0164	12.28
0.0206	21.12
0.0241	29.79
0.0270	34.32
0.0325	39.89
0.0406	46.91
0.0460	50.25
0.0521	53.92
0.0609	58.56
0.0672	65.55
0.0725	75.39
desorption	
0.0697	66.25
0.0603	44.82

run abandoned because of leak.

ISOTHERM DATA

C.2 BENZENE ON CA-1700

Tav = 25.1°C		Tav = 29.9°C	
V ($g.g.^{-1}$)	P (mm.)	V ($g.g.^{-1}$)	P (mm.)
adsorption		adsorption	
0.0111	3.37	0.0113	7.76
0.0130	9.55	0.0136	15.61
0.0186	22.03	0.0151	22.07
0.0226	34.70	0.0183	31.33
0.0271	43.91	0.0225	45.29
0.0310	50.69	0.0283	60.11
0.0386	58.51	0.0331	67.23
0.0446	62.44	0.0432	77.67
0.0614	75.02	0.0514	84.57
0.0669	82.10	0.0607	93.64
0.0726	94.73	0.0659	104.01
		0.0704	117.66
desorption		desorption	
0.0630	75.92	0.0671	99.07
0.0583	53.58	0.0620	76.99
0.0468	38.07	0.0515	56.42
0.0181	19.04	0.0344	34.14
0.0119	4.42	0.0156	16.44
		0.0127	7.78

ISOTHERM DATA

C.2 BENZENE ON CA-1700

Tav = 35.0°C

V ($g.g.^{-1}$)	P (mm.)
adsorption	
0.0125	6.86
0.0136	14.72
0.0160	29.78
0.0218	49.72
0.0270	71.29
0.0363	88.27
0.0446	99.01
0.0533	108.33
0.0591	115.12
0.0643	122.56
0.0712	146.10
desorption	
0.0671	127.74
0.0632	101.60
0.0522	73.89
0.0416	52.85
0.0184	34.07

Tav = 41.2°C

V ($g.g.^{-1}$)	P (mm.)
adsorption	
0.0091	7.27
0.0124	20.75
0.0139	31.01
0.0162	42.67
0.0186	58.22
0.0213	77.08
0.0236	91.10
0.0281	104.64
0.0403	128.03
0.0466	137.71
0.0524	145.24
0.0595	159.78
0.0665	186.68
desorption	
0.0641	156.81
0.0498	121.65
0.0184	52.52

ISOTHERM DATA

C.3 p-CYMENE ON CA-800, CA-1200 and CA-1700

CA-800

Tav = 45.1°C

V ($g.g.^{-1}$)	P (mm.)
0.0353	0.25
0.0510	0.42
0.0629	0.65
0.0762	1.36
0.0876	1.99
0.0955	2.33
0.1094	2.81
0.1173	3.17
0.1303	3.79
0.1453	4.38
0.1580	5.43

CA-1200

Tav = 44.8°C

V ($g.g.^{-1}$)	P (mm.)
0.0006	0.04
0.0159	0.36
0.0322	0.99
0.0336	1.16
0.0431	1.72
0.0500	2.43
0.0573	2.90
0.0633	3.32
0.0695	3.38
0.0801	4.15
0.1054	5.27

CA-1700

Tav = 45.0°C

V ($g.g.^{-1}$)	P (mm.)
0.0049	0.26
0.0079	0.49
0.0120	0.70
0.0145	1.04
0.0156	1.32
0.0185	1.84

CA-1700 (Cont'd.)

V ($g.g.^{-1}$)	P (mm.)
0.0253	2.68
0.0295	3.08
0.0352	3.62
0.0406	4.11
0.0481	4.56
0.0548	4.88

ISOTHERM DATA

C.4 n-BUTANE ON CA-800, CA-1200 and CA-1700

CA-800

Tav = 0°C.

V ($g.g.^{-1}$)	P (mm.)
0.0044	0.68
0.0155	2.04
0.0291	4.92
0.0447	13.02
0.0548	27.13
0.0605	39.76
0.0666	61.29
0.0703	79.14
0.0747	105.89

CA-1200

Tav = 0°C

V ($g.g.^{-1}$)	P (mm.)
0.0073	1.92
0.0147	13.18
0.0171	24.30
0.0189	38.55
0.0200	49.41
0.0218	60.06
0.0226	73.72
0.0241	96.78
0.0252	119.5
0.0272	151.2
.0293	181.5

CA-1700

Tav = 0°C

0.0026	1.51
0.0046	3.86
0.0061	8.30
0.0076	15.21
0.0082	18.25
0.0093	31.26

CA-1700 (Cont'd.)

0.0096	38.19
0.0106	64.60
0.0111	76.37
0.0114	88.63
0.0120	106.60
0.0123	138.13

ISOTHERM DATA

C.5 neo-PENTANE ON CA-800, CA-1200 and CA-1700

CA-800
Tav = 0°C

V ($g.g_o^{-1}$)	P (mm_o)
0.0150	0.76
0.0299	2.24
0.0431	6.64
0.0486	11.44
0.0528	16.25
0.0565	23.43
0.0611	32.19
0.0662	47.61
0.0692	56.47
0.0699	65.61
0.0724	81.46
0.0753	102.02

CA-1200
Tav = 0°C

V ($g.g_o^{-1}$)	P (mm_o)
0.0005	0.69
0.0036	5.55
0.0045	10.83
0.0076	22.26
0.0114	37.75
0.0134	54.08
0.0153	77.25
0.0169	99.17
0.0182	121.28

CA-1700
Tav = 0°C

0.0009	0.46
0.0016	4.62
0.0038	13.40
0.0066	27.88
0.0081	39.88
0.0104	54.90
0.0115	79.77
0.0120	99.55
0.0122	127.01

APPENDIX D.

Pore Size Distributions

D.1 Calculation of Pore Size Distribution from Adsorption Isotherm Data for CA-800 and CA-1700.

D.2 Calculation of Pore Size Distribution from Theoretical Pore Models.

PORE SIZE DISTRIBUTIONS

D.1 CALCULATION OF PORE SIZE DISTRIBUTION FROM ADSORPTION ISOTHERM DATA FOR CA-800 and CA-1700.

CUMULATIVE SURFACE AREAS AND PORE VOLUMES
(Cranston and Inkley Method[220])

NITROGEN ON CA-800 and CA-1700

	CA-800		CA-1700	
Pore Diameter (Å)	Cumulative Σ ($m.^2\ g.^{-1}$)	Cumulative Pore Vol. ($c.c.\ g.^{-1}$)	Cumulative Σ ($m.^2\ g.^{-1}$)	Cumulative Pore Vol. ($c.c.\ g.^{-1}$)
295	-	-	.1	.0004
285	-	-	.1	.0008
275	-	-	.2	.0012
265	-	.001	.2	.0013
255	-	.001	.2	.0015
245	-	.002	.3	.0017
235	-	.002	.3	.0019
225	-	.002	.4	.0023
215	-	.003	.5	.0029
205	1	.004	.5	.0033
195	1	.004	.7	.0039
185	1	.004	.8	.0045
175	1	.005	.9	.0052
165	1	.006	1.1	.0060
155	1	.007	1.4	.0070
145	2	.008	1.7	.0081
135	2	.009	2.2	.0096
125	3	.011	2.6	.0109

Pore Diameter (Å)	CA-800 Cumulative Σ ($m.^2 g.^{-1}$)	CA-800 Cumulative Pore Vol. ($c.c. g.^{-1}$)	CA-1700 Cumulative Σ ($m.^2 g.^{-1}$)	CA-1700 Cumulative Pore Vol. ($c.c. g.^{-1}$)
115	3	.013	3.0	.0122
105	4	.015	3.9	.0145
95	6	.018	4.9	.0168
85	8	.022	6.2	.0196
75	12	.027	8.1	.0232
65	16	.034	10.5	.0271
55	23	.043	14.0	.0319
47.5	29	.050	15.5	.0337
42.5	35	.054	17.4	.0357
37.5	46	.064	19.8	.0380
32.5	60	.076	22.2	.0399
27.5	75	.086	23.0	.0404
22.5	106	.104	25.1	.0417
19	128	.114	26.1	.0422
17	137	.118	27.5	.0427
15	144	.121	27.5	.0428
13	148	.122	-	-
12	-	-		

PORE SIZE DISTRIBUTIONS

D.2 CALCULATION OF CHANGES IN THE PORE SIZE DISTRIBUTION FOR TWO HYPOTHETICAL MODELS OF CONSTRICTION GROWTH

Commencing with the pore size distribution calculated from the experimental data for CA-800, the change in the pore size distributions for two models of constriction growth were calculated.

MODEL I

The growth of constriction into the pore acted as a barrier and reduced the pore diameter by the size of the constriction. For an initial pore diameter of 30 Å, a constriction of 10 Å reduced the pore diameter to 20 Å. The initial pore volume of 47 c.c. $g.^{-1}$ is reduced by the ratio of the square of the pore diameters, to 4.5 c.c. $g.^{-1}$.

MODEL II

The growth of constriction into the pore space occupied a volume proportional to its diameter. The remaining pore diameter was calculated from the remaining pore volume. For an initial pore diameter of 30 Å the area of a circle of diameter 30 Å, A = 705 $Å^2$. The introduction of a 10 Å diameter constriction reduces the available area by 78.5 $Å^2$ to A_2 = 627 $Å^2$. The initial pore volume is reduced from the initial value of 47 c.c. $g.^{-1}$ by the ratio A_R/A to the value V_2 = 42 c.c. $g.^{-1}$. The new pore diameter D_2 is given by $A_R/78.5$.

PORE SIZE DISTRIBUTIONS FOR DIFFERENT VALUES OF THE CONSTRICTION DIAMETER - MODEL I.

STEP I : Experimental Values

D	5	10	15	20	25	30	35	40	50	60	70	80	90	100	110	120
V	12	25	40	54	66	47	37	30	22	17	13	10	8	6	5	4
D^2	25	100	225	400	625	900	1220	1600	2500	3600	4900	6400	8100	10000	12100	14,400

STEP II : Introduce a constriction of D_3^0 = 10 Å

D_2	-	-0	5	10	15	20	25	30	40	50	60	70	80	90	100	110
D_2^2	-	0	25	100	225	400	625	900	1600	2500	3600	4900	6400	8100	10000	12,100
V_2	-	0	4.5	12.5	24	21	19	17	14	12	9.5	7.7	6.3	4.9	4.2	3.4

STEP III : Introduce a constriction of D_2^0 = 25 Å

D_3	-	-	-	-	0	5	10	15	25	35	45	55	65	75	85	95
D_3^2	-	-	-	-	0	25	100	225	625	1220	2025	3025	4225	5625	7225	9025
V_3	-	-	-	-	0	1.3	3	4.2	5.5	5.8	5.4	5.1	4.1	3.4	3	2.5

PORE SIZE DISTRIBUTIONS FOR DIFFERENT VALUES OF THE CONSTRICTION DIAMETER - MODEL 2.

STEP I : Experimental Values

D	5	10	15	20	25	30	35	40	50	60	70	80	90	100	110	120
V	12	25	40	54	66	47	37	30	22	17	13	10	8	6	5	4
D^2	25	100	225	400	625	900	1220	1600	2500	3600	4900	6400	8100	10,000	12,100	14,400
A	19.6	78.5	177	314	490	705	960	1250	1960	2820	3840	5030	6350	7,850	9,500	11,300

STEP II : Introduction of constriction represented by a circle of diameter $D_2^o = 10$ Å, giving an equivalent area of 78.5 $Å^2$.

A_R	-	0	99	236	412	627	882	1172	1872	2742	3762	4952	6272	7,772	9,422	11,222
V_2	-	0	22	40	55	42	34	28	21	16.5	13	10	8	6	5	4
D_2^2	-	0	126	300	525	800	1120	1500	2400	3500	4800	6300	8000	9,850	12,000	14,300
D_2	-	0	11.2	17.3	22.9	28.3	33.5	38.7	49	59.2	69.3	79.4	89.4	99.2	109.5	120

STEP III : Introduction of constriction represented by a circle of diameter $D_3^o = 16$ Å, giving an equivalent area of 200 $Å^2$

A_R	-	-	-	36	212	427	682	972	1672	2542	3562	4752	6072	7,572	9,222	11,022
V_3	-	-	-	6.1	28.6	28.6	26	23	19	15.3	12.3	9.6	7.7	6	5	4
D_3^2	-	-	-	46	270	545	870	1240	2130	3240	4550	6050	7750	9,650	11,800	14,100
D_3	-	-	-	6.8	16.4	23.3	29.5	35.2	46.2	56.9	67.5	77.8	88.0	98.2	108.6	118.7

STEP IV : Introduction of constriction represented by a circle of diameter $D_4^o = 32$ Å, giving an equivalent area of $A_4^o = 800$ Å^2

A_R	-	-	-	-	-	-	160	450	1160	2020	3040	4230	5550	7,050	8,700	10,500
V_4	-	-	-	-	-	-	6.2	10.8	13	12.2	10.3	8.4	7	5.4	4.7	3.8
D_4^2	-	-	-	-	-	-	204	575	1480	2580	3880	5400	7100	9,000	11,100	13,400
D_4	-	-	-	-	-	-	14.3	24	38.5	50.8	62.3	73.5	84.3	94.9	105	116

STEP V : Introduction of constriction represented by a circle of diameter $D_5^o = 50.5$ Å, giving an equivalent area of $A_5^o = 2,000$

A_R	-	-	-	-	-	-	-	-	0	820	1840	3030	4350	5,850	7,500	9,300
V_5	-	-	-	-	-	-	-	-	0	5	6.2	6	5.5	4.5	4	3.3
D_5^2	-	-	-	-	-	-	-	-	0	1050	2340	3860	5500	7,450	9,550	11,500
D_5	-	-	-	-	-	-	-	-	0	32.4	48.4	62.1	74.2	86.3	97.7	109.1

APPENDIX B

Influence of Particle Size on the Adsorptive Capacity of Sintered Carbons - Isotherm Data

ISOTHERM DATA:

ARGON ON CA-800, FINELY GROUND CA-800 AT -196°C and FINELY GROUND CA-1700

CA-800

Tav = -195.7°C

V (c.c.g.$^{-1}$)	P (mm.)
91.2	0.53
102.0	1.81
110.5	4.45
115.9	8.23
122.7	18.52
125.3	25.81
127.2	32.37
129.5	38.50
130.1	47.01
134.6	55.63
138.2	65.07

CA-800 (ground to -200 mesh)

Tav = -195.7°C

V (c.c.g.$^{-1}$)	P (mm.)
99.1	1.24
105.3	2.49
112.4	6.22
119.4	15.00
129.0	35.67
131.1	45.51
135.1	54.32
137.0	60.56

CA-1700

Tav = -195.7°C

0.12	5	x 10^{-5}
0.54	3	x 10^{-4}
1.17	1	x 10^{-3}
3.33	2	x 10^{-2}
6.19	1.1	x 10^{-1}
8.96	3.2	x 10^{-1}
10.77	6.2	x 10^{-1}

CA-1700 (Cont'd.)

13.93	2.37
15.83	7.74
16.74	13.23
17.54	19.45
18.11	28.60
19.93	42.12
22.42	63.30

APPENDIX F.

Kinetics of Adsorption

KINETICS OF ADSORPTION

P.1 ARGON ON CA-800 at -81°C

TIME $\frac{\Delta V_t}{\Delta V_\infty}$

(Chart) Units	(P1 - P2)	(P2 - P3)	(P3 - P4)	(P4 - P5)	(P5 - P6)	(P6 - P7)	(P7 - P8)
0							
1	.295	.352	.377	.396	-	.444	.411
2	.397	.453	.489	.498	.503	.535	.495
3	.459	.517	.553	.558	.564	597	.556
4	.514	.568	.604	.604	.610	639	.598
5	.551	.606	.642	.641	.645	673	.631
6	.586	.640	.675	.672	.676	705	.657
7	.616	.665	.703	.698	703	730	.682
8	.644	.689	.727	.721	727	754	.704
9	.668	.710	.748	.741	750	775	723
10	.685	.729	.768	.758	778	794	.741
12	.709	.763	.802	.789	803	824	.765
14	.736	.792	.840	.818	822	850	.789
16	.760	.816	.856	.840	856	873	.811
18	.777	.833	.875	.860	876	893	.829
20	.798	.847	.892	.877	892	911	.843
22	.815	.860	.905	.891	905	926	.857
24	.832	.875	.917	.900	918	938	.869
26	.846	.888	.928	.909	928	949	.880
28	.860	.898	.937	.917	937	960	.890

(contd.)

$\frac{V_t}{V}$

(Chart) Units	(P1 - P2)	(P2 - P3)	(P3 - P4)	(P4 - P5)	(P5 - P6)	(P6 - P7)	(P7 - P8)
30	.866	.903	.945	-	946	-	.899
32	.873	.909	.951	-	953	.975	.907
34	-	-	.958		960	-	.914
36	.890	.915	.963		965	-	.921
38	-	-	.968		971	-	.927
40	.907	.928	.972		974	.996	.934
50	.945	.955	.985		991	-	.966
60	.990	.979	.995		-		.989
	-	-	-				-

Where P1 = $0.465.10^{-1}$ CM.
P2 = 0.130 CM.
P3 = 0.297 CM.
P4 = 0.881 CM.
P5 = 1.97 CM.
P6 = 3.78 CM.
P7 = 4.70 CM.
P8 = 3.74 CM.

Note: For ease of tabulation the readings were taken directly from the recorder chart. For the majority of experiments the chart speed was such that

10 'chart units' = 3.75 min.

For the remainder of the experiments the time could be read from the chart directly in minutes.

KINETICS OF ADSORPTION

F.1 ARGON ON CA-1700 at -183°C

TIME (Chart Units)	$\frac{\Delta V_t}{\Delta V_\infty}$ (P1 - P2)	(P2 - P3)	(P3 - P4)	(P4 - P5)
0				
1	.567	.562	.515	.531
2	.633	.631	.577	.586
3	.663	.683	.621	.632
4	.726	.725	.658	.672
5	.765	.760	.692	.702
6	.797	.794	.717	.731
7	.825	.815	.745	.756
8	.850	.342	.770	.780
9	.867	.863	.790	.801
10	.887	.884	.809	.819
12	.918	.913	.840	.848
14	.942	.936	.865	.875
16	.960	.957	.886	.894
18	.973	.968	.907	.910
20	.982	.978	.927	.924
22	.988	.986	.940	.935
24	.992	-	.953	.946
26	.995	.995	.965	.956
28	-	-	.975	.963
30			.984	.970
32			-	-

where P1 = 0.151 CM. P4 = 0.453 CM.
P2 = 0.215 CM. P5 = 0.821 CM.
P3 = 0.265 CM.

KINETICS OF ADSORPTION

F.1 ARGON ON CA-1200 at -196°C

TIME (Chart Units)	$\frac{\Delta V_t}{\Delta V_\infty}$					
	P1 - P2	P2 - P3	P3 - P4	P4 - P5	P5 - P6	P6 - P7
0						
1	332	.385	.405	.346	.417	.433
2	371	.436	.456	.408	.464	.496
3	406	.480	.498	.433	.501	.535
4	439	.514	.534	.478	.536	.573
5	467	.540	.566	.509	.568	.608
6	494	.570	.598	.540	.595	.638
7	520	.596	.625	.565	.620	-
8	545	.617	.647	.592	.642	.680
9	586	.640	.672	.614	.662	.718
10	606	.660	.693	.635	.680	.738
12	626	.696	734	.674	.716	.777
14	657	-	.765	.704	.743	.812
16	685	.755	.795	.731	.767	.840
18	710	.779	.820	.762	.792	.861
20	734	.800	.840	.783	.807	.882
22	753	.815	.864	-	.825	.900
24	770	.832	.880	.817	.836	.915
26	787	.846	.893	.835	-	.927
28	802	.857	-	-	.856	.942
30	814	.870	.915	.860	-	.950
35	-	.892	-	.888	.880	.968
40	-	.914	.957	.914	-	.980
45	878	.932	.972	.938	.910	-
50	890	-	.985	.956	-	-

(Chart Units)	P1 - P2	P2 - P3	P3 - P4	P4 - P5	P5 - P6	P6 - P7
55	908		-	-	.937	
60	915			.984	-	
65	925			-	.941	
70	928				-	
75	940				-	
80	946				.955	
85	974				-	
90	980					

where P1 = 1×10^{-4} CM.
P2 = 0.035 CM.
P3 = 0.075 CM.
P4 = 0.121 CM.
P5 = 0.173 CM.
P6 = 0.187 CM.
P7 = 0.170 CM.

KINETICS OF ADSORPTION

P.2 ARGON ON CA-800, CA-1200 and CA-1700 at -81°C

TIME (Chart Units)	$\frac{\Delta V_t}{\Delta V_\infty}$		TIME (Min.)	$\frac{\Delta V_t}{\Delta V_\infty}$
	CA-800	CA-1200		CA-1700
0				
1	.234	.564	.3	.709
2	.340	.678	.5	.751
3	.403	.725	.7	.775
4	.458	.756	.9	.794
5	.505	.780	1	.800
6	.543	.802	1.5	.830
7	.576	.818	2	.845
8	.606	.833	3	.877
9	.636	.845	4	.894
10	.662	.857	5	.911
12	.705	.876	6	.924
14	.735	.890	7	.934
16	.764	.901	8	.944
18	-	.912	9	.954
20	.810	.921	10	.956
22	.829	.927	12	-
24	.842	.936		
26	.858	.940		
28	.874	.946		
30	-	-		
32	.900	-		
34	.910	.958		
36	-	-		

TIME (Chart Units)	$\frac{\Delta V_t}{\Delta V_\infty}$ CA-800	CA-1200
38	-	-
40	.930	.972
50	.963	-
60	-	

KINETICS OF ADSORPTION

F.2 ARGON ON CA-800, CA-1200 and CA-1700 at -183°C

TIME (Min.)	$\frac{\Delta V_t}{\Delta V_\infty}$ CA-800	TIME (Chart Units)	$\frac{\Delta V_t}{\Delta V_\infty}$ CA-1200	CA-1700
0		0		
1	.086	1	-	.531
2	.119	2	.456	.586
3	.151	3	.480	.632
4	.181	4	.506	.672
5	.205	5	.526	.702
6	.228	6	.547	.731
7	.249	7	.567	.756
8	.268	8	.587	.780
9	.286	9	.606	.801
10	.302	10	.624	.819
12	.333	12	.654	.848
14	.360	14	.682	.875
16	.382	16	.703	.894
18	.405	18	.724	.910
20	.424	20	.744	.924
24	.461	22	.762	.946
28	.493	24	.778	.963
30	.508	26	.792	.970
36	.544	28	804	.985
40	.565	30	.818	.992
46	.595	32	.828	-
50	.614	34	.840	
56	.640	36	850	
60	.657	38	.860	

TIME (Min.)	$\frac{\Delta V_t}{\Delta V_\infty}$ CA-800
70	.692
80	.724
90	.753
100	.778
150	.877

TIME (Chart Units)	$\frac{\Delta V_t}{\Delta V_\infty}$ CA-1200	CA-1700
40	.867	
50	.905	
60	.924	
70	.943	
80	960	

KINETICS OF ADSORPTION

P.2 ARGON ON CA-800, CA-1200 and CA-1700 at -196°C

TIME (Min.)	$\frac{\Delta V_t}{\Delta V_\infty}$ CA-800	CA-1700	TIME (Chart Units)	$\frac{\Delta V_t}{\Delta V_\infty}$ CA-1200
0			0	
1	.114	.698	1	.405
2	.165	.785	2	.456
3	.208	.847	3	.498
4	.242	.890	4	.534
5	.273	.923	5	.566
6	.299	.943	6	.598
7	.324	.959	7	.625
8	.345	.968	8	.647
9	.365	.977	9	.672
10	.385	.984	10	.693
12	.418	.994	12	.734
14	.462	-	14	.765
16	.487		16	.795
18	.514		18	.820
20	.534		20	.840
25	.582		22	.864
30	.617		24	.880
35	.654		26	.893
40	.682		28	-
45	.707		30	.915
50	.732		32	.925
			34	.935
			38	.950
			42	.964
			46	.974
			50	.985

KINETICS OF ADSORPTION

F.3 ARGON ON SA-800, SA-1200, SA-1400 and SA-1700 at -196°C

TIME (Min.)	$\frac{\Delta V_t}{\Delta V_\infty}$			
	SA-800	SA-1200	SA-1400	SA-1700
0				
1	.290	.282	.122	.612
2	.420	.404	.169	.740
3	.517	.501	.212	.805
4	.597	.579	.248	.835
5	.660	.644	-	-
6	.712	.694	.287	.840
7	.747	.736	.314	.872
8	.794	.775	.337	.900
9	.825	.805	.360	-
10	.851	.830	.380	.920
12	.891	.872	-	-
14	.920	.902	.460	
16	.941	.927	-	
18	.956	.947	.523	
20	.968	.962	-	
22	.977	.972	.562	
24	.982	.981	-	
26	.987	.988	.601	
28	-	.993	-	
30		-	.665	
32			-	
34			-	
36			.702	
38			-	
40			.725	

TIME (Min.)	$\frac{\Delta V_t}{\Delta V_\infty}$			
	SA-800	SA-1200	SA-1400	SA-1700
55			.806	
70			.857	
85			.884	
			-	

F.4 NUMERICAL SOLUTION OF FICK'S SECOND LAW FOR THE CASE OF A SPHERE OF RADIUS r_o

Equation (40) is

$$\frac{Vt - Vo}{V_\infty - V_o} = 6\left(\frac{Dt}{r_o^2}\right)^{\frac{1}{2}}\left[\pi^{-\frac{1}{2}} + 2\sum_{n=1}^{\infty} \text{ierfc } n\left(\frac{Dt}{r_o^2}\right)^{-\frac{1}{2}}\right] - \frac{3Dt}{r_o^2}$$

Let $T1 = 6\left(\frac{Dt}{r_o^2}\right)^{\frac{1}{2}}$

$$T2 = \pi^{-\frac{1}{2}} + 2\sum_{n=1}^{\infty} \text{ierfc } n\left(\frac{Dt}{r_o^2}\right)^{-\frac{1}{2}}$$

$$T3 = -\frac{3Dt}{r_o^2}$$

$\left(\frac{Dt}{r_o^2}\right)^{\frac{1}{2}}$	T1	T2	T3	$\frac{Vt - Vo}{V_\infty - Vo}$
.05	.3	.566	.0075	.162
.075	.45	.566	.0168	.235
.1	.6	.566	.03	.310
.15	.9	.566	.0675	.442
.2	1.2	.566	.12	.560
.25	1.5	.566	.1875	.662
.3	1.8	.566	.27	.750
.35	2.1	.566	.3675	.822
.4	2.4	.566	.48	.880
.45	2.7	.566	.6075	.921
.5	3.0	.568	.75	.954

Values of the function ierfc x were obtained from Crank[123].

APPENDIX G

Thermodynamics of Adsorption

G.1 Differential Heats and Entropies of Adsorption of Argon and Benzene on CA-800, CA-1200 and CA-1700

G.2 Accuracy of Thermodynamic Measurements

THERMODYNAMICS OF ADSORPTION

G.1 DIFFERENTIAL HEATS AND ENTROPIES OF ADSORPTION OF ARGON ON CA-900

V/V_m	q_{st} (cal. mole^{-1})	$\bar{s}_s$ (cal. mole^{-1} deg.$^{-1}$)
0.091	2,460	23.9
0.183	2,190	25.0
0.274	2,120	23.9
0.320	2,010	24.3
0.366	2,020	23.4
0.412	2,060	22.1
0.457	2,040	21.4
0.548	1,970	20.0
0.640	1,890	18.7
0.732	1,830	18.1
0.821	1,770	16.7
0.914	1,760	15.1
1.005	1,730	14.0
1.100	1,710	12.9
1.193	1,670	12.3
1.284	1,670	11.9
1.375	1,670	11.6
1.465	1,670	11.4

THERMODYNAMICS OF ADSORPTION

G.1 DIFFERENTIAL HEATS AND ENTROPIES OF ADSORPTION OF ARGON ON CA-1200

V/V_m	q_{st} (cal. mole^{-1})	$\bar{s}_s$ (cal. mole^{-1} deg.$^{-1}$)
0.187	2,810	13.4
0.281	2,750	12.5
0.374	2,700	11.6
0.467	2,620	11.2
0.556	2,540	11.0
0.655	2,460	10.9
0.795	2,300	11.3
0.843	2,120	11.7
0.888	1,990	12.4
1.030	1,895	13.0
1.125	1,880	12.6
1.170	1,853	11.6
1.235	1,895	11.9
1.405	1,765	11.6
1.871	1,710	11.2

THERMODYNAMICS OF ADSORPTION

G.1 DIFFERENTIAL HEATS AND ENTROPIES OF ADSORPTION OF ARGON ON CA-1700

V/V_m	q_{st} (cal. mole^{-1})	$\bar{s}_s$ (cal. mole^{-1} deg.$^{-1}$)
0.057	2,840	15.5
0.103	2,710	15.1
0.207	2,640	13.6
0.315	2,500	14.1
0.414	2,460	13.3
0.517	2,420	12.7
0.620	2,300	12.8
0.724	2,120	12.6
0.827	1,950	13.3
1.031	1,800	12.4
1.243	1,720	12.4
1.451	1,730	11.7
1.662	1,730	11.3
1.865	1,730	11.0
2.074	1,710	11.0

THERMODYNAMICS OF ADSORPTION

G.1 DIFFERENTIAL HEATS AND ENTROPIES OF ADSORPTION OF BENZENE ON CA-800

V/V_s	q_{st} (cal. mole^{-1})	$\bar{s}_s$ (cal. mole deg.$^{-1}$)
0.499	8,950	44.7
0.533	8,880	45.1
0.571	8,760	45.4
0.612	8,640	45.7
0.650	8,600	45.8
0.685	8,490	45.9
0.730	8,450	45.8
0.771	8,400	45.8
0.809	8,290	45.9
0.847	8,370	45.5
0.893	8,420	45.1
0.938	8,510	44.6
0.980	8,650	44.1

THERMODYNAMICS OF ADSORPTION

G.1 DIFFERENTIAL HEATS AND ENTROPIES OF ADSORPTION OF BENZENE ON CA-1200

$V/\bar{V}_s$	q_{st} (cal. mole^{-1})	$\bar{s}_s$ (cal. mole^{-1} deg.$^{-1}$)
0.274	9,400	44.5
0.307	9,240	44.7
0.341	9,010	44.8
0.412	8,340	46.5
0.486	8,590	45.8
0.545	8,550	45.0
0.606	8,320	45.3
0.684	8,350	45.5
0.727	8,020	45.8
0.828	8,010	46.2
0.887	8,060	46.4
0.953	8,050	46.5

THERMODYNAMICS OF ADSORPTION

G.1 DIFFERENTIAL HEATS AND ENTROPIES OF ADSORPTION OF BENZENE ON CA-1700

V/V_s	q_{st} (cal. mole^{-1})	$\bar{s}_s$ (cal. mole^{-1} deg.$^{-1}$)
0.214	11,300	38.5
0.266	10,850	40.4
0.285	10,200	40.9
0.367	10,200	41.2
0.425	9,810	41.3
0.497	9,430	42.0
0.563	9,350	42.6
0.632	9,120	43.0
0.695	9,030	43.4
0.794	8,860	44.1
0.835	8,810	43.8
0.948	8,440	45.2
0.971	8,240	45.3

C.2 ACCURACY OF THERMODYNAMIC MEASUREMENTS

(a) Argon Isotherms

The accuracies of the three measured variables temperature, amount adsorbed and pressure will be considered in turn.

Temperature: $90 \pm .05^{\circ}K$ or approx. 1 in 2,000.

Amount Adsorbed: The weight change is calculated from the difference between two cathetometer readings. As the error for one reading is $\pm$ 0.002 cm., the error involved in calculating the extension is $\pm$ 0.004 cm. The sensitivity of the springs is 80 cm. $g.^{-1}$, so the error in the amount adsorbed on a 0.1 g. sample is $\pm$ 0.0004 g. Taking into account spring calibration errors of $\pm$ 0.0002 g., the total error becomes $\pm$ 0.0006 g.

Pressure:

(1) Below a pressure of 2mm. Hg., the pressure is read from the McLeod gauge to an accuracy of $\pm$ 2%.

(2) Pressures above 2mm. Hg. are read from the mercury U-tube manometer. Between p = 2 mm. and p = 1.0 cm. the error is estimated to be $\pm$ 0.004 cm. Therefore for a pressure reading of just greater than 2 mm. the error is $\pm$ 2%. Above p = 1.0 cm. the error reduces to $\pm$ 0.3%. Thus by far the largest error occurs in the pressure measurements.

The calculation of the heat of adsorption involves measuring the slope of a plot of log p versus $^{1}/T$. As pointed above the main error occure in the pressure measurements. For a difference in pressures the error is doubled.

(1) For pressures below p = 2mm.:

$$q_{st} \approx 2,500 \pm 4\% \text{ cal. mole}^{-1}$$

$$= 2,500 \pm 100 \text{ cal. mole}^{-1}$$

(2) For pressures between p = 2mm. and p = 1.0 mm.

$q_{st} \sim 2{,}000 \pm 4\%$ cal. mole^{-1}

$= 2{,}000 \pm 100$ cal. mole^{-1}

(3) For pressures above p = 1.0 cm.

$q_{st} \sim 1{,}500 \pm 0.6\%$ cal. mole^{-1}

$= 1{,}500 \pm 10$ cal. mole^{-1}

(b) Benzene Isotherms

Similar accuracies occur for the measurement of temperature, amount adsorbed and the pressure. However, as most of the q_{st} values correspond to pressures above p = 1.0 cm., the error involved is $\pm$ 0.5%. For $q_{st} \sim 9{,}000$ cal. mole^{-1} the error is $\pm$ 50 cal. mole^{-1}.

G.3 Models of the Adsorbed State

Three basic models that will be examined are:

(a) a localized monolayer,

(b) an ideal mobile gas, and

(c) a non-ideal mobile gas with one or two degrees of translational freedom.

The effect of molecular interactions on the entropy of the localized model has been shown by Garden and Kington[210] to be negligible for the adsorption of argon on zeolite, while for the non-ideal gas model molecular interactions do not affect the entropy[218]. Adopting the methods of analysis similar to that used by Barrer[194], Everett[170] and Garden and Kington[218], the characteristics of the above models will now be compared with the experimental data.

(a) Localized Monolayer Model

This model gives rise to Langmuir's isotherm and the differential molar entropy $\bar{s}_S$ is given by

$$\bar{s}_S = \bar{s}_c + \bar{s}_{th}$$

where $\bar{s}_c = R \ln \frac{1}{\theta - 1}$, $\theta = V/V_m$ and V_m = monolayer capacity. Values of $\bar{s}_S$, $\bar{s}_c$ and $\bar{s}_{th}$ for the adsorption of argon on CA-800, CA-1200 and CA-1700 are listed in TABLE I.

TABLE I

Values of the Differential Entropy $\bar{s}_S$, the Configurational Entropy $\bar{s}_c$ and the Thermal Entropy $\bar{s}_{th}$ for the Adsorption of Argon on CA-800, CA-1200 and CA-1700.

CA-800

θ	$\bar{s}_g$ (cal.mole^{-1} deg.$^{-1}$)	$\bar{s}_c$ (cal.mole^{-1} deg.$^{-1}$)	$\bar{s}_{th}$ (cal.mole^{-1} deg.$^{-1}$)
0.091	23.9	4.6	19.3
0.183	25.0	2.9	22.1
0.274	23.9	1.9	22.0
0.320	24.3	1.5	22.8
0.366	23.4	1.0	22.4
0.412	22.1	0.7	21.4
0.457	21.4	0.4	21.0
0.548	20.0	-0.3	20.3
0.640	18.7	-1.1	19.8
0.732	18.1	-1.8	19.9
0.821	16.7	-3.0	19.7
0.914	15.1	-4.5	19.6

CA-1200

θ	$\bar{s}_s$ (e.u.)	$\bar{s}_c$ (e.u.)	$\bar{s}_{th}$ (e.u.)
0.187	13.4	2.8	10.6
0.281	12.5	1.8	10.7
0.374	11.6	1.0	10.6
0.467	11.2	0.3	10.9
0.556	11.0	-0.4	11.4
0.655	10.9	-1.2	12.2
0.795	11.3	-2.7	14.0
0.843	11.7	-3.3	15.0
0.888	12.4	-4.1	16.5

CA-1700

0.057	15.5	5.6	9.9
0.103	15.1	4.2	10.9
0.207	13.6	2.6	11.0
0.315	14.1	1.5	12.6
0.414	13.3	0.7	12.6
0.517	12.7	0	12.7
0.620	12.8	-0.9	13.7
0.724	12.6	-1.9	14.5
0.827	13.3	-3.1	16.4

According to Garden and Kington[218] the thermal entropy must obey certain criteria if the model of the adsorbed state can be declared valid. The values of the thermal entropy $\bar{s}_{th}$

(1) must be positive quantities and have a reasonable physical magnitude, and

(2) must be independent of θ .

(b) An Ideal Mobile Gas Model

This model yields a linear isotherm where the surface concentration is directly proportional to the pressure (Henry's Law). The isotherm for the adsorption of argon on CA-800 is not linear so clearly this model is not applicable.

(c) Non-ideal Mobile Model

The preceding model is based on molecules possessing only a point area and is therefore grossly over-simplified. The first step is to introduce a co-area for each molecule. The isotherm corresponding to this model is Volmer's equation

$$p = k\left(\frac{\theta}{1-\theta}\right) \exp\left(\frac{\theta}{1-\theta}\right) .$$

The molecules are mobile and may possess one or two degrees of freedom. The differential molar entropy for one degree of translational freedom is given by equation (50) where l = co-length of the argon atoms. For two degrees of translational freedom the differential entropy is given by equation (51) where a, the co-area of argon atoms[218] is taken as 11.6 Å^2. Values of $\bar{s}_S$, $_1\bar{s}_T$, $_2\bar{s}_T$, $\bar{s}_{th}'$ and $\bar{s}_{th}''$ are given in TABLE II. For one degree of translational freedom $\bar{s}_{th}'$ can be equated to $_2\bar{s}_v$ and for two degrees of translational freedom $\bar{s}_{th}''$ can be equated to $_1\bar{s}_v$, where $_n\bar{s}_v$ is the entropy associated with the vibration of the atom against the solid. If the model is valid then values of $_n\bar{s}_v$ should be independent of θ and possess reasonable positive physical magnitudes.

TABLE II

Values of the Differential Molar Entropy $\bar{s}_S$, the Translational Entropies $_1\bar{s}_T$ and $_2\bar{s}_T$ and the Vibrational Entropies $_2\bar{s}_V$ and $_1\bar{s}_V$ for Carbons CA-800, CA-1200 and CA-1700.

CA-800

θ	$\bar{s}_S$ (e.u.)	$_1\bar{s}_T$ (e.u.)	$_2\bar{s}_V$ (e.u.)	$_2\bar{s}_T$ (e.u.)	$_1\bar{s}_V$ (e.u.)
.20	25.0	8.4	16.6	13.9	11.1
.25	24.3	7.7	16.6	13.1	11.2
.30	23.6	6.9	16.7	12.5	11.1
.35	22.9	6.3	16.6	11.8	11.1
.40	22.2	5.5	16.7	11.1	11.1
.45	21.5	4.8	16.7	10.5	11.0
.50	20.8	4.1	16.6	9.6	11.2
.55	20.0	3.4	16.6	8.9	11.1
.60	19.3	2.4	16.9	7.9	11.4
.65	18.6	1.3	17.3	6.8	11.8
.70	18.0	-0.2	18.2	5.3	12.7
.75	17.4	-2.0	19.4	3.7	13.7
.80	16.7	-4.8	21.5	1.1	15.6
.85	16.0	-	-	-2.7	18.7

CA-1200

θ	$\bar{a}_S$ (e.u.)	$1^3\bar{a}_T$ (e.u.)	$2^3\bar{a}_V$ (e.u.)	$2^3\bar{a}_T$ (e.u.)	$1^3\bar{a}_V$ (e.u.)
0.20	13.2	8.4	4.8	13.9	-0.7
0.25	12.7	7.7	5.0	13.1	-0.5
0.30	12.3	6.9	5.4	12.5	-0.2
0.35	11.9	6.3	5.6	11.8	0.1
0.40	11.6	5.5	6.1	11.1	0.5
0.45	11.3	4.8	6.5	10.5	0.8
0.50	11.1	4.1	7.0	9.6	1.5
0.55	11.0	3.4	7.6	8.9	2.1
0.60	10.9	2.4	8.5	7.9	3.0
0.65	10.9	1.3	9.6	6.8	4.1
0.70	11.0	-0.2	11.2	5.3	5.7
0.75	11.0	-2.0	13.0	3.7	7.3
0.80	11.4	-4.8	16.2	1.1	10.3
CA-1700					
0.10	15.2	10.1	5.1	15.7	-0.5
0.15	14.9	9.2	5.7	14.9	0
0.20	14.6	8.4	6.2	13.9	0.7
0.25	14.3	7.7	6.6	13.1	1.2
0.30	14.0	6.9	7.1	12.5	1.5
0.35	13.7	6.3	7.4	11.8	1.9
0.40	13.4	5.5	7.9	11.1	2.3
0.45	13.1	4.8	8.3	10.5	2.6
0.50	12.9	4.1	8.8	9.6	3.3
0.55	12.7	3.4	9.5	8.9	3.8
0.60	12.6	2.4	10.2	7.9	4.7
0.70	12.6	-0.2	12.8	5.3	7.3
0.80	12.7	-4.8	17.5	1.1	11.6

For CA-800, values of $_2\bar{s}_v$ and $_1\bar{s}_v$ are approximately constant over the range $\theta = 0.2$ to 0.6, indicating that either the 1t, 2v or 2t, 1v states of the adsorbed argon are equally reasonable. However, the physical magnitude of the vibrational entropies for both states is higher than that predicted from the theoretical equation for the entropy of vibration, i.e.

$$_1\bar{s}_v = R\,u(e^u-1)^{-1} - \ln(1-e^{-u}) ,$$

where $u = h\nu/kT$, ν being the vibrational frequency. At 90°K Garden and Kington[218] have calculated that $_1\bar{s}_v$ for physical adsorption should be approximately 2 to 3 e.u. The state of the adsorbed molecules giving a value of $_1\bar{s}_v$ nearest to the theoretical value is that possessing only one degree of translational freedom. It appears that the high entropy of vibration values are associated with a low heat of adsorption (c.f. the heats of adsorption of argon on zeolites[194]).

For CA-1200 and CA-1700 it is evident that values of $_2\bar{s}_v$ and $_1\bar{s}_v$ do not comply with the above conditions. Evidently the surface is sufficiently heterogeneous to prevent a satisfactory solution.

APPENDIX H

Crystallite Size Data for Heat Treated Cellulose Acetate, Cellulose, Phenol-formaldehyde, Polyvinylidene Chloride, Polyvinyl Chloride and Cal Carbons

CRYSTALLITE SIZE DATA :

CELLULOSE ACETATE CARBON	CRYSTALLITE SIZE L_c (Å)	CRYSTALLITE SIZE L_a (Å)
CA-700	9.8	27.5
CA-800	9.9	26.3
CA-1000	10.6	31.8
CA-1200	11.0	37.2
CA-1400	11.2	41.6
CA-1700	11.9	44.8
CA-2200	23.3	51.4
CA-2600	45.4	62.2
CA-2900	50.5	62
CELLULOSE CARBON		
CELL-800	10.0	30.2
CELL-1200	10.0	33
CELL-1400	11.2	35.5
CELL-1700	12.5	42.4
PHENOL-FORMALDEHYDE CARBON		
PF-800	10.3	29.4
PF-1200	14.6	41.6
PF-1400	18.1	42.6
PF-1700	20.6	46.0

CRYSTALLITE SIZE DATA (Cont'd.)

POLYVINYLIDENE CHLORIDE CARBON	CRYSTALLITE SIZE L_c (Å)	L_a (Å)
SA-800	8.0	22.2
SA-1200	8.0	35.1
SA-1400	9.1	39.3
SA-1700	10.6	47.2
POLYVINYL CHLORIDE CARBON		
PVC-800	15.5	28.6
PVC-1200	36.2	36.9
PVC-1400	75.3	50.3
PVC-1700	227	71.0
PVC-2200	*	180
PVC-2600	*	284
PVC-2900	*	*
CAL CARBON		
CAL-original	12.4	37.0
CAL-1700	14.5	45.1

* Reflection too narrow to measure with sufficient accuracy.

APPENDIX I

Carbonization Apparatus

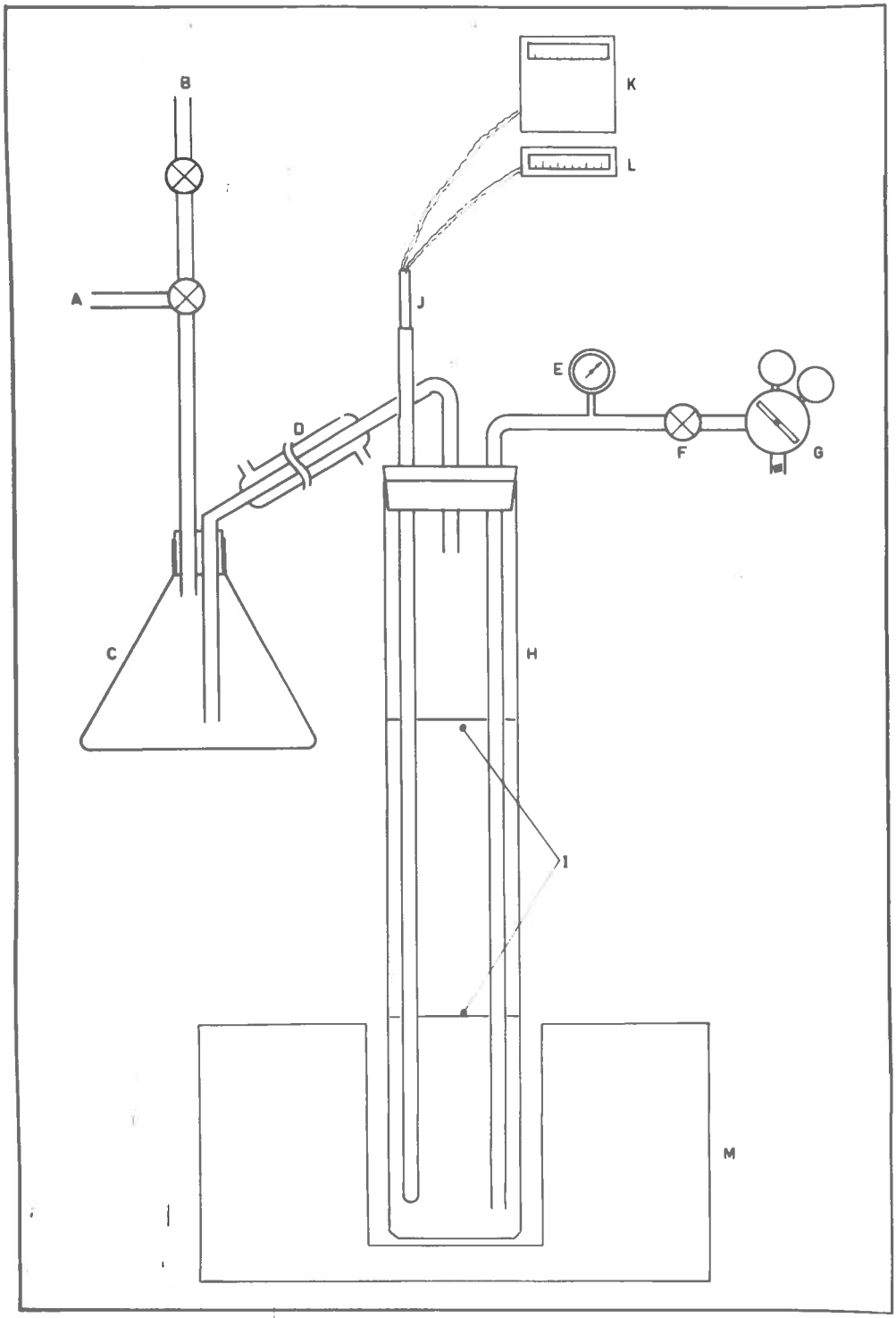

Carbonization Apparatus

KEY TO FIGURE

Carbonization Apparatus

A. Vacuum line
B. Furnace hood
C. Condensate flask
D. Condenser
E. Vacuum gauge
F. Fine control needle valve
G. Cylinder of 'oxygen free' nitrogen
H. Silica tube, length 90 cm., I.D. = 10 cm.
I. Stainless steel heat baffles
J. Four bore silica tubing and two chromel-alumel thermocouples
K. Furnace controller
L. Temperature indicator
M. Furnace

APPENDIX J

Steam Activation Apparatus

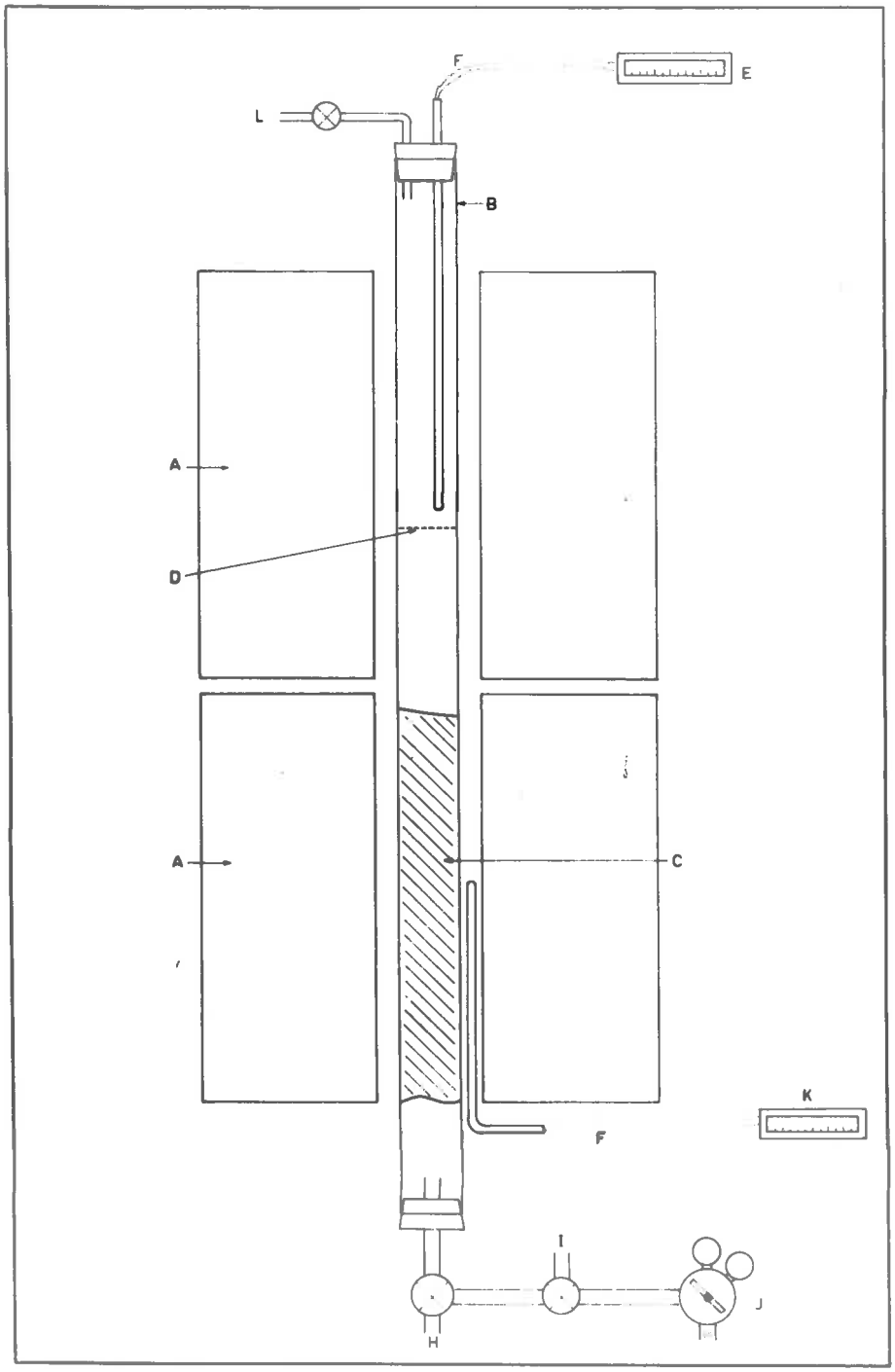

Steam Activation Apparatus

KEY TO FIGURE

Steam Activation Apparatus

A. 2.7-kW furnace
B. Silica tube, length 160 cm., I.D. = 3 cm.
C. Silica chips packing
D. Stainless steel mesh
E. Temperature indicator - top furnace
F. Chromel-alumel thermocouple
G. Furnace controller
H. Vacuum line
I. 200-W steam flash boiler
J. Cylinder 'oxygen free' nitrogen
K. Temperature indicator - bottom furnace
L. Outlet to atmosphere

APPENDIX K

Induction Heated Furnace

APPENDIX L

Graphite Furnace

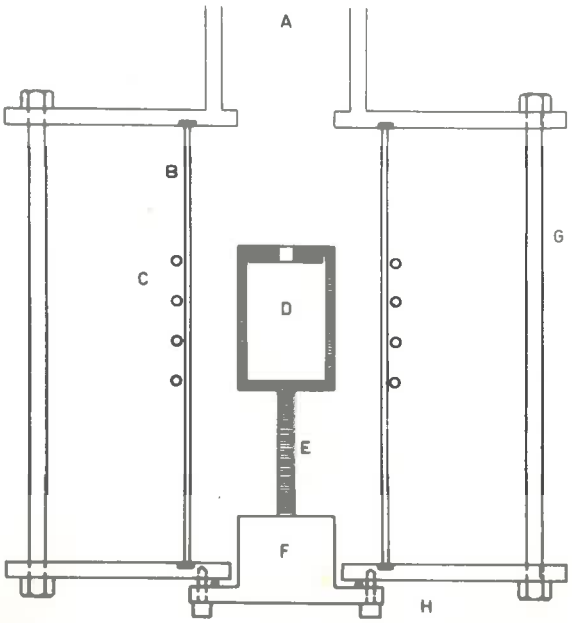

Induction Heated Furnace

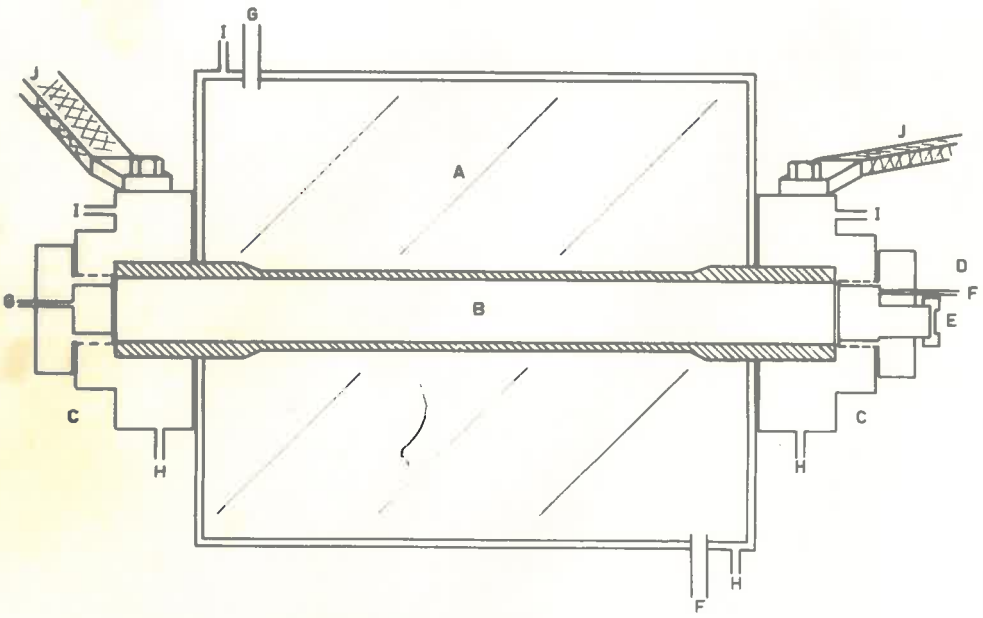

Graphite Furnace

KEY TO FIGURE

Induction Heated Furnace

A. Vacuum line

B. Transparent silica tube, length 40 cm., thickness 0.25 cm., I.D. = 6 cm.

C. $\frac{1}{4}$" copper coils from generator

D. Graphite crucible, length 4.5 cm., thickness 0.25 cm., I.D. = 2.5 cm.

E. Graphite pedestal

F. Water cooled base

G. Tension bolts

H. Neoprene gaskets

KEY TO FIGURE

Graphite Furnace

A. Carbon black insulation

B. Graphite element

C. Water cooled brass blocks clamped to graphite element

D. Brass cover

E. Sight hole

F. Inert gas inlet

G. Inert gas outlet

H. Water inlet

I. Water outlet

J. Power supply - low voltage, high amperage

APPENDIX M

Fine Control Vacuum Valve

APPENDIX N

Gas Introduction Device

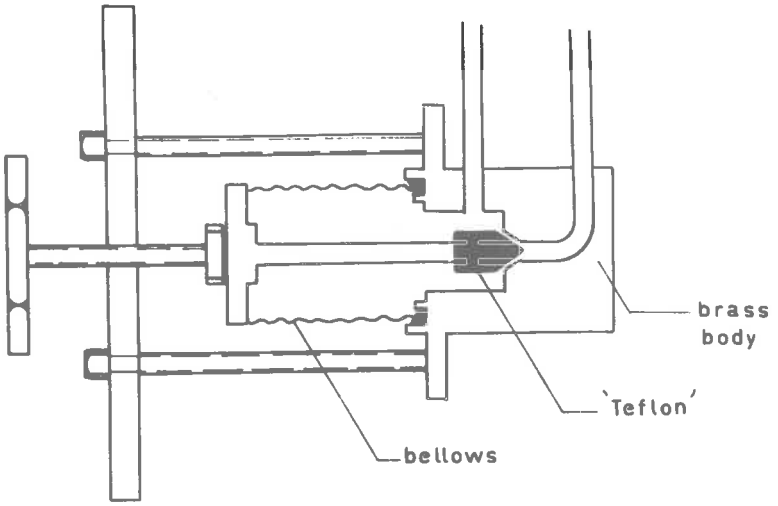

Greaseless Fine Control Vacuum Valve

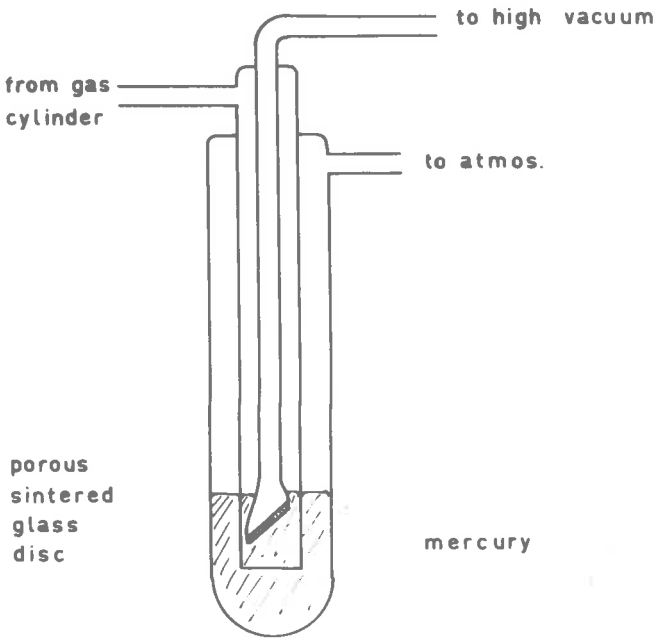

Gas Introduction Device

APPENDIX O

Micro balance Antivibration Mounting

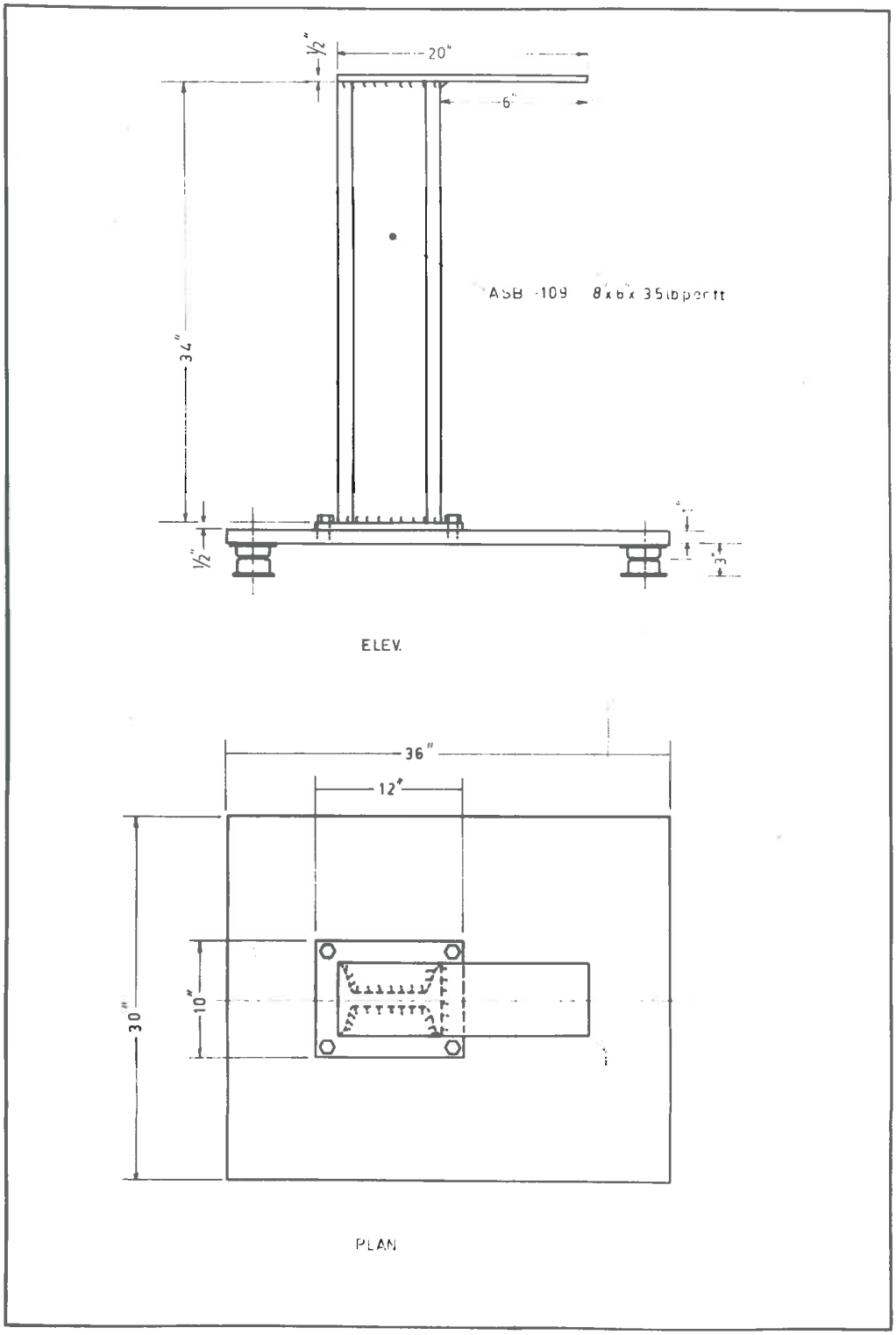

Microbalance Antivibration Mounting

GLOSSARY OF SYMBOLS

c	concentration
C_p	heat capacity of the gas at constant pressure
d	interlayer spacing
d_L	bulk liquid density
D	diffusion coefficient
D_e	effective diffusion coefficient
E	activation energy
G_S	Gibbs free energy of the adsorbate
H_G	molar heat content of the vapour in the standard gas state = H_G/n_G
H, s	- molar quantities
$\bar{H}_S$	differential heat of adsorption of adsorbed molecules = $(\partial H_S/\partial n_S)_{P,T}$
$\bar{H}$, $\bar{s}$	- differential quantities
H_G	total heat content of gas phase
H_S	total heat content of the adsorbed molecules
H, S	- total thermodynamic functions
k_B	Boltzmann's constant
K	Henry's Law constant
L_a	crystallite size in a direction
L_c	crystallite size in c direction
m	mass of a molecule

Glossary of Symbols (Cont'd.)

M	molecular weight
M_a) M_c)	denote a macro-unit of crystallites which are roughly aligned
n_A	moles of adsorbent
n_G	moles of gas in gas phase
n_S	moles of gas adsorbed
N	Avogadro's number
p	pressure
p	proportion of disorientated layers
p_o	saturation pressure
p^0	standard pressure 760 mm. Hg.
P	pressure
P_c	critical pressure of the bulk phase
q	differential heat
q_{st}	isosteric heat of adsorption
Q	total heat
r_k	Kelvin pore radius
$\bar{r}_p$	average pore radius
R	gas law constant
s_G	molar entropy of the gas = S_G/n_S

Glossary of Symbols (Cont'd.)

s^0_G	molar entropy of the gas at a standard pressure and temperature
$\bar{s}_S$	differential entropy of adsorbed molecules $= (\partial S_S/\partial n_S)_{P,T,\Sigma}$
S_G	total entropy of the gas phase
S_S	total entropy of the adsorbed molecules
t	multi-layer thickness
T	temperature
T_c	critical temperature of the bulk phase
U	internal energy
U_{OA}, S_{OA} etc.	internal energy, entropy, etc. of the pure adsorbent
v_S	$= V_G/n_G$ molar volume of the gas phase
$\bar{v}_S$	differential volume, defined as $= (\partial V_S/\partial n_S)_{P,T,\Sigma}$
V	volume
V	molecular volume of adsorbate
V	volume adsorbed c.c. per g.
V_H	pore volume not accessible to argon but accessible to helium
V_m	mono-layer capacity
V_{MAC}	pore volume in macro-pores not taken into account in V_{SL}

Glossary of Symbols (Cont'd.)

V_o	amount adsorbed at time zero
V_p	pore volume calculated from helium and mercury densities
V_s	saturation capacity
V_{SL}	pore volume calculated from the adsorption isotherm saturation capacity at $P/P_o = 1.0$
V_t	amount adsorbed at time t
V_∞	amount adsorbed at time ∞
$\bar{V}_s$	average saturation capacity
x	distance

Greek Letters

α	correction for non-ideality
β	peak breadth
Γ	surface concentration
γ	surface tension
Δ	'foot'
θ	Bragg diffraction angle
θ	contact angle
λ	wavelength
μ_A	chemical potential of the adsorbent, defined as $(\partial U/\partial n_A)_{S,V,n_S}$

Glossary of Symbols (Cont'd.)

Greek Letters (Cont'd.)

μ_S	chemical potential of the adsorbate, defined as $(\partial U/\partial n_S)_{S,V,n_A}$
ρ	density
ρ_{He}	helium density
ρ_{Hg}	mercury density
Σ	surface area
σ, π	bond type
σ_m	molecular area
τ	time spent by a molecule in the adsorbed state
ϕ	'spreading pressure', defined as $(\partial U/\partial \Sigma)_{S_S,V_S,n_S}$

BIBLIOGRAPHY

1. BERNAL, J.D.: Proc.Roy.Soc.(London), 106A, 749 (1924).
2. DEBYE, P., and SCHERRER, P.: Phys.Z., 8, 291 (1918).
3. BACON, G.E.: Acta Cryst., 3, 320 (1956).
4. UBBELOHDE, A.R., and LEWIS, F.A.: "Graphite and its Crystalline Compounds" (Oxford Clarendon Press, 1960).
5. BISCOE, J., and WARREN, B.E.: J.Appl.Phys., 13, 364 (1942).
6. WARREN, B.E.: in "Proc. of the First and Second Conf. on Carbon" (University of Buffalo, Buffalo, 1956), p.49.
7. BACON, G.E.: Acta Cryst., 4, 558 (1951).
8. STEWARD, E.G., and COOK, H.P.: General Electric J., 28, No.1, 35 (1960-61).
9. STEWARD, E.G., and COOK, H.P.: Z.Krist., 114, 245 (1960).
10. LANGMUIR, I.: J.Am.Chem.Soc., 40, 1361 (1918).
11. PULLMAN, B.: in "Proc. of the Third Conf. on Carbon" (University of Buffalo, Buffalo, 1959), p.3.
12. GASSER, C.G., and KIPLING, J.J.: in "Proc. of the Fourth Conf. on Carbon" (University of Buffalo, Buffalo, 1960), p.55.
13. HALLUM, J.V., and DRUSHEL, H.V.: J.Phys.Chem., 62, 110 (1958).
14. SMITH, R.N.: Quart.Rev. (London Chem.Soc.), 13, 287 (1959).
15. HARKER, H., MARSH, H., and WYNNE-JONES, W.F.K.: in "Chemisorption" (Butterworths, London, 1957), p.251.
16. GARTEN, V.A., and WEISS, D.E.: in "Proc. of the Third Conf. on Carbon" (University of Buffalo, Buffalo, 1959), p.295.
17. CULVER, R.V., and WATTS, H.: Rev. of Pure and Appl.Chem. (Australia), 10, No.2, 95 (1960).
18. WEISS, D.E.: Aust.J.Chem., 14, 157 (1961).
19. UBBELOHDE, A.R.: Nature, 180, 380 (1957).

20. HEDLEY, J.A., and ASHWORTH, D.R.: J.Nuclear Materials, 4, 70 (1961).

21. TSUZUKU, T.: in "Proc. of the Third Conf. on Carbon" (University of Buffalo, Buffalo, 1959), p.433.

22. BACON, R., and SPRAGUE, R.: in "Proc. of the Fifth Conf. on Carbon" (University of Buffalo, Buffalo, 1962), VOL.1, p.466.

23. FRANK, F.C.: in "Chemistry of the Solid State", Ed. Garner, W.E., (Butterworths, London, 1955), p.1.

24. STONE, F.S.: in "Chemistry of the Solid State", Ed. Garner, W.E., (Butterworths, London, 1955), p.20.

25. HENNIG, G.R.: in "Proc. of the Fourth Conf. on Carbon" (University of Buffalo, Buffalo, 1960), p.221.

26. GRISDALE, R., PFISTER, A., and VAN ROOSBROECK, W.: Bell. Syst.Tech.J., 30, 271 (1951).

28. HENNIG, G.: J.Chem.Phys. 20, 438 (1952).

29. FRANKLIN, R.E.: Proc.Roy.Soc. (London), 209A, 196 (1951).

30. MROZOWSKI, S.: in "Proc. of the First and Second Conf. on Carbon" (University of Buffalo, Buffalo, 1956), p.31.

31. MIZUSHIMA, S.: in "Proc. of the Fourth Conf. on Carbon" (University of Buffalo, Buffalo, 1960), p.417.

32. CASTLE, J.G.L. in "Proc. of the First and Second Conf. on Carbon" (University of Buffalo, Buffalo, 1956), p.13.

33. DAVIDSON, H.W., and LOSTY, H.H.W.: in "Proc. of the Fourth Conf. on Carbon" (University of Buffalo, Buffalo, 1960), p.585.

34. GREEN, L.: in "Proc. of the Fourth Conf. on Carbon" (University of Buffalo, Buffalo, 1960), p.497.

35. FLORY, P.J.: "Principles of Polymer Chemistry" (Cornell University Press, New York, 1953).

36. AUSTIN, A.E.: in "Proc. of the Third Conf. on Carbon" (University of Buffalo, Buffalo, 1959), p.389.

37. NELSON, J.B., and RILEY, D.P.: Proc.Phys.Soc.(London), 57, 477 (1945).

38. BLACKMAN, L.C.F., SAUNDERS, G., and UBBELOHDE, A.R.: Proc. Roy.Soc.(London), 264A, 19 (1961).

39. CONROY, J.S., SLYSH, R.S., MURPHY, D.B., and KINNEY, C.R.: in "Proc. of the Third Conf. on Carbon" (University of Buffalo, Buffalo, 1959), p.395.

40. KIPLING, J.J., and WILSON, R.B.: in "Proc. Conf. Science in the Use of Coal" (Institute of Fuel, London, 1958), p.C6.

41. TANG, M.M., and BACON, R.: in "Abstracts of Papers for the Sixth Conf. on Carbon" (University of Buffalo, Buffalo, 1963), No.125 and 126.

42. SMITH, R.C., and HOWARD, H.C.: J.Am.Chem.Soc., 59, 234 (1937).

43. BLAYDEN, H.E., RILEY, H.L., and TAYLOR, A.: J.Am.Chem. Soc., 62, 180 (1940).

44. BOLTON, K., CULLINGWORTH, J.E., GHOSH, B.P., and COBB, J.W.: J.Chem.Soc., 252 (1942).

45. RILEY, H.L.: Chem. and Ind., 17, 391 (1939).

46. OUCHI, K., and HONDA, H.: Fuel, 38, 429 (1959).

47. WINSLOW, F.H., MATREYEK, W., and YAGER, W.A.: in "Ind. Carbon and Graphite" (London Chem.Soc., 1958), p.190.

48. DACEY, J.R., and BARRADAS, R.G.: Canad.J.Chem., 41, 180 (1963).

49. EVERETT, D.H., REDMAN, E., MILES, A.J., and DAVIES, D.H.: Fuel, 42, 219 (1963).

50. WINSLOW, F.H., BAKER, W.O., and YAGER, W.A.: J.Am.Chem. Soc., 77, 4751 (1955).

51. WINSLOW, F.H., BAKER, W.O., and YAGER, W.A.: in "Proc. of the First and Second Conf. on Carbon" (University of Buffalo, Buffalo, 1956), p.93.

52. GRASSIE, N.: "Chemistry of High Polymer Degradation Processes" (Butterworths, London, 1956).

53. GILBERT, J.B., and KIPLING, J.J.: Fuel, 41, 249, 493 (1962).

54. HEUSER, E.: "The Chemistry of Cellulose" (John Wiley and Sons, London, 1944), p.545.

55. MROZOWSKI, S.: in "Kinetics of High Temp. Processes", Ed. Kingery, W.D., (Wiley and Chapman, 1959), p.264.

56. DIAMOND, R., and HIRSCH, P.B.: in "Ind. Carbon and Graphite" (London Chem.Soc., 1958), p.197.

57. STEWARD, E.G., and DAVIDSON, H.W.: in "Ind. Carbon and Graphite" (London Chem.Soc., 1958), p.207.

58. KMETKO, E.A.: in "Proc. of the First and Second Conf. on Carbon" (University of Buffalo, Buffalo, 1956), p.21.

59. BARANIECKI, C., RILEY, H.L., and STREATER, E.: in "Ind. Carbon and Graphite" (London Chem.Soc., 1958), p.283.

60. KINNEY, C.R.: in "Proc. of the First and Second Conf. on Carbon" (University of Buffalo, Buffalo, 1956), p.83.

61. OKADA, J., SEKIGUCHI, A., and ISHI, T.: in "Proc. of the Fifth Conf. on Carbon" (University of Buffalo, Buffalo, 1962), VOL.1, p.497.

62. HOGAN, J.F., RAKSZAWSKI, J.F. and REDMOUNT, M.B.: in "Abstracts of Papers for the Sixth Conf. on Carbon" (University of Buffalo, Buffalo, 1963), No.91.

63. MIZUSHIMA, S.: in "Proc. of the Fifth Conf. on Carbon" (University of Buffalo, Buffalo, 1963), VOL.2, p.439.

64. STRANSKI, I.N.: Adv.Catalysis, 9, 406 (1957).

65. FELDMAN, M.H., GOEDDEL, W.V., DIENES, G.J., and GOSSEN, W.: J.Appl.Phys., 23, 1200 (1952).

66. KANTER, M.A.: in "Kinetics of High. Temp. Processes", Ed. Kingery, W.D., (Wiley and Chapman, 1959), p.61.

67. AKAMATU, H., and KURODA, H.: in "Proc. of the Fourth Conf. on Carbon" (University of Buffalo, Buffalo, 1960), p.355.

68. DIAMOND, R.: in "Proc. of the Third Conf. on Carbon" (University of Buffalo, Buffalo, 1959), p.367.

69. SEAL, M.: Nature, 182, 1264 (1958).

70. PINNICK, H.T.: J.Chem.Phys., 20, 756 (1952).

71. TSUZUKU, T.: in "Proc. of the Fourth Conf. on Carbon" (University of Buffalo, Buffalo, 1960), p.403.

72. LOCH, L.D., and AUSTIN, A.E.: in "Proc. of the First and Second Conf. on Carbon" (University of Buffalo, Buffalo, 1956), p.65.

73. SUTTON, A.L., and HOWARD, V.C.: in "Abstracts of Papers for the Sixth Conf. on Carbon" (University of Buffalo, Buffalo, 1963), No.48.

74. COLLINS, F.M.: in "Proc. of the First and Second Conf. on Carbon" (University of Buffalo, Buffalo, 1956), p.177.

75. DAVIDSON, H.W., and LOSEY, H.H.W.: General Electric J., 30, No.1, 22 (1963).

76. LEMON, H.B.: Phys.Rev., 14, 281 (1919).

77. HOWARD, H.C., and HULETT, G.A.: J.Phys.Chem., 28, 1082 (1924).

78. McBAIN, J.W., and SESSIONS, R.F.: J.Phys.Chem., 40, 603 (1936).

79. SMITH, T.: J.Chem.Soc., 923 (1952).

80. BOOCOCK, G., and HOLDSWORTH, S.D.: Atomic Energy Research Establishment, Harwell, CE/M220, HRGP/p.72 (1958).

81. WYNNE-JONES, W.F.K.: in "The Structure and Properties of Porous Materials", Ed. Everett, D.H., and Stone, F.S., (Butterworths, London, 1958), p.35.

82. KISELEV, A.V., and KOVALYOVA, N.V.: Zhur.Fiz.Khim., 30, 2775 (1956).

83. KISELEV, A.V., and KHRAPOVA, E.V.: Izvest.Akad.Nauk S.S.S.R., Otdel.khim.Nauk, 1 (1958).

84. AVGUL, N.N., KISELEV, A.V., KOVALYOVA, N.V., and KHRAPOVA, E.V.: in "Proc. of the Second International Congress on Surface Activity" (Butterworths, London, 1957), VOL.2, p.218.

85. DUBININ, M.M., ZAVERINA, E.D., IVANOVA, L.S., KAVEROV, A.T., and KASATOCHKIN, V.I.: Izvest.Akad.Nauk S.S.S.R., Otdel.khim.Nauk, 17, 29 (1961).

86. DUBININ, M.M.: in "Proc. of the Fifth Conf. on Carbon" (University of Buffalo, Buffalo, 1962), VOL.1, p.81.

87. DUBININ, M.M.: in "Ind.Carbon and Graphite" (London Chem. Soc., 1958), p.219.

88. DUBININ, M.M.: Chem.Rev., 60, 235 (1960).

89. DUBININ, M.M.: Izvest.Akad.Nauk S.S.S.R., Otdel.khim.Nauk, 1153 (1960).

90. BRUNAUER, S.: "Physical Adsorption of Gases and Vapours" (Oxford University Press, 1942).

91. FRANKLIN, R.E.: Trans.Faraday Soc., 45, 274, 668 (1949).

92. SPALARIS, C.N., BUPP, L.P., and GILBERT, E.C.: J.Phys. Chem., 61, 350 (1957).

93. SPALARIS, C.N.: in "Proc. of the Third Conf. on Carbon" (University of Buffalo, Buffalo, 1959), p.575.

94. AMPHLETT, C.B., and GREENFIELD, B.F.: Atomic Energy Research Establishment, Harwell, AERE C/R2632, 1958.

95. HASSLER, J.W.: "Active Carbon" (Chem.Pub.Co.Inc., New York, 1951).

96. MANTELL, C.L.: "Industrial Carbon" (Van Nostrand, New York, 1946).

97. WICKE, E., and KOPPER, H.H.: J.Chem.Phys., 58, 25 (1961).

98. COAL RESEARCH IN C.S.I.R.O., No.4, May, p.4, (1958).

99. DAVIDSON, H.W.: in "Nuclear Graphite" (Dragon Project, Organization for European Economic Co-operation, 1959), p.209.

100. BOLLMAN, W.: in "Proc. of the Fifth Conf. on Carbon" (University of Buffalo, Buffalo, 1963), VOL.2, p.303.

101. KLUG, H.P., and ALEXANDER, L.E.: "X-ray Diffraction Procedures for Polycrystalline and Amorphous Materials" (Chapman and Hall, 1954).

102. FRANKLIN, R.E.: Acta Cryst., 3, 107 (1950).

103. WARREN, B.E.: Phys.Rev., 59, 693 (1941).

104. HOUSKA, C.R., and WARREN, B.E.: J.Appl.Phys., 25, 1503 (1954).

105. SCHERRER, P.: Gottinger Nachrichten, 2, 98 (1918).

106. DIAMOND, R.: Acta Cryst., 11, 129 (1958).

107. ALEXANDER, L.E., and SOMMER, E.C.: J.Phys.Chem., 60, 1646 (1956).

108. ALEXANDER, L.E., and DARIN, S.R.: J.Chem.Phys., 23, 594 (1955).

109. JAMES, R.W.: "The Optical Principles of the Diffraction of X-rays, The Crystalline State" (Bell and Sons, London, 1956), VOL.2.

110. FOWLER, R.H.: Proc. Cambridge Phil.Soc., 32, 144 (1936).

111. FOWLER, R.H.: Proc. Cambridge Phil.Soc., 31, 260 (1935).

112. EMMETT, P.H., and BRUNAUER, S.: J.Am.Chem.Soc., 59, 1553 (1937).

113. BRUNAUER, S., EMMETT, P.H., and TELLER, E.: J.Am.Chem.Soc., 60, 309 (1938).

114. BRUNAUER, S., DEMING, L.S., DEMING, W.E., and TELLER, E.: J.Am.Chem.Soc., 62, 1723 (1940).

115. HALSEY, G.D.: Discuss.Faraday Soc., 8, 54 (1950), Adv. Catalysis, 4, 259 (1952).

116. JURA, G., and POWELL, R.E.: J.Chem.Phys., 19, 251 (1951).

117. PIERCE, C., and SMITH, R.N.: J.Phys.Colloid Chem., 54, 795 (1950).

118. HILL, T.L., EMMETT, P.H., and JOYNER, L.G.: J.Am.Chem.Soc., 73, 5102 (1951).

119. CONNOR, P.: Industrial Chemist, 37, 178, 224 (1961).

120. YOUNG, D.M., and CROWELL, A.D.: "Physical Adsorption of Gases" (Butterworths, London, 1962).

121. ARNELL, J.C., and BARSS, W.M.: Canad.J.Res., 26A, 236 (1948).

122. EVERETT, D.H.: in "The Structure and Properties of Porous Materials", Ed. Everett, D.H., and Stone, F.S., (Butterworths, London, 1958), p.95.

123. DUBININ, M.M.: Quart.Rev., (London Chem.Soc.), 9, 101 (1955).

124. CULVER, R.V., and HEATH, N.S.: Ph.D. Theses, University of Adelaide, (1954).

125. BRECK, D.W., EVERSOLE, W.G., MILTON, R.M., REED, T.B., and THOMAS, T.L.: J.Am.Chem.Soc., 78, 5693 (1956); REED, T.B., and BRECK, D.W.: J.Am.Chem.Soc., 78, 5972 (1956).

126. BARRER, R.M.: Quart.Rev., (London Chem.Soc.), 3, 293 (1949), Brit.Chem.Eng., 4, 267 (1959).

127. DACEY, J.R., and THOMAS, D.G.: Trans.Faraday Soc., 50, 740 (1954).

128. McBAIN, J.W.: "The Sorption of Gases and Vapours by Solids" (Routledge, London, 1932).

129. ALMOND, J.: J.Sci.Instr., 35, 70 (1958).

130. SCHULL, C.G.: J.Am.Chem.Soc., 70, 1405 (1948).

131. BARRETT, E.P., JOYNER, L.G., and HALENDA, P.P.: J.Am.Chem. Soc., 73, 373 (1951).

132. PIERCE, C.: J.Phys.Chem., 57, 149 (1953).

133. CRANSTON, R.W., and INKLEY, F.A.: Adv.Catalysis, 9, 143 (1957).

134. JUHOLA, A.J., and WIIG, E.O.: J.Phys.Chem., 71, 2069 (1949).

135. JUHOLA, A.J., PALUMBO, A.J., SMITH, S.B.: J.Am.Chem.Soc., 74, 61 (1952).

136. BIORCI, G., and PESCETTI, D.: in "Proc. of the Fifth Conf. on Carbon" (University of Buffalo, Buffalo, 1962), VOL.1, p.88.

137. DE BOER, J.H.: in "The Structure and Properties of Porous Materials", Ed. Everett, D.H., and Stone, F.S., (Butterworths, London, 1958).

138. WASHBURN, E.W.: Proc.Nat.Acad.Sci. U.S.A., 7, 115 (1921).

139. RITTER, H.L., and DRAKE, L.C.: Ind.Eng.Chem.Analyt., 17, 782 (1945).

140. INGLES, O.G.: Aust.J.Appl.Sci., 9, 120 (1958).

141. HOLMES, J., and EMMETT, P.H.: J.Phys.Colloid Chem., 51, 1276 (1947).

142. WELLER, K.: Ph.D. Thesis, University of Adelaide, (1963).

143. WHEELER, A.: Adv.Catalysis, 3, 250 (1951).

144. DE BOER, J.H.: "The Dynamical Character of Physical Adsorption" (Oxford, 1953).

145. CARMAN, P.C.: "Flow of Gases Through Porous Media" (Butterworths, London, 1956).

146. KNUDSEN, M.: Ann.Phys., 28, 75 (1909).

147. CRANK, J.: "The Mathematics of Diffusion" (Oxford, London, 1956).

148. BABBITT, J.D.: Canad.J.Res., 28A, 449 (1950), Canad.J. Phys., 29, 427, 437 (1951).

149. HABGOOD, H.W.: Canad.J.Chem., 36, 1384 (1958).

150. NELSON, E.T., and WALKER, P.L.: J.Appl.Chem., 11, 358 (1961).

151. BENSON, G.W., and TOMPKINS, F.C.: J.Phys.Chem., 60, 220 (1956).

152. BARRER, R.M.: "Diffusion In and Through Solids" (Cambridge University Press, London, 1941).

153. JOST, W.: "Diffusion in Solids, Liquids and Gases" (Academic Press, 1952).

154. CARMAN, P.C., and HAUL, R.A.W.: Proc.Roy.Soc. (London), 222A, 109 (1954).

155. BARRER, R.M., and FENDER, B.E.F.: Phys. and Chem. of Solids, 21, 1,12 (1961).

156. TIMOFEEV, D.T., and KABANOVA, O.N.: Izvest.Akad.Nauk S.S.S.R., Otdel.khim.Nauk, 1539 (1961).

157. NAPHTALI, L.M., and POLINSKI, L.M.: J.Phys.Chem., 67, 369 (1963).

158. BARRER, R.M.: Proc.Roy.Soc.(London), 167A, 392, 406 (1938).

159. BARRER, R.M., and IBBITSON, D.A.: Trans.Faraday Soc., 40, 195, 206 (1944).

160. BARRER, R.M., and BROOK, D.W.: Trans.Faraday Soc., 49, 1049 (1953).

161. BARRER, R.M., and RILEY, D.W.: J.Chem.Soc., 133 (1948).

162. BARRER, R.M.: Trans.Faraday Soc., 45, 358 (1949).

163. ZWIETERING, P., OVEREEM, J., and VAN KREVELEN, D.W.: Fuel, 35, 66 (1956).

164. MAGGS, F.A.P.: Research, 6, 513 (1953).

165. JOY, A.S.: in "Proc. Conf. Science in the Use of Coal" (Institute of Fuel, London, 1958), p.A67.

166. BOLT, B.A., and INNES, J.A.: Fuel, 38, 333 (1959).

167. DACEY, J.R., YOUNG, D.M., and McDOUGALL, H.J.: Canad.J. Chem., 35, 689 (1957).

168. HILL, T.L.: J.Am.Chem.Soc., 72, 5347 (1950).

169. HILL, T.L.: Adv.Catalysis, 4, 212 (1952).

170. EVERETT, D.H.: Trans.Faraday Soc., 46, 453, 942, 957 (1950), Proc.Chem.Soc., 38 (1957).

171. COULSON, C.A.: in "Proc. of the Fourth Conf. on Carbon" (University of Buffalo, Buffalo, 1960), p.215.

172. AUSTIN, A.E., and ADELSON, E.: in "Proc. of the Fifth Conf. on Carbon" (University of Buffalo, Buffalo, 1962), VOL.1, p.485.

173. EVERETT, D.H., and WHITTON, W.I.: Proc.Roy.Soc.(London), 230A, 91 (1955).

174. PIERCE, C., WILEY, J.W., and SMITH, R.N.: J.Phys.Colloid Chem., 53, 669 (1949).

175. WICKE, E., and VOIGT, U.: Angew.Chem., B19, 94 (1947).

176. CLAUSING, P.: Ann.Phys.Chem., 7, 489, 569 (1930); DAMKOHLER, G.: Z.Phys.Chem., 174A, 222 (1935).

178. PITTSBURGH COKE and CHEMICAL CO., Activated Carbon Division, Grant Building, Pittsburgh 19, PA.: Brochure on Pittsburgh Granular Carbon.

179. MORGAN, J.J., and FINK, C.E.: Ind.Eng.Chem., 38, 219 (1946).

180. KIRK, P.L., and SCHAFFER, F.L.: Rev.Sci.Instr., 19, 785 (1948); ERNSBERGER, F.M., and DREW, C.M.: Rev.Sci. Instr., 24, 117, 998 (1953).

181. DELL, R.M., and WHEELER, V.J.: United Kingdom Atomic Energy Authority, AERE -R3424, (1960).

182. McBAIN, J.W., and SESSIONS, R.F.: J.Colloid Sci., 3, 213 (1948).

183. GAST, Th., and VIEWIG, R.: Kunstoffe, 34, H 6/7, 117 (1944); GAST, Th.: Feinwerktechnik, Nr.6, 167 (1949); GAST, Th.: Z.angew.Phys.Bd., 8, H4, 164 (1956).

184. BARR, W.E., and ANHORN, V.J.: "Scientific and Industrial Glass Blowing and Laboratory Techniques" (Instrument Pub.Co., Pittsburgh, 1949).

185. DIN, F.: "Thermodynamic Functions of Gases" (Butterworths, London, 1956), VOL.2.

186. ARMSTRONG, G.T.: J.Res.Nat.Bur.Stand., 53, 263 (1954).

187. LOPEZ-GONZALEZ, J.D., CARPENTER, F.G., and DIETZ, V.R.: J.Res.Nat.Bur.Stand., 55, 11 (1955).

188. SANDERSON, R.T.: "Vacuum Manipulation of Volatile Compounds" (Wiley, New York, 1948).

189. HOGE, H.J.: J.Res.Nat.Bur.Stand., 44, 321 (1950).

190. PUDDINGTON, I.E.: Rev.Sci.Instr., 19, 577 (1948).

191. AMERICAN PETROLEUM INSTITUTE RESEARCH PROJECT 44: "Selected Values of Physical and Thermodynamic Properties of Hydrocarbons and Related Compounds", (1952).

192. McCREERY, G.L.: J.Am.Ceram.Soc., 32, 141 (1949).

193. WINFIELD, M.E., and SUTHERLAND, K.L.: Aust.J.Chem., 6, 221, 234, 244 (1953).

194. BARRER, R.M., and STUART, W.I.: Proc.Roy.Soc.(London), 249A, 464, 484 (1959).

195. McKINSTRY, H.A., and SHORT, M.A.: in "Proc. of the Fifth Conf. on Carbon" (University of Buffalo, Buffalo, 1963), VOL.2, p.507.

196. JONES, F.W.: Proc.Roy.Soc.(London), 166A, 16 (1938).

197. CULVER, R.V., and HEATH, N.S.: Trans.Faraday Soc., 51, 1569 (1955).

198. BANGHAM, D.H., and RAZOUK, R.I.: Trans.Faraday Soc., 33, 1463 (1937).

199. KINI, K.A.: private communication, C.S.I.R.O., Division of Coal Research, Australia, 1963.

200. THURSTAN, E.G., and WALL, G.C.: Australian Atomic Energy Commission, TM 85, March 1961.

201. MEYER, H.I.: J.Appl.Phys., 24, 510 (1953).

202. EMMETT, P.H.: Chem.Rev., 43, 69 (1948).

203. CAMERON, A., and STACY, W.O.: Aust.J.Appl.Sci., 9, 283 (1958); 10, 449 (1959).

204. DIETZ, V.R., and CARPENTER, F.G.: Adv. in Chem. Series, Solid Surfaces, No. 33, p. 146, (1961).

205. OLDENKAMP, R.D., and HOUGHTON, G.: J.Phys.Chem., 67, 303 (1963).

206. BEEBE, R.A., BISCOE, J., SMITH, W.R., and WENDELL, C.B.: J.Am.Chem.Soc., 69, 95 (1947).

207. ROBERTS, J.K., and ORR, W.J.C.: Trans Faraday Soc., 34, 1346 (1938).

208. MILLER, A.R.: "The Adsorption of Gases on Solids" (C.U.P., 1949).

209. DE BOER, J.H., and CUSTERS, J.F.H.: Z.Phys.Chem., 25B, 225 (1934).

210. BARRER, R.M.: in "The Structure and Properties of Porous Materials", Ed. Everett, D.H., and Stone, F.S., (Butterworths, London, 1958).

211. FIELD, G.J., WATTS, H., and WELLER, K.R.: Rev.Pure and Appl.Chem.(Aust.), 13, 1 (1963).

212. ISIRIKYAN, A.A., and KISELEV, A.V.: J.Phys.Chem., 65, 601 (1961).

213. FRANKLIN, R.E.: Acta Cryst., 4, 253 (1951).

214. GRAY, T.J.: "The Defect Solid State", (Interscience Pub., N.Y., 1957).

215. RIES, H.E.: Adv. Catalysis, 4, 87 (1952).

216. BLAYDEN, H.E., GIBSON, J., and RILEY, H.L.: in "Proc. of a Conf. on the Ultra-fine Structure of Coals and Cokes", (B.C.U.R.A., London, 1944), p.176.

217. BARRER, R.M.: in "The Structure and Properties of Porous Materials", Ed. Everett, D.H., and Stone, F.S., (Butterworths, London, 1958).

218. GARDEN, L.A., and KINGTON, G.L.: Proc.Roy.Soc.(London), 234A, 24, 35 (1956).

219. HILL, T.L.: J.Chem.Phys., 17, 762 (1949).

220. DRAIN, L.E., and MORRISON, J.A.: Trans.Faraday Soc., 48 845 (1952); 49, 660 (1953).